Biodegradable Polymers for Biomedical Additive Manufacturing

Dario Puppi[1,*] *and Federica Chiellini*[1,*]

[1]Department of Chemistry and Industrial Chemistry – University of Pisa, UdR INSTM Pisa, Via G. Moruzzi 13, 56124 Pisa (Italy)
*E-mail: dario.puppi@unipi.it, federica.chiellini@unipi.it

Keywords: biodegradable polymers, additive manufacturing, natural polymers, aliphatic polyesters, 3D printing

Abstract

The tremendous interest received by additive manufacturing (AM) within the biomedical community is a consequence of the great versatility offered in terms of processing approach, materials selection, and customization of the resulting device. In particular the unparalleled control over structural and compositional features at the macro- and microscale, as a result of the large design freedom and high reproducibility, is making AM the technology of election for the fabrication of biodegradable medical devices. This article is aimed at providing an update overview of scientific literature on biodegradable polymers for AM application in the biomedical field. The main AM techniques applied so far to biodegradable polymers are outlined by presenting relevant materials processing requirements. The different classes of biodegradable polymers investigated for AM (i.e., proteins, polysaccharides, aliphatic polyesters of either natural or synthetic origin, polyurethanes, as well as other synthetic polymers under AM implementation) are described by highlighting their source of extraction, chemical modification, or synthesis route, and their physical-chemical and processing properties in relationship to AM. Relevant literature on their AM processing for medical and pharmaceutical applications is accordingly reviewed.

Summary

List of acronyms
AM: additive manufacturing
ASCs: adipose-derived stem cells
ASTM: American society for testing and materials
BC: bacterial cellulose
BG: bioactive glass
BJ: binder jetting
BMP-2: bone morphogenetic protein-2
BMP-7: bone morphogenetic protein-7
BMSCs: bone marrow stromal cells
Ca-P: calcium phosphate
CAD: computer-controlled design
CAM: computer-controlled manufacturing
CAWS: computer-aided wet-spinning
CLSM: confocal laser scanning microscopy
CT: computer tomography
DEF: diethyl fumarate
DLP: digital light processing
DMPA: 2,2-bis(hydroxymethyl) propionic acid
EC: ethyl cellulose
ECM: extracellular matrix
EDA: ethylenediamine
EFDP: electrofluidodynamic printing
FDM: fused deposition modeling
GelMA: gelatin methacryloyl
Gly: glycine
Hyp: hydroxyproline
ME-AM: melt extrusion-additive manufacturing
HA: hyaluronic acid
Hap: hydroxyapatite
HAMA: hyaluronic acid methacryloyl
HA-pNIPAAM: poly(*N*-isopropylacrylamide)-grafted hyaluronic acid
HMDI: hexamethylene diisocyanate
IPDI: isophorone diisocyanate
MEW: melt-electrospinning writing
MRI: magnetic resonance imaging
MSCs: mesenchymal stem cells
Mw: molecular weight
NC: numerical control
NIPS: non-solvent-induced phase separation
NVP: N-vinyl-2-pyrrolidone
PA11: polyamide 11
PA12: polyamide 12
PC: polycarbonate PC
PCL: poly(ε-caprolactone)
*PCL: star poly(ε-caprolactone)
PDLLA: poly(d,l-lactide)
PED: precision extrusion deposition
PEEK: polyether ether ketone
PEG: poly(ethylene glycol)
PEGDA: polyethylene glycol diacrylate

PEUs: poly(ester urethanes)
PGA: poly(glycolic acid)
PHA: polyhydroxyalkanoates
PHB: poly(3-hydroxybutyrate)
PHBHHx: poly[3-hydroxybutyrate-*co*-3-hydroxyhexanoate)
PHBV: poly(3-hydroxybutyrate-*co*-3-hydroxyvalerate)
PHV: poly(3-hydroxyvalerate)
P[3HB-co-4HB]: poly(3-hydroxybutyrate-*co*-4-hydroxybutyrate)
PLGA: poly(lactide-*co*-glycolide)
PLA: poly(lactide)
PLATMC: poly(l-lactide-*co*-trimethylene carbonate)
PLACL: poly(l‐lactide‐*co*‐ε‐caprolactone)
PDLACL: poly(d,l-lactide-*co*-ε-caprolactone) ()
PLLA: poly(l-lactide)
PMMA: poly(methyl methacrylate)
PPF: poly(propylene fumarate)
PPFDA: poly(propylene fumarate)-diacrylate
Pro: proline
PS: polystyrene
PTMC: poly(trimethylene carbonate)
PUs: polyurethanes
PVA: poly(vinyl alcohol)
PVP: poly(vinyl pyrrolidone)
RGD: arginine-glycine-aspartic acid
rhBMP-2: recombinant human bone morphogenetic protein-2
rhBMP-7: recombinant human bone morphogenetic protein-7
ROP: ring-opening polymerization
SLA: stereolithography
SE-AM: solution extrusion-additive manufacturing
μSLA: microstereolithography
SLS: selective laser sintering
SSLS: surface selective laser sintering
S/O/W: solid in oil in water
STL: standard tessellation language
TE: tissue engineering
TCP: β-tricalcium phosphate
TPP: two-photon polymerization
TPUs: thermoplastic polyurethanes
T_g: glass transition temperature
T_m: melting temperature
T_{deg}: degradation temperature
UV: ultraviolet
Vis: visible
2D: two-dimensional
3D: three-dimensional
3HB: 3-hydroxybuytrate
3HHx: 3-hydroxyhexanoate
3HV: 3-hydroxyvalerate
4HB: 4-hydroxybutyrate

1 Introduction

Additive manufacturing (AM) was defined in 2012 by the American Society for Testing and Materials (ASTM) as "the process of joining materials to make objects from three-dimensional (3D) model data, usually layer upon layer, as opposed to subtractive manufacturing methodologies" [1]. A diversified terminology has been adopted over time to refer to AM by employing various terms used interchangeably, such as 3D printing, rapid prototyping, solid freeform fabrication, additive fabrication, additive processes, and additive layer manufacturing. Due to the increasing interest on AM industrialization, the ASTM and International Organization for Standardization have been working also on relevant aspects other than terminology, such as measuring the performance and safety of relevant materials, process and equipment, ensuring the quality of the finished parts and end products, and specifying procedures for the calibration of machines [2].

AM techniques are based on computer-controlled design (CAD) and manufacturing (CAM) approaches to process a wide range of materials (i.e., metals, polymers, ceramics, and composites) into final products with geometry and size resembling those of digital models. 3D computer solid models of the object can be directly drawn by means of a CAD or math software. In addition, 3D model data can be derived from medical imaging techniques used for diagnostic purposes, e.g., computer tomography (CT) and magnetic resonance imaging (MRI). The digital model is converted into a standard tessellation language (STL) file containing the information of the object's surface geometry, and then expressed as a series of cross-sectional layers with predefined thickness originating a slice file. A numerical control (NC) programming language file is finally loaded digitally in the machine to drive the motion of the fabricating parts.

The fabrication process involves starting from the bottom and building layers up through a sequential delivery of energy and/or materials, with each newly formed layer adhering to the previous one. In laser-based AM techniques, a beam or projection of light is selectively directed to i) a photosensitive resin bath to form patterns of photopolymerized/crosslinked material, in the case of vat photopolymerization techniques, e.g., stereolithography (SLA) and microstereolithography (μSLA) [3] or ii) a powder bed to generate local heat and form patterns of sintered/fused material, in the case of selective laser sintering (SLS).[4] Regarding binder jetting (BJ), also referred to as 3D printing, a liquid binder is selectively deposited on a powder bed [5]. In extrusion-based AM techniques, a polymer as melt [6] or dissolved/suspended in a suitable solvent [7] is extruded in a given environment, for instance in air at a controlled temperature or in a coagulating medium, and deposited with a predefined pattern on a fabrication platform.

Overall the main challenging aspects for new developments are related to build speed and resolution, biocompatibility and mechanical properties of fabricated parts, controlled composition of multi-material parts, as well as other peculiar requirements of specific biomedical applications [8]. AM has the potential of fastening the product development process by reducing the time required for design validation and functional prototypes development. However, at the current stage AM processes are still slow in comparison to those based on large scale production technologies, such as injection molding. Even if this limitation is offset in customized medicine applications by AM flexibility, the perspective of broadening and optimizing its applicative spectrum encourages research on the enhancement of fabrication efficiency with a good compromise between the spatial resolution and the time of production.

Insufficient resolution can result in a significant dimensional discrepancy between the CAD virtual model and the fabricated object, with influence on its resulting quality, structural and functional properties. Besides dimensional accuracy at the macroscale, different biomedical applications require morphological features structured at the micro/nanoscale, for instance as a means to steer cell behaviors in tissue engineering (TE). For these reasons, μSLA and melt-electrospinning writing (MEW) have been attracting great attention for the development of porous polymeric constructs structured at the submicrometric scale [3, 9]. In this optic, combination of AM with other materials processing techniques at different integration levels (i.e., assembly, fabrication or technique level) is a hot topic in the scientific community with the aim of optimizing conflicting scaffold structural requirements, such as high mechanical strength/multi-scale porosity, 3D structure/high resolution, high quality/high fabrication velocity, and structural role/bioactivity [10, 11].

From a mechanical point of view, parts fabricated by AM have often lower properties than those produced by subtractive and formative techniques. Depending on the AM technique employed, such drawback can be the result of a limited choice among suitable materials (e.g., in the case of photosensitive polymers[3]), limited materials engineering freedom (e.g., in the case of composite materials processing by laser- or melt extrusion-based techniques[12]), unwanted porosity and other structural defects (e.g., in the case of uncomplete particles fusion in SLS or marked/insufficient fiber-fiber fusion in extrusion AM [13]). The anisotropic mechanical behavior of additive manufactured parts as a consequence of the layered manufacturing process [14, 15] is particularly pronounced in scaffolds for TE due to the highly porous structure necessary for tissue growth processes. Ongoing research is aimed at developing new software able to analyze the relationship between AM process parameters and material performance [16]. In the next future, machine learning capabilities will allow the selection of the appropriate AM

process parameters given a target mechanical performance, and the analysis in real time of material morphological features and irregularities in order to quantify their relationship with the resulting mechanical performance.

Personalized medicine is emerging as one of the most successful and promising applications for AM. The possibility of using tomographic images from X-ray and MRI scan to manufacture objects customized to anatomical parts of the human body is revolutionizing the approach to surgical planning, building prosthetics, dentistry, and TE. Tens of articles have reported the clinical applications of devices made from metals, polymers or their combination, like in the case of maxillofacial surgery in which AM is used for anatomic models, surgical guides, occlusal splints, implants (e.g., osteosynthesis plates and skeletal reconstruction parts) and facial epithesis [17]. Research on biomedical polymers for AM is resulting in a tremendous impact on clinical treatment of human tissue failure defects, as well as on materials science and technology for polymeric devices development. Recently, a considerable literature has grown up around polymeric materials for AM with the aim of optimize and broaden the range of applications of this class of techniques for biomedical purposes. Significant progress has been achieved on the synthesis of biocompatible and biodegradable photoreactive macromers for SLA to replace conventional lithographic acrylic resins which may cause toxic effects [8, 18, 19]. The decades-long history of clinical employment of polymeric implants made by conventional melt-processing techniques [20] is being exploited to implement in melt-based AM processes both polymers already approved for use in humans and those under development. *In vivo* outcomes on implantation in animals and humans of polymeric devices made by fused deposition modeling (FDM) or SLS stimulate research for their permanent introduction in the interventional surgery routine [21-23]. AM techniques based on polymers in solution or as suspension offer the advantages of processing naturally-derived polymers with inherent bioactive and biomimetic properties to develop production processes with enhanced environmental sustainability. In addition, solution-based AM is the election approach to functionalize materials with drugs and other bioactive agents, such as in the case of hydrogels with controlled porosity and external shape encapsulating cells or growth factors [24, 25], and to endow the polymeric matrix with a nano/microporosity [7, 26]. Great efforts have been also made to develop nanocomposite implants by AM in order to increase the mechanical properties and bioactivity of polymers already in the clinical practice, such as poly(l-lactic acid) (PLLA) and poly(ε-caprolactone) (PCL), as well as other polymeric materials currently under investigation for biomedical purposes [27].

This article aims to provide an updated overview of literature focused on biodegradable polymers tailored to the application of AM in biomedical science and technology. In particular, relevant applicative fields are introduced by highlighting the peculiar advantages and the most challenging issues of AM. The technological and methodological aspects of the different AM techniques applied so far to biodegradable polymers are presented and their specific processing requirements discussed. The different classes of biodegradable polymers under investigation for AM are introduced by highlighting their source of extraction, chemical-physical modification or synthesis route, and their physical-chemical and processing properties in relationship to AM. Relevant literature on their AM processing for medical and pharmaceutical applications is accordingly reviewed. While the range of polymers for AM is being increasing, the article is focused specifically on those that have been more extensively investigated showing promising outcomes for their commercial translation.

2 Additive Manufacturing (AM) in Biomedical Science and Technology

As previously introduced, AM of polymeric materials has found application in different biomedical areas, including 3D anatomical models and surgical training, surgical equipment, prosthetics and implants, TE, *in vitro* tissue modelling, and drug discovery (**Figure 1**). The advanced technological level of AM, in terms of automation degree, reproducibility, design freedom of the manufactured details, processing of medical digital images and their accurate reproduction as solid anatomical objects, is fastening its translation to clinical research and practice in different medical branches, including orthopedic, urogenital, cardiovascular, and neurological surgery.

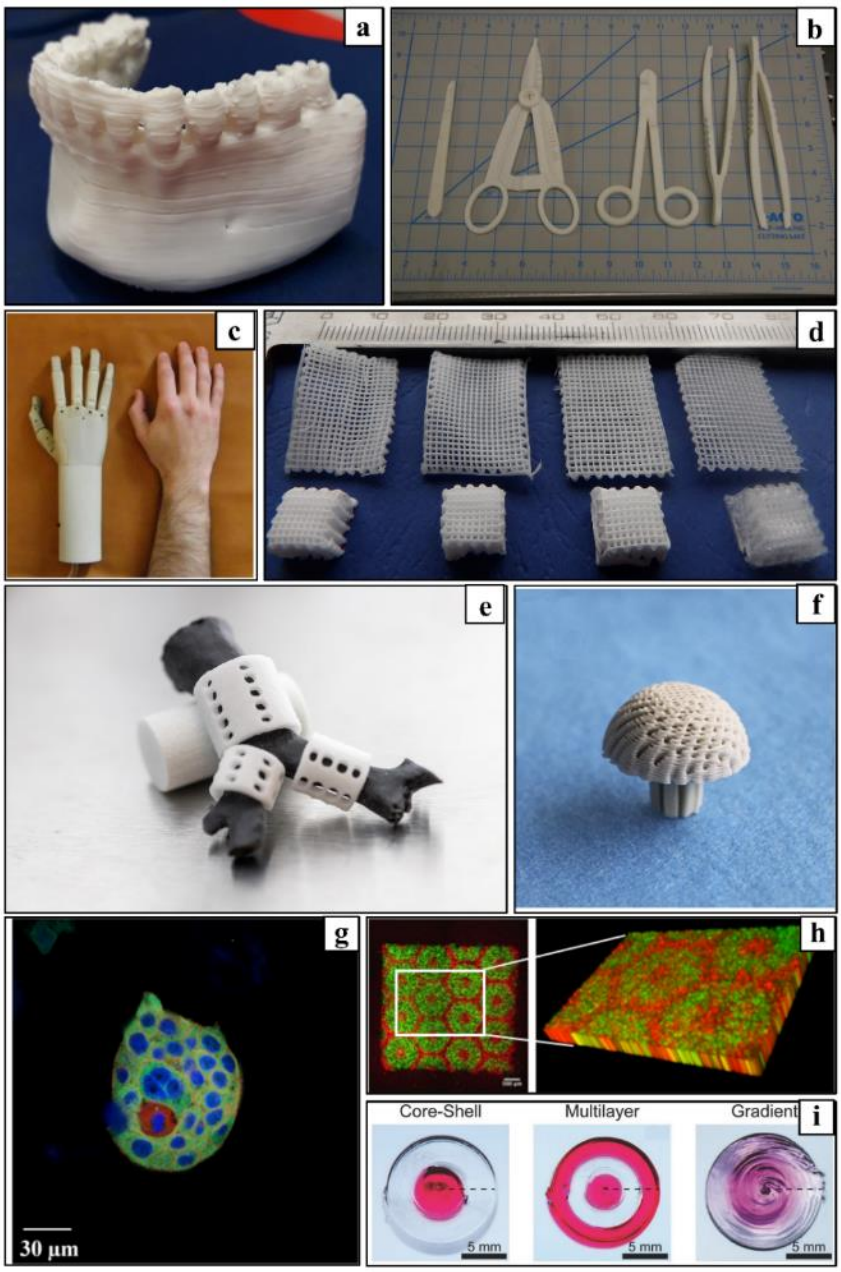

Figure 1. Representative examples of AM biomedical applications. (a) 3D anatomical models: picture of poly(d,l-lactide) (PDLLA) mandibular model by FDM [28]. (b) Surgical instruments: picture of customized nylon surgical set by SLS (reproduced with permission [29]). (c) Exoprostheses: multifunctional prosthetic hand prototype made of a fiber-reinforced nylon (Duraform® HST) and fabricated by SLS (reproduced with permission [30]). (d) Surgical implants: picture of porous poly(methyl methacrylate) (PMMA) implants prototypes fabricated by computer-aided wet-spinning (CAWS) and submitted to different post-processing treatments (reproduced with permission [31]). (e) Biodegradable surgical implants: picture of pediatric tracheal splints made of PCL and fabricated by SLS (reproduced with permission [32]). (f) Scaffold-guided tissue engineering (TE): picture of a PCL/hydroxyapatite (Hap) bone scaffold by FDM modelled on a goat femoral head and equipped with an intramedullary stem (reproduced with permission [33]). (g) 3D tissue modelling: confocal laser scanning microscopy (CLSM) micrograph of a spheroid of human pancreatic cancer cells grown *in vitro* on a 3D microstructured polyelectrolyte complex by CAWS (reproduced with permission [34]). (h) Integrated organ-on-a-chip: CLSM micrograph of a 3D bioprinted hepatic construct with patterns of hepatic cells (green) in gelatin methacryloyl (GelMA) and supporting cells (red)

(scale bar, 500 μm) (reproduced with permission [35]). (i) Drug release systems: picture of polypills with core-shell, multilayer, or concentration gradient configuration of drug loading (reproduced with permission [36]).

3D models for anatomical study and surgical training was one the first successful biomedical applications of AM (**Figure 1a**). Different articles have highlighted the potential of physical anatomical models developed by AM for understanding microsurgical anatomy details and acquiring surgical skills without the ethical, legal and infection problems related to cadaver material. Since they are not considered medical devices, anatomical models can be easily manufactured without following any regulation. Patient-specific phantoms and surgical guides have been used increasingly in different surgery disciplines including among others craniofacial surgery [37-40], neurosurgery [41-43], spine surgery [44-46], cardiovascular surgery [47-49], and pelvic surgery [50-52]. Personalized anatomical models are used also as prototypes for designing medical implants and surgical guides, assistive devices when planning and during surgery, as well as means for academic and clinical teaching, communication to patient, and dissemination [53].

Functional surgical instruments design and fabrication were recently investigated as potential applications of AM to enhance customization and ease of modification according to a clinician's preference. As an example, Kondor *et al*. [54, 55] developed by FDM a generic surgical set that was functionally tested by laparotomy, splenectomy and suturing on a surgical simulator. A recent study showed that functional surgical instruments fabricated by SLS offer some advantages compared to traditional manufacturing methods, including no cost raising for increased complexity, accelerated design to production times, and surgeon specific modifications (**Figure 1b**) [29].

Exoskeleton devices and exoprostheses that can easily fit upper and lower limbs are designed and printed all over the world. AM is bringing different advantages to this therapeutic field including the possibility of making products out of one part, easily personalizing and customizing the device with large design freedom, and producing parts cheaply and quickly [56]. Besides decorative devices, a technologically-advanced field of application in this area is represented by functional prostheses. In particular, a great number of upper limb prostheses with different types of actuation and control of hand kinematics are described in literature and specialized internet websites [57]. Most of these prostheses are available on the market and developed by recurring to different polymers such as acrylonitrile butadiene styrene (ABS), poly(d,l-lactide) (PDLLA), poly(ether ether ketone) (PEEK) and thermoplastic polyurethanes (TPUs) processed by FDM, polyamides 12 and 11 (PA12, PA11) processed by SLS, or

photopolymer resins processed by SLA. For instance, Andrianesis and Tzes [30] recently described a SLS-manufactured anthropomorphic hand chassis made of fiber-reinforced PA12, that integrates a modular actuation system providing the prosthesis with the necessary dexterity, tactile sensing, and controlled digits position (**Figure 1c**).

Surgical implants are among the biomedical applications currently benefiting of AM clinical translation. Virtual planning and guided surgery with additive manufactured patient-specific implants are becoming particularly common in mandibular reconstruction.[58] For instance, Tarsitano *et al*. [59] demonstrated that the employment of customized reconstructive titanium plates manufactured by laser sintering technology facilitated restoration of native mandibular contour. The potential of AM for processing biostable polymers already employed in reconstructive surgery has been recently demonstrated, e.g., in an article describing FDM fabrication of customized osteosynthesis plates as well as cranioplasty and maxillofacial implants made of PEEK [60]. Other polymeric devices intended to optimize surgical intervention and planning, such as occlusal splints and surgical guides, are widely employed by clinicians around the globe [17]. The evidence that a porous structure can favor implant integration, as consequence of tissue formation across the material creating a mechanical interlocking that minimizes micromovements and stress shielding effects, is propelling research on direct AM of biostable porous architectures made of biocompatible polymers, such as poly(methyl methacrylate) (PMMA) [31, 61, 62] and PEEK [63] (**Figure 1d**). As in the case of endovascular stents, surgical implants intended for children require to be made of a biodegradable material allowing for the physiological expansion of tissues and organs during child growth (**Figure 1e**). Research on AM application to this aspect recently resulted in the clinical implantation of personalized 3D printed tracheal and cardiovascular splints made of polymers (e.g., PCL) designed to be absorbed into the body [22, 23].

Tissue engineering (TE) is by far the most extensively investigated biomedical field of application of AM mainly as a consequence of the strict requirements in terms of scaffold porosity, pore size and anatomical structure not attainable by means of other fabrication approaches [64, 65]. Indeed, TE relies on the implantation of a biodegradable scaffold with an interconnected porous structure, possibly in combination with cells and bioactive molecules, which acts as a temporary template providing mechanical support and cell adhesion substrate to guide the tissue regeneration process (**Figure 1f**) [66]. It is well known that scaffold chemistry, topography, porosity, and mechanical stiffness influence cell shape, cytoskeletal organization, function, protein expression, and differentiation [67-70]. AM techniques customized to TE purposes enable an advanced control over scaffold composition and

architecture at different size scales (from macro- to micrometric scale) in terms of design freedom and resolution, with relevant effects on mechanical and biological properties [21, 65]. Structural control can be pushed down to a sub-micrometer resolution scale by employing hybrid AM approaches and μSLA with the aim of providing nanometric instructive cues to cells [21, 31, 71, 72]. In addition, cutting edge advancements on computer-aided design and manufacturing approaches are leading to the fabrication of clinically-sized, anatomically-shaped scaffolds with a tailored porous structure [73, 74]. Fast progress on novel technological tools for processing a wide array of biomedical polymers and relevant composite materials is resulting in the customization of 3D scaffolds for engineering tissues with different structural and functional features, such as complex solid organs (e.g., liver and bone) and tubular structures (e.g., urethra and blood vessels) [66, 75, 76]. The great efforts spent on this research trend are giving the first clinical results like in the case of PCL devices by FDM implanted in humans for craniofacial and dentistry reconstruction [21, 77].

3D tissue modelling for tissue physiology, cancer research and drug evaluation is an emerging field of application of AM that is benefiting of the great knowledge generated by TE research and the resulting powerful technological tools. In particular, the growing interest of the AM community on experimental modelling of healthy and pathological tissues stems from the evidence that 3D scaffolds enable the development of culture microenvironments more closely resembling those found in native tissues in comparison to what achieved with two-dimensional (2D) cell culture systems [78]. Seminal works on polymeric scaffolds for cancer modelling [79-86] showed that tumor cells grown in 3D tend to form proliferative masses or aggregates not detected in monolayer cultures, resulting in different metabolic characteristics and gene expression profiles, as well as in increased tumor proliferation and decreased sensitivity to induced apoptosis. Indeed, 3D scaffolds culture allow more accurate and reproducible information on drug toxicity and tissue chemoresistance for early-stage drug discovery and high-throughput screening of drug candidates [87, 88]. Owing the aforementioned advantages of AM in controlling and customizing scaffold properties, a number of articles have been published on the investigation of additive manufactured systems to develop 3D models of different pathologically-relevant tissues, such as bone metastases [89] and pancreatic cancer [34] (**Figure 1g**). In addition, bioprinting versatility has been exploited to recapitulate certain features of solid tumor tissues, e.g., gradient distribution of chemical and biological factors. In this optic, complex tissue models based on synthetic or natural polymers, cells, growth factors, and well-defined vasculature were developed as systems scalable to mechanistic and high-throughput screening assays related to different biological phenomena, such as wound healing,

vascularization and chondrogenesis [90, 91]. Humanized tumor tissue models in animals were recently developed as alternative to the injection of human cancer cells in order to better mimic species-specific mechanisms occurring in human diseases [92]. This approach involves the ectopic implantation of an additive manufactured scaffold seeded and cultured with human cells in combination with growth or differentiation factors, into an immunodeficient host. Partially humanized organs have been engineered *in vivo* to study prostate or breast metastasis to bone by employing PCL/β-tricalcium phosphate (TCP) composite scaffolds produced by FDM [93] or PCL microfiber tubular scaffolds fabricated by MEW and coated with calcium phosphate (Ca-P) [89, 94, 95].

Integrated organ-on-a-chip research is supported by the great progress made by AM in supplying advanced tools for fabricating in a single continuous procedure the four key elements, i.e., a microfluidic chip, live cells/microtissues that will be cultured in this chip, components for stimulus loading to mature the microtissues, and sensors for results readout.[96] In particular, the ability of bioprinting to precisely positioning multiple materials, including hydrogels, cells, growth factors, and even bacteria [97], in a sequential order with a high spatial resolution enables the development of heterogenous and sophisticated microenvironments mimicking those found in native tissues [98] (**Figure 1h**). Fabricating energy actuators (e.g., electrical and mechanical transducers) and sensors on chips to apply stimuli to cells and monitor their activities is an effective way to make micronized organs mature and functional. A few articles described the possibility of integrating on the same chip mechanical strain-inducing actuators and electrochemical sensors, together with complex fluid handling modules [99]. Other microfluidic approaches explored to induce mechanical stimuli to cells on demand involves the employment of magnetic particles [100] or actuators made from memory shape materials [101].

Drug release from additive manufactured implants is one of the most challenging aspects that could greatly influence the future trend of AM applied to biomedical polymers [102]. Direct drug loading of AM implantable devices during fabrication has been intensively investigated for hydrogel-forming materials (e.g., crosslinked alginate) and other hydrophilic polymers that can be processed by using aqueous solutions at room temperature [103, 104]. Indeed, most of relevant studies were based on solution extrusion-AM (SE-AM) and BJ, with few examples reporting on drug loading of implants fabricated by FDM, SLA or SLS, mainly by recurring to post-processing loading strategies because of the tough processing conditions required (i.e., high temperatures, high energy laser) that can lead to drug degradation. In particular, SE-AM offers great opportunities for loading either hydrophilic or hydrophobic polymers with a drug by simply adding it as solute or suspension to the solution to be processed at room temperature

[105, 106]. Advanced pharmaceutical AM technologies can be used to produce controlled drug delivery systems and personalized dosages for the future of personalized medicine [107]. Different oral dosage forms by AM are currently under investigation resulting in the recent approval of the first additive manufactured drug-releasing tablet for oral administration, Spritam®. In particular the versatility of AM has been investigated to tune dosage macroshape [108], drug concentration gradients [109], and complex inner porous structures [110] as a means to control drug release kinetics (**Figure 1i**). The first successful results suggest that AM has the potential to offer high versatility in controlling drug release profiles, personalized customization, complex designs, and multi-drug incorporation, enabling a new paradigm of controlled release and local delivery of drugs. The high technological readiness level of AM techniques will facilitate the maturation of advanced fabrication approaches to drug delivery eventually adhering to GMP-standards and industrial scale-up.

3 Polymeric Materials Requirements for AM

In addition to fundamental requirements of polymeric biomaterials (e.g., biocompatibility), biomedical devices should assure structural and functional roles tailored to the specific application they are intended to. As an example, those designed for interfacing with cells and actively supporting a biological regenerative process should provide biochemical and/or physical cues to influence cell behaviors. Moreover, each AM technique requires distinct physical-chemical polymer properties in agreement with its processing principles. The employment of polymers in the fabrication of ceramic-based devices (e.g., as binding/reinforcing agents in BJ, sacrificial materials in SLA, or molding systems in indirect AM [111]) further widens the relevant AM requirements window.

This chapter is dedicated to a synthetic description of the fundamental scientific and technological aspects involved in the processing of biodegradable polymers by different AM techniques. Various criteria have been adopted to classify AM techniques on the basis of different aspects, such as the processing principles, the technological solutions, or the physical state of the material. This review specifically deals with techniques applied to biodegradable polymers by following a classification commonly used in the biomedical field in agreement to their working principles, i.e., stereolithography (SLA), selective laser sintering (SLS), binder jetting (BJ), melt extrusion-AM (ME-AM), solution extrusion-AM (SE-AM), and bioprinting (**Figure 2**). Materials processing properties required by each AM technique will be discussed by highlighting advanced strategies for polymer structure design and formulation. The integration of AM with other fabrication methods will be properly presented as an effective

means to develop hybrid polymeric architectures with complementary structural features. The most successful attempts of AM combination with electrospinning [112], salt leaching [113], gas foaming [114], freeze drying [115], and wet-spinning [7] will be described in this and the following chapters, showing how the integration can be achieved at: i) the assembly level by combining substructures fabricated by different technologies into a bi/multiphasic construct, ii) at the fabrication level by simultaneously incorporating multiple-length scale networks (e.g., macro-, micro- and nanofeatures) within a single final bi/multimodal scaffold, iii) at the technique level by fusing the working principles of different fabrication techniques within a single, novel hybrid AM technology [10, 11].

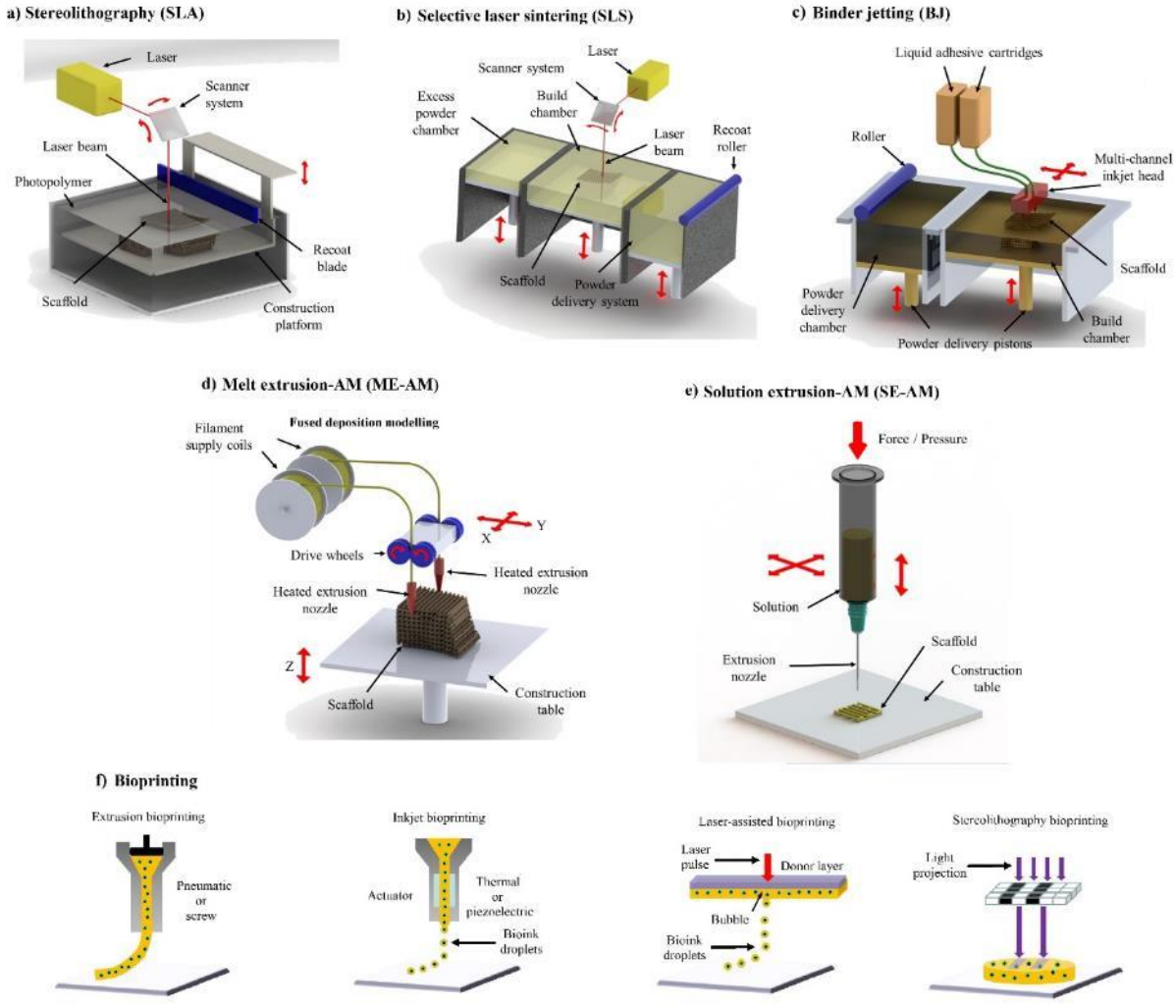

Figure 2. AM techniques commonly employed for biodegradable polymers processing [65, 98]. (a) Stereolithography (SLA): a light source is irradiated over the surface of a vat filled with a photosensitive resin. (b) Selective laser sintering (SLS): based on selective sintering of a powder bed made of polymer, ceramic or hybrid particles by means of a computer-controlled laser beam. (c) Binder jetting (BJ): a liquid binder is selectively deposited on a bed of polymer, ceramic, metallic or composite powder by means of an inkjet head. (d) Melt extrusion-AM (ME-AM): e.g., fused deposition modelling (FDM), based on the extrusion of a polymeric

filament through a nozzle kept at a temperature higher than the polymer T_g. (e) Solution extrusion-AM (SE-AM): a polymer, ceramic or composite solution is extruded through a translating nozzle by means of a pneumatic or mechanical-driven dispensing system. (f) Extrusion bioprinting: based on pneumatics or mechanical force to continuously extrude cells suspended in a hydrogel solution; inkjet bioprinting: based on a piezoelectric or thermal actuator to sequentially eject small droplets made of cells and a hydrogel; laser-assisted bioprinting: based on a laser pulse to vaporize a region in the donor layer (top) forming a bubble that propels a suspended bioink to fall onto the substrate; stereolithography bioprinting: based on projected light to selectively crosslink bioinks layer-by-layer.

3.1 Stereolithography (SLA)

SLA has been used for years in large-scale industrial processes in the microelectronics sector as well as in the biomedical industry for the production of custom hearing and dentistry devices. One of the main advantages of SLA approaches over other AM techniques is their higher resolution which is limited by the system's optics rather than the extrudate or powder particles size.

SLA, also referred to as vat photopolymerization, is based on the controlled polymerization and/or crosslinking of a photosensitive resin to fabricate an object layer-by-layer by using light, usually in the ultraviolet (UV) and sometimes in the visible (Vis) spectrum [116]. Resin curing can be based on vector scanning SLA, mask projection SLA or two-photon polymerization (TPP). In all cases, a light source is irradiated over the surface of a vat filled with a photosensitive resin. Once a layer is photopolymerized, the build stage is submerged further into the photopolymer vat and the next layer is built directly on top of the previous one (**Figure 2a**). Alternative technological solutions developed for processing polysaccharide derivatives into biocompatible hydrogels, involve pumping PBS after the fabrication of each layer to rinse away partially-reacted resin, and then dispensing fresh monomer to fabricate the next layer [117].

In the case of vector scanning SLA, a laser beam is scanned over the vat surface, while in the case of mask projection SLA, often referred to as digital light processing (DLP), light is reflected off a set of dynamic micromirrors to irradiate simultaneously the entire surface of the photopolymer vat. In both approaches the resin is selectively solidified through photopolymerization reactions wherever the laser is scanned. TPP relies on the simultaneous absorption of two lower energy photons at high wavelength, typically in the range 780–820 nm.[118] In this case, features on the nanometer scale can be achieved, even if the time required to obtain physiologically relevant sizes makes this technique in most of the cases an impractical choice for 3D biomedical implant fabrication [119].

μSLA approaches have the potential to create devices with feature sizes in the scale of tens of micrometers and overall dimensions of centimeters [3]. They are based on either high-resolution vector scanning or mask projection systems using UV lamps, LEDs or lasers. A top-down approach in which the light is projected from above the vat, or a bottom-up approach involving light projection from below can be either adopted. A layer of fresh resin with controlled thickness is applied over the solidified layer by means of a process based on dipping, spreading, pumping or gravity.

μSLA has been having a great impact on the biomedical market in large-scale production of customized removable teeth aligners (Invisalign®) and hearing aid device parts [120, 121], as well as in different surgery applications such as anatomical models for surgical planning, models and molds for customized implants, custom surgical guides and templates [122]. The tremendous progress made on resolution increasing, and on the variety of photosensitive materials for biodegradable scaffolds fabrication, encourages research on SLA employment for TE [3]. Indeed, as it will be further discussed, the great ability of SLA to control pore size, geometry, porosity and interconnectivity is being exploited to develop advanced materials engineering strategies for regenerative medicine. In addition, the possibility of incorporating cells during the photopolymerization treatment opens new possibilities for the development of living TE constructs and microscale cell patterning strategies [123, 124].

Materials design and processing requirements. SLA resins are composed by reactive monomers, oligomers and/or polymers that polymerize and/or crosslink when exposed to light in the UV or Vis spectrum. The process is carried out in the presence of a suitable photoinitiator and possible additives such as light absorbers, stabilizers, anti-foaming agents, and other functional components (e.g., ceramic particles and polypeptides) [125]. In order to exploit the precise spatial and temporal control achievable by means of SLA techniques, it is necessary to employ photopolymers with minimized shrinkage and distortion upon polymerization. At the same time, the resin should not be thermosetting and its viscosity should be sufficiently low, typically below 5 Pa·s [18, 126], to achieve the necessary flow properties. Low molecular weight (Mw) macromers with relatively low glass transition temperature (T_g), and a diluent when needed, are typically employed for this reason.

The diluent can be reactive, like in the case of diethyl fumarate (DEF) [127] or N-vinyl-2-pyrrolidone (NVP) [128] that are employed in the photoreaction of macromers containing fumarate groups. When a non-reactive diluent is employed, for instance in the case of solid or highly viscous macromers functionalized with reactive groups (e.g., acrylates), the cured material can undergo shrinkage upon diluent extraction and drying [129]. Since this shrinkage

is usually isotropic and the designed architecture of the object is preserved, this effect is to be accounted for in the design phase. Various photoinitiators with UV or Vis light absorbance have been tested for applications requiring cell-material interactions, including the UV Irgacure photoinitiators, with Irgacure 2959 showing the least toxicity to different cell lines, and the Vis light initiators lithium phenyl-2,4,6-trimethylbenzoylphosphinate and eosin Y disodium salt with increased water solubility [130].

The most employed photopolymer resins for SLA are multifunctional acrylates, methacrylates, and acrylamides submitted to free-radical photopolymerization, as well as epoxides and vinyl ethers submitted to cationic photopolymerization [3, 8]. Photocuring of low-Mw, multi-functional monomers usually results in highly cross-linked networks showing a rigid and brittle behavior. For this reason, a number of articles have focused on the development of macromers with low T_g and relatively high Mw (1-5 kg/mol) to fabricate flexible and elastomeric porous constructs for biomedical applications [131-133]. Cutting edge advancements in SLA materials science and technology deal with polymers with advanced properties including shape memory [134], ionic conductivity [135], high thermomechanical properties [136], biocompatibility for Class IIA devices [137]. In addition, SLA synthetic materials are often surface-treated by using bioactive coatings, such as calcium phosphates and biomimetic peptides, in order to increase their biocompatibility and favor cell adhesion [138, 139].

Biodegradable SLA materials can be obtained by employing oligomers with hydrolysable ester or carbonate linkages in the main chain, and functionalized with photocurable acrylate, methacrylate, or vinyl functional groups. As it will be discussed in detail later, macromers based on poly(propylene fumarate) (PPF) [140], acrylate-endcapped poly(ε-caprolactone-*co*-trimethylene carbonate) [141, 142] or poly(trimethylene carbonate) (PTMC) [143, 144], methacrylate [129] or fumaric acid monoethyl ester [145] end-functionalized PDLLA oligomers, or divinyl fumarate PCL [146] have been successfully employed to fabricate biodegradable scaffolds. The optimization of physical-chemical, rheological and biological properties of new unsaturated polyester resin formulations is a key aspect for SLA application in the TE field [19]. Research on biostable photocurable resins for biomedical purposes is giving promising results as well, such as in the case of polyethylene glycol diacrylate (PEGDA) hydrogels, which are widely investigated as scaffolds for cells growth [147-149]. Various natural polymers, including gelatin [150], keratin [151], collagen [152], chitosan [153], and hyaluronic acid (HA) [117] have been successfully modified with photopolymerizable pendant groups in order to exploit their biocompatibility and high cellular adhesion for photoreaction-based fabrication approaches. However, although the great progress made on gelatin

methacryloyl (GelMA) to fabricate biocompatible scaffolds [124, 150, 154, 155], functionalized natural polymers for SLA still generally result in either 2D structures or 3D constructs with limited porosity in the direction of printing (Z axis). Indeed, the high-water content and low crosslinking groups density in these resins typically cause high depth of penetration of light, not allowing the fabrication of high resolution features in the print direction even by recurring to UV absorbers [3]. However, the great efforts spent by actors in this research area are leading to significant advances in the development of machines and resins for the next generation of naturally-derived SLA polymers. As an example, soybean oil epoxidized acrylate was recently polymerized by SLA into a highly compatible scaffold with shape memory properties suitable for 4D Printing at physiological conditions [156].

3.2 Selective laser sintering (SLS)

SLS is extensively used across different industrial sectors, including electronics, aerospace, and automotive industries, for prototyping devices, small components, and cost-effective consumer good parts.

SLS is based on the selective sintering of a powder bed made of polymer, ceramic or hybrid particles by means of a computer-controlled laser beam [157]. Once the fabrication of a layer is complete, a new powder bed is mechanically spread over it by means of a roller or a blade system (**Figure 2b**). The powder sintering and spreading process is repeated several times to build up the 3D object layer-by-layer. A high intensity laser beam (e.g., CO_2 laser) capable of raising the bed temperature and bonding the particles within a layer and between adjacent layers is employed. Non-sintered powder serves as support for the subsequent layers, thus allowing the manufacturing of complex geometries without the need of implementing support structures and materials.

Further advantages of SLS over other AM techniques include avoiding the use of solvents, diluents or other reactive agents that can be toxic if not completely removed from the device [158]. On the other hand, post-processing treatments (e.g., air blasting and ultrasonic cleaning) are often required to eliminate non-sintered powder that may remain entrapped in porous architectures. SLS resolution is typically in the range of 100 μm depending on laser parameters. As a consequence of the limited laser intensity applied in order to avoid polymer thermal degradation, a poor control over surface roughness, which is defined by particle size and shape, is generally achieved. For this reason, surface finishing treatments (e.g., milling and coating) are typically applied.

SLS has found application in the biomedical field mainly for manufacturing patient-specific anatomical models, exoprostheses, and biostable implantable devices with complex shapes and

controllable internal architectures [159]. Indeed, the great progress made on SLS in combination with medical imaging techniques is being resulting in fastening and improving the quality of surgical procedures, such as preoperative planning, implant design and surgery operations. In addition, the development of tailored powders made of biodegradable polymers, possibly loaded with osteoconductive ceramics, has widened the application of SLS to TE scaffolds and drug delivery devices. The availability in the market of biomaterial powders for SLS is still scarce and most of the methodologies for their preparation are performed at a laboratory scale. However, the successful implantation in humans of medical devices fabricated by SLS witnessed the tremendous potential of this AM technique for tissue reconstruction and pediatric interventional surgery [21]. Indeed, Oxford Performance Materials has received FDA clearance to manufacture patient-specific PEEK implants (OsteoFab®) for cranial, maxilofaccial and spinal surgery [161], while PCL devices are surgically employed to treat infants affected by tracheobronchomalacia [162].

Materials design and processing requirements. SLS is based on laser absorption-induced raising of the local temperature to a level enough to soft and fuse the particles together, typically without causing an actual melting of the polymer. The material processing requirements of SLS concern different aspects including polymer optical, thermal, viscosity, and surface tension properties, as well as particles shape and size distribution [159, 163, 164].

Since the CO_2 laser produces a beam of infrared light, it is necessary that the polymer absorb energy at the laser wave length (10.6 μm). Otherwise an increase of laser energy power can compensate low energy absorption. In the case of semicrystalline polymers, the indicative sintering window can be considered the temperature range between the onset of polymer melting and that of crystallization, as obtained from differential scanning calorimetry [165]. Indeed, it is essential to avoid polymer crystallization that often results in curling or warpage of SLS parts. The fabrication chamber is typically maintained at a temperature just below the melting or softening point of the polymeric powder to speed up and optimize the sintering process by minimizing internal stresses and curl distortions. An inert gas atmosphere in the chamber to hinder oxidative degradation of the polymer during the process is therefore required. In comparison to semicrystalline polymers, amorphous polymers soften gradually over a broader range of temperature between their T_g and flow temperature. For this reason, they typically present lower internal stresses and distortions upon solidification from melt. However, their melt viscosity tends to be relatively high, resulting in limited coalescence of polymer particles.

Indeed, low values of melt zero-shear viscosity (η) and surface tension are necessary to achieve an adequate coalescence of polymer particles during sintering [166]. This aspect is of particular importance considering that unlike other melt processing techniques (e.g., injection molding) additional material compacting under pressure is not provided. Temperature effects together with gravity and capillary forces are the only factors providing the driving force for particles consolidation in SLS [13]. A η not low enough is the cause of imperfections and poor surface quality, resulting in brittleness and instability of sintered parts, as often observed in the case of amorphous polymers [164]. For instance, semicrystalline PA12 (nylon-12) (η=100 Pas) can be fully densified by SLS but polycarbonate (PC) which is amorphous (η=5000 Pas) cannot, even if they show similar surface tension in the melt state [13].

Particles shape, surface and granulometry are crucial parameters since affect powder flowability during spreading to form a bed of a given thickness (usually around 100 µm) and with a density suitable for the sintering process. The required powder properties are generally assured by particles shape close to a spherical geometry and a narrow size distribution between 20 and 80 µm, with a low share of fine particles below 10 µm to avoid their agglomeration [167]. As reviewed by Schmid and Wegener [164], different particle shapes can be obtained by varying the preparation technique. Spherical particles are usually obtained by co-extrusion processes of immiscible mixtures (e.g., oil droplets in water), potato-shaped particles by precipitation processes starting from a polymeric solution, irregularly-shaped particles by cryogenic milling. Polymer/ceramic composite microspheres can be obtained by solid in oil in water (S/O/W) emulsification solvent evaporation methods [168].

Industrial consumption of SLS powder is dominated by PA12 and its blends, with a minor percentage of the market distributed on other polyamides (e.g., PA11) and few other polymers, such as thermoplastic elastomers (i.e., TPUs and polyether block amides) and PEEK, not including the so-called commodity plastics, such as poly(ethylene) and poly(vinyl chloride) [169]. The market offer of amorphous polymers for SLS is limited to polystyrene (PS), with few investigations on other polymers such as PMMA [170] and PC [171]. The reason behind this very limited range of materials is that only a successful combination of the aforementioned intrinsic and extrinsic polymer properties allows a new powder to be implemented in SLS.

As previously mentioned, several attempts have been made to process biodegradable polymers by SLS, mainly aliphatic polyesters for TE scaffolds production.[4, 166, 172-174] In particular, SLS of PCL [4, 174-177], PDLLA [166, 172, 178], and poly(3-hydroxybutyrate-*co*-3-hydroxyvalerate) (PHBV) [179-181] also in combination with osteoconductive calcium phosphates, has been reported.

3.3 Binder jetting (BJ)

Being one of the first AM techniques employed in the biomedical field [182], BJ has been widely investigated for processing biocompatible ceramics and polymers. Although, originally referred to as 3D printing, in this review it will be called BJ in order to avoid misinterpretations related to the frequent use in literature of the term '3D Printing' as synonym of AM.

BJ is based on the selective deposition of a binder, usually in the liquid form, on a powder bed (**Figure 2c**). The binder acts as an adhesive between powder particles to form a solid layer or to bond or fuse adjacent layers together as well [8]. A multi-channel inkjet head can be employed to deposit different binders or increase the manufacturing velocity. After the fabrication of each layer, the construction platform moves downward a given distance and a new powder bed is placed on top of the previous one to carry on with the layer-by-layer process until the 3D object building is completed. Like in the case of SLS, the unbound powder acts as a support for the building of the successive layer. Depending of the properties required, post processing treatments, such as depowering, sintering, infiltration, coating, polishing and machining, are carried out [183]. In particular, post processing sintering and infiltration of a binder are the most common approaches to increase the density and mechanical strength of printed parts.

The liquid binder can be deposited through either drop-on-demand or continuous-jet printheads. In the first case the most common approaches involve ejecting a drop from a nozzle as a consequence of a piezoelectric deformation of the chamber containing the binder or a confined thermal vaporization and subsequent volume expansion of a small liquid volume. Continuous-jet printheads involve pumping the liquid through a gun body equipped with a piezoelectric crystal that creates an acoustic wave generating a constant droplet output.

BJ presents a high versatility in terms of materials selection since it can be applied to powders made of metals, ceramics, polymers, or composites. In addition, the high production rate and the tunable manufacturing scale ranging from millimeter objects that can be scaled up to large-sized models in the meter range, make BJ a flexible technique adaptable to the industrial production [5]. Shape alterations and geometrical defects as consequence of solvent evaporation or post-processing treatments (e.g., dipping in a binder solution [184] and sintering [185]) often required to stabilize the printed structure, are the major peculiar drawbacks of BJ limiting its application. In addition, mechanical properties and surface resolution are lower in comparison to what achieved with other AM techniques, such as SLA and FDM, even after post-processing treatment.

The most investigated biomedical application of BJ is the fabrication of ceramic-based bone implants. Considering the limited ceramic processing versatility of other AM techniques, research on BJ has produced a large body of literature on both *in vitro* and *in vivo* investigation of implantable devices for applications extending from tissue regeneration to bone tumor therapy [111]. In addition, BJ represents the most exploited AM technique in pharmaceutical sciences, as witnessed by the launch on the market of the oral antiepileptic medicine Spritam® [107]. The versatility of BJ in bioactive formulations processing has been also exploited to fabricate polymeric implants made of either a hydrophobic or hydrophilic polymer and loaded with a drug that can be released *in situ* with a controlled kinetics [186].

Materials design and processing requirements. In the case of a ceramic or metallic powder, the binder is composed of a solution or dispersion of a polymer or an inorganic material capable to form a film with adhesive properties upon drying or to react with the particle material. For instance, when powders made of a bioceramic or a bioactive glass (BG) are employed, an aqueous solution of a hydrophilic polymer (e.g., hydroxypropyl methylcellulose and dextrin) or an acidic binder able to react with the ceramic (e.g., phosphoric acid and citric acid) is employed [111]. BJ of a polymeric powder is based instead on material swelling under the action of the binder, and the consequent polymer chains interdiffusion and entanglement at the interface between different particles.

Various BJ parameters, including binder composition, powder bed thickness, powder particles size and shape, printing and post-processing parameters, affect the surface morphology and mechanical properties of the fabricated part. Although literature on BJ parameters/device properties relationship is scarce in the case of polymeric powder, general considerations on this topic can be made relying on what experimentally observed for BJ processing of ceramics [183, 187], as well as for polymer powder processing by SLS [163]. Overall, for a given polymer most of the processing requirements concerns the binder characteristics in relationship to the final application.

A polymer binder should have a strong solvating power to achieve effective particles fusion by quickly dissolving them during the time required to print one layer [183]. It typically consists of a good solvent or solvents mixture, e.g., chlorinated solvents for hydrophobic polymers like aliphatic polyesters and aqueous binders for hydrophilic polymers like polysaccharides. The material fusion degree depends also on particles size since by decreasing it the polymer is more easily dissolved. However, particles with a diameter lower than 20 μm are difficult to spread and tend to agglomerate. In general, polymer particles shape, surface and granulometry should

be taken under control to assure suitable flowability of the powder to form a bed of a given thickness and density, as previously considered for SLS.

The binder formulation should possess suitable viscosity and surface tension to properly eject, spread, and infiltrate in the powder bed without wicking out considerably from the impact area, leaving behind a too rough surface. These parameters can be optimized to enhance printing resolution by employing a polymer solution as a binder, as demonstrated by depositing a 10 wt. % PCL solution in chloroform onto a PCL powder bed [188]. Reference values recommended for commercial BJ printers are a viscosity of 20 cPs and a surface tension of 35 dynes/cm. Binder vapor pressure is another key parameter since a too low evaporation rate can worsen the process resolution, while a too fast evaporation rate will likely result in warping of the printed component as a consequence of internal stresses. For instance, warpage effects in polyester parts are avoided by replacing methylene chloride with chloroform as binder, or using a mixture of them. In the case of a binder based on acetone, which has high volatility and a lower solvating power for aliphatic polyesters in comparison to chlorinated solvents, most of the porosity of the original powder bed is likely to be maintained after printing at room temperature. An effective approach to increase the evaporation rate of binders with low vapor pressure is represented by the employment of a warm powder bed.

Besides being the most employed technique for AM of biomedical ceramics, such as osteoconductive calcium phosphates [189-197], BJ has been applied to process also aliphatic polyesters [198] and hydrophilic polymers, such as poly(vinyl alcohol) (PVA), starch, maltodextrin, and cellulose derivatives [8, 199]. In addition to the binding component, the deposited liquid may contain additives such as surfactants, viscosity modifiers, and bioactive agents, to improve the printing process or functionalize the final device. As previously mentioned, this aspect has been widely investigated to develop orally delivered drugs by adding a pharmaceutical active ingredient to the binder formulation. In addition, extensive research has shown that BJ is suitable for the preparation of drug-loaded implants based on different biodegradable polymers including PCL, poly(lactic-*co*-glycolic acid) (PLGA), and their blends [198], PLLA [200], and PDLLA [201]. Advanced approaches allow the combination of multiple drugs within one implant with a relatively long-term release profile [202].

3.4 Melt extrusion-AM (ME-AM)

The Melt-extrusion class of AM techniques (ME-AM) is finding increasing industrial exploitation particularly in the automotive, aerospace, and medical sectors for rapid production of functional prototypes, models, and parts of civil aircrafts or vehicles produced in small number. In particular, they are the most investigated AM techniques for the fabrication of

polymeric scaffolds for TE as a consequence of the good compromise offered in terms of materials selection versatility, design freedom, automation degree, mechanical properties, and accuracy of deposition details.

ME-AM comprises a set of techniques based on the controlled extrusion through a nozzle of a polymer kept at a temperature above its T_g [203-206]. The raw polymeric material can be in the form of a continuous filament, pellets, or powder, depending of the technological solution adopted. The computer-controlled motion of the extrusion head and/or the construction platform allows the deposition of the extruded polymer following a predefined pattern. After the fabrication of each layer, the distance between the extrusion head and the platform increases of a given distance corresponding to that of the designed layer thickness, to obtain a 3D object with a layer-by-layer process.

FDM or fused filament fabrication, the oldest and most diffuse ME-AM technique, is based on the extrusion of a polymeric filament through a heated nozzle (**Figure 2d**). In the case of a complex geometry of the object to be manufactured, two independent extrusion nozzles can be used to simultaneously deposit a support material and fabricate the 3D object. Other AM techniques involving the thermal processing of polymeric materials as powder or pellets are based on different principles of control over molten polymer flow (i.e., pressurized nozzle, force-controlled plunger, or rotating screw), namely 3D fiber deposition [205], precision extrusion deposition (PED)[204], and bioextrusion [207]. The main advantages brought by these approaches are that they do not require polymer pre-processing into a filament, as they offer the possibility of directly developing composite or blend scaffolds by simply feeding a mixture of the components to the machine. On the other hand, the optimization of the fabrication process is often more difficult than in the case of FDM, and a higher temperature and/or a longer residence at high temperature is required to achieve a uniform extrusion.

A number of articles have reported on the integration of ME-AM with electrospinning at a fabrication level in order to develop multi-scale structures by imparting nanoscale features to macroporous scaffolds [112, 207-209]. This approach couples the 3D shape and mechanical stability of macrostructured scaffolds by AM with the enhanced material/cells interaction of micro/nanosized electrospun fibers. In this way, the hierarchically-organized architecture found in native tissues can be recreated to offer greater surface area for proteins absorption and more binding sites to cell membrane receptors [11]. Cutting edge advancements on technological integration of AM with melt electrospinning recently led to the development of a hybrid technique, that is, melt electrospinning in a direct writing way or melt electrospinning writing (MEW) enabling the fabrication of 3D scaffolds with high resolution of the architectural

features [210]. MEW relies on the deposition of a stable electrified molten jet onto a collector translating at a speed (~1 m min^{-1}) approaching that of the jet [71, 211]. The distance between the spinneret and the collector is typically below 5 cm. Advanced MEW approaches lately resulted in the development of 3D layered polymeric scaffolds composed by axially-aligned submicrometric fibers [212]. In addition, different studies have been carried out to endow a polymeric scaffold with a dual-scale porous structure by a sequential combination of ME-AM and either gas foaming [114, 213] or salt leaching [113].

As it will be described in section 4.2, ME-AM techniques have been extensively investigated for the development of bone scaffolds based on aliphatic polyesters, such as PCL [214], PDLLA [215], and PLGA [215, 216] that were thoroughly characterized both *in vitro* and *in vivo*. In particular, successful clinical trials indicate that PCL implants fabricated by means of FDM meet all the requirements needed to receive approval for use in clinical bone reconstruction [20]. Although the majority of scaffolds by ME-AM have been designed for hard TE, a consistent body of literature has been also dedicated to scaffolds for regenerating cartilage and other soft tissues [217, 218].

Materials design and processing requirements. ME-AM is generally based on polymer melt/softening and crystallization/solidification to shape the material in the desired form. The polymeric material is processed at a temperature above its T_g, and above its melting temperature (T_m) in the case of semicrystalline polymers. As a direct consequence, polymers intended for this application should meet some basic requirements such as suitable viscoelastic properties and good thermal stability at the processing conditions. For this reason, thermoplastic polymers that hold a long history of industrial melt processing have been rapidly implemented in ME-AM.

The polymer molecular structure and the resulting inter- and intramolecular interactions determine the polymer T_g and chain stiffness, which together with polymer Mw and polydispersity index affect its rheological properties in the rubbery/melt state. In the case of FDM, filament viscoelastic properties are also fundamental for successful material processing. A too stiff filament will not permit winding onto spools, a brittle filament can snap, and a soft filament can be squeezed between the driving gears, in any case compromising polymer feeding [219]. Most of the commercial FDM machines on the market require a filament diameter of 1.75 or 2.85 mm. In the case of home-made filaments, dimensional consistency (e.g., 1.75±0.05 mm) should be assured in order to have a constant feed rate during fabrication.

Common feedstock materials for FDM include amorphous thermoplastics, such as ABS. Extending FDM technology to semicrystalline polymers has been more challenging due to

warpage of the deposited part, often occurring as a consequence of crystallization during cooling [220]. Indeed, polymer chains drawing to form more dense, crystalline regions results in shrinkage of the printed object that can warp and become detached from the build platform, reducing its final quality. Anyhow, residual stresses and part warpage can be consequences of thermal gradients within FDM-manufactured objects made of either amorphous or semicrystalline polymers. Manufacturing in a heated chamber often represents a successful means to reduce thermal gradients within the printed material. Loading the polymeric matrix with fillers characterized by high thermal conductivity (e.g., carbon fibers) has been also employed to vary material thermal expansion coefficient. This approach has been found to reduce distortion or warpage effects, die swell, and to influence polymer crystallization rate and crystallinity [220, 221].

The key to achieve high mechanical strength of the final printed part is a successful interdiffusion and re-entanglement of the polymer chains across filament-filament interfaces, as the melt rapidly cools towards its T_g [222]. Interface polymer welding is affected by the macromolecular structure and morphology (i.e., amorphous or semicrystalline) and by different processing parameters, such as the deposition speed, extrusion temperature and environmental temperature. Indeed, thermally-driven filaments welding is affected by polymer chains alignment under extrusion shear forces as well as by post-extrusion anisotropic stresses acting on polymer melt during its deposition. Thermostatically-controlled printing chamber and deposition platform are technological solutions effective to control the non-isothermal polymer chain diffusive process during FDM. While molecularly-aware models and experimental investigations of this aspect have been reported for amorphous polymers [222-224] there is still a gap in literature addressing tools to predict deformation and welding behavior of semi-crystalline melts in FDM.

PLLA is the most used semicrystalline polymer for FDM filaments thanks to its T_m low enough to carry out melt extrusion outside of a dedicated facility and, at the same time, high enough for manufacturing objects that retain their shape at average use temperatures. However, PLLA has been found to partially degrade during thermal processing, particularly when a long residence at high temperatures is required like in the case of pneumatic direct extrusion-based systems [225]. Although FDM allows minimizing the thermal residence time in comparison to other melt extrusion techniques, polymer processing for filament preparation can anyhow involve thermal degradation. In addition, commercial PLA filaments may contain inorganic additives that could react during processing causing changes in polymer macromolecular structure and morphology [226]. Careful drying to remove residual water that can induce melt

hydrolytic degradation, purging with inert gas during extrusion, and thermal stabilizing additives are precautions recommended whenever this risk exists [227]. PCL has also received great interest as biomedical polymer for FDM due to its superior rheological and viscoelastic properties over many of its resorbable-polymer counterparts, which render it easy to manufacture and manipulate into complex macroshapes and microstructures [228]. Although this class of AM techniques is not the election one for fabricating drug-loaded devices, a number of polymers of common use in pharmaceutical formulation, including PCL, PLLA, PVA, poly(ethylene glycol) (PEG), cellulose derivatives, ethylene vinyl acetate, and poly(vinyl pyrrolidone) (PVP) have been evaluated for this application [229, 230]. In addition, a range of biostable biomedical polymers including PEEK, poly(ether ketone ketone), poly(ether imide), polysulfone, ABS, and PMMA are commercially available as filaments for FDM.

3.5 Solution Extrusion-AM (SE-AM)

SE-AM represents the most versatile and employed processing approach to plot hydrogel scaffolds [231], possibly laden with cells or cells aggregates (see section 3.6). In addition, the possibility of avoiding material thermal treatment as well as developing advanced structural and pharmacological functionalization strategies widens the range of applications of SE-AM by including hydrophobic polyesters processing [7].

This class of AM techniques is based on the controlled extrusion through a nozzle of a polymeric solution or suspension by means of a pneumatic or mechanically-driven dispensing system (**Figure 2e**). The extruded material is generally deposited in the form of a continuous filament following a pattern defined by the motion of the extrusion head and/or the building plane. Polymer solidification/gelation can be achieved by means of different mechanisms, including among others: drying through solvent casting [232], physical coagulation in a non-solvent bath [26], ionotropic gelation [233], chemical cross-linking [234], photocrosslinking under UV light [235], and polyelectrolytes complexation [236].

Mechanically-driven dispensing systems rely either on a piston or a rotating screw. The piston-based approach generally results in better control of material feeding rate in comparison with *i*) pneumatically-driven systems in which a delay related to gas volume compression can occur, *ii*) screw-driven systems which are generally indicated only for viscous materials due to the high shear stresses involved. Technological solutions based on arrays of nozzles that can deposit multiple filaments were recently designed to fabricate thick samples in short time [237].

Typical resolution achievable with these techniques is on the scale of hundreds of microns in the case of hydrogels, and can be pushed down to tens of microns by employing aliphatic polyesters [238, 239]. However, the recent application of the layer-by-layer stacking principle

to solution electrospinning, is fastening the translation of AM resolution to a viable micro/nanoscale [240]. Indeed, advanced technological approaches commonly referred to as electrofluidodynamic printing (EFDP) or near-field electrospinning, comprising tailored processing conditions (e.g., short working distance, high translation speed of the fiber collector, low voltage, and high-precision solution feeding) allows enhanced control over high-resolution polymer patterns whose large surface area can be exploited for instance to provide nano/microstructural instructive cues to cells [241-247]. In addition, in this way it is possible to implement AM with the great versatility of electrospinning in terms of drug loading approach and control over drug release kinetics [248]. Similarly, research on the integration of AM with electrofluidodynamic techniques for particles fabrication is aimed at the controlled deposition of assembled polymer particles structures possibly encapsulating cells [249].

SE-AM avoids the shortcomings associated with high temperature processing, particularly the risk of materials thermal degradation. Other relevant advantages include the possibility of processing natural polymers into 3D hydrogels with a controlled shape and porosity, loading the polymeric device with a bioactive agent through direct blending methods, carrying out proof of concept studies with few amounts of polymer (e.g., less than 1 gram), obtaining a dual-scale porosity through integration with other processing techniques [10]. Indeed, hybrid AM techniques integrated at a fabrication level with either wet-spinning [7] or freeze drying [250] enable the combination of an interconnected network of macropores determined by the designed lay-down pattern, with a microporosity in the polymeric matrix that can be pushed down in some cases to the nanometer scale [31]. In particular, the local microporosity can be obtained by extruding an organic solution of a synthetic [26, 251, 252] or natural [238, 253, 254] aliphatic polyester into an ethanol bath, or through the cryogenic extrusion of a polysaccharide [115, 250], polyester [255, 256] or protein [257] solution followed by lyophilization. The size and concentration of the resulting micropores can be tuned in a certain range, particularly in the case of computer-aided wet-spinning (CAWS) by acting on processing and post-processing parameters, in order to tune specific material properties depending on porosity (e.g., biodegradation rate, material/cell interaction and release of loaded drugs). On the other hand, it should be considered that the generation of a microporosity leads to a lower material stiffness as a consequence of the increased specific void volume.

Major shortcomings of this class of techniques are related to the employment of organic solvents with their inherent environmental and industrial impact. In addition, there are risks associated to residual solvents which, if not completely removed, may compromise the biocompatibility of the device, besides altering bioactive factors loaded in the polymer matrix.

However, proper post-processing protocols based on vacuum treatment, washing and drying are effective in completely eliminating organic solvents from polymeric devices [31, 258].

Materials design and processing requirements. As a consequence of the great variety of physical-chemical approaches included in this class of techniques, peculiar materials processing requirements need to be defined depending on the different solidification/gelation mechanisms adopted.

Different technological designs based on extrusion in air have been developed to plot a broad range of materials including solutions of linear or highly branched polymers, acrylic dispersions, inorganic solutions, and inorganic pastes combined with polymeric binders that are then sacrificed by sintering the green part [8]. Particularly referring to biodegradable polymers, tailored SE-AM approaches were optimized to process synthetic aliphatic polyesters [256, 259-261] and/or polysaccharides [115] through their extrusion and controlled deposition in air. An organic solvent that evaporates upon printing eventually resulting in material solidification is typically employed when a hydrophobic polymer is processed. If the solvent vapor pressure is too high or too low, processing shortcomings, such as needle clogging, layered structure distortion or fusion, and unwanted porosity defects can occur upon extrusion [262]. The polymer concentration should be tuned in order to have solution viscosity and surface tension suitable for maintaining the 3D shape of the polymer strand after its deposition. A too high viscosity can hinder a continuous solution feeding, besides causing a too fast solidification of the polymer [260]. Samples with limited thickness are typically obtained by extrusion in air due to the aforementioned constrains on solvent and polymer concentration selection. In the case of integration of SE-AM with freeze drying, a solvent with a relatively high melting point (e.g., 1,4 dioxane for hydrophobic polymers, and water for hydrophilic polymers) is necessary to optimize the lyophilization process [255]. Once the aforementioned polymer solution variables have been fixed, a set of deposition and environmental parameters, including deposition velocity, solution feed rate, and environment temperature, need to be optimized. In the case of EFDP approaches, the basic electrospinning requirements related to solution, electric field and environment variables, analyzed in depth by a vast literature [263, 264], should be specifically considered in relationship to the peculiar technological solutions adopted. For instance, the reduced jet travelling distance related to the short working gap typically employed in EFDP (e.g., 500 μm to 3 mm to have a stable cone-jet mode) [240] should be taken into account to select a solvent with a suitable volatility.

AM approaches relying on polymer solution physical coagulation in a liquid medium are typically based on a non-solvent-induced phase separation (NIPS). Any hydrophobic or

hydrophilic polymer suitable to be processed by wet-spinning for fibers production can be in theory processed by CAWS [7]. High solvent/non-solvent miscibility is a fundamental requirement for NIPS to take place since it is based on polymer desolvation caused by solvent–non-solvent counter-diffusion. In addition, by employing a polymer concentration higher than a critical threshold, the polymer solution can separate into a polymer-lean phase dispersed in a continuous polymer-rich phase, resulting in the formation of a microporous matrix after polymer solidification. Different variables such as polymer concentration, coagulation bath temperature and composition, and deposition parameters (e.g., deposition velocity and solution feed rate) affect thermodynamics and/or kinetics conditions of the NIPS process and, as consequence, can be exploited to tune the macro- and micromorphology of the resulting construct [7]. Warping effects are often observed both for amorphous (e.g., PMMA) [31] and semicrystalline (e.g., PHBHHx) [238] polymers due to free volume variations during coagulation. Variation of processing parameters (e.g., warming up the coagulation bath) and post-processing treatments (e.g., slow drying) can be effective in minimizing residual coagulation stresses in the layered structure. CAWS has been widely investigated to process a range of polyesters either synthetic [26, 105, 251, 252] or derived from natural resources [238, 239, 253, 254, 258], as well as polyelectrolyte complexes of chitosan and poly(γ-glutamic acid) [34, 236].

Besides complexation of polyelectrolytes, various specific crosslinking strategies can be pursued to confer additive manufactured hydrogels with the physical stability necessary to maintain a 3D porous structure and shape. The ability of different natural polymers to undergo physical crosslinking upon extrusion in a liquid medium, through straightforward mechanisms (e.g., temperature-dependent physical gelation of gelatin [265] and ionotropic gelation of alginate in the presence of divalent cations [266]) can be exploited for AM. However, chemical crosslinking is often required to achieve acceptable morphology control and reproducibility. Indeed, as consequence of their poor mechanical properties and hydrophilic behavior, in most of the cases natural hydrogels cannot maintain a filament shape for the required time and eventually collapse under the weight of upper layers during fabrication.

Different chemistries have been proposed for hydrogel crosslinking, such as photoinitiated reactions giving good temporal and spatial control with various naturally-derived macromolecules [124, 267]. Once grafted onto the functional residues of the polymer chain, photoactive moieties can induce the formation of covalent crosslinks when exposed to a specific wavelength of light in the presence of a photoinitiator. In particular, free radical polymerization of acrylate derivatives of proteins and polysaccharides has been widely investigated to design

novel photoreactive inks also suitable for fabricating cell-laden constructs [268, 269]. Synthetic polymers are also investigated for AM of biomedical hydrogels with enhanced processing and mechanical properties. For instance, Liu and Li [270, 271] recently developed a novel strategy based on UV exposure of an extruded pre-gel solution to form a polymeric double network hydrogel composed of covalently crosslinked polyacrylamide and ionically crosslinked k-carrageenan. In any case, concerns about the non-degradability of the backbones resulting from free-radical chain-growth crosslinking as well as the biocompatibility of the preparation process are often raised [272].

Photoinitiated thiol-ene chemistry has been recently implemented in AM as an alternative crosslinking strategy for natural polymers [268, 273]. It is based on dimerization of thiols with reactive carbon–carbon double bonds. In this case the polymerization follows a step-growth radical mechanism resulting in high conversion of functional groups and low polymerization shrinkage. In comparison to free radical polymerized diacrylates, a lower radical initiator concentration is required, the reaction kinetics is generally more rapid, and the photoinitiated thiol-ene can form more homogeneous hydrogel networks [274, 275]. In addition, biodegradable and bioactive molecules containing thiols can be straightforwardly conjugated to the network as pendant groups or crosslinking bridges. Examples of hydrogels fabrication based on thiolated natural (e.g., alginate [274] and gelatin [273]) or synthetic polymers, e.g., poly(glycidol) [276], are reported in studies focused on AM combined with UV exposure.

Hydrogel solutions usually behave as a non-Newtonian shear thinning fluid, whereby an increase in shear rate leads to a decrease in shear viscosity as consequence of chains disentanglement related to attenuation of molecular interactions [277]. Functionalization of proteins and polysaccharides through acrylate derivatization of pendant groups can lead to variation in their solution rheological properties. This is often the case of GelMA showing increased viscosity in comparison to the native polypeptide as a consequence of the increase in lysine side chain length, resulting in increased chains entanglement and intermolecular interactions [278]. Such rheological modifications can on one side help in stabilizing the extruded filament and on the other cause experimental issues such as needle blockage or discontinuous extrusion.

An effective strategy to process hydrogels with low elastic modulus and avoid their collapse is printing and embedding the material within a second hydrogel support bath.[279] Indeed, by selecting a medium with a density close to that of the printing material, it is possible to achieve low-gravity conditions in which soft hydrogels can easily maintain the intended 3D geometry.

3.6 Bioprinting

Bioprinting, also referred to as organ printing, enables patterning and precisely placing biologics, including living cells, nucleic acids, drug particles, proteins and growth factors, to recapitulate tissue anatomy, biology and physiology. The tremendous scientific, diagnostic and therapeutic potential of bioprinting technologies is witnessed by relevant fast-growing literature, together with the marketing of bioprinters and bioprinted tissues for different applications, ranging from TE and *in vitro* modelling to pharmaceutics and high-throughput screening [280]. Bioprinting is based on the ejection from a reservoir of a bioink composed by living cells or cells aggregates suspended in a medium, possibly in combination with biomaterials and bioactive molecules [281]. The different bioprinting techniques applied within the scientific community can be classified on the basis of the mechanism adopted to control the deposition. In particular, extrusion, inkjet and laser-assisted bioprinting are the most employed ones (**Figure 2f**). Analogous attempts of photopatterning cells-encapsulating hydrogels by means of SLA have been reported [282]. In this case, Vis light-based systems are also investigated in order to prevent cells damage related to UV light irradiation [124].

Extrusion bioprinting is based on pneumatically- or mechanically-controlled extrusion of the bioink through a nozzle, as described in the previous section. Pneumatic and piston-based dispensing systems are commonly used to achieve high cell viability, rather than screw-driven dispensing that generates larger pressure drops at the nozzle with potential harm to cells [231]. Multiple-nozzle extrusion systems have been also developed to process and combine different hydrogel materials into a sophisticated living construct and exploit advanced crosslinking strategies. For instance, two-nozzle systems were employed to develop double-hydrogel crosslinking strategies (e.g., ionotropic and enzymatic crosslinking) [283-286], and to combine natural and synthetic polymers with different processing requirements into a hybrid scaffold [287-289]. Extrusion bioprinting processes can rely on hydrogel shear-thinning properties, physically/chemically-triggered gelation inside a liquid bath, extrusion inside a pseudoplastic or granular bath, or simultaneous dispensing of a bioink and a crosslinking agent using co-axial needles assemblies [290].

Inkjet bioprinting involves ejecting a bioink from a nozzle in the form of droplets (~10-50 μm in diameter) to a building surface [291]. The bioink is forced through the nozzle under the action of a pressure commonly generated by either a piezoelectric actuator or a thermal element that superheats the ink and creates an expanding vapor bubble. Alternative technological solutions are based on electromagnetic pin actuators, or interdigitated gold rings generating acoustic waves. The bioink is typically composed by a suspension of cells in a solution of a polymer that

is either physically or chemically crosslinked upon deposition. Other strategies involve ejecting cells suspended in a solution of a crosslinking agent (e.g., $CaCl_2$ or thrombin) over a biopaper substrate (e.g., alginate or fibrinogen) which is crosslinked upon bioink deposition [292, 293]. Laser-based bioprinting involves coating a bionk layer with a laser-absorption layer (e.g., titanium oxide or gold) which is fixed to an optically-transparent support (e.g., glass). Laser pulses are focused through the glass side into the absorbing layer which heats either evaporating or decomposing a small portion of the hydrogel in contact with it [294-296]. The generated high-pressure bubble propels a small droplet of bioink towards a building stage through an orifice-free process.

A vast literature is focused on the development of bioinks for the aforementioned techniques, based on either natural polymers and their derivatives (e.g., gelatin [124] and collagen [297]) or synthetic polymers (e.g., PEG [298], pluronic [299], and PVP [300]). They have been combined with a wide array of cells for the engineering and *in vitro* modelling of health and pathological tissues such as bone, cartilage, cardiac tissue, nerves, and lung tissue, as well as ovarian and cervical cancer [280].

The main advantages of these techniques are related to the possibility of directly fabricating customized living tissue engineered constructs with timely and spatially-controlled deposition of cells and other biologics. This allows the development of controlled biomimetic microenvironments by exploiting the self-organizing properties of cells and tissues. Currently, the applicative potential of bioprinting is mainly related to *in vitro* applications rather than surgical approaches. Indeed, before bioprinted organs are ready to be transplanted into humans, several important ethical concerns and regulatory issues need to be addressed [301]. Aspects like risks of significant harm associated with human testing, lack of a specific regulatory framework, combined with ethical questions of irreversibility, loss of treatment opportunity, and replicability still represent restrictions to bioprinting for humans.

Materials design and processing requirements. The strict processing requirements related to printing living materials through a mild and cell-friendly process, greatly limit the range of technological solutions and materials for bioprinting [291, 302]. FDM and SLS do not meet bioprinting requirements since high temperature processing conditions are unsuitable for cell viability. As previously mentioned, a few attempts on SLA-based bioprinting have been made. Although Vis light employment allows preventing UV-related cell DNA damages, concerns related to cytotoxic photoinitiators, photoreactive oligomers, and crosslinking agents still exist. For these reasons, extrusion and inkjet bioprinting are the most exploited techniques along with a number of studies showing that laser-assisted bioprinting can be suitably employed to print

cell-laden hydrogels. As it will be discussed in detail throughout the whole paper, various natural polymers, including proteins and polysaccharides from different sources, have been successfully employed in combination with crosslinking agents, cells, growth factors and other proteins to develop bioinks designed for bioprinting.

Bioink properties are generally tailored to meet the peculiar technological requirements and constrains of a selected fabrication technique. In general, a non-Newtonian shear thinning behavior is fundamental for extrusion and inkjet bioprinting of cell-laden hydrogels in order to achieve high print fidelity and cells viability [303, 304]. In any case, bioink viscosity is a crucial parameter that needs to be optimized considering that highly viscous polymer solutions on one side can hold the deposited shape for long time with high print fidelity, on the other side they require higher pressure to be processed resulting in higher stresses acting on cells and obvious limitations on gauge size and print resolution. This issue becomes relevant in the case of inkjet bioprinting that involves relatively high shear rates (10^5-10^6 s^{-1}), while in the case of extrusion bioprinting the processing viscosity window is much wider. Reference bioink viscosity ranges are 1-10 mPas for inkjet bioprinting, 30 to 6 x 10^7 mPas for extrusion bioprinting, and 1–300 mPas for laser-assisted bioprinting [291].

Another relevant limitation is on cell density which is typically maintained lower than 10^6 cells·mL^{-1} to avoid constrains such as cell settling and sedimentation, nozzle clogging, droplet spreading, and worsened resolution [305]. Concerns about the deleterious effects on cells viability of high temperatures (~300 °C) generated in thermal inkjet have been overcome by modern technologies in which thermal heating lasts few microseconds (~2 µs) [306]. In laser-assisted bioprinting the volume of the transferred material as consequence of laser pulse absorption is a function of the laser energy and spot size, biomaterial composition, and coating thickness [294]. In general, only the small fraction of the bioink in the immediate vicinity of the absorbent layer is volatilized and the bulk biomaterial undergoes only little to no heating.

The hydrogel molecular design strategies outlined in section 3.5 should take into account constraints related to the use of cells in the case of bioprinting. Many approaches exploit the capability of different natural polymers to form physically-stable hydrogels under mild conditions, such as in the case of ionotropic gelation of alginate or enzymatic crosslinking of fibrinogen. As previously discussed, photoinitiated radical chain polymerization of acrylate derivatives and step-growth thiol-ene reaction are the most exploited strategies to chemical crosslink cell-laden hydrogels during extrusion or after deposition, as well as for direct SLA biopatterning. Advanced approaches rely also on combined photoreactive acrylate and thiol-ene chemistries to develop complex living constructs starting from bioinks with low viscosity

[268]. In any case, a good compromise among physical printability related to bioink rheology, mechanical stability given by polymer crosslinking, and biological functionality as a result of cells viability and migration in the polymer network, is a challenging bioprinting aspect. Representative examples of efforts spent on this topic are studies on bioprinted GelMA optimized through two-step thermo/photo-crosslinking strategies [269] or new Vis light photoinitiating approaches [307].

As it will be described in detail in section 4, various proteins including collagen, gelatin, fibrin and silk fibroin, and polysaccharides including alginate, cellulose, chitosan and agarose, have been widely investigated for bioprinting resulting in the development of a large number of bioink formulations currently under investigation or on the biomaterials market. Multiple polymers bioinks (e.g., alginate with gelatin/fibrin, cellulose with alginate) have been often employed to meet different processing, mechanical, and functional requirements necessary to develop biomimetic tissue-like constructs [308].

4 Biodegradable Polymeric Biomaterials for AM

The most widely investigated polymeric materials for AM biomedical applications are those susceptible to be degraded in physiological environments. As previously discussed, this is justified by the tremendous advantages of AM over other materials processing techniques in controlling key compositional, structural, and functional parameters of polymeric systems designed for TE and other advanced biomedical applications.

The following sections are dedicated to an overview of the most exploited classes of polymers in this context, obtained from natural sources or through synthetic routes. Critical aspects regarding their extraction or synthesis, purification, and physical-chemical modification to make them processable by means of specific AM techniques are highlighted. Cutting edge advancements on their development into functional biomaterials are outlined by discussing representative articles focused on relevant key aspects.

4.1 Polymers from Natural Sources

After the oil crisis in the seventies, the use of polymers that could be obtained from renewable resources and eventually susceptible of degradation in the environment was seriously considered as a reliable industrial alternative in agreement with the increasing awareness of ecological issues. The parallel growing interest on regenerative therapeutic approaches, as well as on controlled and targeted pharmacological strategies involving the employment of biodegradable materials has further encouraged research on polymers derived from natural sources. Specifically referring to biomedical applications, natural polymers offer different

advantages over their synthetic counterparts, generally including intrinsic biological signaling, surface chemistry promoting cell adhesion, and cell-responsive degradation and remodeling. In addition, the pendant functional groups present in the repeating units of proteins and polysaccharides provide many options for chemical derivatization tailored to bioactive functionalization [309].

One of the most challenging aspects involved in the biomedical application of naturally-derived polymers regards their shaping into a given geometry and a porous architecture that can be maintained for predefined time under physiological, aqueous conditions. For this reason, a large body of literature has been dedicated to physical-chemical modification of natural materials aimed at their processing into devices with adequate physical properties. An appealing aspect of many natural polymers is the possibility of forming biocompatible hydrogels providing a highly hydrated 3D environment for the cells. Additive manufactured hydrogels made from proteins (e.g., collagen and gelatin) or polysaccharides (e.g., alginate and chitosan) are commonly employed for TE and other biomedical applications. As it will be discussed in depth in the following sections, the huge progress made by biomaterials researchers has enabled the successful application of different AM approaches to naturally-derived polymers, including SLA of photocrosslinkable derivatives of proteins and polysaccharides, BJ of hydrogels using water as a binding agent, and extrusion of hydrogel-forming aqueous solutions. Indirect AM has been also proposed as an effective tool for the production of self-supporting porous hydrogels with a predefined shape. For instance, Van Hoorick *et al*. [310] employed an additive manufactured sacrificial polyester scaffold that was selectively dissolved after UV crosslinking of the infiltrated hydrogel phase.

As previously introduced, natural polymers are more challenging to build into scaffolds by AM in comparison to synthetic polymers, and generally result in poor resolution, particularly along the print (build) direction. However, cutting edge advancements on hydrogels physical-chemical tailoring are showing the possibility of integrating an enhanced fabrication reproducibility and resolution with the superior biocompatibility and bioactivity of natural polymers. In addition, the recent application of AM to microbial polyesters [311] is leading to the development of the next generation of load-bearing scaffolds with physical and mechanical properties comparable to those of synthetic aliphatic polyesters, but complying with the concept of sustainable development.

The most investigated proteins, polysaccharides and microbial polyesters in this field are following described by highlighting the different strategies developed to optimize their AM processing into biocompatible and biofunctional devices (**Table 1**). Although also other

naturally-derived macromolecules are employed as blend components for AM due to their biomechanical (e.g., elastin [312]) and gelation properties (e.g., agarose [313]) this review specifically focuses on those polymers that have been giving the most promising results as main material constituent.

Table 1. Naturally-derived biomedical polymers for AM.

Polymer	AM technique	Processing conditions and material design
Collagen	SE-AM (bioprinting)	- Extrusion and stabilization of collagen solutions through: cryogenic plotting [257, 314], *in situ* crosslinking [315], hybrid inks (e.g., fibrin/alginate–collagen) [316, 317], high density collagen dispersions at controlled pH [318, 319], heated printing chamber [297].
	BJ	- Collagen dissolved into the binder solution plotted onto a ceramic bed [320].
Gelatin	SE-AM (bioprinting)	- Extrusion of: a warm solution containing gelatin into a cold environment and stabilized through chemical crosslinking [234], enzymatic crosslinking [321] or combination with other natural polymers (e.g., alginate [322, 323], fibrinogen [24], chitosan [324] and HA [325]) suitable to be more stably crosslinked; a solution of GelMA followed by post-processing UV crosslinking [124, 235, 307]; a solution of norbornene-modified gelatin solutions followed by photocrosslinking [273, 326, 327];
	SLA	- Photocrosslinking of: GelMA [19, 31-33]; a thiol–ene clickable derivative (e.g., allylated gelatin) [273].
Fibrin	Bioprinting	- Controlled deposition of a thrombin solution containing cells or growth factors onto a fibrinogen substrate used as a biopaper [293, 328, 329]. - Mixing fibrinogen/thrombin at low temperature in a dual-chamber single nozzle extrusion system just before their deposition [330]. - Controlled deposition of a solution containing fibrinogen and other hydrogel-forming materials (e.g., gelatin and HA) followed by enzymatic crosslinking [331-333].
Silk fibroin	SE-AM (bioprinting)	- Controlled deposition of aqueous solutions of fibroin: stabilization with glycerol [334], blending with other natural polymers acting as (sacrificial) bulking agent amenable to be physically [335-337] or enzymatically [338] crosslinked.
	SLA	- Photocrosslinking of methacrylate derivatives of fibroin [339].
Chitosan	SE-AM	- Acetic acid solution of chitosan: NaOH pipetting on deposited fiber [340]; extrusion into a coagulation bath [341, 342]; optimizing acid solution composition (acetic acid/lactic acid/citric acid) followed by post-processing NaOH immersion [343, 344]; cryogenic deposition followed by lyophilization/gelation [345-347]. - Polyelectrolyte complexation: extrusion of a PEC suspension into ethanol [34, 236]; extrusion of a chitosan suspension in an alginate solution and post-processing pipetting of HCl [348].
	SLA	- Combination with photocrosslinkable polymers (e.g., PEGDA) [153].
Alginate	SE-AM (bioprinting)	- Extrusion of: an (cell laden) aqueous solution of alginate stabilized through submerged crosslinking [233, 349-353] or aerosol spraying [354]; norbornene functionalized alginate and UV-induced thiol-ene crosslinking [274].
	SLA	- Photoreticolation of alginate derivatives with pendant phenolic hydroxyl groups [267].
Cellulose	SE-AM (bioprinting)	- Extrusion of aqueous solutions/suspensions containing cellulose: blending with physically-crosslinkable polymers (e.g., alginate [353, 355-358]), coagulation by means of a non-solvent [359], chemical crosslinking [360, 361], extrusion of cellulose acetate dissolvent in a highly volatile solvent followed by cellulose regeneration [362] .
	ME-AM	- Cellulose fillers (e.g., nanocrystals, fibers and wood flour) for thermoplastic polymers (e.g., PLLA, PCL or PVA) [363].
	SLA	- Cellulose nanofillers for stereolithographic resins [364, 365].
Hyaluronic acid	SE-AM (bioprinting)	- Extrusion followed by photoreticolation of: HA solutions containing photocrosslinkable hydrogels (e.g., GelMA [366] and hydroxyethyl-methacrylate-derivatized dextran [367]); HAMA formulations containing other polymers (e.g., Gel-MA [368] and poly(N-isopropylacrylamide)-grafted HA [369]); HAMA modified with moieties giving supramolecular assembly [303, 370]; thiolated HA formulation containing a suitable crosslinker [371-373].
	SLA (bioprinting)	- Photoreticolation of HAMA-based formulations possibly containing cells and other photocrosslinkable polymers [117, 374].
PHA	SLS	- Sintering of: PHB powder [375-377]; Ca-P-loaded PHBV microspheres [179-181].

	ME-AM	- FDM of filaments made of PCL/PHBV blend [378] or PHB/PLA blend containing a plasticizer [379].
	SE-AM	- CAWS extrusion into an ethanol bath of a PHBHHx-based solution in chloroform or THF [238, 239, 253, 258], or a PHBHHx/chloroform/ethanol mixture [254].

4.1.1 Proteins

The rich landscape of proteins as a result of biological evolution offers a variety of genetically encoded structures and properties spanning many length scales. Indeed, the proteins repetitive nature facilitates the formation of long-range ordered molecular secondary structures capable to self-assemble into complex 3D hierarchical architectures characterized by peculiar mechanical, chemical, electrical, electromagnetic, and optical properties [380]. As a consequence of the aforementioned advantages, various proteins (e.g., collagen, gelatin, silk fibroin, and keratin) have been investigated for biomedical applications resulting in commercial products introduced in the surgical routine.

Because of their poor thermal stability, AM of proteins mostly relies on extrusion of aqueous solutions or suspensions. Proteins physical stabilization in physiological environments is achieved by exploiting their inherent gelation properties and/or applying physical-chemical crosslinking. The high cell affinity of proteins is particularly exploited in bioprinting approaches. Indeed, as discussed in Section 3.6, most of the bioinks for AM are based on collagen, gelatin, and/or fibrin (**Figure 3**). Chemical modification of proteins, as witnessed by the large body of literature on gelatin derivatives, has been also investigated as a means to endow protein with photocrosslinkable moieties exploitable for SLA or photocrosslinking of extruded polymers.

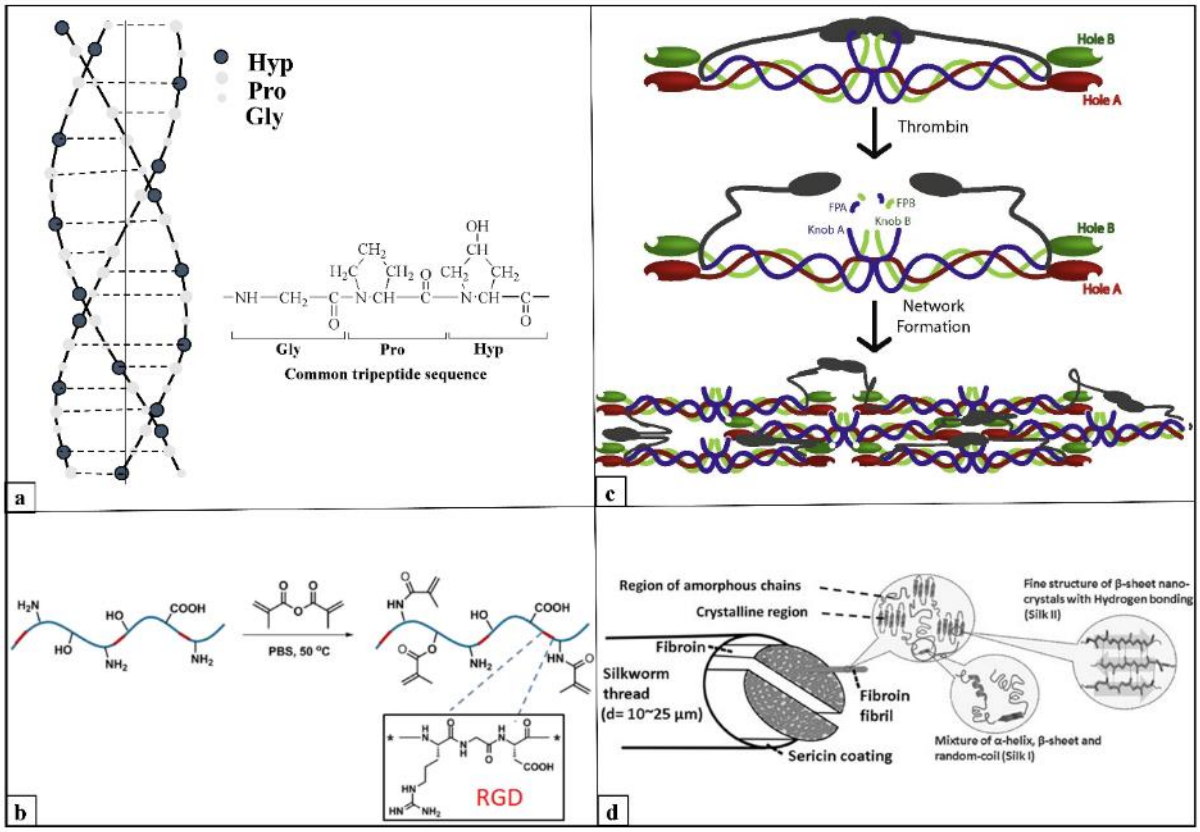

Figure 3. Structure of proteins commonly employed in biomedical AM. (a) Triple chain structure of collagen fibrils and chemical structure of the most common tripeptide sequence found in collagen, composed of glycine (Gly), proline (Pro) and hydroxyproline (Hyp) sequences (reproduced with permission [66]). (b) Scheme for the preparation of photocrosslinked GelMA through reaction of gelatin and methacrylic anhydride for grafting methacryloyl substitution groups (RGD domains illustrated as red segments, and their chemical structure is depicted within the inset) (reproduced with permission [381]). (c) Fibrin polymerization (α chains shown in blue, β chains in green, and γ chains in red; αC domains are in gray) (reproduced with permission [382]). (d) Schematic of silk fibroin structure (insets showing the fibril overall structure and the fine β-sheet antiparallel alignment of polypeptide chains) (reproduced with permission [383]).

4.1.1.1 Collagen

Collagen biodegradability, relatively low antigenicity, cell-binding properties, and peculiar biomechanical behavior have attracted great interest for different biomedical applications ranging from dermal dresses to TE [384].

Source of extraction. Collagen is a structural protein of native extracellular matrix (ECM) of various biological tissues, including skin, bone, cartilage, teeth, tendons, and blood vessels [231]. Types I–IV are the most common among over twenty-two types of collagen found in mammals. Collagen for biomedical applications is extracted from bovine or porcine skin, as well as from Achilles tendon of bovine or equine origin using neutral/slightly alkaline salt, acidic, alkaline, or acidic/proteolytic enzymes solutions followed by repeated salt precipitation

[385]. Engineered recombinant bacterial collagen is under investigation as a reliable and cost-effective alternative to avoid immunogenicity, infection transmission, and batch variability [386].

Physical-chemical modification. Collagen is composed of three polypeptide chains, with similar compositions at high content of glycine (Gly) (near 33%) and imino acids (near 20%), that wrap around one another with a right-handed twist forming a tightly packed triple helix (**Figure 3a**) [387, 388]. Collagen fibrils are stabilized by covalent crosslinks between amino acid residues of different chains. However, in the human body collagen undergoes degradation *via* proteolytic enzymes (e.g., collagenases) causing a fast impairment of its structural role as implant biomaterial [389]. Collagen stability in physiological environments can be increased through its combination with mineral crystals [390], or polymers of either natural (e.g., elastin and glycosaminoglycans [391], HA [392]) or synthetic (e.g., acrylates [393, 394]) origin. In addition, various chemical crosslinking strategies have been developed, to covalently bind the amine side groups of polypeptide chains. Concerns raised towards the potential toxicity of the crosslinking agents, e.g., glutaraldehyde [395], have encouraged research on alternative approaches involving chemical modification of collagen side groups to enable crosslinking by free radical polymerization [396] or via enzymatic reaction [397].

Biomedical use. Collagen in the form of sponges [398], gels [399, 400], or electrospun ultrafine fibers [401] has been widely investigated for bone and cartilage TE. In addition, a large body of literature has been focused on collagen-based materials for skin repair and blood vessel engineering to exploit its thrombogenic properties. For instance, electrospinning has been widely investigated to fabricate micro/nanostructured collagen in combination with other natural [402] or synthetic polymers [403, 404] . The tremendous progress achieved is witnessed by a number of collagen-based devices currently available in the biomedical market worldwide, such as dermal membranes and sponges for localized delivery of antibiotics (e.g., Sulmycin® Implant, Collatamp® G, Septocoll E) [405], skin engineered substitutes (e.g., Apligraft®) [406, 407], as well as hemostatic sealants made from bovine collagen either in combination or not with thrombin (e.g., Sulzer-Spine® Tech, CoStasis® Surgical Hemostat, Floseal®, Gelfoam®, UltraFoam™) [408]. Two of the first TE clinical trials involved the implantation of engineered autologous bladder [409] or vaginal organs [410] based on scaffolds made from collagen or a collagen/poly(glycolic acid) (PGA) composite.

AM application. The aforementioned advantages in terms of biocompatibility and bioactivity have been widely exploited in AM by employing collagen as main solution extrusion component, in the formulation of inks for **bioprinting**, and in **BJ** binders to fabricate collagen-

Ca-P composites [320]. The low viscosity of collagen solutions, gels, or dispersions commonly employed for biomedical purposes, and the slow gelation of collagen, are main disadvantages for direct fabrication of predesigned scaffolds [411]. Different strategies have been adopted to increase the reproducibility, geometrical accuracy, and control over structure of additive manufactured collagen. These include among others extruding directly on a cryogenic stage followed by lyophilization [257, 314], applying a crosslinking agent (e.g., aerosolized or nebulized $NaHCO_3$) during extrusion [315], extruding hybrid inks containing polymers more readily crosslinkable (e.g., fibrin and alginate) [316, 317], extruding a high density collagen dispersion at a controlled pH [318, 319], and heating the printing chamber [297] (**Figure 4a**). The plotted structures can be further stabilized by freeze-drying or chemical crosslinking. In this way the scaffold can exhibit high shape and dimensional fidelity with the designed model, being composed by fibrillar collagen strands with diameter of few hundreds of micrometers that are stable after incubation in cell culture medium.

The fast progress on AM of collagen has led to the successful free-form fabrication of complex living architectures. For instance, a proof of concept study on human skin bioprinting involved the use of keratinocytes and fibroblasts as constituent cells to reproduce the epidermis and dermis, and collagen to reproduce the dermal matrix of the skin [315]. Different bioprinting processes and bioinks are currently marketed for drug screening and *in vitro* modelling of soft and hard tissues. Some examples are the exVive3D™ Human Liver Model for drug screening [412], the BioInk™ [413], the Lifeink® 200, and the OsteoInk™ [414]. Living tissue engineered constructs based on collagen were also developed by means of indirect AM. As an example, external ear anatomical constructs with biomechanical properties recapitulating those of native auricular cartilage were fabricated by injecting a chondrocytes-containing collagen hydrogel in an ABS mold fabricated by FDM [416].

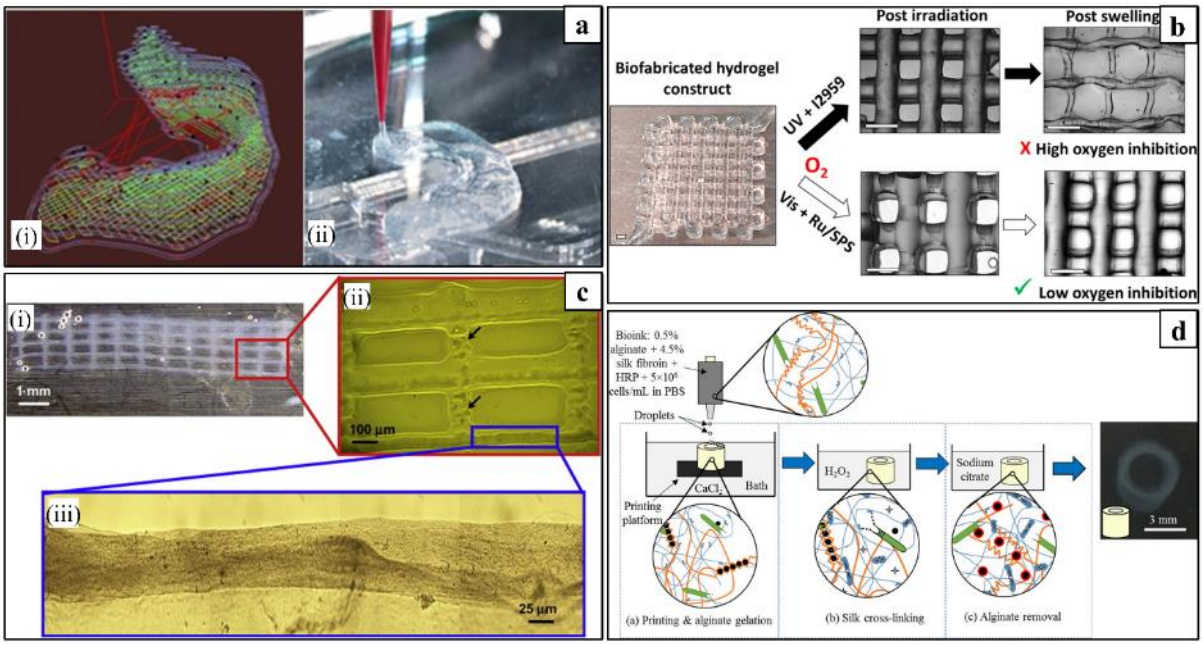

Figure 4. AM of proteins. (a) Digital model of print path (i) and printed collagen hydrogel (ii) developed starting from a CT scan of sheep meniscus (reproduced with permission [297]). (b) Gel-MA-based hydrogel constructs fabricated by extrusion followed by either UV- or Vis-light photoreticolation (reproduced with permission [307]). (c) Representative images of hydrogels by inkjet printing of a suspension of human microvascular endothelial cells in a thrombin solution onto a fibrinogen substrate, showing a printed grid (i), minor defects (ii) and fiber alignment (iii) (reproduced with permission [328]). (d) Schematic of inkjet bioprinting strategy for 3D silk fibroin cellular constructs using sacrificial alginate (reproduced with permission [337]).

4.1.1.2 Gelatin

Gelatin is widely employed in biomedical applications thanks to its biocompatibility, biodegradability, and versatility in forming physically-crosslinked hydrogels in physiological environments [417].

Source of extraction and physical-chemical modification. Gelatin is derived from denaturation of collagen through hydrolysis of amide groups into carboxyl groups through an alkaline or acid process, yielding to a higher and lower conversion, respectively [418]. The proteins resulting from the two processes have different isoelectric points as a consequence of a different carboxyl groups density. They can interact with charged molecules at a physiological pH to form polyion complexes as positively- (Type A) or negatively-charged (Type B) basic gelatin. This aspect has been widely exploited for the controlled release of charged biomolecules including proteins and plasmid DNA, with potential application in different biomedical sectors [419]. Differently to collagen, gelatin from different sources typically show reduced structural variations as a result of the denaturation of the protein tertiary structure. Such molecular and supramolecular modifications usually leads to better solubility and less antigenicity of gelatin

as compared to collagen [420]. However, gelatin retains the polyaminoacid structure of collagen containing arginine-glycine-aspartic acid (RGD) sequences promoting cell attachment, together with the target sequences of enzymes involved in its degradation *in vivo*. Gelatin can be either physically- or chemically-crosslinked to form hydrogels with controlled stability in physiological environments. For instance, in the case of glutaraldehyde crosslinking aldehyde carbonyl groups react with free amino groups of lysine and hydroxylysine aminoacidic residues to form covalent bonds between gelatin molecules at either intramolecular or intermolecular scale. In this case, by varying the crosslinking density it is possible to tailor *in vivo* gelatin degradation by matrix metalloproteinases (e.g., collagenase) [421].

Biomedical use. Due to the aforementioned biocompatible and bioactive properties, as well as the demonstrated hemostatic and adhesive behavior, research on gelatin eventually resulted on the marketing and clinical use of various biomedical products, including biological glues, topical hemostatic agents, hemostatic sponges (e.g., Gelfoam®), films used in neurological, thoracic and ocular surgery (e.g., Gelfilm®), and microcarriers for cell culture (e.g., CultiSpher-G®).[422] In addition, a large body of literature has been published on gelatin in the form of disks, 3D hydrogels or microparticles, as carriers for the delivery of growth factors (e.g., transforming growth factor beta-1, bone morphogenetic protein-2 and -7 (BMP-2 and BMP-7), and insulin-like growth factor [423-426]) or for encapsulating different cells including chondrocytes [427, 428], osteoblasts [429], mesenchymal stem cells (MSCs) [430, 431], and preadipocytes [432]. In addition, gelatin has been often used in combination with synthetic polymers to develop hybrid materials with enhanced bioactivity, like in the case of composite polyurethane (PUs)/gelatin constructs with optimized human umbilical vein endothelial cells adhesion and proliferation [433].

AM application. At the physiological temperature (37 °C), gelatin dissolves as a colloidal sol and it can reversibly form a gel when cooled (< 29 °C) because of a conformational change from coil to helix that leads to chain association and eventually the formation of a 3D network [265]. This temperature-dependent gelation property represents a noteworthy advantage for **SE-AM** allowing extrusion of a warm gelatin solution into a cold environment to form a gel with a customizable shape. Low mechanical resistance and structural stability in aqueous environments are major shortcomings of additive manufactured gelatin. Indeed, even if physically crosslinked, gelatin tends to dissolve again when exposed to physiological conditions. Different strategies for gelatin stabilization to form 3D hydrogels by AM has been followed, such as glutaraldehyde crosslinking [234] and combination with other natural polymers suitable to be more stably crosslinked (e.g., alginate [322, 323], fibrinogen [24],

chitosan [324], and HA [325]). Nanoapatite coating represents a further way to increase the mechanical properties of printed gelatin-based interpenetrating polymeric networks [434]. A successful example of native gelatin employment for bioprinting is represented by a recent study on controlled extrusion of a suspension of human corneal epithelial cells in a solution of gelatin/alginate/collagen followed by $CaCl_2$ crosslinking of the polysaccharide to achieve well-defined porous hydrogels stable in PBS for more than 2 weeks [435]. An alternative AM approach for material patterning, proposed also for other biomedical polymers (e.g., fibrin and alginate) is represented by inkjet printing a crosslinker (e.g., glutaraldehyde) onto a gelatin bed [436].

Gelatin can be made susceptible to **photocrosslinking** into a hydrogel stable in physiological conditions through a simple and straightforward procedure involving its direct reaction with methacrylic anhydride in phosphate buffer (pH 7.4) at 50 °C [437]. In this way methacryloyl substitution groups are introduced on the reactive amine and hydroxyl groups of the aminoacidic residues **(Figure 3b**). GelMA photocrosslinking can be carried out in aqueous environments under mild conditions with the presence of a photoinitiator. This inherent advantage makes GelMA the most exploited naturally-derived polymer for photoinduced free-radical crosslinking [381]. GelMA formulations enable good control over their rheological properties and chemical reactivity depending on the degree of methacryloylation and polymer concentration. The resulting crosslinked hydrogels retain the intrinsic polypeptide biological properties, such as enzyme-degradability and cell-adhesion promotion. Different microfabrication techniques have been used to microstructure photocrosslinked GelMA hydrogels, including photopatterning, AM approaches, micromolding, self-assembling, microfluidics, and biotextile [381]. Nichol *et al*. [150] were among the first to micropattern functionalized gelatin with a top-down approach involving UV irradiation of preformed arrays of GelMA, resulting in a variety of biocompatible shapes and configurations with tunable hydration and mechanical properties.

The first articles on layer-by-layer **SLA** crosslinking of GelMA to fabricate 3D patterned structures were published in 2012 [154, 155]. After that, several studies have reported the SLA processing of resins based on GelMA to fabricate substrates with low toxicity and excellent cell-adhesion properties [124]. For instance, human meniscus cells-seeded GelMA scaffolds by SLA were placed *ex vivo* in surgically created defects in human meniscus tissue resulting in good integration and new bonding tissue at the interface after 3 weeks of culture.[438] The fabrication of patterned hydrogels possibly encapsulating cells was also investigated by means of SE-AM of GelMA followed by post-processing UV crosslinking. As an example, Billiet *et*

al. [235] proposed the use of a photoinitiator with enhanced biocompatibility, i.e., 2,2′-Azobis[2-methyl-*N*-(2-hydroxyethyl)propionamide] (VA-086) compared to the conventional Irgacure 2959, and successfully fabricated GelMA scaffolds with fully-interconnected pores networks. This approach was exploited to fabricate mechanically stable hepatocarcinoma cell line-laden GelMA scaffolds with high cell viability (>97%) through the optimization of printing pressure and needle shape. Vis-light-induced photoreticolation was also proposed as a means to crosslink GelMA in order to avoid cells damage risks related to UV irradiation [124, 307]. Wang *et al*. [124] employed a mixture of PEGDA and GelMA with eosin Y as Vis-light photoinitiator to encapsulate NIH 3T3 fibroblast cells in 3D structures with 50 μm resolution, achieving 85% cell viability for at least five days. Analogously, Lim *et al*. [307] described a new Vis-light initiating system based on the water-soluble initiators ruthenium and sodium persulfate, which yielded higher viability of cells encapsulated in Gel-MA in comparison to what achieved with conventional UV systems based on Irgacure 2959 (**Figure 4b**). In any case, extrusion of GelMA requires a strict control of the bioink, nozzle, and deposition platform temperature. Otherwise viscosity modifiers, such as HA[366] and gellan gum [439], should be employed. In particular, the addition of gellan gum was demonstrated to enhance the processing properties of GelMA bioinks by increasing their viscosity, yield stress, and speed of gelation. Optimized formulations (10/0.5% w/v GelMA/gellan gum) resulted in improved filament deposition and increased stiffness of UV-cured hydrogels encapsulating chondrocytes able to produce cartilage matrix *in vitro* [440]. GelMA was also co-deposited with photocrosslinkable methacrylate poloxamer macromers, functioning as reinforcing gel, to fabricate 3D hydrogels with the shape of the femoral condyle or the auricular cartilage [441].

Thiol–ene click chemistry has been also successfully employed to crosslink norbornene-modified gelatin for cells encapsulation [326, 327]. A recent article described the application of allylated gelatin as a thiol–ene clickable bioink for SLA or SE-AM combined with light irradiation to fabricate porous constructs with relatively high shape fidelity to CAD models [273]. An alternative approach to photocuring is represented by enzymatic protein crosslinking as shown by Irvine *et al*. [321] who crosslinked gelatin as a blend with PEG by employing microbial transglutaminase to print cell-laden constructs.

4.1.1.3 Fibrin

Fibrin is a fibrous protein whose clinical relevance is related to its use for developing versatile biomaterials with inherent biocompatibility, biodegradability and injectability, exploitable for advanced applications in TE, drug delivery, cell encapsulation, and surgical adhesives [442].

Source of extraction and synthesis route. Fibrin is naturally polymerized during blood clot formation starting from thrombin-catalyzed proteolysis of fibrinogen, a protein present in the blood as soluble component (**Figure 3c**) [443]. Fibrinogen is composed of two sets of three polypeptide chains (α, β, and γ) joined together by six disulfide bridges. Cleavage of fibrinopeptide A from the Aα chains and fibrinopeptide B from the Bβ chains leads to fibrinogen conformational changes and exposure of polymerization sites. Fibrin monomer with great tendency to self-associate and to form insoluble fibrin, is thus formed [442, 444]. Once polymerized, the fibrin network is stabilized by covalent crosslinking in the presence of the factor XIIIa. The resulting fibrous structure is characterized by extreme extensibility and compressibility, as well as an interconnected porosity suitable for hemostasis, fibrinolysis, and wound healing.

Biomedical use. Various clinically-available formulations allow the combination of fibrinogen and thrombin derived from plasma to form fibrin products for different applications, such as hemostats in surgery, adhesives for skin graft attachment, and sealants in colostomy closure [445]. Surgically employed sealants comprise those sourced from human pooled plasma (e.g., Tisseel VH®), autologous plasma (e.g., Cryoseal®), and bovine plasma (e.g., Vitagel™). In addition, thanks to its inherent advantages, including good cell seeding and cell encapsulation efficiency, combined with the possibility to be produced from the patient's own blood, fibrin has been widely investigated in the form of 3D gels or microbeads to engineer different tissues (e.g., cardiac, cartilage, and adipose tissues), often in combination with growth factors [422, 442].

Fibrin is degraded and remodeled *in vivo* by enzymatic activity. Fibrinolysis is mediated by serine protease plasmin cleavage at specific sites on either fibrinogen or crosslinked fibrin to yield various degradation products [446]. Rapid degradation of fibrin gels can cause losing of the necessary material structural features, especially in the case of TE in which a mechanical role is required before a sufficient formation of the growing tissue is achieved. Many studies have been addressed to tuning morphological, rheological, adhesive and other functional properties of fibrin gels by optimizing the crosslinking conditions (i.e., pH, and concentration of fibrinogen, thrombin, and calcium ion), using low cell density, or adding specific protease inhibitors [382, 442]. For instance, a challenging task is to develop an optimal fibrous network density trough tailoring fibrinogen and thrombin concentration in order to achieve a good balance between mechanical properties and cell infiltration.[447] Other strategies adopted to develop fibrin-based materials with advanced properties include PEGylation of either self-

assembled peptides [448] or fibrinogen [449], genipin crosslinking [450], and combination with synthetic [451] or natural polymers [452].

AM application. The use of fibrin in AM has been mainly related to **bioprinting** of cell-laden constructs. One of the first approaches involved the alternate deposition by thermal inkjet printing of two bioinks, one composed of a thrombin solution and the other one composed of a thrombin solution containing NT2 neuronal precursor cells, onto a fibrinogen substrate used as biopaper [293]. Similarly, Cui and Boland [328] developed a process to deposit a thrombin solution containing human microvascular endothelial cells onto a fibrinogen substrate to fabricate 3D channel structures forming a tubular microvasculature stable *in vitro* over 3 weeks (**Figure 4c**). The high crosslinking versatility represents the main advantage of fibrinogen for AM encapsulation of cells and growth factors, as shown by Lee *et al*. [329] who printed a thrombin solution onto a printed fibrinogen solution, both containing vascular endothelial growth factors.

Another AM strategy includes the employment of a dual-chamber single nozzle extrusion system that allows blending fibrinogen and thrombin solutions at a low temperature just before their deposition, in order to prevent crosslinking in the needle [330]. Attempts have been also made to combine fibrinogen with other hydrogel-forming materials to improve its processing properties and stability once extruded as droplet or filament. Indeed, its fibrous nature represents a disadvantage for AM, since it often results in clogging issues and unstable printed geometry [333]. For instance, fibrinogen can be combined with gelatin to endow the resulting bioink with thermoreversible gelation behavior exploitable to print cell-laden hydrogels with predefined shape and porous structure. Fibrinogen/gelatin constructs fabricated by means of pneumatic SE-AM were crosslinked through a dual-enzymatic strategy, involving thrombin and transglutaminase, to support multiple cell types, including human umbilical vein endothelial cells, human neonatal dermal fibroblasts, and human bone marrow-derived MSCs [332]. Laser bioprinting of fibrinogen/HA solutions containing a cells suspension, followed by thrombin crosslinking was also investigated as a suitable method to fabricate 3D multicellular arrays [331].

4.1.1.4 Silk Fibroin

Silk fibroin is widely investigated for different biomedical applications thanks to its processability in aqueous environments at room temperature, biodegradability to amino acids, biocompatible crosslinking processes, high tensile strength, and elasticity [453, 454].

Source of extraction and chemical structure. Silks are proteins produced in fiber form by silkworms and spiders. Differences in primary aminoacidic sequence among silks of different

species, as well as within a species, result in different functional properties, which are significantly affected also by the extraction, purification, processing and environmental conditions [455, 456]. Fibers from the filaments of silkworm (*Bombyx mori*) are composed by core structural fibroin proteins held together by sericin, which is a family of glue-like proteins [457]. Adequate fibroin purification from sericin is necessary to avoid immune reaction and elicit acceptable *in vivo* foreign body response [458]. Silk fibers are composed by two major fibroin proteins, light and heavy chains (25 and 325 kDa, respectively), consisting of polypeptides organized in layers of antiparallel β sheets forming crystalline regions (**Figure 3d**) [459, 460].

Biomedical use. Silk fibroin materials in the form of hydrogels, fibers, sponges, particles, and membranes have been widely investigated for various biomedical applications, including sutures, wound dressing, hemostatic devices and scaffolds for the engineering of a wide array of tissues (e.g., vascular, neural, cartilage, ligament, and bone tissue) [461]. Fibroin non-woven meshes, porous sponges, and electrospun nanofibers have been employed for *in vitro* growth of different human cell types, such as epithelial cells, keratinocytes, endothelial cells and bone marrow-derived MSCs [455, 462-470]. Various strategies have been pursued to biofunctionalize fibroin materials, including immobilization of growth factors and combination with osteoconductive ceramics [471-475].

AM application. The ability of fibroin to form physical crosslinks through intra- and intermolecular hydrogen bonding between hydrophobic domains can be exploited to stabilize materials manufactured by **SE-AM**. Self-assembled fibroin hydrogels have a relatively high mechanical strength, even if low flexibility and brittle behavior can represent major disadvantages depending on the application [476]. Glycerol was investigated as non-toxic additive to stabilize an intermediate conformation of crystallized fibroin with good flexibility [334]. Blending with other natural polymers acting as bulking agents and amenable to be physically crosslinked can be also exploited. For instance, silk-based printing efficacy and resolution were enhanced by using gelatin as bulking agent and glycerol to induce physical crosslinking [335]. Silk fibroin-gelatin blend hydrogels were also recently bioprinted and stabilized in physiological conditions through either enzymatic crosslinking by mushroom tyrosinase or physical crosslinking via sonication [338]. The resulting microstructured hydrogels supported the multilineage differentiation of encapsulated human nasal inferior turbinate tissue-derived mesenchymal stromal cells. A recent study was focused on inkjet printing of a fibroblasts-laden blend of alginate and silk fibroin through a two-step gelation process [337]. First sodium alginate was crosslinked by means of $CaCl_2$ during printing, then

fibroin was chemically-crosslinked at tyrosine residues through post-printing horseradish peroxidase catalysis, and finally alginate was sacrificed through its liquefaction as consequence of Ca ions chelation (**Figure 4d**).

A novel strategy for 3D freeform fabrication of silk fibroin relies on a one-step physical gelation process involving the extrusion into a nanoclay colloidal suspension containing low-Mw PEG that acts as physical crosslinker by inducing the formation of the β sheet secondary structure [336]. In addition, Kim *et al*. [339] chemically modified the primary amines of silk fibroin by glycidyl methacrylate. The resulting **photocurable** formulation was processed by means of DLP to fabricate complex structures reproducing the anatomical details of different organs (e.g., heart, trachea, and ear).

4.1.2 Polysaccharides

Polysaccharides are the first choice of polymers meeting the principles of sustainability, eco-efficiency, and green chemistry for the development of biomedical materials. Various polysaccharides with peculiar chemical nature and physical-chemical properties can be obtained from different sources (i.e., vegetable, animal, and microbial sources) generally with lower impact and production costs in comparison with proteins. In this optic, great interest is given to novel biotechnologies to recover polysaccharides from bioagro-wastes [477] and algal waste biomasses [478], and to process them into high value added materials.

Alginate, an anionic polymer typically extracted from brown algae, HA, an anionic polymer of animal source that can be also produced via microbial fermentation, and chitosan, a positively charged polymer obtained from crustacean shell and fungal biomass, can be mentioned among the most investigated biomedical polysaccharides for AM. The well ascertained biocompatibility of polysaccharides and their high chemical versatility conferred by the functional groups present in the structural units, label them as materials of election for various biomedical applications.[309] Indeed, the wide plethora of chemical modification reactions developed for this class of polymers provides powerful tools to tune polymer bioactivity, biodegradability, processing, and physical properties.

The great knowledge acquired by the scientific community on polysaccharides chemical-physical functionalization has been exploited to optimize and widen their AM processing potential, for instance by tailoring solution rheological properties for extrusion-based processing, introducing photoreactive moieties to stabilize extruded hydrogels, or optimizing novel SLA strategies. The increasingly rapid advances made in the past two decades on polysaccharides science and technology applied to AM is summarized in the next paragraphs

by highlighting critical aspects for each of the most investigated polymer in this area (**Figure 5**).

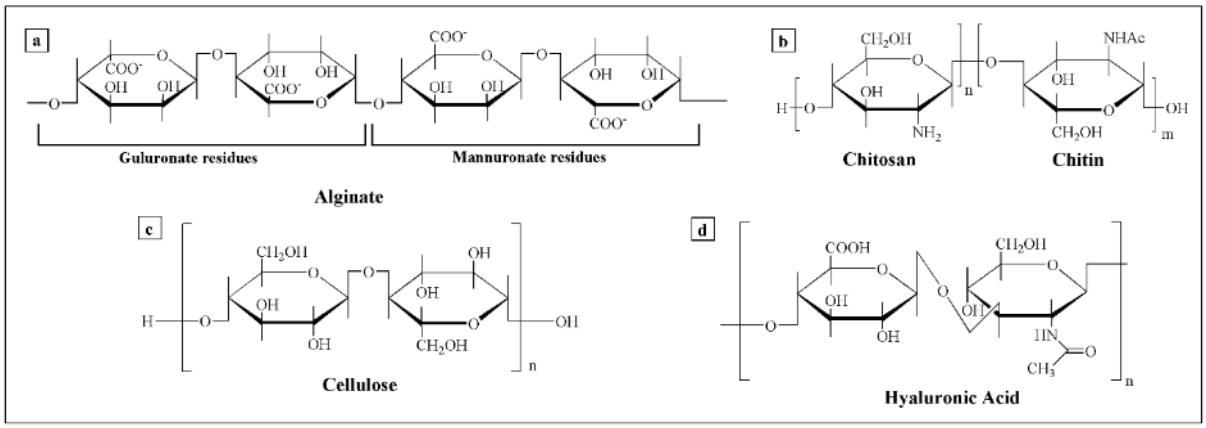

Figure 5. Representative chemical structure of the most investigated polysaccharides for AM. (a) Chain portion of alginates, linear copolymers consisting of blocks of continuous mannuronate residues, guluronate residues or alternating guluronate/mannuronate residues. (b) Chemical structure of chitosan, commercially produced by deacetylation of chitin yielding a heteropolymer. (c) Chemical structure of cellulose, a linear polymer of β-1,4-linked glucose residues. (d) Chemical structure of hyaluronic acid (HA), consisting of alternating disaccharide units of α-1,4-D-glucuronic acid and β-1,3-N-acetyl-D-glucosamine.

4.1.2.1 Alginate

Alginate is a natural polysaccharide widely used in different biomedical fields thanks to its high biocompatibility as carrier for cell encapsulation and drug delivery, scaffold for TE, and anti-adhesion material [479].

Source of extraction. Alginate is found as structural polysaccharides in marine brown algae (e.g., *Laminaria hyperborea*, *Ascophyllum nodosum*, and *Macrocystis pyrifera*) and as capsular polysaccharide in some soil bacteria (e.g., *Azotobacter vinelandii*) [480]. Alginate macromolecular structure is constituted by (1-4)-linked β-D-mannuronic acid and α-L-guluronic acid units (**Figure 5a**), whose sequence changes along the polymer chain. Many authors referred to this polysaccharide as 'alginates' in the plural form to highlight an extreme variability in material chemical-physical behavior, as a consequence of batch-to-batch variations in composition, Mw, and extent of the residues sequence, related to environmental conditions of the source and relevant climate changes. Industrial extraction processes are based on soaking acidified seaweeds in a sodium carbonate solution to convert insoluble alginic acid into soluble sodium alginate [481]. Some *in vivo* studies on alginate have reported immunogenicity and inflammatory responses, likely attributed to impurities (heavy metals, endotoxins, proteins, and polyphenolic compounds) [482, 483]. A proper purification is

therefore necessary to consider alginate biocompatible and to guarantee an acceptable control over its chemical-physical properties, aqueous stability, and biodegradation rate [484].

Physical-chemical modification and biomedical use. The marked hydrophilicity of alginate, mainly imparted by its carboxylic groups, does not favor the necessary proteins adsorption allowing for mediated biological phenomena, including immunogenicity, but also cell adhesion [485]. A widely exploited approach to increase alginate cell affinity is based on covalent linking of oligopeptides containing the RGD sequences, through straightforward chemical reactions mediated by carbodiimide-based reagents [486-492]. Although conventionally considered as a biodegradable polymer, bioabsorbability of alginate can be limited due to the lack of specific enzymes in mammals as well as the relatively high Mw of some commercial alginate batches, larger than the renal clearance threshold [493]. Partial oxidation of backbone has been demonstrated as an effective means to make alginate degradable in physiological media [494, 495].

Alginate tends to form insoluble hydrogels in aqueous solutions via ionotropic gelation based on ionic interactions between carboxylic acid groups and chelating cations [496]. In its native form, alginate is mainly present as Ca^{2+} crosslinked gel, but it forms physiologically stable hydrogels also in the presence of other multivalent cations (i.e., Sr^{2+} and Ba^{2+}). In general, Ca^{2+} crosslinking is preferred because of the milder reaction conditions and less toxicity involved in comparison to the use of other cations [266]. The biocompatibility and ease of gelation of alginate make it attractive in a wide range of biomedical applications, including wound healing, drug delivery, and tissue engineering. Various alginate-based wound dressings, such as Algicell™ (Derma Sciences), AlgiSite M™ (Smith & Nephew) and Comfeel Plus™ (Coloplast) are commercially available [408, 479]. However, ionotropic gelation suffers poor reproducibility in physiological environments due to monovalent cations that can interact with polymer carboxylic groups [497]. The reversible nature of ionic bridges between adjacent polymer chains represents one of the main shortcomings of alginate, resulting in weak hydrogels with poor physiological stability. Another approach followed to stabilize alginate exploited also for AM, as discussed in the following section relevant to chitosan-based materials (*see section 4.1.2.2*), is based on its complexation with a polycation. A number of covalent crosslinking strategies have been successfully pursued to enhance mechanical integrity and reproducibility of alginate hydrogels, even if in many cases they present different drawbacks, including lack of biological inertness and cross-reactivity with encapsulated cells and proteins [498-503].

AM application. The most exploited AM strategy for the fabrication of alginate hydrogels, possibly encapsulating cells, involves the **extrusion** of an aqueous polymer solution and then its crosslinking immediately after dispensing, for instance by means of submerged crosslinking [233] or aerosol spraying [354]. By employing low sodium alginate concentrations (1 to 2% w/v), Khalil *et al*. [233] developed endothelial cells-laden hydrogels through extrusion into a calcium-containing bath. Good cell viability was achieved by this approach even if the elastic modulus was low and decreased along time after incubation in a cell culture medium bath. A recent study reported on fibroblasts-laden scaffolds with tunable stiffness by varying sodium alginate concentration in the range 2-10% w/v, with a resulting significant influence on cell migration and morphology (**Figure 6a**) [349]. It was shown that at low concentration the 3D porous structure was compromised, while at too high concentrations cell migration was hindered due to high chain packing density. Other studies have shown decreased viability of various cell lines by increasing alginate concentration, explainable with the increased shear stresses acting on cells during extrusion [350, 351]. Rheological modifiers, such as cellulose nanofibrils, have been investigated as suitable means to enhance viscosity and processing properties of alginate-based bioinks, without compromising cell viability [352, 353].

Although the development of methacrylated alginate has been reported [501], its use for photocrosslinking-based AM has not been extensively investigated mainly because of the high control over hydrogel properties achievable through ionotropic gelation. One of the few exceptions is represented by a recent study on Vis-light-induced **SLA** hydrogelation of an alginate derivative with chemically incorporated phenolic hydroxyl groups, mediated by ruthenium II trisbipyridyl chloride ([Ru(bpy)3]2+) and sodium persulfate [267]. Thiol-ene chemistry has been investigated as approach alternative to methacryloyl functionalities crosslinking also for alginate-derived AM materials. Ooi *et al*. [274] reported the development of a norbornene functionalized alginate system as a cell-laden bioink for extrusion bioprinting with a rapid UV-induced crosslinking mechanism. The mechanical and swelling properties of the developed hydrogels were tunable by varying the concentration, length, and structure of dithiol PEG crosslinkers. A recent article reported on the development of viscoelastic, bioprintable aldehyde-containing oxidized alginates that could be combined with different imine-type dynamic covalent chemistries (i.e., oxime, semicarbazone, and hydrazone) to tune the rheological, mechanical and self-healing properties of the resulting hydrogels [504].

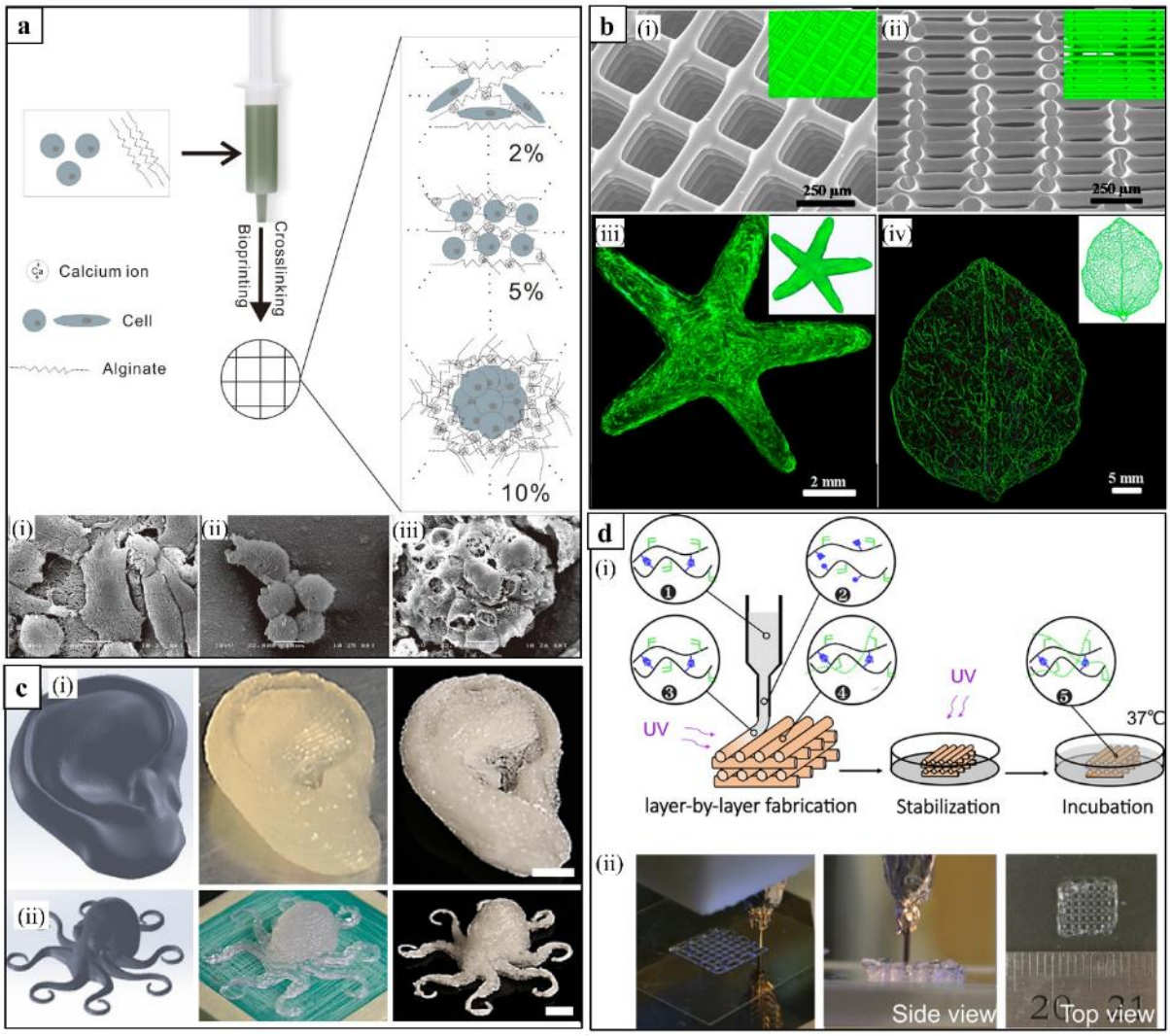

Figure 6. AM of polysaccharides. (a) Schematic representation of influence of alginate concentration (2, 5 and 10% w/v) on cell migration and morphology: after 7 days of *in vitro* culture, (i) in 2% constructs cells could stretch themselves showing a spindle like shape, (ii) in 5% constructs cells had a spherical shape due to the restrictions from the surrounding polymer networks, (iii) in 10% constructs cells spheroids were clearly observed as a consequence of cells tightly packing (reproduced with permission [349]). (b) Chitosan extrusion directly in air and at room temperature: top (i) and side view (ii) SEM images of a chitosan scaffold; fluorescent microscopy image of 3D printed chitosan with starfish (iii) or leaf (iv) shape (inset images show relevant CAD models) (reproduced with permission [344]). (c) Cellulose ear model (i) and octopus structure (ii) by extrusion (direct-ink-write): first column is SolidWorks models, second column is manufactured gel structures, and third column is resultant structures after freeze-drying (displayed scale bars are 1 cm) (reproduced with permission [360]). (d) Schematic of fabrication, stabilization, and incubation processes for dual-crosslinking of methacrylated HA hydrogels (i): (1) supramolecular hydrogel assembly with guest–host bonds within the syringe chamber; (2) guest–host bond disruption when extruded through the narrow needle, due to shear; (3) rapid self-healing of the supramolecular hydrogel and guest–host bonds when shear is removed and the material is deposited; (4) UV treatment to photo-crosslink methacrylates within the printed hydrogels; and (5) stabilization to enforce the polymerized network; (ii) representative images of the printing process and a resulting multilayer hydrogel structure (reproduced with permission [303]).

4.1.2.2 Chitosan

Different inherent properties make chitosan appealing for biomedical applications, such as a good biocompatibility, a hydrophilic surface favoring cell adhesion, and a well-assessed antibacterial activity [505].

Source of extraction and physical-chemical properties. Chitosan is the deacetylated form of chitin, a polysaccharide found in the exoskeleton of crustaceans, insects, and some fungi [506]. For this reason, it is often classified as semisynthetic rather than natural polymer. Chitosan is typically obtained by alkaline hydrolysis of the acetated groups of chitin to produce on an industrial scale a linear copolymer of β-(1–4) linked 2-acetamido-2-deoxy-β-D-glucopyranose and 2-amino-2-deoxy-β-D-glycopyranose (**Figure 5b**). It is commercially available with different N-deacetylation degree, conventionally classified as low (55-70%), medium (70-85%), high (85-95%) and ultra-high (>95%) degree.

The source chitin, existing in three polymorphic crystalline structures (α, β, γ) [507], the extraction and purification conditions, and the resulting deacetylation degree greatly influence chitosan physical-chemical, morphological and functional properties, including chemical reactivity, degree of crystallinity, solubility, hydrophilicity, solution viscosity, mucoadhesion, and antimicrobial activity [508]. After refinement, at the dry state chitosan macromolecules can organize in a rigid polymorphic, semicrystalline structure through inter- and intra-molecular hydrogen bonding. In general, crystallinity degree is maximum for both chitin (i.e., 0% deacetylated form) and fully deacetylated chitosan [509]. As a consequence of a wide variability in degree of deacetylation and M_w between different commercially available batches, various chitosan T_g values within a representative range of 140-200 °C, have been reported.

While chitin is insoluble in aqueous solutions and most of organic solvents, chitosan is readily soluble in acid aqueous solutions at pH below its pKa, as a consequence of amino groups protonation into positively charged groups (NH_3^+). The viscosity of chitosan solutions increases with an increase in polymer concentration or deacetylation degree, while decreases with increasing the shear rate, resulting in a pseudoplastic behavior [508]. From a chemical point of view, chitosan behaves in solution as a polycationic base due to the presence of amino groups along its backbone, differently to other polysaccharides that are neutral (e.g., starch) or acidic (e.g., alginate, ulvan, carrageenan, fucoidan) owing the exclusively presence of hydroxyl and acid groups along their structure [309]. This polycationic structure confers chitosan with a well-documented antimicrobial activity against many Gram-positive and Gram-negative bacteria, whose mechanism is likely related to an electrostatic interaction with the anionic components

of bacterial surface (e.g., peptidoglycan and lipopolysaccharide) leading to cell damage or death [510].

Biomedical use. Chitosan has been reported to be highly biocompatible, displaying low immunogenicity when interfaced with living organisms, with acceptable host response upon implantation [511, 512]. *In vivo* it is susceptible to enzymatic biodegradation through hydrolysis of glucosamine–glucosamine, glucosamine–N-acetyl-glucosamine, and N-acetyl-glucosamine–N-acetyl-glucosamine linkages, mainly by lysozyme, an enzyme present in various human body fluids and tissues [513]. Besides affecting the previously mentioned chemical-physical properties, the degree of deacetylation affects chitosan biodegradation rate and biocompatibility since the presence of free amino groups favors the interaction with cells [514, 515].

Chitosan has been widely investigated in the form of membrane, gel, or micro/nanoparticles for the controlled release of various bioactive agents, ranging from growth factors, antibiotics and anti-inflammatory drugs [508, 516]. A large and growing body of literature has been dedicated to the development of chitosan-based scaffolds for engineering various human tissues, including bone, cartilage, skin, liver and nerves [517]. In order to enhance its mechanical strength and ability to maintain a predefined shape once processed, chitosan has been combined with numerous polymers of synthetic (e.g., PVA [518] and PLLA [519]) or natural (e.g., alginate [520] and collagen [521]) origin as well as with bioactive ceramics (e.g., Ca-P [522] and natural coralline [523]). In addition, the high chemical reactivity of the amino groups has been exploited to functionalize and tailor chitosan macromolecular structure, as shown by Park *et al*. [524] who developed thermosensitive chitosan–g–pluronic copolymers as injectable hydrogels encapsulating bovine chondrocytes.

AM application. **SE-AM** of a diluted acetic acid solution in air or into a coagulation/crosslinking medium represents the most direct approach to AM of chitosan-based hydrogels. One of the first attempts in this context was made in 2002 by Ang *et al*. [341] who extruded an acetic acid solution of chitosan into a bath composed of NaOH and ethanol. By optimizing the composition of the coagulation bath, they were able to fabricate 3D scaffolds that maintained square macropores after washing and freeze drying. The reproducibility of the fabrication process was increased by Geng *et al*. [340] who designed a dual dispensing method to simultaneously extrude a chitosan acid solution and dispense NaOH onto the deposited polymeric strand. Chitosan constructs fabricated through the same processing strategy were more recently investigated in comparison with PDLLA-based constructs to evaluate *in vitro* the inflammatory response elicited by them in terms of cytokine profile of human

monocytes/macrophages [525]. A recent study reported on the extrusion of a silk particles dispersion (up to 300% w/w) into a chitosan solution to fabricate scaffolds with enhanced mechanical properties and printing accuracy, by manually pipetting a NaOH solution onto each printed layer [526]. Extruding a chitosan solution into a bath of isopropyl alcohol is a reliable alternative for manufacturing scaffolds able to induce *in vitro* the chondrogenesis of infrapatellar fat pad adipose-derived stem cells (ASCs) cultured on them [342].

A different AM approach is based on freezing the extruded chitosan solution during its deposition onto a low-temperature platform, followed by its lyophilization [345]. In this way, a defined open porosity along the Z-axis building direction can be achieved. In order to avoid the expensive and time-consuming lyophilization step, the frozen chitosan structure can be directly dipped into a KOH coagulation bath to induce polymer gelation, even if this treatment can diminish the fabrication accuracy [346]. Anyhow, scaffolds fabricated by this method were recently validated both *in vitro* using human fibroblasts/keratinocytes co-culture and *in vivo* in a diabetic rat model resulting in improved wound healing in comparison to what observed with a commercial product (**Figure 7**) [347]. High porous structure regularity was recently achieved through extrusion in air of concentrated chitosan solutions in a solvent mixture (acetic acid/lactic acid/citric acid) with optimized volatility (**Figure 6b**) [343, 344]. The resulting chitosan filaments showed relatively high strength and pronounced extensibility that were further increased after NaOH bath immersion (ultimate strain ~ 400%), as a consequence of polymer physical crosslinking through hydrophobic interactions and hydrogen bonds.

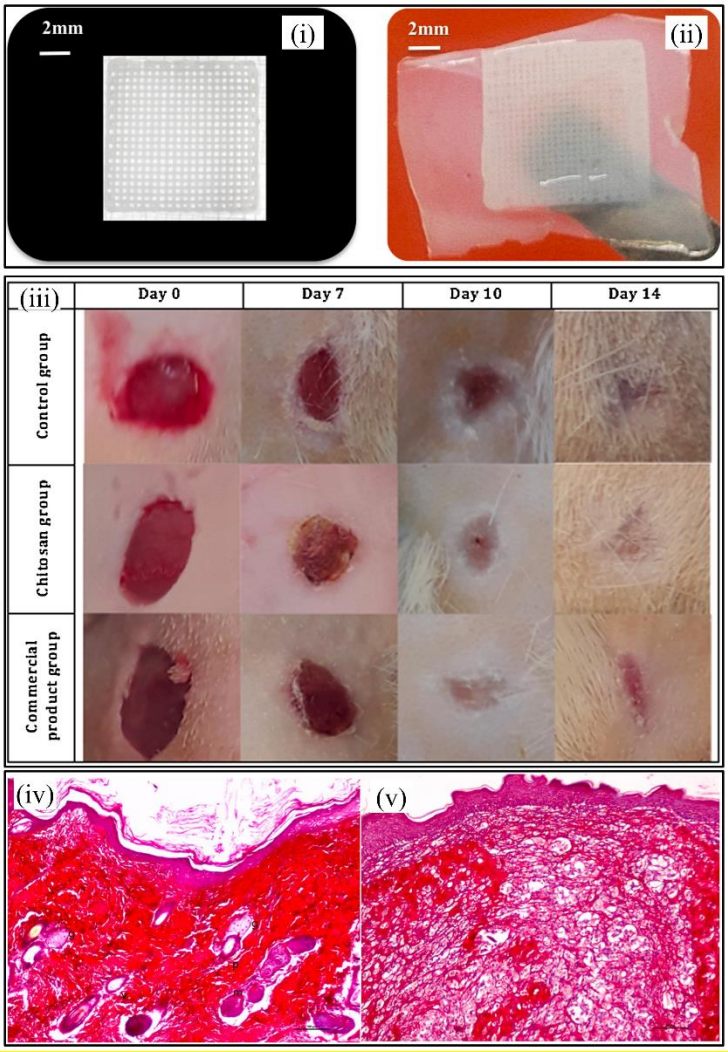

Figure 7. *In vivo* investigation of additive manufactured chitosan. Representative picture of chitosan scaffold without (i) and with (ii) a film of chitosan at the base; representative images (each photo corresponds to an area of 1 cm^2) of wound healing in treated and untreated groups (iii); histological staining Hematoxylin + picro-sirius red of tissue excised from wounds treated with chitosan scaffolds (iv) or with a commercial product (v) for 14 days (v: blood vessels, g: sebaceous glands, p: hair follicles, m: arrector pili muscles; scale bar 100 μm) (reproduced with permission [347]).

Ionic complexation with a polyanion is another effective way to stabilize extruded chitosan, which represents one of the main advantages of polycations for AM purposes. The first successful example of this strategy applied to AM was represented by CAWS fabrication of hydrogels with defined porous structure and enhanced mechanical properties through the extrusion in an ethanol bath of an aqueous suspension of a chitosan/poly(γ-glutamic acid) polyelectrolyte complex (PEC) [236]. The resulting PEC hydrogel scaffolds were successfully investigated in combination with the human cancer cell line BxPC-3 for long-term *in vitro* 3D modelling of the pancreatic ductal carcinoma [34]. Reeds *et al*. [527] used a chitosan-alginate PEC aqueous mixture and fabricated scaffolds through indirect AM by employing negative

molds made by FDM and positive molds by BJ. The method developed by Liu *et al*. [348] involved extruding a suspension of chitosan in an alginate solution and spraying a HCl solution on the deposited fiber in order to protonate the chitosan amino groups. In this case, scaffold structure reproducibility and manufacturing accuracy were enhanced by increasing the molar concentration of chitosan in the mixture.

Chitosan was also recently added to a PEGDA-based resin up to a 1:5 weight ratio for the **SLA** fabrication of ear-shaped scaffolds with optimized properties by controlling chitosan Mw and photoinitiator concentration [153].

4.1.2.3 Plant and bacterial cellulose

Plant cellulose, particularly in micro- and nanostructured forms, has been widely investigated for different biomedical applications to exploit its surface chemistry, biocompatibility and biodegradability, in particular in the case of skin repair treatment thanks to its suitability in accelerating the process of epithelialization [528].

Source of extraction and physical-chemical properties. Cellulose is the most abundant renewable polymer on earth, found primarily in lignocellulosic material in forests. Algae, agriculture residues, bacteria biosynthesis, and chemical synthesis represent other sources [529]. Cellulose is an unbranched polymer of β-1,4-linked glucose residues (**Figure 5c**). In native cellulose (i.e., cellulose I), hydroxyl groups tend to form hydrogen bonds resulting in monoclinic and triclinic crystallites interspersed with amorphous regions [530]. Native cellulose can be converted through physical-chemical and biological treatments to other crystalline forms with different unit cell dimensions, such as in the case of cellophane and rayon.

Like other polysaccharides, cellulose is not thermoplastic and it undergoes degradation when thermally processed. In addition, the high degree of polymerization and the complex pattern of intra- and intermolecular hydrogen bonding result in cellulose insolubility in water and in many organic solvents, making solution processing challenging. However, the possibility of dissolving cellulose in ionic liquid solutions and then regenerating it in a non-solvent after processing has been shown by several studies [531]. This enables the application of different solution-based processing techniques, including casting, molding, wet-spinning, and electrospinning.

Plant cellulose derivatives from various sources and subjected to different treatments are available on the market as biomaterials, including microfibrillated cellulose and nanocrystalline cellulose [532]. The first one is typically in the form of 5-60 nm wide and several microns long nanofibers, obtained by mechanical delamination of wood pulp followed by chemical or

enzymatic treatment. Nanocrystalline cellulose, in the form of nanofibrils with a cross-sectional size as low as 5 nm and hundreds of nm in length, is obtained through wood pulp acid hydrolysis with concentrated sulfuric acid to dissolve the cellulose non-crystalline domains, followed by high pressure treatment.

Bacterial cellulose (BC) possesses peculiar physical-chemical and structural features making it appealing for biomedical applications, including high purity, high crystallinity, high Young's modulus, excellent biodegradability, high water holding capacity, and good biological affinity [533]. BC is synthesized by bacteria such as *Acetobacter xylinum*, and its unique properties are the result of a typical nanostructured fibrous architecture. BC fibril diameter is typically in the range of 30 nanometers, hundred times thinner than that of plant cellulose fibers [534]. This nanosized structure, together with the absence of residual contaminants typical of plant cellulose (e.g., lignin, hemicelluloses, and pectin), are the reasons of the aforementioned advantages.

Biomedical use. Many attempts have been made to exploit BC properties for different biomedical applications. In particular, BC porous structure and hydrophilicity have been shown to be suitable for wound dressing by accelerating granulation, ensuring tissue healing, absorbing exudates, and providing a physical barrier from the surrounding environment to prevent microbial colonization [535]. Wound dressings from BC are nowadays available on the market (e.g., Biofill®, Bioprocess®, and XCell®) and applied in patients affected by burns and chronic ulcers showing accelerated healing and pain relief in comparison with other commercial wound patches [536]. BC growing typically results in pellicles rising to the surface of the reactor, and agglomerating to form a membrane with high purity that can be either used as it is, processed into nanofibrils, solubilized, or dispersed in a liquid. BC can be also shaped and molded into 3D structures directly during *in vitro* cultures, depending on the bacterial culture conditions (i.e., static culture, agitated culture, or airlift reactor) that also affect the resulting mechanical properties and micro/macrostructural features [537]. This aspect has accelerated research on BC application for developing implantable scaffolds tailored to different tissues, including blood vessels, cartilage, and bone. For instance, a number of bone engineering devices based on BC in combination with other naturally-derived polymers, e.g., collagen, agarose, PHB, and chitosan, or bioactive nanofillers, e.g., hydroxyapatite (Hap), are available on the market [538].

AM application. The possibility of obtaining filaments suitable to be printed by **FDM** and based on different cellulose derivatives commonly-used for pharmaceutical formulations (i.e., ethylcellulose, hydroxypropyl methylcellulose acetate succinate, and hydrophilic cellulose

derivatives) was recently demonstrated. However, poor thermal stability represents one of the main shortcomings of lignocellulose materials limiting their use in ME-AM as reinforcement components. As recently reviewed by Wang *et al*. [363], cellulose-containing filaments for FDM are typically composed of PLLA, PCL, or PVA reinforced with cellulose-based fillers in different forms, such as nanocrystals, fibers, and wood flour, at weight percentages up to 50%. Few studies also involved cellulose crystals as nanofillers for SLA manufacturing [364, 365].

Raw formulations for **SE-AM** have been optimized through combination of cellulose solutions or suspensions with other hydrogel-forming polymers (e.g., alginate) and proper additives in order to tailor their rheological and processing properties, as well as the stability of the printed hydrogel once in a physiological environment [363]. The resulting nanocellulose formulations show a shear-thinning behavior suitable for extrusion through a nozzle into 3D shapes that can be retained as a result of different gelation/solidification methods (e.g., physical/chemical crosslinking, air dry, and freeze-drying). A number of studies recently focused on the controlled deposition of nanofibrillar cellulose-alginate formulations that were crosslinked by using $CaCl_2$ to develop 3D hydrogels possibly encapsulating cells [353, 355-358]. The same crosslinking strategy was followed in the case of methylcellulose-alginate bioinks [539]. A successful AM approach involves printing cellulose dissolved in an ionic liquid (e.g., 1-ethyl-3-methylimidazolium acetate) followed by coagulation in a non-solvent bath to obtain spatially-structured hydrogels [359]. In this case, co-solvents (e.g., 1-butanol and dimethyl sulfoxide) have been investigated as rheological modifiers to ensure consistent printing.[540] An alternative way to stabilize cellulose-based materials after extrusion relies on freeze drying followed by chemical crosslinking (**Figure 6c**) [360]. 3D structures printed adopting this strategy are characterized by a dual-scale porosity, due to the lyophilization process, facilitating cell growth. Free-standing gels can be also obtained by adding xylan conjugated with tyramine to cellulose nanofibrils suspensions to make them susceptible to enzymatic crosslinking [361]. A recent article described an AM process based on the extrusion in air of an acetone solution of cellulose acetate [362]. After solvent evaporation and material solidification, cellulose acetate was reconverted to cellulose through NaOH deacetylation.

4.1.2.4 Hyaluronic acid (HA)

HA is widely exploited as injectable or implantable biomedical polymer thanks to its inherent advantages, such as no immunogenic properties, widespread availability, ease of chain size manipulation, and ability to interact with cell-surface receptors [541].

Source of extraction. HA is found in the ECM of different connective tissues as major structural and functional macromolecular element that contributes to the water balance regulation, serves

as lubricant and shock absorber, and at the same time, acts as scavenger for free radicals. Besides functioning as selective and protective coat around the cell membrane, HA interacts with bioactive molecules and is recognized by specific cell receptors that regulate cell behaviors, such as migration and ECM remodeling [541, 542].

HA is a high molecular mass (10^3 to 10^7 Da) linear copolymer consisting of alternating disaccharide units of α-1,4-D-glucuronic acid and β-1,3-N-acetyl-D-glucosamine, linked by β(1→3) bonds (**Figure 5d**) [543]. It is often referred to as 'hyaluronan', since it exists *in vivo* as polyanion and not in the protonated acid form. It is produced on an industrial scale through extraction from animal tissues (e.g., umbilical cord and rooster comb) [422] or microbial fermentation [544]. Medical grade HA is obtained by means of separation techniques, such as protease digestion, HA ion-pair precipitation, membrane ultrafiltration, non-solvent precipitation, and lyophilization, necessary for its purification from other biopolymers and molecules to which is complexed [545].

Biomedical use and physical-chemical modification. HA medical applications include, among others, viscosupplementation by injection into joints to treat arthritis and relieve pain, ophthalmic surgery, tissue augmentation and protection in cosmetic and reconstruction surgery, and advanced applications, such as TE and cells encapsulation [546]. HA combination with other polysaccharides, proteins, and ceramics has been investigated in order to provide artificial ECM environments to enhance cell interaction since the hydrophilic, polyanionic nature of HA does not favor cell adhesion [547].

HA tends to aggregate in aqueous environment as a consequence of hydrophobic interactions and hydrogen bonding between acetamido and carboxylate groups [548]. However, these interactions are fairly weak, thus polymer aggregates tend to dissociate under physiological conditions. For this reason, a large body of literature has been devoted to chemical modification of HA to reduce water solubility and control its biodegradation through, for instance, esterification. Various HA derivatives with different degrees of esterification (e.g., HYAFF ® and ACP™) are currently available on the biomedical market. A wide range of other HA chemical modification approaches have been developed, including hydrazide modifications, crosslinking with polyfunctional epoxides, glutaraldehyde crosslinking, reaction with divinyl sulfone, and crosslinking with carbodiimides [547].

AM application. Solutions of unmodified HA alone are not suitable for **SE-AM** owing their high viscosity, slow gelation behavior, and low stability upon printing. These shortcomings justified research on HA combination with other hydrogels for AM, like in the case of blending

with photocrosslinkable hydrogels (e.g., GelMA [366] and hydroxyethyl-methacrylate-derivatized dextran [367]).

Chemical modification represents a powerful tool to widen the possibilities of HA processing by AM and optimize hydrogel stability through crosslinking. Suri *et al*. [117] developed a novel method for the layered photoreticolation of HA methacryloyl (HAMA) into a set of 3D scaffolds with different geometry and porous structure. A similar approach allowed high survival of encapsulated MSCs after HAMA photocrosslinking [374]. HAMA has been also employed in photocrosslinkable multimaterial ink formulations. Skardal *et al*. [368] developed a processing method based on partial photochemical co-crosslinking of GelMA with HAMA giving an extrudable gel-like fluid, that was then printed under irradiation to fabricate tubular constructs encapsulating cells. Kesti *et al*. [369] developed bovine chondrocytes-laden hydrogels with a well-defined porous structure by blending poly(*N*-isopropylacrylamide)-grafted HA (HA-pNIPAAM) with HAMA. HA-pNIPAAM provided fast gelation and immediate post-printing structural fidelity, while HAMA ensured long-term mechanical stability upon photocrosslinking.

Separately coupling adamantane and β-cyclodextrin moieties to HA is an effective means to create two hydrogel-precursors that form a supramolecular assembly upon mixing [370]. By integrating this approach with photocrosslinkable methacrylate groups, Ouyang *et al*. [303] developed a dual-crosslinking strategy enabling the fabrication of layered hydrogels with a predefined porous structure that were stable over a month in physiological conditions with no loss in mechanical properties (**Figure 6d**). Other attempts to optimize ink rheology and stability of the printed hydrogel, were based on thiolated HA crosslinked by either poly(ethylene glycol tetraacrylate) [371] or gold nanoparticles [372]. 3D double printed constructs were recently developed by alternating strands of PCL and a precursor solution composed of thiolated HA, allyl-functionalized poly(glycidol) as cytocompatible cross-linker, and native HA as thickener to optimize ink rheology [373]. By grafting PLGA to HA, Park *et al*. [549] were able to obtain chloroform solutions that could be processed under a heated air stream to fabricate 3D scaffolds encapsulating BMP-2/PEG nanosized complexes. A recent strategy integrated photoreactive acrylate and thiol-ene chemistries by developing HA functionalized with both methacrylate and norbornene, suitable to processed by AM into cell-laden hydrogels [268].

4.1.3 Microbial polyesters

Polyhydroxyalkanoates (PHA) are microbial polyesters widely investigated for biomedical applications thanks to their biocompatibility and *in vivo* degradability into monomeric and

oligomeric products not exerting toxic effects [309]. From an applicative and technological perspective, the great interest raised on PHA is justified by the possibility of combining the advantages of a potentially sustainable production, starting from renewable resources, with a thermoplastic behavior and processing versatility comparable to those of chemically synthesized aliphatic polyesters.

Synthesis and source of extraction. PHA are produced as intracellular carbon and energy storage compounds by many Gram-positive and Gram-negative bacteria under unbalanced growth conditions [550, 551]. Extensive market penetration of PHA is hindered by production costs related to the need of maintaining axenic cultures and providing refined carbon substrates [552]. For this reason, several attempts have been made to enhance the competitiveness of PHA large-scale commercialization through novel metabolic engineering, synthetic biology, and bioinformatics approaches [553]. Ongoing research is investigating carbonaceous (agro)industrial waste streams as alternative feedstocks for PHA production, such as waste glycerol from biofuel production, lignocellulose waste from the food industry and forestry, and even petrochemical plastic waste [554]. Waste substrates coupled with mixed microbial consortia in three-stage systems, comprising feedstock fermentation, enrichment of PHA-producing bacteria, and PHA production, have been investigated as means to optimize process commercial potential [555].

Chemical structure and physical-chemical properties. PHA class is composed by aliphatic polyesters generally consisting of 1000-10000 monomeric units with different pendant groups, or a hydrogen atom, at the beta-position **(Figure 8)**. They can be classified as short-chain-length or medium-chain-length PHA if they consist of 3–5 or 6–14 carbon monomers in the 3-hydroxyalkanoate unit.

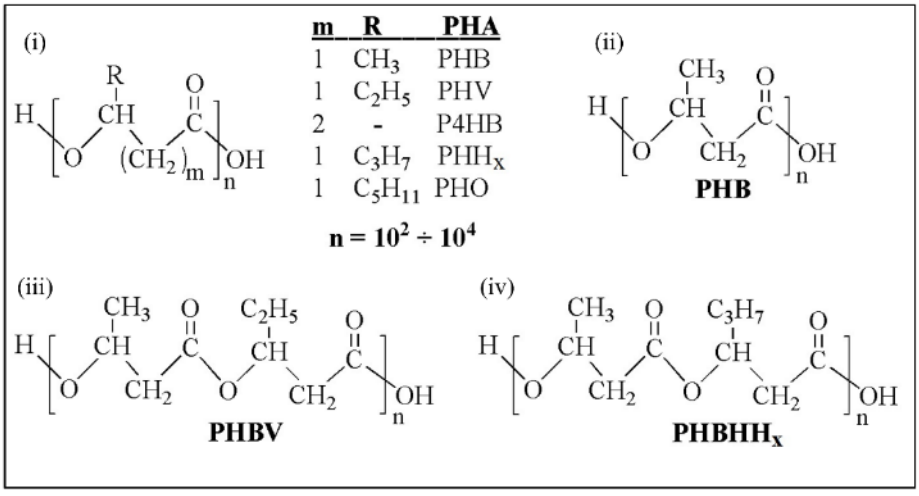

Figure 8. Chemical structure of polyhydroxyalkanoates (PHA) investigated for biomedical AM. General structure of PHA (i); structure of poly(3-hydroxybutyrate) (PHB) (ii); structure of poly(3-hydroxybutyrate-*co*-3-hydroxyvalerate) (PHBV) (iii); structure of poly[3-hydroxybutyrate-*co*-3-hydroxyhexanoate) (PHBHHx) (iv).

Since the discovery in the Twenties of poly(3-hydroxybutyrate) (PHB) [556], which has a pendant methyl group, an array of PHA macromolecular structures have been identified starting from poly(3-hydroxyvalerate) (PHV), with an ethyl pendant group, and the copolyester poly(3-hydroxybutyrate-*co*-3-hydroxyvalerate) (PHBV). The structural, processing and mechanical properties of PHA depend on both the length of the pendant groups and the distance between ester linkages [311]. PHB has a high degree of crystallization in the range 60-80%, as a consequence of the high stereochemical regularity, resulting in a stiff and brittle mechanical behavior (elongation at break<10%) (**Table 2**). The different molecular structure of poly(4-hydroxybutyrate) (P4HB) generally results in reduced degree of crystallization (~35%), higher flexibility, and better processing properties in comparison to PHB. Indeed, P4HB has a T_g (~-50°C) and a T_m (~60°C) much lower than those of PHB (T_g~0°C and T_m~180°C) [557]. The copolymerization between 3-hydroxybuytrate (3HB) and 4-hydroxybutyrate (4HB) monomers results in poly(3-hydroxybutyrate-*co*-4-hydroxybutyrate) (P[3HB-co-4HB]) co-polyesters with morphological, thermal and mechanical parameters intermediate between those of the two relevant homopolymers [558]. Since 3HB and 3-hydroxyvalerate (3HV) units co-crystalize in a single crystalline unit cell as a consequence of the small difference in size of the side group, PHBV crystallinity is not much reduced in comparison to PHB, being around 60% throughout a wide range of composition from 0 to 95% 3HV [559]. However, inhibition of secondary crystallization in PHBV results in increased flexibility and ductility (elongation at break up to 50%), as well as a reduced T_m (down to 130 °C) broadening its melt processing window in comparison to PHB. The longer alkyl side chain confers to poly[3-hydroxybutyrate-*co*-3-hydroxyhexanoate) (PHBHHx) even a broader processing window and higher elasticity which can be exploited for tailored biomedical applications [560]. Indeed, experimental investigations have demonstrated that by increasing 3-hydroxyhexanoate (3HHx) content, the T_m and degree of crystallization can be decreased from 177 to 54°C and 60 to 18%, respectively [561, 562]. The tensile strength can be correspondingly reduced from 43 to 20 MPa, while the elongation at break can be increased from 5 to 850%.

In vivo PHA biodegradation is the result of two different mechanisms, i.e., nonenzymatic and enzymatic hydrolysis of the ester bond, the latter by the action of nonspecific lipases and esterases being more extensive at the later stages [563, 564]. Besides polymer characteristics like chemical composition, Mw, and crystallinity, PHA biodegradation rate greatly depends on

the specific physiological environment. P4HB sutures complete biodegradation can require from 8 to 52 weeks , while no significant degradation of PHB implants was observed after 9 months in a rat femoral defect [565].

Biomedical use and physical-chemical modification. PHA molecular structure similarity with synthetic aliphatic polyesters results in processing and mechanical properties generally superior to the other classes of natural polymers, suggesting their use for the fabrication of devices with high resolution and reproducibility intended to be used in load-bearing applications (e.g., bone TE). In addition, the numerous homopolymers and copolymers belonging to this class of renewable materials, combined with the possibility of tuning their Mw and comonomers percentages by changing microbial fermentation conditions, offer the possibility to tune the resulting material biodegradation, mechanical and processing properties over a wide range. For these reasons, PHA have been widely investigated for the development of various biodegradable devices such as orthopedic screws, skin patches, implantable and injectable systems for drug delivery, scaffolds for the regeneration of different tissues, including bone, cartilage, nerves, and blood vessels [605]. Indeed, various biomedical products mainly based on PHB and P4HB, are commercially available for research and clinical applications, such as sutures (e.g., TephaFlex®, Phantom Fiber™, and MonoMax®), scaffolds (e.g., BioFiber™ scaffold), and surgical meshes (e.g., GalaFLEX and Tornier®) [606].

A large body of literature has been dedicated to combining PHA with other bioactive materials in order to tailor their biodegradation, thermal, mechanical and processing properties, as well as their hydrophilicity and cell interaction. Numerous osteoinductive ceramics in the form of nano/microsized fillers (e.g., HA, BG, TCP, and zirconia) have been loaded into PHA implants designed for bone repair [607]. Multi-block copolymerization with other acids/lactones (e.g., PLLA [608]) or ethers (e.g., PEG [609]) as well as linking of functional proteins [610] have been also investigated to tailor PHA physical-chemical, structural and functional properties. In addition, the microbial production of novel oligomers were recently investigated by co-feeding *Escherichia coli* with diethylene glycol, resulting in the formation of lactate-HB oligomers that can undergo polyaddition reaction with diisocyanate to yield biodegradable PUs [611].

Table 2. Reference data available in literature relevant to thermal transitions, mechanical properties, biodegradation rate, and suitable solvents of high-Mw natural and synthetic aliphatic polyesters investigated for AM [557, 562, 566-578].

Polymer	T_g (°C)	T_m (°C)	C (%)	Tensile modulus (GPa)	Tensile strength (MPa)	Elongation at break (%)	*In vivo* absorption time[f]	Scaffold compressive properties			Solvents
								AM technique (material)	Modulus (MPa)	Strength (MPa)	
PHB	0-5	170-180	60-80	0.9-4.0	15-60	5-20	2-3 years	SLS (PHB) [376]	0.4-24	0.1-1.7	Halogenates (e.g., chloroform and dichloromethane), dimethylformamide
P4HB	-47 to -52	57-69	35	0.05-0.23	35-50	>1000	2-18 months	n/a	n/a	n/a	
PHBV	0-5	130-180	35-70	0.5-3.5	10-40	5-50	> 1 year	SLS (PHBV; PHBV/Ca-P) [179, 181] FDM (PHBV/PCL) [378]	2.4-6.5 n/a	0.2-0.6 6.8-15.1	
PHBHHx	0-2	54-180	15-45	0.1-0.5	4-21	5-850	> 6 months	CAWS (PHBHHx) [238, 258] CAWS (PHBHHx/PCL) [239]	0.7-1.5 0.2-0.4	1.3-2.0 0.4-0.6	
PCL	-60	56-65	> 50	0.2-0.5	4-42	80-1100	> 2 years	FDM (PCL) [579, 580] FDM (PCL/TCP) [581] FDM (PCL/PLGA 1:1) [582] ME-AM (PCL/Hap) [583] CAWS (PCL; PCL/Hap) [26, 252] CAWS (*PCL; *PCL/Hap) [251] SLS (PCL) [4] SLS (PCL/Hap) [175] SLS (PCL/TCP) [584, 585]	20-40 124 50 27-56 0.1-1.3 1.4-7.3 52-67 24-103 0.1-14	2.0-6.8[b] 4.2-5.2 6.1 1.9-4.5 0.3-5.2 0.5-1.5[c] 2.0-3.2[b] 2.5-11.5 n/a	Halogenates, toluene, cyclohexanone, tetrahydrofuran, acetone, dimethylformamide
PLLA	55-80	170-190	37-50	2.7-4.1	15-150	<10	2-5 years	ME-AM (PLLA)[586] SE-AM/freeze drying (PLLA/TCP) [255] SLS (PLLA; PLLA-Hap) [179]	195 60 5.8-6.1	8.3 4.7 0.5-0.6	Chloroform, dichloromethane, furan, dioxane, dioxolane
PDLA	40-50	120-160	30-45	3.4-3.8	58-67	<10	n/a	n/a	n/a	n/a	In addition to PLLA solvents: acetone, ethyl lactate, tetrahydrofuran, ethyl acetate, dimethylsulfoxide, N,N xylene, dimethylformamide
PDLLA[a]	43-60	120-170	15-40	1-3.5	28-50	<10	2-16 months	FDM (PDLLA) [218, 587-589] SE-AM (PDLLA/PEG) [261, 590] SE-AM (PDLLA/PEG/BG) [261, 590] SSLS (PDLLA/TCP) [591] SLA (PDLLA derivative) [592] SLA(PDLLA-co-PCL derivative) [593] SLA (Hap-loaded PDLLA derivative) [594]	3-600 28-92 44-100 2.5-4.0 150-360 0.1 12-31	8.5-22 n/a n/a 6-11 n/a 0.6-1.2	
PGA	34-44	200-231	45-55	6.1-7.2	12-70	<10	6 weeks	n/a	n/a	n/a	Highly fluorinated organics, e.g., hexafluoro isopropanol
PLGA	44-55	---[d]	---[d]	1.4-2.8	40-55	<10	1-6 months	FDM (PLGA) [215] ME-AM (PCL/PLGA) [582, 595] ME-AM (PCL/PLGA/TCP) [582] SE-AM/freeze drying (PLGA/TCP) [596] SE-AM/freeze drying (PLGA/pearl) [597] SLS (PLGA/TCP) [598]	2.6 50-52 51 18 23 130	n/a 3.2-6.0 8.4 0.7 0.8 12	PDLLA solvents
PPF	-25-30	---[d]	---[d]	0.02-1[e]	20-70[e]	<5[e]	Several months[g]	µSLA (PPF/DEF) [599-601] DLP (PPF/DEF) [602] SE-AM (Hap-loaded PPF/DEF) [603]	8-50 135 50	77-290 n/a n/a	Chloroform, dichloromethane, tetrahydrofuran, acetone, ethyl acetate

n/a: not available data. [a] Amorphous when d-lactide>20%.[604] [b] Values corresponding to yield strength. [c] Values calculated at stresses corresponding to 50% strain. [d] Amorphous. [e] Values measured for crosslinked PPF/DEF samples. [f] Values relevant to full polymer resorption upon implantation either in human or animal, depending on material morphology and site of application. [g] Data on *in vivo* full absorption of PPF not available in literature; based on *in vitro* studies, several months are needed for full absorption depending on crosslinking degree.

The combination of different PHA, including PHB, PHBV and P[3HB-*co*-4HB] copolymers, with other blend polymers such as PLLA, PCL, starch, cellulose and chitosan has been also widely described [612]. However, PHA do not show the same blending versatility of synthetic polyester counterparts, with which they generally show poor miscibility, mainly due to processing issues. Short-chain PHA, particularly PHB, are soluble in very few solvents, i.e., halogenated solvents (e.g., chloroform and dichloromethane) and dimethylformamide, often resulting only in a partial solubilization at concentrations required by specific processing techniques (e.g., solvent casting and electrospinning) [613]. In addition, thermal processing is often challenging due to the narrow window between T_m and degradation temperature (T_{deg}). Indeed, PHA processing at temperatures above 150 °C generally results in the production of trans-crotonic acids [606, 614].

AM application. The limited PHA thermal processing properties is a major shortcoming for AM application. A few articles reported on the employment of **SLS** for PHA scaffolds fabrication. In particular, PHB was successfully processed by SLS without any variation in polymer thermal properties and chemical composition [375-377]. However, although the resulting scaffolds macroscopically showed geometrical fidelity to the virtual model, they were characterized by poor resolution, high surface roughness, and unwanted macropores in the polymeric matrix due to not completely sintered particles. Duan *et al.* [179-181] fabricated nanocomposite scaffolds through SLS of Ca-P-loaded PHBV microspheres (ϕ~50 μm) prepared by means of a S/O/W emulsion-solvent evaporation method (**Figure 9a**). They developed PHBV scaffolds with interconnected porous geometries that were biofunctionalized by binding the recombinant human BMP-2 (rhBMP-2) to a heparin-gelatin conjugated coating that was physically entrapped onto the surface. High surface roughness as a result of limited coalescence of composite microspheres was observed also in this case.

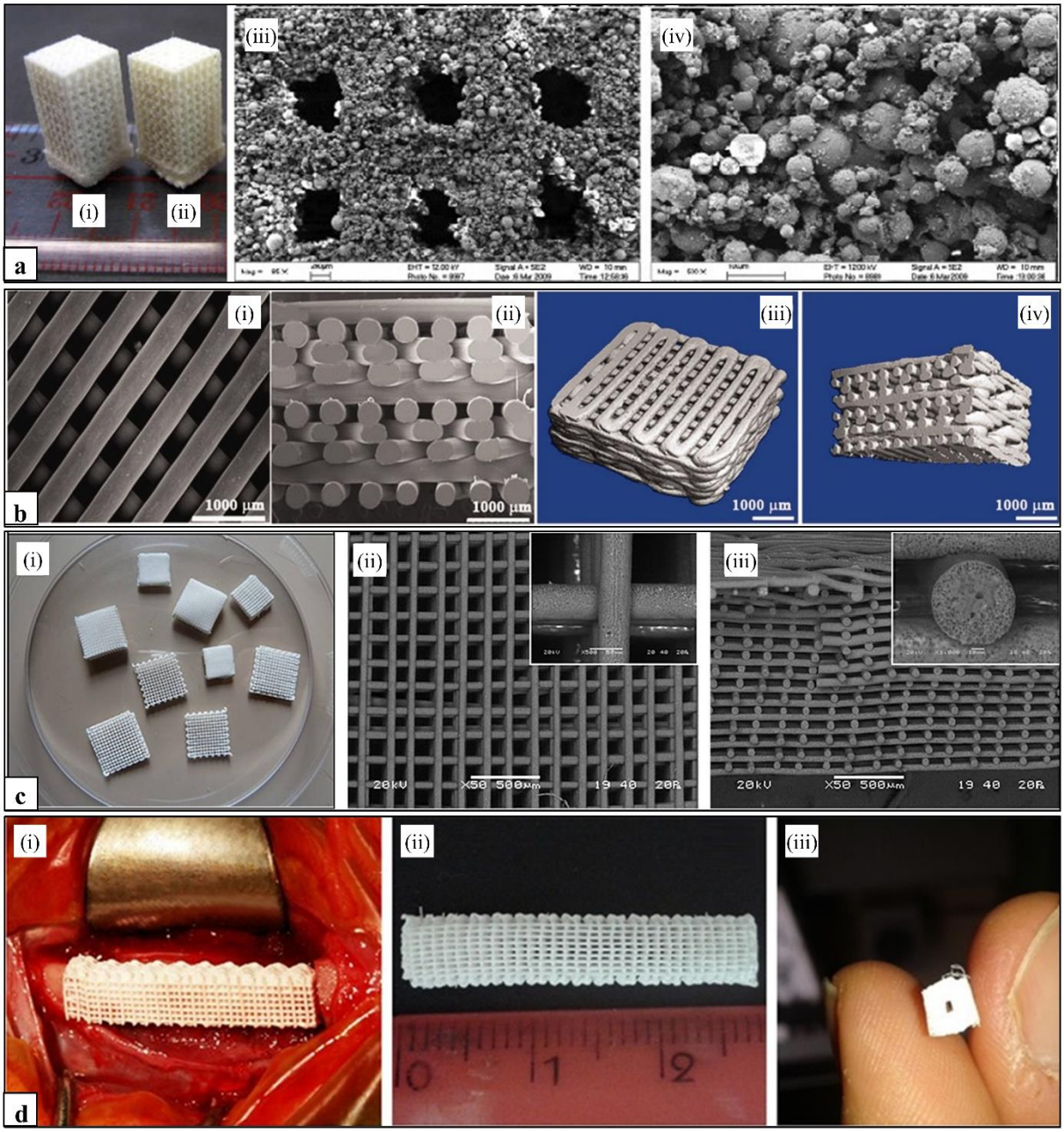

Figure 9. AM of PHA scaffolds. (a) SLS of poly(3-hydroxybutyrate-*co*-3-hydroxyvalerate) (PHBV): picture of PHBV (i) and PHBV-CaP (ii) scaffolds; SEM micrographs 85 x (iii) and 500x (iv) of PHBV-CaP scaffolds (reproduced with permission [179]). (b) FDM of PHBV: representative SEM micrographs and µ-CT images of top view (i) and (iii) and cross-section (ii) and (iv) of PHBV/PCL blend scaffolds (50:50 weight ratio) (reproduced with permission [378]). (c) CAWS of poly[3-hydroxybutyrate-*co*-3-hydroxyhexanoate) (PHBHHx): picture of PHBHHx scaffolds with different external size and porosity (i) and SEM micrographs of PHBHHx scaffold top view (ii) and cross-section (iii) (inset high magnification micrographs show polymer microporosity) (reproduced with permission [238]). (d) Anatomical PHBHHx scaffold by CAWS with shape and dimensions resembling those of a critical size segment of the New Zealand rabbit radio: representative pictures showing an implanted scaffold (i), the top view (ii) and the macrochanneled edge (iii) of the scaffold prototypes (reproduced with permission [258]).

Few articles reported on successful application of **FDM** to PHA processing, in all cases through their blending with other polymers and/or plasticizers. In particular, PCL/PHBV blend scaffolds at different weight ratios (75:25, 50:50 and 25:75) were recently fabricated by FDM (**Figure 9b**) [378]. The proliferative capacity and chondrogenic potential of porcine chondrocytes cultured on these scaffolds were enhanced by increasing the PHBV content and by treating the surface with low pressure oxygen plasma. A recent study reported on the development of a PHB/PLA blend in the weight ratio 60/25, containing also 15% wt. of an ester of citric acid (Citroflex®) acting as plasticizer, that was processed by FDM into 3D dog bone shapes for tensile mechanical characterization [379]. Other studies dealt with the development of composite filaments made of maleic anhydride-grafted PHBV reinforced with either palm fiber [615], wood flour [616], or multi-walled carbon nanotubes [617], even if FDM processability was not tested in any case.

The versatility of **SE-AM** for 3D PHA constructs fabrication has been described by various articles reporting on different CAWS approaches to process polymeric solutions through their coagulation in an ethanol bath. The possibility of obtaining PHBHHx scaffolds with tunable pores size and geometry as well as predefined external shape and dimensions was shown by varying CAWS design and fabrication parameters (**Figure 9c**) [238]. Optimized PHBHHx scaffolds developed through this approach supported the *in vitro* proliferation of MC3T3-E1 murine preosteoblast cells. A peculiar feature of this kind of PHBHHx scaffolds is a homogenous microporosity in the polymer matrix as a result of the NIPS process leading to polymer solidification [7]. A recent study showed the possibility of tuning this local micromorphology in terms of concentration of micropores by processing ternary PHBHHx/solvent/non-solvent mixtures with variable composition [254]. Anatomical PHBHHx scaffolds with dimensions and shape resembling those of a critical size segment of a New Zealand rabbit's radius were endowed with a longitudinal macrochannel designed to support host tissue infiltration from the edges of the resected bone once implanted (**Figure 9d**) [258]. Mechanical characterization highlighted the anisotropic behavior under tension and compression of these scaffolds whose compressive stiffness was increased by the presence of the longitudinal channel. CAWS approach was also successfully applied to fabricate scaffolds based on a blend of PHBHHx/PCL with tunable weight ratio between the two polymers.[239] In addition, by employing a rotating mandrel as auxiliary dynamic fiber collector, tubular PHBHHx constructs were recently developed as potential biodegradable intravascular stents for small caliber blood vessels [253].

4.2 Synthetic Biodegradable Polymers

Chemically-synthesized biodegradable polymers present many advantages over natural macromolecules favoring their processing, application and industrialization. Indeed, physical-chemical, mechanical, biodegradation, and functional properties of synthetic polymers can be precisely tailored by changing the synthesis/modification strategy and conditions to meet specific application-related requirements.

A wide range of synthetic biodegradable polymers have been developed for medical and pharmaceutical applications, including among others, polyesters, polyoxalates, polyanhydrides, PUs, polydioxanones, and polyphosphazenes [618]. They are susceptible of hydrolytic and/or enzymatic degradation *in vivo* through hydrolysis of ester, urethane, urea, or anhydride linkage depending on the molecular structure. The biodegradation rate of the polymer is directly related to the backbone linkage stability together with other factors, such as local pH, degree of crystallinity, equilibrium water content, and material porosity.

This section is mainly dedicated to aliphatic polyesters that represent the most widely investigated biodegradable synthetic polymers for AM thanks to their decade-long history of clinical use and processing as a melt, solution, or solid (**Table 3**). As nicely reviewed by Coulembier *et al*. [619], polyesters synthesis can be carry out through either homopolycondensation of a hydroxycarboxylic acid, hetero polycondensation of a diol with a dicarboxylic acid, or ring-opening polymerization (ROP) of lactones and related cyclic monomers. The latter method has become the most exploited one to obtain high molar mass polyesters thanks to its simplicity and suitability to control Mw distribution. The successful application of aliphatic polyesters in the biomedical field is related to a combination of different factors including biocompatibility of the polymer and relevant degradation products, tunable degradation kinetics in agreement to the envisaged application, high processing versatility, and mechanical properties suitable to a large range of applications [571, 572, 574, 577, 620]. As a consequence, numerous fabrication processes based on different AM techniques, ranging from ME-AM and SLS to SE-AM and BJ, have been developed to process aliphatic polyesters and poly(ester urethanes) (PEUs). Together with PPF, which was the first biodegradable polyester investigated for SLA, methacrylate-functionalized derivatives of PCL, PLA, and other biodegradable polymers, e.g., PTMC [143, 144], have been investigated as suitable photoreactive resin components for AM.

Table 3. Synthetic biodegradable polymers for biomedical AM.

Polymer	AM technique	Processing conditions and material design
PCL	ME-AM	- FDM processing of filaments made of PCL possibly loaded with HA, TCP or a drug [203, 579, 581, 621]. - Melt extrusion of PCL and relevant bioceramic-loaded composites, driven by pneumatic pressure [622, 623], force-controlled plunger [583, 624, 625], or screw extruder [204, 207, 626-630]. - Hybrid AM through: combination of melt-extruded strands with electrospun fibers [112, 207, 631-635], fully integration of FDM and electrospinning at a technique level (i.e., MEW) [210, 211, 636-640], sequential combination of FDM and pore-forming processes (e.g., thermally-induced phase separation [641], salt leaching [113, 642]), MEW of a photocrosslinkable PCL derivative followed by UV exposure [643].
	SE-AM	- Deposition onto a platform of a PCL solution extruded in air [259]. - Hybrid AM through: extrusion and deposition of a PCL solution, possibly containing Hap particles or a drug, into a non-solvent bath (i.e., CAWS) [26, 74, 105, 252, 253, 644], inkjet printing of a mixture of PCL dimethylacrylate and PEGDA followed by UV curing [645].
	SLS	- Processing of a PCL powder [4, 646-650], also in combination with polysaccharides (i.e., starch, dextran, or gellan) [651], Hap [162, 168, 175, 652], or TCP [584, 585], possibly surface-coated with collagen [585] or gelatin [653].
	SLA	- Photocrosslinking of methacrylate [654] or divinyl-fumarate [655] PCL derivatives, or poly(ester amide) copolymers [656].
Poly(α-hydroxy acids)	ME-AM	- FDM processing of filaments made of PLLA [14, 657-659], PDLLA [218, 587, 660-663] or PLGA [664], possibly loaded with TCP, Hap, or drugs. - Pneumatic-driven extrusion of PLLA [586], PLLA/Hap [665], PLGA [215], or PLGA/PCL blends [595]; plunger-driven extrusion of PLGA/PCL blends loaded with TCP [582, 666-668]. - Hybrid AM of PLA through combination of FDM and gas foaming [114, 213].
	SE-AM	- Extrusion of: a solution of PDLLA, containing PEG as plasticizer and possibly a suspension of CaP or BG particles [261, 262, 590], a concentrated PDLLA solution in a volatile solvent (e.g., dichloromethane) [232]; inkjet printing of a PLGA solution to form 2D micropatterns [669]. - Hybrid AM of: PLLA/TCP [255, 670], PLGA [671], PLGA/TCP [596] and PLGA/pearl [597] by sequential combination of SE-AM and freeze drying; PLGA through a CAWS process involving the controlled deposition of a tetraglycol solution into ethanol [672].
	SLS	- Sintering of a powder made of: PLLA [673], PLLA/carbonated Hap [179, 674, 675], PDLLA [676], PDLLA/TCP [166, 173], PLGA/TCP [598], carbon-loaded PDLLA [172, 677, 678], carbon-loaded PDLLA/Hap [178], or TCP/carbon-loaded PDLLA [591].
	BJ	- Hybrid AM through controlled deposition of chloroform, possibly containing Pluronic®, onto a PLGA/NaCl powder bed, followed by salt leaching [679]. - Controlled deposition of an acetone/ethanol mixture, containing a drug, onto a PLLA [200, 680] or PDLLA [201, 202] powder bed.
	SLA	- Photocrosslinking of PDLLA functionalized with fumaric acid [145] or methacrylate [129, 592, 681], possibly loaded with Hap [594, 682, 683].
PPF	SLA	- Photocrosslinking of PPF diluted in its monomer (i.e., DEF) [567, 599-601, 684], possibly functionalized with ceramic and peptide coatings [138, 139, 685, 686] or with BMP-2-loaded PLGA microparticles that were suspended in the photopolymer resin [687, 688].
	SE-AM	- Hybrid AM through extrusion in air of a solution of PPF and DEF, containing a suspension of Hap, followed by UV exposure [603].
PEUs	ME-AM	- FDM processing of PCL-based PEUs [689-692], also blended with PVA [693]
	SE-AM (bioprinting)	- Extrusion of: a dimethylformamide solution of a blend of two aromatic PEUs directly into a water bath [694], a hexafluoro-2-propanol solution containing a poly(ester urethane urea) and paclitaxel [695], an organic PEU solution onto a low T platform followed by freeze drying [696] possibly by means of a dual nozzle [287-289, 697-699], an aqueous dispersion of a thermoresponsive waterborne PEU for bioprinting [700-703]. - Inkjet printing of an acid aqueous medium onto a film of a pH-sensitive PU based on PCL diols [704, 705].
PTMC	SLA	- Photocrosslinking of formulations containing: PTMC functionalized with methacrylate end groups, possibly as copolymer with PCL [141, 142], and either Hap [143, 144, 706] or β-TCP [707].
	FDM	- FDM processing of a copolymer with PLLA [708, 709].
PVA	BJ	- Deposition of PVA aqueous binders on a polysaccharide powder bed [8].
	SE-AM	- Extrusion of a drug-containing PVA aqueous solution [106], inkjet printing of PVA aqueous solutions containing additives (e.g., humectant and pigments) [710].
	ME-AM	- FDM processing of PVA filaments loaded with either carbon nanotubes [711] or cellulose nanocrystals [712].

4.2.1 Poly(ε-caprolactone) (PCL)

PCL represents one of the most investigated synthetic polymers for biomedical applications thanks to its biocompatibility, inexpensive production routes, controlled biodegradation and mechanical properties, high permeability to many drugs, and good blend-compatibility.

Synthesis route and physical-chemical modification. PCL is a semicrystalline aliphatic polyester with thermoplastic behavior (**Figure 10a**). High-Mw PCL is industrially synthesized by ROP of ε-caprolactone monomer using tin bis(2-ethylhexanoate) (stannous octoate) as catalyzer in the presence of a higher alcohol initiator (e.g., 1-dodecanol) [619]. PCL has a T_g of *ca* -60 °C, a T_m in the range 60-65 °C, and a degree of crystallinity usually exceeding 50% (**Table 2**). At the physiological temperature PCL shows an elastic and ductile behavior since its amorphous domains are in a rubbery state. As a consequence of a highly hydrophobic nature and a high crystallinity degree, PCL has a slow biodegradation (years for complete *in vivo* absorption [713]) suggesting its use for long-term applications (e.g., load-bearing tissue scaffolds). Overall, PCL biodegradation *in vivo* involves first the non-enzymatic hydrolytic cleavage of ester groups, and eventually intracellular degradation once the Mw is decreased to less than 3000 g/mol [228]. The role and efficacy of enzymes, mainly esterases and lipases, in PCL degradation is not clear and difficult to isolate from other contributions. This aspect greatly depends also on the specifics of the local environment, like in the case of subcutaneous and intramuscular *in vivo* PCL degradation in which an absence of enzymatic activity is suggested [714]. Co-polymerization with other co-monomeric units (e.g., d,l-lactide, l-lactide, and ethyl ethylene phosphate) represents an effective means to accelerate the biodegradation rate, and to tune other physical-chemical and mechanical properties of PCL [715-717]. The incorporation of bioactive ceramic particles, including HA, TCP, $CaCO_3$, and Wollastonite, into PCL matrices has been also investigated to develop osteoconductive bone implants with enhanced mechanical properties, to increase polymer hydrophilicity, as well as to create a pH buffer against the acidic degradation products of the polymer [66].

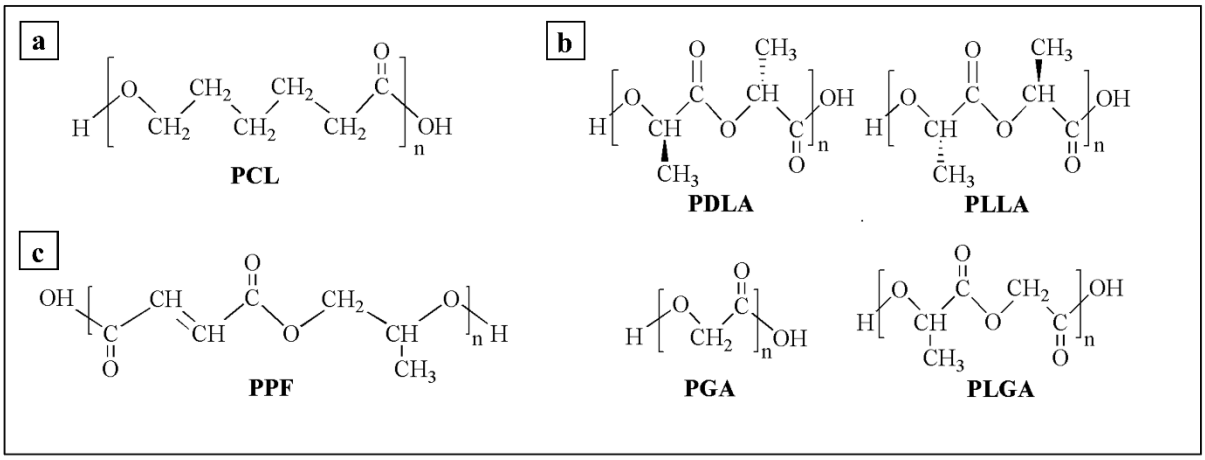

Figure 10. Chemical structure of biodegradable polyesters investigated for biomedical AM. (a) Poly(ε-caprolactone) (PCL). (b) poly(α-hydroxyacids), i.e., poly(d-lactide) (PDLA), poly(l-lactide) (PLLA), poly(glycolide) (PGA), and poly(lactide-*co*-glycolide) (PLGA). (c) poly(propylene fumarate) (PPF).

Processing properties and biomedical use. Thanks to its low melting temperature, high thermal stability, broad processing window (T_{deg}>300 °C), and suitable melt viscoelasticity, PCL can be easily processed by conventional melting techniques to develop composites and 3D devices [718]. PCL is soluble in different solvents, including halogenates, toluene, cyclohexanone, tetrahydrofuran, acetone, and dimethylformamide, making it suitable to be processed also as an organic solution [719]. This aspect has motivated a vast literature to investigate electrospinning as a suitable technique for the fabrication of PCL micro/nanofibrous meshes for different biomedical applications [720]. In addition, PCL insolubility in water, ethyl alcohol, diethyl ether, and petroleum ether can be exploited to employ NIPS approaches [721].

The suitable rheological and viscoelastic properties of PCL, both as melt or in solution, have been exploited to fabricate a wide range of medical devices and drug release systems. These include among others polymeric rods, micro- and nanoparticles for drug delivery, sutures, wound dressings, contraceptive implants, fixation devices, dentistry materials, and scaffolds for bone, cartilage, blood vessels, skin, and nerve regeneration [228, 620]. In particular, PCL-based sutures (e.g., Monocryl®) [722] and subcutaneous contraceptive implants (e.g., Capronor®) [723] have been clinically used for years. In addition, PCL is employed in the production of other commercial products, such as tissue repair patches manufactured by Ethicon Inc. and filling agents for non-load bearing bone cavities [606].

AM application. PCL is the most widely employed biomedical polymer in ME-AM thanks to its well-assessed melt processing properties, as witnessed by its employment for the fabrication of biodegradable devices used in the clinical practice (**Figure 11a**). PCL physical properties and thermoplastic behavior meet also the basic requirements of SLS. Its solubility in different

organic solvents and the suitable rheological properties of the resulting PCL solutions have also encouraged research on its processing by means of SE-AM techniques (e.g., CAWS). In addition, the well ascertained melt- and solution-blending compatibility of PCL with a number of commercial polymers offers many possibilities to develop innovative AM materials for biomedical applications.

Hutmacher *et al*. [203] were the first to develop PCL scaffolds by means of **ME-AM** (**Figure 11b**). In particular, they employed FDM to fabricate scaffolds made of PCL or PCL/Hap composites and endowed with a tailored porous architecture well supporting the *in vitro* proliferation, differentiation, and ECM synthesis of primary human fibroblasts and periosteal cells [579]. *In vivo* trials showed that this kind of PCL scaffolds promoted the formation of new bone tissue in an orbit defect model surgically created in Yorkshire pigs [724], and in a defect on medial femoral condyle of adult New Zealand White rabbits as well [580]. Afterwards, PCL plug scaffolds by FDM were tested in a clinical pilot study involving five patients needing cranioplasty surgery [725]. Twelve months after implantation, the scaffolds were well integrated in the surrounding calvarial bone with new bony tissue filling the porous space. Clinical trials eventually led to FDA approval of a set of PCL scaffolds by FDM for craniofacial applications. They are currently marketed by Osteopore International in the form of 3D implants (i.e., Osteoplug^{TM}) or thin interwoven meshes (i.e., Osteomesh^{TM}) [726]. Implantation of Osteoplug^{TM} scaffolds into burr holes of twelve patients treated for a chronic subdural hematoma, resulted in good osteointegration without any adverse events, with a mean follow-up of 16 months [727]. Osteomesh™ implants were recently investigated for orbital floor fracture repair in 20 patients. The study led to good functional and aesthetic outcomes with no signs of inflammation or reduction in limitation of ocular mobility, while neobone formation was evident on CT scan performed 18 months after implantation [728]. A pilot randomized controlled clinical trial involving thirteen patients was aimed at evaluating the feasibility and effectiveness of using a conical shape PCL scaffold, supplied by Osteopore International, in fresh extraction sockets for ridge preservation (**Figure 11a**) [729]. The implants were used as space fillers and resulted after 6 months in better bone healing and maintenance of ridge height as compared to extraction sockets without the scaffold. PCL scaffolds by FDM were also recently shown to be good candidates for soft tissue regeneration upon *in vitro* culture in combination with human adipose tissue-derived precursor cells [730]. 2 and 4 weeks after implantation in nude mice, angiogenesis and adipose tissue formation were observed throughout the engineered constructs by using a femoral arteriovenous flow-through vessel loop.

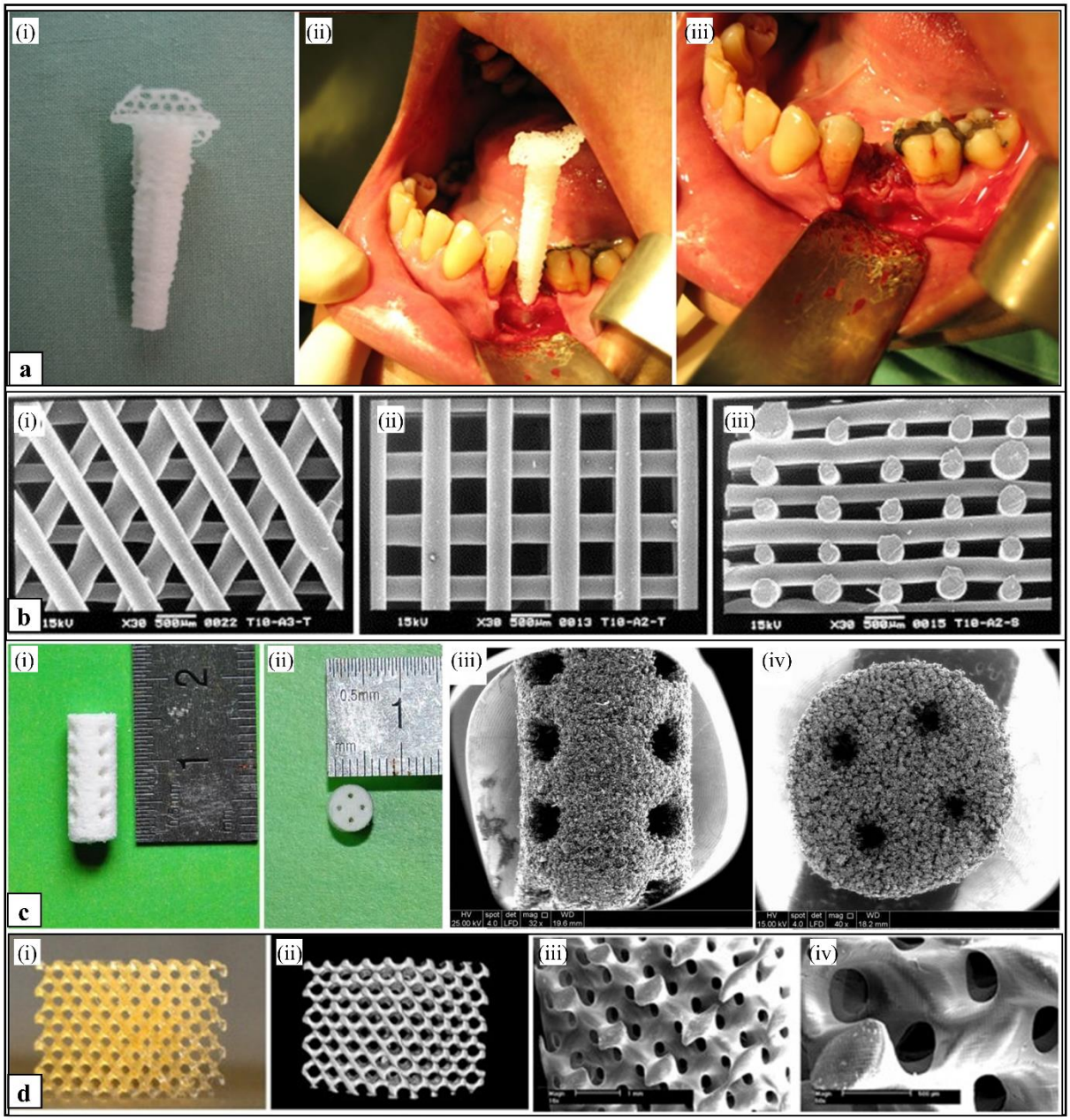

Figure 11. AM of PCL scaffolds. (a) Clinical application of additive manufactured PCL scaffolds: pictures of PCL conical scaffold by FDM for bone healing (i), scaffold insertion in a fresh extraction socket (ii), scaffold trimming off with a scalpel after insertion (iii) (reproduced with permission [729]). (b) FDM: top-view of 0/60/120° lay-down pattern (i); top view (ii) and cross-section (iii) of 0/90° lay-down pattern (reproduced with permission [731]). (c) SLS: pictures and SEM micrographs of side view (i) and (iii) and top view (ii) and (iv) of PCL/Hap scaffold (reproduced with permission [652]). (d) SLA: photograph (i), μCT visualization (ii) and SEM micrographs (iii) and (iv) of a PCL-based scaffold (reproduced with permission [654]).

A large body of literature has investigated FDM manufacturing of PCL/TCP composite scaffolds with enhanced mechanical strength, osteoconductive potential, and tailored biodegradation kinetics [581, 732-738]. Probst *et al.* [739] implanted in a human patient an anatomical PCL/TCP scaffold shaped on the basis of a CT scan of a complex calvaria defect,

observing bone healing and no palpable defect area after 6 months. Different strategies have been followed to enhance the bioactivity of PCL/TCP scaffolds, such as platelet rich plasma treatment [740], collagen coating [735], NaOH treatment [738], *in vitro* culture with animal [733], or human MSCs [736], and combination with growth factors [741, 742]. For instance, PCL/TCP scaffolds by FDM were cultured *in vitro* with human MSCs and then implanted in nude rat critical-sized femoral defects leading to cell survival for up to 3 weeks post-transplantation, as well as 50% of new bone grown success rate [736]. Biphasic constructs composed by a PCL cartilage scaffold coupled to a PCL/TCP osseous matrix, both fabricated by FDM, were resurfaced with a PCL/collagen electrospun mesh, seeded with MSCs, and implanted into critically-sized osteochondral defects in pigs [737]. Bone ingrowth and remodeling with high mineralization rate, functional cartilage restoration, and low occurrence of fibrous tissue were observed after 6 months. Biphasic scaffolds were also investigated for the regeneration of the goat femoral head by combining an anatomical PCL/Hap scaffold by FDM (**Figure 1f**) with a non-woven scaffold composed by PLA-coated PGA fibers [33]. These scaffolds were seeded with chondrocytes and bone marrow stromal cells (BMSCs) and subcutaneously implanted in nude mice leading after 10 weeks to histological structures and biophysical properties similar to those of native goat femoral head. Chhaya *et al*. [2] described a clinical case in which a 70-year old female patient received a customized scaffold loaded with autologous bone marrow and BMP-7 for the treatment of a non-union tibial defect of 4 cm. After 18 months of follow-up, the scaffold was filled with 75% newly regenerated bone with no reported post-operative discomfort.

As previously mentioned, FDM has lately come into focus as potential fabrication technique for drug-releasing medical implants and pharmaceutical dosage forms. PCL is often investigated in this field since its low T_m allows the preparation of drug-loaded filaments by melt extrusion without compromising the molecular structure of the therapeutic agent. By following this approach, Teo *et al*. [621] developed gentamicin sulphate-loaded PCL/TCP meshes with effective antibacterial activity in an infected full thickness wound mouse model. Similarly, T-shaped PCL prototypes of an intrauterine contraceptive device were fabricated by FDM and optimized to release *in vitro* indomethacin under sink conditions over a period of 30 days [743]. Kempin *et al*. [229] developed hollow cylinder model implants made of PCL, PLLA, ethyl cellulose (EC), or the methacrylic polymer Eudragit® RS, by processing quinine-loaded filaments prepared by solvent casting followed by hot melt extrusion (**Figure 12a**). In particular, the PCL-based formulation allowed an advanced control over *in vitro* quinine release kinetics by varying the filament drug loading. A recent case study was focused on custom-prepared PCL

filaments to manufacture disk-shaped model oral dosage forms [230]. In particular, feedstock indomethacin-loaded filaments with optimized mechanical and rheological properties for FDM were developed by tuning the drug loading. PCL was also investigated as a blend component in combination with hydrophilic polymers, i.e., poly(1-vinylpyrrolidone-*co*-vinyl acetate) and PEG, to modulate material processing properties and the release kinetics of the model drug caffeine from relevant FDM-printed tablets [219].

The successful application of FDM to PCL has encouraged research on alternative ME-AM technological solutions based on either pneumatic pressure-, piston- or screw-driven extrusion. As an example, Yilgor *et al*. [622] developed PCL scaffolds with different fibers stacking organization by using a Bioplotter® (Envisiontec GmbH) with a pressurized cartridge unit heated at 140 °C. Implantation in a rat pelvis model showed that bone regeneration within the scaffold was enhanced by increasing the pores size and endowing the scaffold with a sequential release of BMP-2 and BMP-7 from polymeric nanoparticles. A multi-head deposition system equipped with pressure-assisted melt and solution syringes was employed to alternatively plotting layers made of either PCL or chondrocytes-encapsulated alginate [623]. A ME-AM system using a steel syringe was employed to fabricate 3D scaffolds made from a composite of PCL, PLGA, and TCP, and ornamented with cell-laid ECM that was shown to enhance bone formation in ectopic and orthotopic rat models [624]. A similar approach was applied to fabricate PCL scaffolds loaded with synthetic [625] or bio-derived Hap [583]. The screw-based PED technology was employed to develop a set of PCL scaffolds with resolution at the microscale [204]. Optimized PCL scaffold prototypes developed by PED were seeded with primary fetal bovine osteoblasts and then subcutaneously implanted in nude mice showing increased osseous ingrowth during a 8 weeks study period [626]. Cell attachment to this kind of scaffolds can be increased by applying a coating made of a polysaccharide (e.g., chitosan) after *in situ* plasma treatment [627]. Bioextruder is another screw-based system investigated to develop PCL scaffolds with tunable pores size and mechanical properties by varying processing parameters, such as screw rotation velocity and nozzle translation velocity [207, 628]. This technology has been optimized to develop PCL scaffolds with high accuracy, possibly loaded with BGs (e.g., FastOs®BG) [629] or surface-modified through plasma treatment during fabrication [630].

PCL processing versatility has been greatly exploited to develop **hybrid AM** techniques designed to combine hierarchical structural features. A number of articles have reported on the alternating deposition of PCL strand layers by ME-AM and ultrafine fibrous layers by electrospinning (**Figure 13a**). Indeed, the integration of PCL-based additive manufactured

structures with electrospun fibers made of PCL [631], PCL/silk fibroin blend [632], PCL/collagen blend [112], or PLGA [207] has been reported to significantly influence cell adhesion, proliferation, morphology, and migration. In addition, intercalating collagen nanofibrous layers into a PCL scaffold by ME-AM was shown to enhance the mechanical properties of the resulting construct [633]. A more sophisticated fabrication process was developed by alternating PCL strand layers with electrospun PCL and osteoblast-like cells-laden alginate struts in order to achieve homogeneous cell proliferation throughout the scaffold [634]. A multiscale hybrid AM approach was also investigated by Yoon and Kim [635] who integrated an electrospun mesh made of rhodamine-B-loaded core/shell PEG fibers into a PCL scaffold fabricated by ME-AM. In this case, drug release could be tailored by sandwiching the hydrophilic mesh between two electrospun PCL meshes with adjustable thickness.

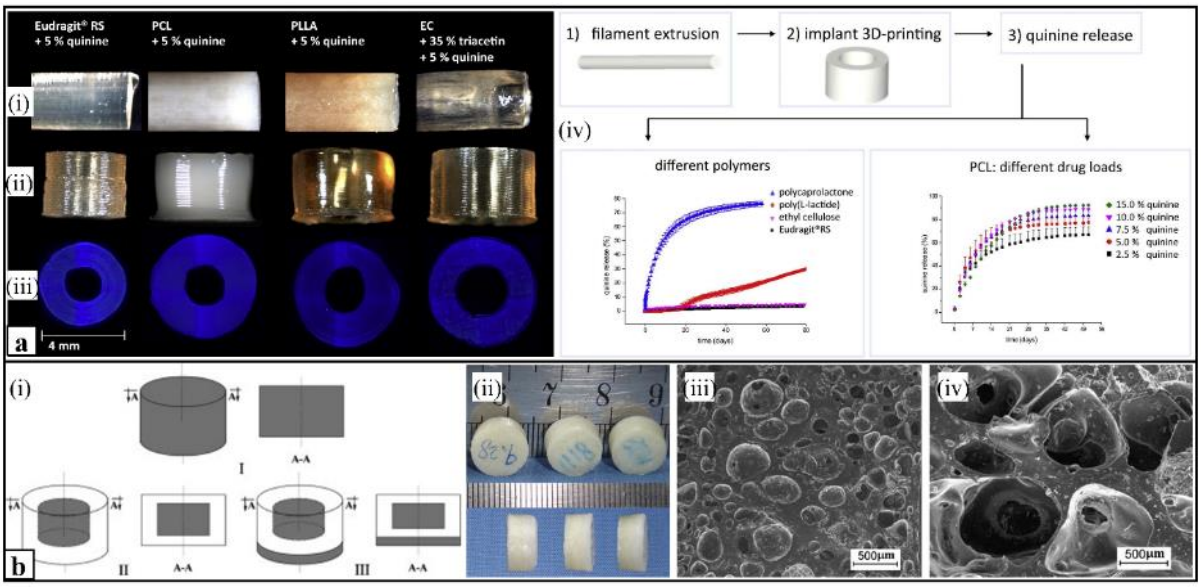

Figure 12. AM of drug-loaded biodegradable implants. (a) FDM manufacturing of quinine-loaded implants made of different polymers, i.e., the methacrylic polymer Eudragit® RS, PCL, PLLA or EC: reflected light microscopic images of side view of the filaments employed (i) and the resulting implants (ii), fluorescence microscopic images of the implants top view (iii); *in vitro* cumulative drug release profiles of implants made from different polymers, and of PCL implants loaded with different quinine percentages (iv) (reproduced with permission [229]). (b) Levofloxacin-loaded PLLA implants by BJ: schematics of implant structures (i.e., matrix, capsule, and double-layer/capsule structures) (i), picture of fabricated implants (ii), SEM micrographs of the manufactured implants before (iii) and after *in vitro* release for 40 days (iv) (reproduced with permission [200]).

MEW represents a successful example of AM and electrospinning integration at a technique level to fabricate PCL structures up to 10 mm in height over relatively large build areas, approaching single micron filament resolution and 20 µm placement resolution (**Figure 13b**) [210, 211]. PCL has been processed by MEW into scaffolds with cuboid [211, 636] or tubular

geometry [637, 638], and as fibers integrated in a hydrogel as pore-forming sacrificial material [639] or reinforcing network [640]. Bicompartmental scaffolds were also developed by combining different PCL constructs fabricated by FDM and MEW for periodontal TE [744] or by combining a PCL construct by MEW with an alginate gel for osteochondral TE [745]. *In vitro* studies have demonstrated that PCL scaffolds developed via MEW can support cell attachment, proliferation, ECM formation, and cell infiltration throughout the thickness of the scaffold, facilitated by the large pores and the high pores interconnectivity [746]. Different articles have reported animal experiments involving the subcutaneous implantation in immunocompromised rodents of this kind of PCL scaffolds, often functionalized with recombinant human BMP-7 and CaP coatings. In particular, as previously mentioned, PCL tubular constructs by MEW were investigated to develop humanized bone organ models in mice for studying metastatic sites of prostate and breast cancer cells [89, 94, 95].

The sequential combination of **FDM with a pore-forming** processing technique is an effective strategy to develop PCL scaffolds with a dual-scale porosity. For instance, Jensen *et al*. [641] incorporated a surface microporous structure into a FDM-manufactured PCL scaffold by infusing it with a ternary mixture of PCL, 1,4-dioxane, and water that underwent thermally-induced phase separation followed by lyophilization. In order to fasten and optimize drug release from PCL scaffolds by FDM, Visscher *et al*. [113] introduced a tunable microporosity in the polymeric matrix through salt leaching, and then applied a Gel-MA coating achieving a sustain release of cefazolin for up to 3 days (**Figure 13c**). The microporosity was also shown to facilitate the scaffold degradation during an accelerated test in NaOH. The combined FDM-salt leaching approach was also recently employed to control the *in vitro* release of different drug models (i.e., doxorubicin, paclitaxel, and cefazolin) from PCL scaffolds [642].

PCL scaffolds with a dual-scale porosity can be also fabricated through a one-step **CAWS** process involving the extrusion of an acetone polymeric solution into an ethanol bath (**Figure 13d**) [26]. The scaffold can be functionalized by adding to the PCL solution an osteoconductive ceramic [252] or a drug [105] that is then incorporated in the polymeric matrix upon coagulation. PCL scaffolds by CAWS were shown to support the adhesion, proliferation, differentiation, and mineralized matrix deposition of murine preosteoblast cells [26] and human ASCs [644]. Combining these PCL scaffolds with an integrated chitosan-based hydrogel is an effective means to endow them with antimicrobial properties [252]. PCL tubular constructs can be fabricated by using a rotating mandrel into the coagulation bath as an auxiliary fiber collector [253]. In addition, CAWS was employed to process a three-arm star PCL (*PCL) into dual-scale porous scaffolds with enhanced mechanical properties comparing to analogous constructs

made from PCL with a linear molecular structure [251]. This kind of *PCL scaffolds was endowed with an anatomical geometry, and implanted in critical size defects created in a rabbit radius model, showing good interaction with the host tissue without inflammatory response [74]. After 3 months, the defects were bridged with new bone tissue covering the scaffolds and penetrating into the first fibrous layers. AM of PCL-based solutions through their extrusion and deposition in air was also investigated to fabricate porous structures, achieving a limited development along building direction (Z axis) [259]. Overall, PCL scaffolds fabricated by CAWS show less accurate geometrical and dimensional fidelity to the CAD model in comparison to what observed when ME-AM is applied to PCL because of different factors, such as volumetric shrinkage and geometrical distortion during coagulation, as well as fluid dragging forces acting on the depositing filament. On the other hand, the aforementioned advantages of CAWS in terms of versatility in microstructural and drug loading functionalization should be also taken into account.

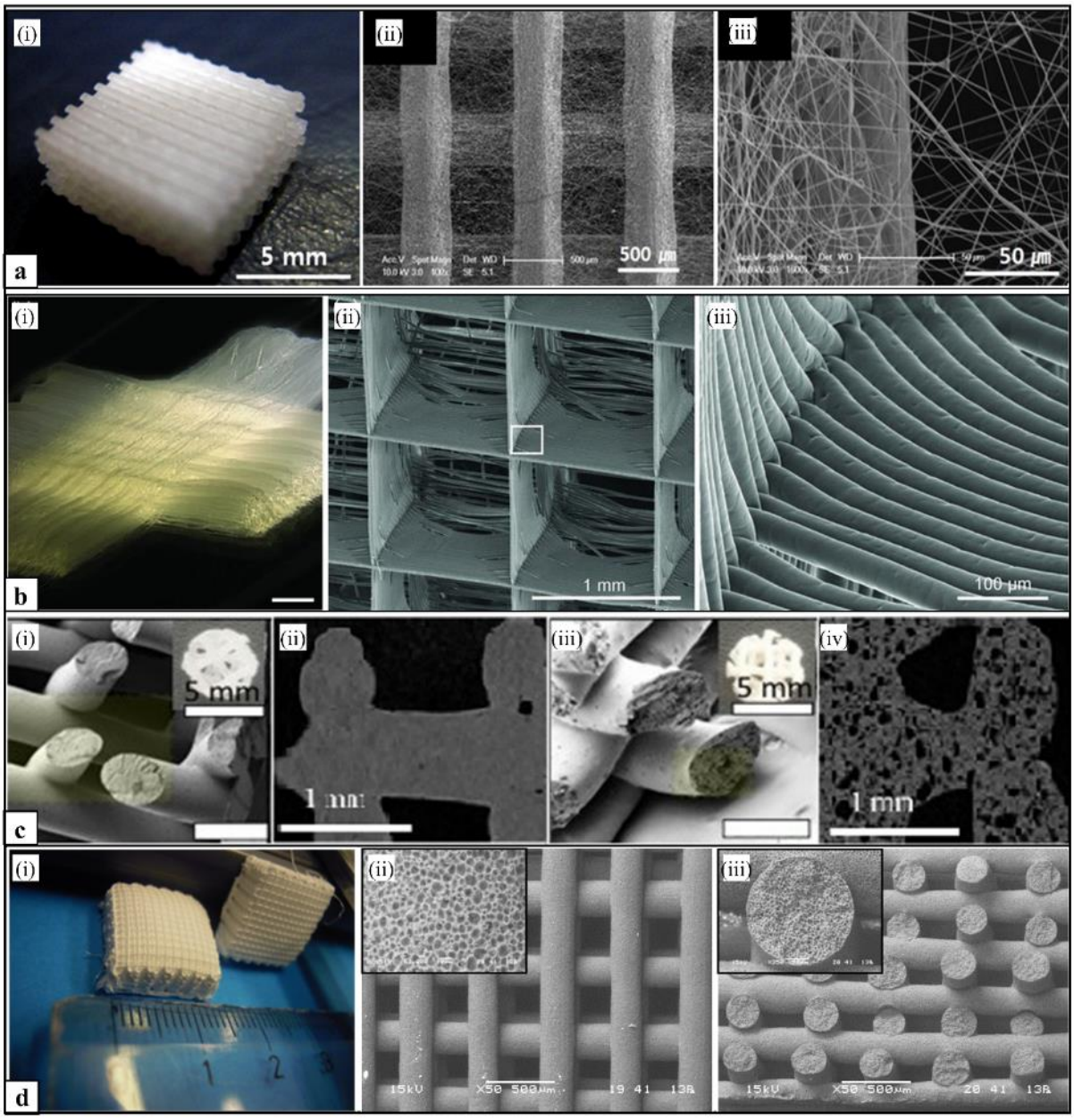

Figure 13. Hybrid AM of PCL. (a) Dual-scale fibers scaffolds by FDM and electrospinning integrated at a fabrication level: representative picture (i) and SEM micrographs 100x (ii) and 1000x (iii) of scaffold composed of PCL macrostrands and PCL nanofibers (reproduced with permission [112]). (b) Microfiber scaffolds by MEW: representative picture (i) and SEM micrographs (ii) and (iii) of scaffold composed by PCL microfibers (reproduced with permission [211]). (c) Dual-scale porous scaffolds by sequential FDM and salt-leaching: representative cross-section SEM and µ-CT micrographs of dense PCL scaffold by FDM (i and ii) and microporous PCL scaffold by FDM/salt leaching (iii) and (iv) (reproduced with permission [113]). (d) Dual-scale porous scaffolds by CAWS: representative picture (i) and SEM micrographs of top view (ii) and cross-section (iii) of PCL scaffolds (inset high magnification micrographs show polymer microporosity) (reproduced with permission [26]).

SLS was first applied to PCL in 2005 for the fabrication of scaffolds that were subcutaneously implanted in an immunocompromised mice model to study their suitability to support bone in-growth [4]. After that, several studies investigated SLS to process PCL also in combination

with polysaccharides (i.e., starch, dextran, or gellan) [651], Hap [168, 175, 652], or TCP [584], possibly surface-coated with collagen [585] or gelatin [653] for bone and cartilage TE. In general, these kinds of scaffold are characterized by a lower resolution and a higher surface roughness than PCL scaffolds obtained by other AM techniques (**Figure 11b**). Smith *et al*. [646] computationally designed and fabricated a condylar ramus unit PCL scaffold for temporomandibular joint reconstruction in a Yucatan minipig animal model. Once implanted and fixed in the mandible using mini-plates, the scaffold could support masticatory function as well as both osseous and cartilage regeneration. Nano-Hap inclusion into PCL scaffolds by SLS led to enhanced bone formation and increased biodegradation velocity after seeding with human MSCs and implantation in a critical femoral bone defect in rabbits [652]. Composite microspheres made by S/O/W methods can be employed, in place of mechanically mixing PCL and Hap particles, in order to obtain more uniform granulometry and particles shape, even if mechanical properties worsening can occur [168]. A recent study reported on the development of PCL/TCP scaffolds by loading the ceramic phase up to 30% wt. with a resulting significant increase in the compressive modulus [585]. The *in vitro* osteogenic differentiation of porcine ASCs seeded on these scaffolds was enhanced by applying a collagen type I coating that also favored *in vivo* bone formation and vascularization after intramuscular implantation of the construct in nude mice. Analogously, collagen type II coating favored the *in vitro* and *in vivo* proliferation of porcine chondrocytes seeded on PCL scaffolds.[653] Zopf *et al*. [22] described for the first time in 2013 the implantation of a PCL device in an infant suffering from tracheobronchomalacia to prevent airway collapsibility (**Figure 1e**). From 2012 to 2018, 15 subjects with a median age of 8 months received 29 splints on their trachea, right and/or left mainstem bronchi [747]. The tracheobronchial splints were developed on the base of a 3D model of the patient's airway and fabricated by SLS starting from a powder made of PCL [647] or a blend of PCL with Hap (4 wt.%), added as a flowing agent during the sintering process [162]. The same technology was investigated to develop patient-specific PCL scaffolds for craniofacial soft tissue reconstruction that were tested *in vitro* [648, 649]. As an example, auricular scaffolds seeded with primary porcine auricular chondrocytes and cultured in a pro-chondrogenic medium were subcutaneously implanted in rats [650]. After 4 weeks, diffuse chondrogenic tissue formation was observed in both the peripheral and central aspects of the explants.

Attempts to fabricate PCL-based constructs by **photoreticolation AM** were also reported. For instance, three-arm *PCL oligomers of various Mw were end-functionalized with methacrylic anhydride, and processed by SLA to fabricate 3D biodegradable scaffolds with a predefined

porous structure (**Figure 11c**) [654]. BG incorporation up to 20 wt. % into the polymer matrix, through its dispersion in the photoreactive resin, allowed enhancement of fibroblasts proliferation. An alternative fabrication approach is based on inkjet printing of a mixture of PCL dimethylacrylate and PEGDA followed by UV curing to manufacture mesh structures with different patterns [645]. Divinyl-fumarate PCL was also recently investigated as an alternative photocurable polymer to overcome problems related to substances leached out from acrylic resins, such as inflammation and allergic reactions [655]. The polymer was successfully employed in combination with NVP, as a reactive diluent, to fabricate by μSLA porous scaffolds with gyroid and diamond architectures supporting the adhesion and spreading of human MSCs. SLA fabrication of 3D scaffolds through photocrosslinking of poly(ester amide) copolymers based on ε-caprolactone and l-alanine was also reported [656].

4.2.2 Poly(α-hydroxy acids)

Poly(α-hydroxy acids), including PLA, PGA, and their copolymers (**Figure 10b**), are widely investigated in the biomedical area, and clinically employed for various applications thanks to their biocompatibility, controlled biodegradability into safe byproducts that can be resorbed through normal metabolic pathways, and mechanical properties suitable for different applications.

Poly(lactide) (PLA). As a consequence of the chirality of lactic acid (2-hydroxy propionic acid) that can exist in optically active d- or l- isomers, different forms of PLA exist as poly(l-lactide) (PLLA), poly(d-lactide) (PDLA), poly(d,l-lactide) (PDLLA), and poly(l-lactide-*co*-d,l-lactide) (PLDLLA). The polymer stereochemical structure can be easily modified by polymerizing a controlled mixture of l- and d-isomers to yield semicrystalline or amorphous polymers. On an industrial scale, high-Mw PLAs are commonly synthesized by ring-opening polymerization of dilactide (3,6-dimethyl-p-dioxane-2,5-dione), the cyclic dimer of lactic acid. The nomenclature adopted for PLAs is often confused and contradictory. As a rule of thumb polymers obtained by polycondensation of lactic acid should be referred to as poly(lactic acid), while those synthesized by ROP of lactide as poly(lactide).

Considering that lactic acid is generally obtained by microbial fermentation and that the resulting macromolecule in turn can degrade down back to lactic acid, PLA is generally considered as an environmentally friendly material [309]. Dilactide is synthesized with high yield and selectivity by using weakly basic catalysts (e.g., tin and zinc oxides, organostannates and -titanates) [748]. The l-isomer is the preferred feedstock for dilactide since the majority of lactic acid from microbial fermentation exists in this form and it provides high dilactide yield

for the synthesis of high-Mw PLAs with high crystallinity and mechanical strength [604]. A large range of properties can be obtained by copolymerization with the d-isomer of lactic acid as well as with other oxygenated functional monomers, such as glycolide, ε-caprolactone, and polyether polyols. A l-lactide content above 90% typically results in a semicrystalline structure with enough toughness and high tensile strength. When the l-lactide percentage is below 80%, an amorphous morphology is obtained. Unfortunately, some companies do not clearly specify the composition and stereoisomeric form of the marketed PLA batches. In some cases, commercially available PLAs are blends of PLLA and PDLLA. Relevant information can be however deduced from polymer T_m, crystallinity, and macroscopic appearance (i.e., translucent or opaque).

PLLA has been reported to have a T_g in the range 55-80 °C, a T_m in the range 170-180 °C, and a crystallinity degree in the range 40-50% (**Table 2**) [566, 569]. Since the amorphous domains of PLLA are in a glassy state at the physiological temperature, the polymer behaves as a brittle material when employed for clinical use. PDLA has typically lower T_g and T_m values than PLLA [568]. In addition, by increasing the d-stereoisomer content in PDLLA the T_g and T_m are significantly decreased [749]. In general, commercial PLAs are soluble in different solvents, such as dioxane, acetonitrile, chloroform, methylene chloride, 1,1,2-trichloroethane, and dichloroacetic acid, and partly soluble in ethyl benzene, toluene, acetone and tetrahydrofuran [570]. However, in the case of highly crystalline PLLA the list of suitable solvents is restricted. Water, alcohols (e.g., methanol, ethanol, and propylene glycol) and unsubstituted hydrocarbons (e.g., hexane and heptane) are non-solvents exploited for PLA precipitation procedures.

The development of new routes for the production of high-Mw polymer batches together with the growing environmental awareness in the general public have expanded the PLAs use for consumer products and packaging applications [750]. In the biomedical field PLLA has been investigated for different applications requiring a mechanical role, leading to various biodegradable products on the market and used in the clinical practice, including long lasting sutures, suture reinforcements, suture anchors, meniscal darts, and a wide range of devices for guided tissue regeneration barrier, osteosynthesis, and orthopedic fixation (e.g., Atrisorb® Freeflow™, Bio Interference Screw®, BioScrew®, Biotrak®, and Bio-Anchor®) [573, 576, 606, 751, 752]. In addition, PLLA is considered as the reference biodegradable material for intravascular biodegradable stents thanks to its relatively low T_g above the physiological temperature, which can be exploited for balloon expansion implantation procedures [753]. As a consequence of its more brittle behavior, lower mechanical properties, and higher hydrophilicity, amorphous PDLLA is mainly investigated for drug release applications [408].

Poly(α-hydroxy acids) are degraded in the human body mainly through hydrolysis into oligomers and monomeric acids, which can enter the tricarboxylic acid cycle and be excreted in the form of carbon dioxide and water via respiratory route and renal filtration [754]. Depending on the application, the complete resorption of PLLA devices takes long time, such as in the case of interference orthopedic screws, which persist *in vivo* for up to 5 years and require 7 to 10 years for complete resorption [755, 756]. Amorphous PDLLA is in general subjected to a faster biodegradation than semicrystalline PLLA [757]. In addition, the methyl pending group confers to PLAs repeating unit a more hydrophobic character, generally causing a slower biodegradation in comparison to PGA. The main biodegradation stage of poly(α-hydroxy acids) involves a non-specific, bulk hydrolytic scission of ester bonds. After that, the cleavage of the chain end groups (chain unzipping) takes place together with the solubilization of the degradation products [620]. The carboxylic acid end groups and the carboxylic degradation by-products can catalyze the hydrolytic process causing sometimes undesired effects, such as premature fail of the implant, tissue inflammation due to local acidification, denaturation of loaded drugs and/or poor control over their release kinetics [758, 759]. Inclusion of bioceramics (e.g., Hap nanopowder) into polymeric matrices, besides enhancing material osteoconductivity and mechanical strength [760, 761], can represent a strategy to counteract the acidic degradation by stabilizing the pH of the local environment [762, 763].

Poly(glycolide) (PGA). It is highly crystalline (45-55%), with a T_g between 35 °C and 40 °C, relatively high T_m (> 200 °C) and tensile strength (12.5 GPa) [575]. High-Mw PGA is typically synthesized by ROP of glycolide, the cyclic dimer of glycolic acid, commonly using as catalysts organo-tin, antimony, or zinc.[578] Although PGA was used in the manufacturing of the first synthetic absorbable suture (DEXON®) in the sixties [764] and in the production of internal bone pins (Biofix®) until 1996 [765], its rapid degradation in aqueous environment and insolubility in common solvents have limited its investigation as main component of load-bearing devices and drug release systems. Besides a quick decrease of scaffold mechanical properties, PGA fast biodegradation can lead to local glycolic acid concentration and subsequent inflammation [766]. Anyhow, a few studies investigated PGA as a filler material in combination with other biodegradable polymers, or in the form of non-woven fabrics to support the regeneration of different tissues, including bone [767, 768], cartilage [769, 770], and tendon [771].

PLGA copolymers. They have been extensively employed in the biomedical field to exploit the possibility of tailoring their biodegradation, mechanical, and processing properties by varying the lactide/glycolide molar ratio, the end groups, and the lactide isomeric form (i.e., l- or d,l).

For instance, the degradation time can be decreased from 5-6 months to 1-2 months by varying the d,l-lactide/glycolide molar ratio from 85:15 to 50:50 [772]. Indeed, as a consequence of their higher hydrophobicity, the lactic acid moieties are hydrolyzed slower than the glycolic acid ones, resulting in a variation of their ratio during biodegradation. The processing technique and the resulting macromolecular morphology also play a key role in the resulting biodegradation kinetics, as reported by an article demonstrating a significantly slower biodegradation of PLGA electrospun fibers in comparison to dense films made from the same raw copolymer [773]. This finding was explained with the high packing density and axial orientation of polymer chains during electrospinning, slowing down water diffusion in spite of the much higher surface area of electrospun fibers in comparison to monolithic films. PLGA copolymers have been particularly investigated for different biomedical applications, such as electrospun fibers [773] or micro/nanoparticles [774] for drug release, and 3D porous scaffolds for TE [775]. Various PLGA-based products are available on the medical market, including injectable formulations for the treatment of prostate cancer and endometriosis (LUPRON DEPOT®), opioid and alcohol dependence (Vivitrol®), human growth hormone deficiency (Nutropin Depot®), or macular edema and non-infectious uveitis (OZURDEX®). Other commercial PLGA devices are absorbable sutures (Vicryl®, Vicryl Rapide®, Polysorb® and Purasorb®), patches for wound treatment and skin regeneration (Vicryl® mesh, Dermagraft®, CYTOPLAST Resorb®), bioresorbable fixation plates, screws, and pins for bone fracture stabilization and craniofacial reconstruction (Rapidsorb® plates, LactoSorb®, RFS™ Screw and Pin System) [752, 776].

AM application. Highly crystalline PLAs (e.g., **PLLA**) are among the most employed materials in **FDM** thanks to their relatively low T_m (<180 °C) enabling their processing outside of a dedicated facility without the use of a heated construction platform.[777] However, as previously mentioned, PLAs can be susceptible to degradation during thermal processing [227]. In addition, drawbacks related to low melt elasticity and strength, often resulting in melt rupture during processing, have been connected to PLLA high chain stiffness and low entanglement density [778, 779]. As discussed before, small percentages of d-lactide are enough to significantly decrease the crystallinity degree and change polymer melt rheology. Macromolecular chain stiffness and morphological properties can be also modulated through copolymerization with other co-monomeric units. For instance, poly(l-lactide-*co*-ε-caprolactone) (PLACL) and poly(l-lactide-*co*-trimethylene carbonate) (PLATMC) can be engineered in order to be endowed with a chain flexibility optimized for melt processing [708,

709]. Indeed, commercial PLACL and PLATMC are characterized by a significant lower T_g (e.g., 13 and 32 °C, respectively) in comparison to PLAs [709].

The fabrication of PLLA scaffolds by means of ME-AM was reported for the first time in 2001 by employing a pneumatic system designed to process polymeric grains [586]. The possibility to extrude PLLA filaments for FDM, possibly loaded with TCP, was subsequently shown [657]. Different studies demonstrated that FDM-manufactured dog bone shaped samples made of different commercial PLAs have tensile modulus and strength comparable to those reported for PLLA-based films prepared by means of solvent casting or compression molding [14, 657, 658]. In particular, Chacón *et al*. [15] showed that PLA samples fabricated by FDM exhibited anisotropic mechanical behavior that could be changed by acting on build orientation, layer thickness, and feed rate. Chhaya *et al*. [218] employed FDM to fabricate PDLLA scaffolds with a geometry modelled *in silico* via a laser scanning data set from a patient who underwent breast reconstruction surgery. These breast-shaped scaffolds were employed for *in vivo* modelling of angiogenesis and adipose tissue formation in athymic nude rats. FDM was also recently employed to fabricate a porous PLLA screw-like scaffold that was coated with Hap and loaded with MSCs [659]. *In vivo* assessment in a rabbit anterior cruciate ligament model showed that PLLA screw constructs supported significant bone ingrowth and bone-graft interface formation. A recent article reported on FDM fabrication of scaffolds composed of semicrystalline PLA strands (~115 μm) and with different pore size (150, 200, 250 μm), achieving high reproducibility and good dimensional fidelity to the CAD model [660]. However, thermal processing caused a significant reduction of polymer Mw and T_{deg}, even if the scaffolds well-supported the proliferation of human BMSCs. Low porosity PLA scaffolds with enhanced mechanical properties were recently fabricated by FDM and investigated for bone TE [588]. Another study showed that by optimizing pore size (i.e., 750 μm) of PLA scaffolds fabricated by FDM, osteoblasts proliferation, metabolic activity, and osteogenic matrix protein production were enhanced [587].

Lately, PLLA/Hap scaffolds fabricated by a piston ME-AM system were seeded with BMSCs and implanted in a rabbit model used as *in vivo* bioreactor to generate a large vascularized tissue engineered bone (**Figure 14**) [665]. In particular, the scaffold was designed with a central channel and crossed with the saphenous vessel bundle. Other attempts to biofunctionalize PLA scaffolds fabricated by FDM involved coating them with gelatin/polylysine interpenetrating polymer networks, designed to release different growth factors with a spatiotemporal controlled mechanism [589], or incorporating in the polymer matrix RGD-conjugated gold nanoparticles.[780] In addition, PLAs are among the pharmaceutical grade polymers that can

be extruded into filaments loaded with drugs to produce custom-made oral dosage forms or implantable drug-releasing systems. For example, printing PDLLA model disk geometries incorporating the antimicrobial nitrofurantoin was described in details by different articles [661-663].

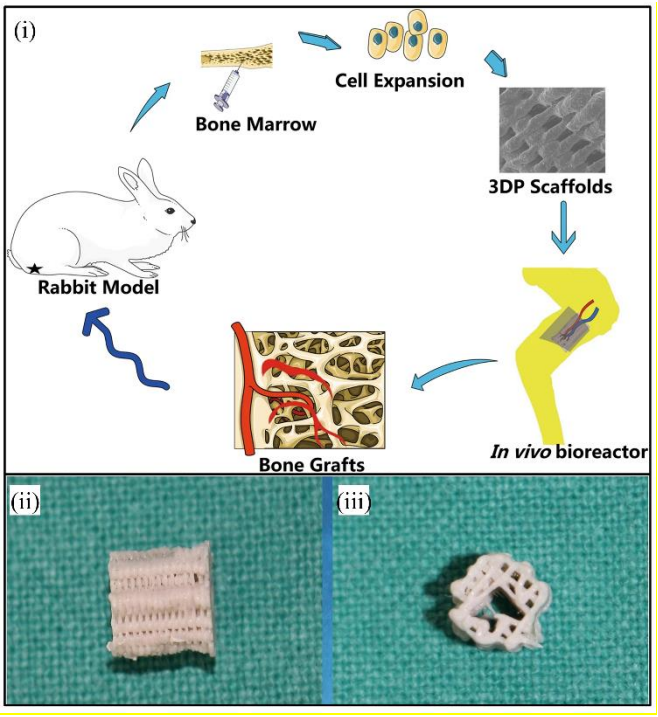

Figure 14. Bone development research on poly(α-hydroxy acids) scaffolds by FDM: simplified diagram of vascularized tissue engineered bone development through *in vivo* bioreactor culturing of scaffolds seeded with BMSCs (i), representative pictures of side view and top view of a channeled PLLA/Hap composite scaffold for *in vivo* cell culturing (reproduced with permission from [665].

Nanocomposite scaffolds by **FDM** were recently developed through solvent casting blending of **PLGA** (lactide/glycolide ratio: 65/35) and TCP in a 75:25 weight ratio before melt extrusion into a continuous filament.[664] The resulting scaffolds were coated with Hap and implanted in a rabbit femoral defect model showing good osteointegration, bone regeneration throughout the construct, and marked biodegradation after 12 weeks. Another study reported almost complete degradation of PLGA (lactide/glycolide ratio: 50:50) scaffolds fabricated by pneumatic ME-AM after 8 weeks of their implantation in a rabbit tibia model (**Figure 15a**) [215]. Since this degradation rate is too fast for bone TE, a few articles described the processing of PLGA blended with PCL (typically in a 1:1 weight ratio) by means of pneumatic ME-AM. For instance, Hong *et al*. [595] showed that the surface-functionalization of PCL/PLGA scaffolds by means of RGD fused on a coating of mussel adhesive proteins significantly enhanced the attachment, proliferation, and osteogenic differentiation of human ASCs. Another study demonstrated that by including TCP into PCL/PLGA scaffolds fabricated by mechanical

pressure ME-AM, the resulting compressive strength was increased and bone regeneration was enhanced after implantation in a rabbit calvarial defect model.[582] The same approach was used to manufacture PCL/PLGA/TCP membranes for guided bone regeneration in beagle implant models [666, 667]. Song *et al*. [668] dispensed an alginate hydrogel, containing PLGA microspheres loaded with the immunosuppressive drug cyclosporin, between strands made of a PLGA/PCL blend that were fabricated by ME-AM. The resulting 3 layers-integrated construct was seeded with xenogeneic cells (i.e., human lung fibroblasts) and subcutaneously implanted into the BALB/c mouse, resulting in significant suppression of T-cell-mediated rejection for 4 weeks.

Zhou *et al*. [114] were the first to report the possibility of obtaining PLA scaffolds endowed with a dual-scale porosity by a sequential application of **FDM and gas foaming**. They successfully integrated macropores (100–800 μm) determined by the designed lay-down pattern, with interconnected micropores (1–10 μm) in the polymer matrix formed by submitting the printed scaffold to CO_2 saturation and foaming. Marascio *et al*. [213] further developed this approach by submitting PLA-based filaments to CO_2 saturation and then achieving polymer gas foaming during FDM due to the high processing temperature (**Figure 16a**). This method was validated by developing PLLA/TCP and PLACL scaffolds with macropore size of tens of microns and composed by strands with an interconnected microporosity in their cross-section.

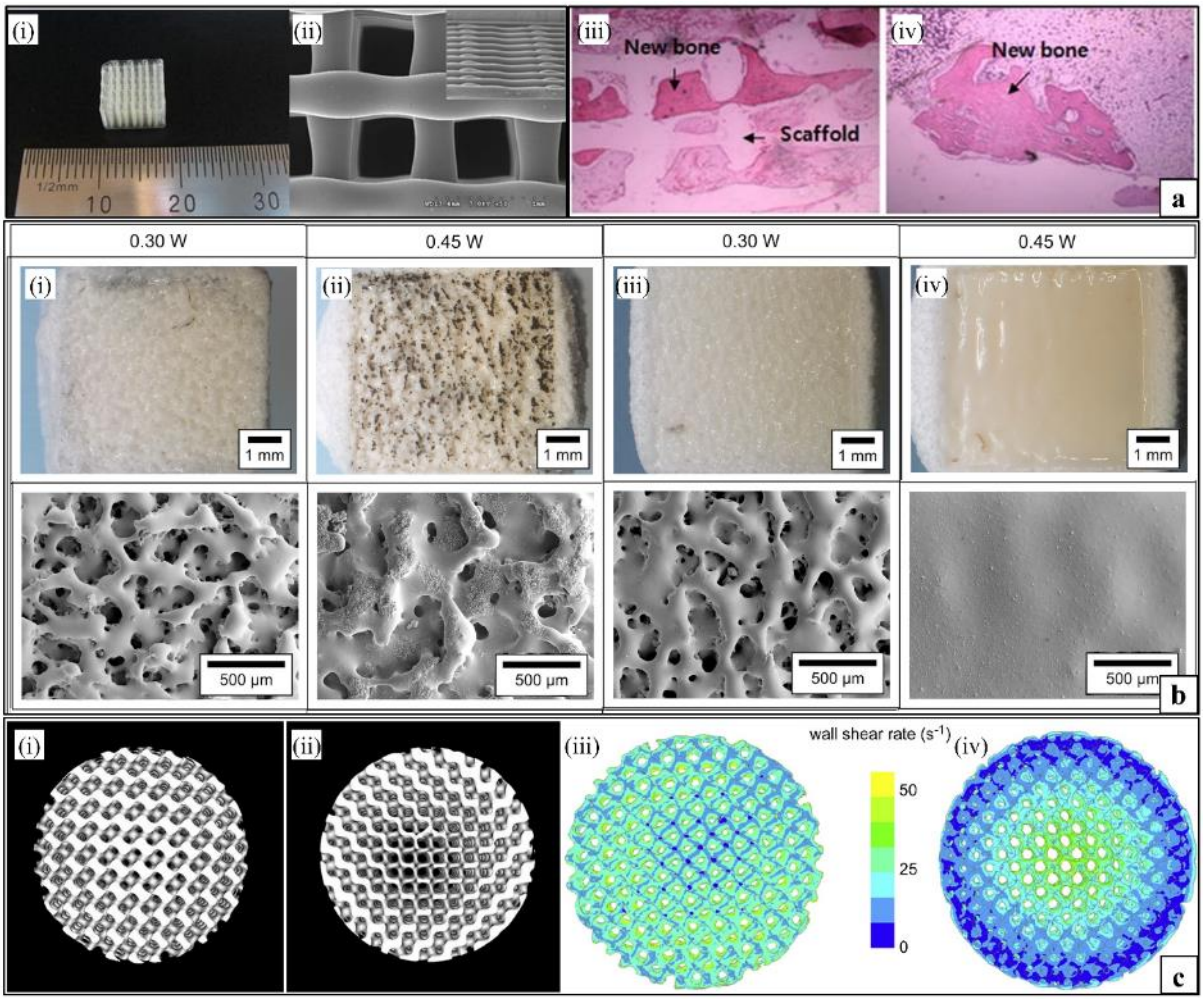

Figure 15. AM of poly(α-hydroxy acids). (a) PLGA scaffolds by FDM: picture (i) and SEM micrograph of top view (inset high magnification micrograph shows scaffold lateral view) (ii) of 3D scaffolds; histological specimens stained with hematoxylin and eosin (×40) of PCL (iii) and PLGA (iv) constructs at 8 weeks after implantation (reproduced with permission [215]). (b) PDLLA/TCP composites (50:50 weight ratio) by SLS: light microscope and SEM images of the top surfaces of test specimens (6×6×6 mm) for different laser power settings; batch 1 with higher Mw, higher polymeric particles size, and lower ceramic particle size (i) and (ii) showed signs of carbonization (black dots) and a more porous surface than batch 2 (iii) and (iv) (reproduced with permission [166]). (c) PDLLA derivative scaffolds by SLA: top-view µCT-visualization and thresholded z-stacks of confocal microscopy images (500 µm thickness) showing the distribution of cells densities and wall shear rates in isotropic (i) and (iii) and gradient (ii) and (iv) scaffolds (reproduced with permission [681]).

Xiong *et al*. [255] extruded a dioxane solution of PLLA in which TCP was suspended by using a low-temperature deposition **SE-AM** system. The subsequent sublimation of dioxane created a microporosity in the polymeric matrix forming a dual-scale porosity. Similar technological approaches were adopted to fabricate PLGA [671], PLGA/TCP [596], and PLGA/pearl composite scaffolds [597]. A multi-nozzle low-temperature deposition system was employed to obtain gradient compositions and morphologies in PLLA scaffolds, as well as to load them with BMP-2 [670]. 12 weeks after their implantation, the developed scaffolds were effective in

repairing a 15-mm segment defect created in a rabbit radius model. However, the described SE-AM approaches did not allow an accurate control over deposition details and the resulting scaffold porous structure. Serra *et al*. [261] achieved enhanced resolution of the deposition parts by employing PEG as a plasticizer to facilitate PDLLA solution extrusion in air without any post-processing treatment (**Figure 16b**). The scaffolds could be loaded with CaP particles after their suspension in the starting chloroform solution, leading to increase in surface roughness, hydrophilicity, and adhesion of primary MSCs. The variation of PEG percentage in the solution could be exploited too to vary scaffold surface roughness, wettability, mechanical properties, and biodegradation rate [262]. This approach was further developed to fabricate a biphasic osteochondral construct, composed of a PDLLA scaffold coupled to a PDLLA/BG composite scaffold, that was subcutaneously-implanted in a mice model for a preliminary *in vivo* evaluation [590]. The potential of SE-AM for novel drug delivery systems development was shown by developing a multilayer system composed by a dexamethasone disodium salt-loaded PVA layer sandwiched between PLGA layers [106]. Mironov *et al*. [672] recently described a novel CAWS method for scaffold fabrication based on the controlled deposition of a tetraglycol solution of PLGA directly into an ethanol bath. A solvent-cast AM approach was followed to fabricate different kinds of 3D self-supporting microstructures (e.g., square spiral, circular spiral, micro-cup, and layered scaffolds) by extruding a concentrated PDLLA solution in a highly volatile solvent (i.e., dichloromethane) [232]. In addition, an **inkjet printing** process was lately employed to deposit a N,N-dimethylformamide solution of PLGA on a PS substrate for patterning human ASCs adhesion [669].

Various efforts have been spent on applying **SLS** to PLAs for the fabrication of porous scaffolds, possibly in combination with bioceramics [781]. In particular, 3D scaffolds made of PLLA [673], also loaded with carbonated Hap [179, 674, 675], or PLGA/TCP [598] were successfully fabricated. However, limited polymer particles fusion generally resulted in marked porous defects that worsened the mechanical answer of this kind of scaffolds (compression strength < 3MPa) [675, 782]. A high-density polymer matrix could be manufactured when PDLLA was completely melted [676]. In general, with increasing laser power unwanted porosity decreased until a fully coalesced structure was obtained, with the risk, however, of local carbonization. PDLLA/TCP composites (50:50 weight ratio) with a close and dense surface morphology can be obtained by melting the polymer powder in order to glue the ceramic particles together [173]. In this case, a small polymer particle size, a large filler particle size, as well as a low polymer Mw can allow melt viscosity and sintering rate suitable to fabricate dense parts (**Figure 15b**) [166]. In 2004 Antonov *et al*. [172] reported on an AM method called surface-SLS (SSLS)

based on near-infrared (λ=0.97 μm) laser radiation of PDLLA particles that were loaded on the surface with carbon microparticles to enhance localized heating. The authors demonstrated that it was possible to load the scaffold with Hap or the ribonuclease A enzyme without compromising its activity, as well as to change scaffold topography by varying polymeric particles size and carbon content [178]. The use of carbon does raise issues of concern regarding safety and biocompatibility. However, optimized PDLLA scaffolds fabricated by SSLS sustained human fetal femur-derived cells viability, growth, and osteogenesis *in vitro*, and favored bone formation when implanted into murine critical-sized femur segmental defects [677]. Moreover, these scaffolds were seeded with human bone marrow MSCs and subcutaneously implanted in rats maintaining cells adhesion for 90 days without cytotoxicity signs [678]. SSLS approach was also suitable to fabricate scaffolds made of composites with TCP/PDLLA weight ratio up to 80:20, showing compressive properties comparable to those of trabecular bone [591].

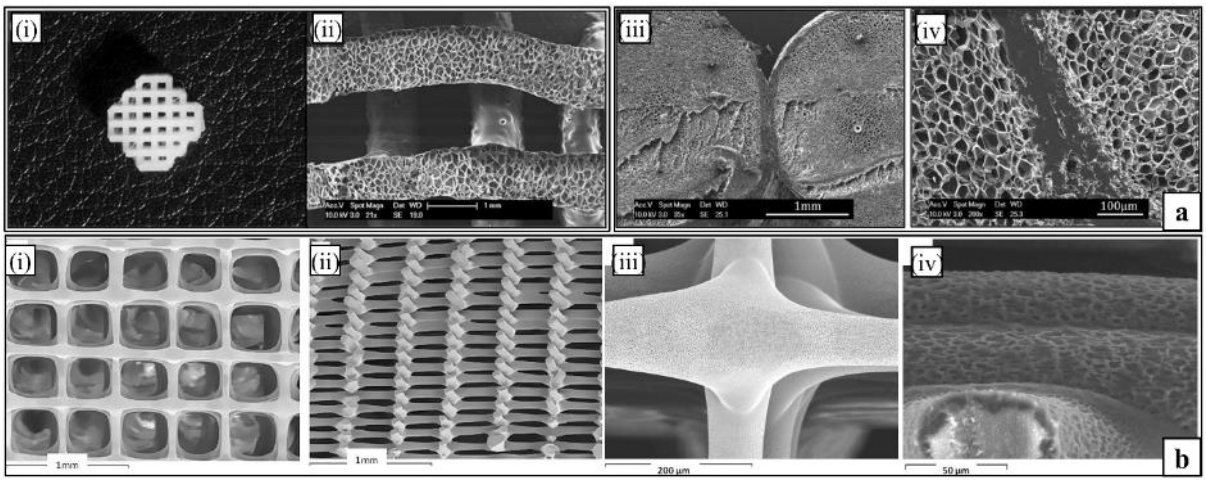

Figure 16. PLA scaffolds with dual-scale porosity. (a) PLLA/TCP foamed scaffold structure by sequential gas foaming and FDM: picture (i) and SEM micrographs of top-view (ii) and fiber-fiber contact points (iii) and (iv) (reproduced with permission [213]). PDLLA scaffolds by SE-AM: SEM micrographs at different magnifications of top-view (i), transversal cross-section (ii), fiber-fiber contact point (iii) and fiber surface microporosity (reproduced with permission [261]).

One of the earliest attempts to apply **BJ** to poly(α-hydroxyacids) involved the controlled deposition of chloroform to pattern PLGA powder surfaces and to fabricate 3D porous scaffolds by combination with salt leaching.[679] In addition, several efforts have been spent on the use of BJ for fabricating drug-eluting PLA implants for the treatment of infected bone [783]. Notably, PLLA implant prototypes loaded with a drug (e.g., antibiotic and antituberculosis agents) that was either dispersed in the polymeric matrix or contained in an inner reservoir were developed [200, 784]. For instance, Huang *et al*. [200] added the antibiotic levofloxacin to a

binder solution composed of a mixture of acetone and ethanol, in order to fabricate PLLA implants with different loading design, drug distribution, and *in vitro* release kinetics (**Figure 12b**). By following similar approaches, a set of implants with complex layered structures were developed in order to achieve a sequential release of different antibiotics [201, 202, 680]. As an example, levofloxacin and tobramycin were recently incorporated into multi-layered concentric cylinders made of PDLLA to achieve a sustained and programmed multi-step release kinetics optimized for chronic osteomyelitis treatment [202].

One of the first published studies on **SLA** application to PLA derivatives involved photocrosslinking fumaric acid monoethyl ester-functionalized three-armed PDLLA oligomers using NVP as diluent and comonomer [145]. Other studies were based on methacrylate end-functionalized PDLLA and its copolymers. In particular, PDLLA oligomers with 2, 3, or 6 arms were synthesized, end-functionalized with methacryloyl chloride, and photo-crosslinked in the presence of ethyl lactate as a non-reactive diluent, to fabricate high-resolution 3D scaffolds supporting *in vitro* preosteoblast cells proliferation [129, 592]. These photo-polymerizable PDLLA macromers were investigated for the fabrication of scaffolds with isotropic or gradient pore size to control the distribution of cells seeded under perfusion (**Figure 15c**) [681]. Porous scaffolds built by employing a poly(d,l-lactide-*co*-ε-caprolactone) (PDLACL)-based resin showed excellent fidelity to the CAD design and controlled compressive properties ranging from rigid and strong to highly flexible and elastic [593]. Composite scaffolds with different pore sizes were also fabricated by mixing Hap particles to photocurable methacrylate end-functionalized PDLLA oligomers [594, 682, 683]. Hap nanoparticles inclusion increased the scaffold mechanical properties and osteoconductive potential without affecting the morphology of the structure [594, 683]. Ultrafine fibers scaffolds for soft TE with high resistance to tensile dynamic loading were recently developed by processing poly(l-lactide-*co*-ε-caprolactone-*co*-acryloyl carbonate) by means of MEW followed by UV photocrosslinking [643].

4.2.3 Polypropylene fumarate (PPF)

Owing the presence of a double carbon-carbon bond in its repeating unit, which allows crosslinking into a covalent polymer network, PPF is the most investigated synthetic biodegradable polymer for photoreactive AM strategies.

Synthesis route. PPF is a linear polyester consisting of repeating units containing one unsaturated bond in trans configuration (**Figure 10c)**. Optimized protocols to synthesize PPF on a lab scale are based on a two-step reaction of DEF and propylene glycol through a bis(hydroxypropyl) fumarate diester intermediate [785]. Since its development in the late

1980's [786, 787], various lab procedures for the synthesis of PPF for biomedical applications have been developed. However, many shortcomings related to the step-growth polymerization of PPF are hindering its moving into clinical materials market. Indeed, issues influencing the final material properties, such as low conversion, poor control over molecular mass distribution, conjugate-addition side reactions, and unwanted crosslinking, are reported in literature [788].

Photoreticolation and biomedical use. Photochemical crosslinking of PPF has been broadly explored to obtain biomedical materials with suitable mechanical and degradation properties. The crosslinked network can be tailored by varying the molecular properties of the starting macromers, such as the Mw, which is typically in the range 500-4000 Da [789, 790]. PPF photoreaction can be achieved in the presence of different crosslinking agents, such as NVP [789], PPF-diacrylate (PPFDA) [791], and methyl methacrylate [792]. Since PPF oligomers are in a liquid state before crosslinking, custom-shaped implants can be easily obtained by molding before crosslinking.

Given its relatively high stiffness (i.e., compressive modulus up to 200 MPa and tensile modulus up to 1 GPa [793, 794]), crosslinked PPF has been considered for hard tissue repair. In addition, its copolymerization with other biodegradable monomeric units (e.g., l-lactide) was investigated as an effective route to tune the processing, morphological, thermal, and mechanical properties of the resulting biodegradable construct [795]. PPF biocompatibility to bone-forming cells was demonstrated both *in vitro* and *in vivo* [796, 797]. PPF undergoes *in vivo* bulk degradation through hydrolysis of the ester linkages into propylene glycol and fumaric acid, which are readily removed from the body, even if the acidic degradation products can elicit inflammatory response [790]. Factors affecting crosslinked PPF biodegradation are, among others, the Mw of PPF macromer, the crosslinking agent, the crosslinking density, the scaffold porosity and pore size, the environmental pH, and the presence of additives. For instance, the biodegradation rate of crosslinked PPF-diacrylate was shown to decrease by increasing the crosslinking density [798]. Like in the case of PLAs, ceramic fillers inclusion can act as a pH buffer inhibiting polymer autocatalytic degradation [799]. Composites based on PPF loaded with bioactive ceramics (e.g., Hap and TCP) were investigated as scaffolding materials with improved osteoconductivity, mechanical properties, and hydrophilicity [792, 799-802]. Different studies have investigated both *in vitro* and *in vivo* the combination of PPF matrices with PLGA microspheres loaded with the osteogenic peptide TP508 [790, 803-805] In particular, composite PPF scaffolds with optimized TP508 release kinetics resulted in 80% of defect length bridging after 12 weeks of implantation in a rabbit radius model [804].

AM application. Most of the first attempts to fabricate biodegradable devices by **SLA** focused on processing PPF diluted in its monomer (i.e., DEF) to reduce resin viscosity (**Figure 17a**) [684]. Both vector scanning and DLP techniques have been investigated for PPF reticulation under selective UV irradiation by employing a free radical photoinitiator (e.g., Irgacure 819), typically without including a light absorber. Cooke *et al*. [567] were the first to employ SLA for processing PPF into implants with a predefined shape. The employment of µSLA vector or projection scanning allowed the fabrication of high resolution PPF structures (**Figure 17b**) [599, 793]. Lee *et al*. [599] systematically investigated the effect of µSLA vector scanning speed and working temperature on solidification depth of PPF/DEF mixtures with 75:25 or 50:50 weight ratio. They eventually fabricated 3D scaffolds with different pore size characterized by a compressive ultimate strength (20-40 MPa) and an elastic modulus (200-300 MPa) comparable to those of trabecular bone. Various studies investigated PPF scaffold porous structure tuning to affect cell behaviors. For instance, the possibility of controlling the proliferation of pre-osteoblast cells by varying PPF scaffold pores size and architecture was demonstrated [600]. Another experimental investigation showed that changes in DEF concentration and pore size significantly affected scaffold mechanical stiffness and osteogenic signal expression of rat BMSCs [601].

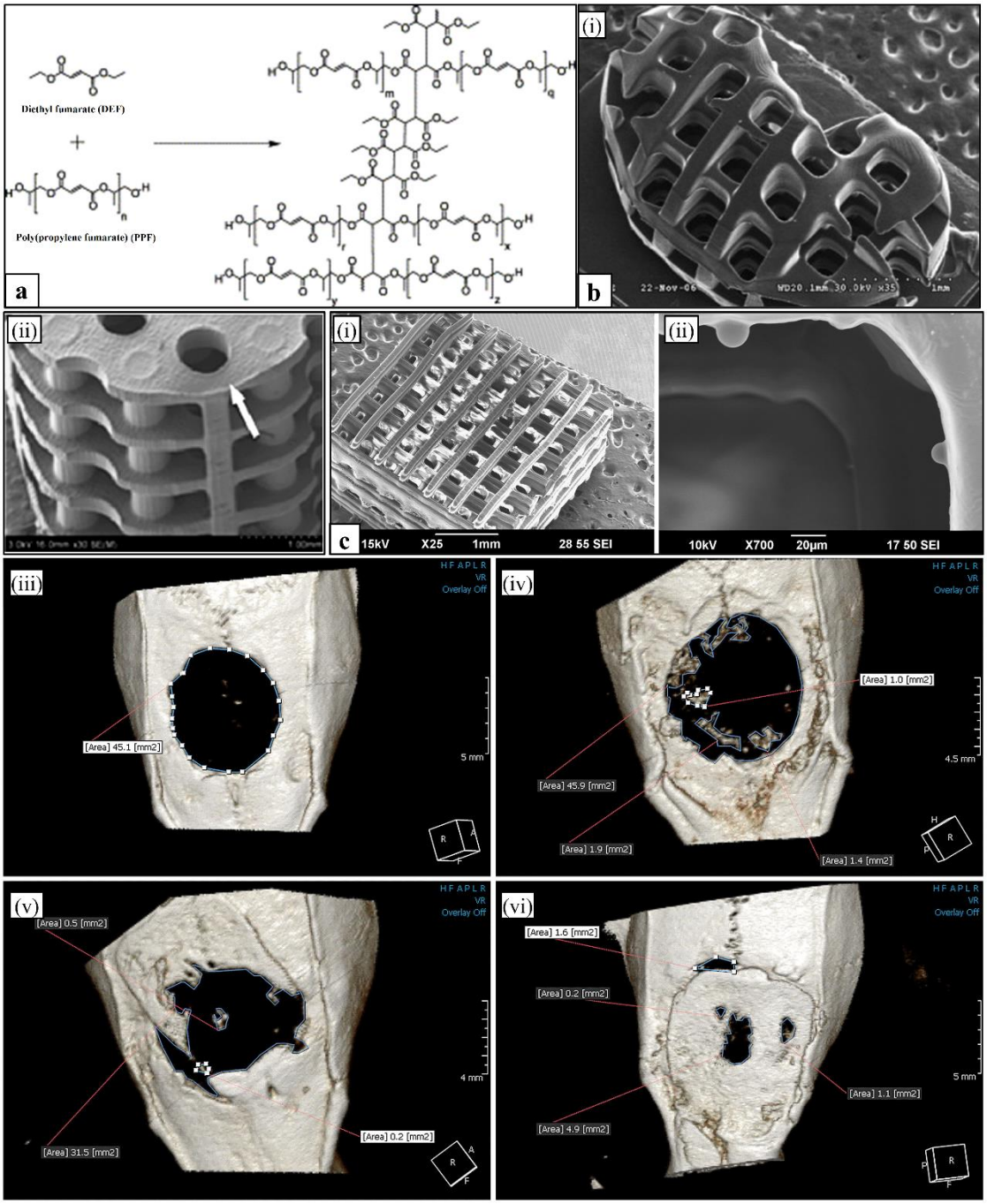

Figure 17. (a) Schematics of polyaddition reactions that occur between PPF and DEF, including the direct addition between two PPF chains and the crosslinking of two PPF chains by polymerized DEF (reproduced with permission [793]). (b) Customized PPF structures by SLA techniques: SEM micrographs of kidney scaffold (i) (reproduced with permission [684]), cylindrical scaffold with continuous channel geometry (ii) (reproduced with permission [601]). (c) Biofunctionalized PPF scaffold by SLA: SEM micrographs at different magnifications of PPF scaffold incorporating BMP-2-loaded PLGA microparticles (i) and (ii) (protrusion in (ii) are microparticles embedded in the PPF matrix); micro-CT images of rat cranial bone at 11 weeks after scaffold implantation: negative control (iii), PPF scaffold by a combined particulate leaching/gas foaming method (iv), PPF scaffold by SLA (v), and BMP-2-loaded PPF scaffold by SLA (vi) (reproduced with permission [687]).

PPF scaffolds with a 3D porous architecture obtained by alternating layers composed of either lattices or columns were dip coated with biomimetic apatite and RGD to biofunctionalize the surface [138]. *In vitro* investigations showed that preosteoblast cells proliferation in these biofunctionalized scaffolds was improved compared to non-coated samples. Similarly, Shin *et al*. [139] submitted PPF/DEF scaffolds to three different peptide coating modifications that altered the material hydrophobic surface properties and promoted cell adhesion. This kind of scaffolds were also functionalized by suspending BMP-2-loaded PLGA microspheres in the PPF/DEF resin (**Figure 17c**) [687]. The effective release of BMP-2 was assessed both *in vitro* and *in vivo* in a rat calvarial defect model, leading after 11 weeks to significantly increased bone formation in the growth factor-loaded group compared to the non-loaded one. BMP-2-loaded PPF scaffolds were also seeded with human ASCs and implanted in rat crania showing that the synergistic effect of growth factor release and cell differentiation led to enhanced bone formation [688]. Dadsetan *et al*. [685] evaluated the role of a coating made of a calcium phosphate (i.e., either TCP, carbonate HA, or biphasic CaP) and the simultaneous surface loading with rhBMP-2 on the *in vivo* bone regeneration capacity of porous PPF scaffolds. After implantation in a critical-size calvarial defect model, enhanced bone healing was observed in the case of rhBMP-2-loaded scaffolds. By using a different approach, PPF scaffolds by SLA were either spray-coated or dip-coated with a PLGA solution containing a dispersion of Hap or TCP. The hybrid coating enabled new bone ingrowth within 4 weeks after implantation of scaffolds in a canine femoral multi-defect model [686].

PPF was also recently employed to validate a continuous DLP system for the fabrication of scaffolds through the use of a dye-initiator package, i.e., TiO_2 and bis (2,4,6-trimethylbenzoyl)phenylphosphine oxide, facilitating high accuracy along the Z dimension [602]. In this way, PPF/DEF scaffolds with high resolution, accurate pore geometries, and high compressive modulus (i.e., 135 MPa) were fabricated. In addition, Dilla *et al*.[806] developed diblock and triblock copolymers of PEG-PPF that were processed by DLP into hydrogels with a 10-fold increase in elongation at break (>150%) compared to those fabricated by traditional DEF-based AM. A novel approach was developed to fabricate PPF scaffolds loaded with a layered gradient of Hap by means of **SE-AM** coupled with photoreticolation [603]. For this purpose, Hap was suspended in the presence of a surfactant in a solution of PPF, DEF, and Irgacure, and UV crosslinking was carried out after extrusion of each layer.

4.2.4 Polyurethanes (PUs)

PUs have been used over the past 50 years in the biomedical industry as flexible and rigid materials for different applications, including cardiovascular devices, spinal grafts, breast implants, and more recently, biodegradable tissue scaffolds.

Synthesis and chemical structure. PUs are a class of polymers characterized by urethane groups (—NHCOO—) in their chemical structure, obtained by reaction of an aliphatic or aromatic diisocyanate, a macrodiol (i.e., a polyether, polyester, or polycarbonate, with 1000 < M_w < 5000 Da), and a chain extender which can be a diol or a diamine with a low M_w (typically < 400 Da). Poly(ether urethanes), e.g., those obtained from PEG or poly(tetramethylene ether) glycol, show high flexibility, hydrolytic resistance, low oxidative and thermal stability [807]. Poly(ester urethanes) (PEUs), e.g., those synthesized from poly(ethylene adipate) diols or poly(butylene adipate) diols, show higher mechanical strength, and are susceptible to hydrolysis of the ester groups [808]. Poly(carbonate urethanes), e.g., those obtained from reaction of poly(hexamethylene carbonate) diols, have good mechanical properties and hydrolytic resistance, even if they can undergo long-term *in vivo* enzymatic and oxidative degradation [809].

PUs can be synthesized through either a one-step or a two-step method. In the first one, a diisocyanate, a macrodiol, and a chain extender are mixed to react together. The second method, which is most often used thanks to the possibility of achieving a better control on the resulting macromolecular structure, involves first reacting a macrodiol with a slight excess of a diisocyanate to obtain a prepolymer, which is then reacted with a chain extender. In this way, a linear copolymer with alternating blocks of soft and hard segments is eventually synthesized [810].

In the case of biodegradable PUs, the soft segment is typically represented by an aliphatic polyester, (e.g., PCL, PGA, or PDLLA), a copolymer between two aliphatic polyesters, or a poly(ester-ether) copolymer (e.g., PCL-*co*-PEG), while a linear diisocyante, e.g., 1,6 hexamethylene diisocyanate (HMDI), is employed as the hard segment to avoid carcinogenic products from degradation of aromatic units (**Figure 18**). The resulting copolymers are also referred to as thermoplastic PUs (TPUs), since they can soften, melt, and be processed under heat application, in addition to the possibility of being processed upon dissolution in a proper organic solvent. So-called waterborne PUs are synthesized by incorporating in the chemical structure hydrophilic monomers containing ionic functionality, including quaternary ammonium, carboxylate, or sulfonate groups, in order to achieve stable dispersions of copolymer particles in a continuous aqueous phase, also without recurring to emulsifiers [811].

Thermosetting PUs have been also synthesized by using a multifunctional chain extender, or introducing a crosslinking agent [812].

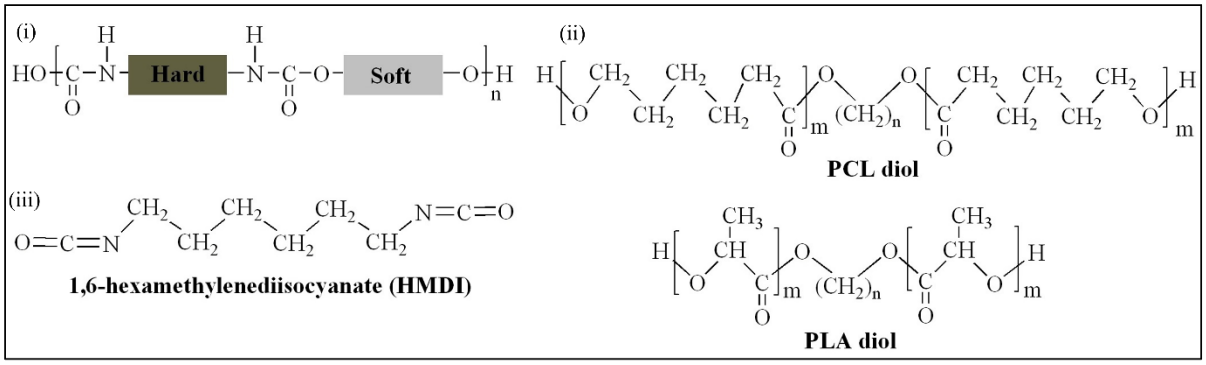

Figure 18. General chemical structure of biodegradable poly(ester urethanes) (PEUs) (i); chemical structure of representative macrodiols and a linear diisocyanate commonly used for PEUs synthesis.

Soft segments are composed by reacted macrodiols with a low T_g, in a rubbery state at room temperature, while hard segments are composed by diisocyanates reacted with the chain extender, organized in semicrystalline or highly ordered domains with high T_g. Microphase separation due to incompatibility between soft and hard segments occurs as a consequence of their different polarity and free energy [813]. Hard segments form hydrogen bonds and act as dispersed rigid fillers and physical crosslinks, conferring the material with high material elastic recovery. By varying different factors, such as the length and chemical structure of macrodiols, the nature of the chain extender, and the NHCOO/OH ratio, material mechanical response can be tuned from low-modulus elastomeric to rigid behavior [814]. Other polymer properties, such as thermal stability, hydrophilicity, biodegradation rate, and solvent solubility, can be varied accordingly.

Biomedical use. The tunable elastomeric properties of PUs have attracted great interest in different biomedical areas requiring advanced mechanical performance, such as high flexibility and fatigue resistance. For instance, PUs are used for the manufacturing of elastics and cavity liners for dentistry, cardiovascular catheters and cardiac valves, breast implants, wound dressing membranes, bone adhesives, and condoms [815]. Cardiothane, a silicone-urethane copolymer invented by Kontron Inc., Chronoflex®, a class of poly(carbonate urethanes) marketed by AdvanSource Biomaterials, Tecoflex®, aliphatic polyether-based TPUs from The Lubrizol Corporation, are only few examples of the wide variety of biomedical PUs available in the market. Biomedical applications of biodegradable PUs are mainly related to tissue engineering and drug release systems [816]. As a consequence, their chemistry has been optimized to meet relevant requirements in terms of biocompatibility, degradation kinetics

tailored to specific tissue formation rate or drug release profile, nontoxicity of absorbable degradation products, and tissue-mimicking mechanical properties.

The overall *in vivo* degradation rate of PEUs is governed mainly by the hydrolysis of the ester groups, yielding α-hydroxy acids degradation products [817]. Hydrolysis of the urethane groups in the hard segments, resulting in urethane and urea fragments with terminal acid groups, occurs at a slower rate. The concentration of acidic degradation products related to bulk hydrolysis can cause autocatalyzed degradation and adverse tissue reaction [818].

AM application. Different AM technologies have been investigated to process biodegradable PUs and their composites with synthetic polymers, polysaccharides, or proteins [819, 820]. One of the first attempts to apply AM to PUs was made in 2004 and relied on **FDM** to process PCL-based PEUs into porous scaffolds [689]. However, the preparation of continuous PU filaments with a consistent diameter suitable for reproducible FDM processing is still a challenge nowadays [690]. This is due to some inherent shortcomings related to thermal extrusion of PUs, including pirohydrolysis of polyester segments, low thermal and oxidative polyether stability, as well as the elastomeric behavior of PEUs, which can hinder a steady extrusion process for producing and processing an FDM filament (see section 3.4). Anyway, Güney *et al*. [691] recently developed a TPU based on a PCL-*b*-PEG-*b*-PCL triblock copolymer and HMDI, that behaved like a tough hydrogel and could be processed by FDM. Blending with a more rigid polymer is an effective way to achieve filament viscoelastic properties suitable for FDM. By adopting this strategy, Castro *et al*. [693] processed filaments made from a PEU blended with PVA, the latter leached out from the scaffolds by water immersion, leaving behind a porous microfilamentous surface topography exploitable for directional cell migration. FDM was also recently applied to process a PEU based on a PCL-*co*-PDLLA soft segment and a block urethane hard segment, composed by 1,4-butanediisocyanate and 1,4-butanediol, to fabricate scaffolds with two different structures (500 μm pore size and 90° or 60° deposition angle) [692]. The scaffolds were shown to support the dynamic compression-relaxation loads physiologically applied onto the knee, and to promote the chondrogenic differentiation of human BMSCs (**Figure 19a**).

SE-AM represents the most exploited approach in this context. Agrawal *et al*. [694] employed a CAWS technique to extrude a dimethylformamide solution of a blend of two aromatic PEUs directly into a water bath. The fabricated 3D porous scaffold was then impregnated with an epoxy-based hydrogel to form a fiber-reinforced gel with optimized mechanical strength, modulus, and toughness. Another article described the layer-by-layer deposition on metallic substrates of a hexafluoro-2-propanol solution containing a poly(ester urethane urea) and

paclitaxel, to develop novel drug-releasing coatings for surgical implant devices [695]. Xu *et al*. [696] deposited at a low temperature (-28 °C) a dioxane solution of a PU based on PCL, PEG, and HMDI, to fabricate 3D macrochanneled and porous scaffolds. The fabricated structures were then submitted to freeze drying for solvent removal, resulting in the formation of a microporous matrix morphology. This approach was further developed through the use of a double nozzle AM system allowing the simultaneous deposition of the PU organic solution and an aqueous solution of gelatin, to fabricate a hybrid construct engineered as a model for bioartificial liver manufacturing [287]. The double nozzle system was also exploited for double-layer nerve conduits fabrication through a sequential deposition of an acetic acid solution of collagen and a dioxane solution of PU, then stabilized by means of chemical crosslinking and freeze-drying, respectively [697, 698]. Another application of this dual-deposition strategy was the fabrication of tubular PU constructs sandwiching a gelatin/alginate/fibrinogen hydrogel laden with ASCs [699]. In this case, a cell-compatible organic solvent (i.e., tetraglycol) was employed for PU, while a cryoprotectant (i.e., DMSO or glycerol) was incorporated in the hydrogel phase to guarantee cell survival during fabrication and freeze-thawing steps. More complex sandwiched geometries endowed with an intrinsic grid network and branched channels for oxygen and cell nutrients supply were also developed [288, 289]. Merceron *et al*. [821] used a four cartridges system to fabricate a single integrated muscle–tendon unit by co-printing a TPU with a C2C12 myoblasts-laden hydrogel, and PCL with a hydrogel encapsulating NIH3T3 fibroblasts.

The employment of aqueous dispersions of waterborne PUs enables direct cell-compatible **bioprinting** approaches. Some studies focused on the copolymerization of polyester diols with isophorone diisocyanate (IPDI), as a hard segment, and two chain extenders, i.e., ethylenediamine (EDA), and 2,2-bis(hydroxymethyl) propionic acid (DMPA), to synthesize thermoresponsive PUs that could be dispersed in water as nanoparticles and form a gel when printed at physiological temperature [700-702]. By varying the composition of the soft segment (i.e., PCL, PCL-*co*-PLLA, PCL-*co*-PDLLA, PLLA-*co*-PEG, or PDLLA-*co*-PEG) it was possible to tune nanoparticles size and zeta potential, the rheological properties of the dispersion, and the mechanical properties of the printed cell-laden hydrogel. Stacked gel fibers encapsulating either murine neural stem cells [701] or human umbilical cord derived MSCs [702] were developed by following this approach. Blending soy protein with this kind of thermoresponsive PU dispersions was proved to be an effective strategy for fastening gel formation process and enhancing structural integrity during the layer-by-layer deposition [703]. The liquid-frozen deposition manufacturing previously described was applied also to

waterborne PUs. For instance, a PCL diol and a polyethylene butylene adipate diol (2:3 molar ratio) were reacted as soft segment with the previously described IPDI/EDA/DMPA hard segment chemistry to obtain a water dispersion that was printed on a platform maintained at -30 °C. The addition of PEG as a water-leachable viscosity enhancer [822], or HA as a thickener and constitutive blending material [823], enabled the optimization of PU dispersion rheological properties. In this way, the porous structure of the resulting scaffolds, possibly loaded with growth factors, was tailored to chondrogenic tissue engineering (**Figure 19b**).

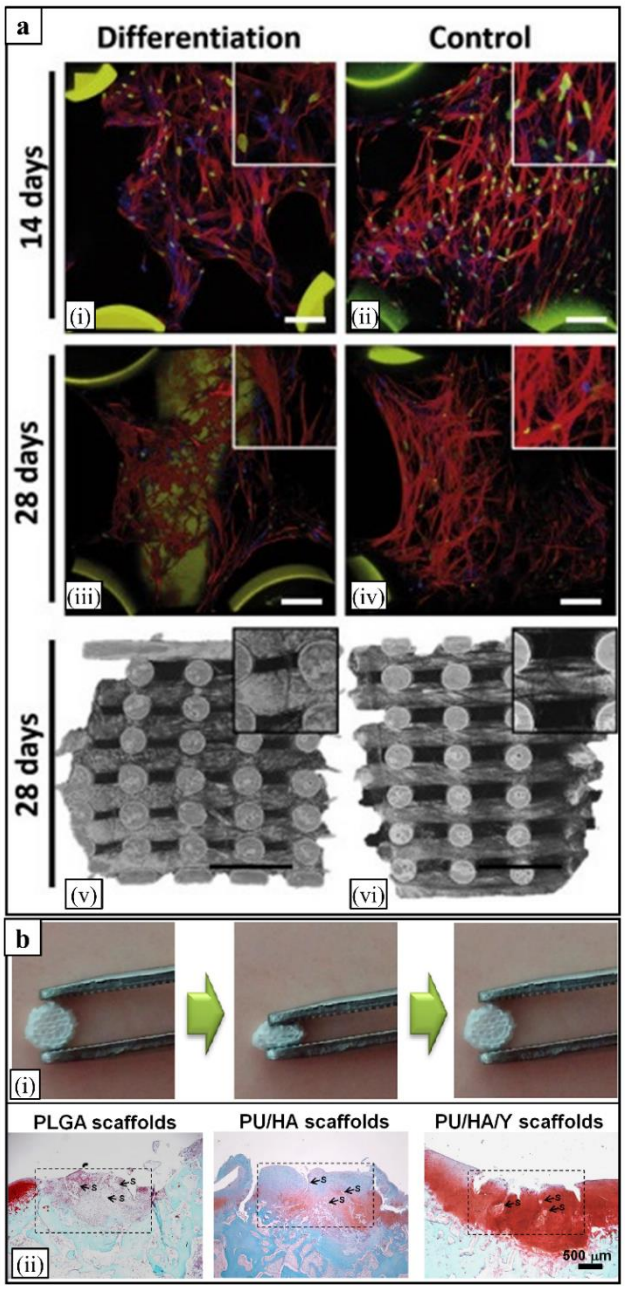

Figure 19. AM of biodegradable PUs. (a) CLSM micrographs of human BMSCs cultured *in vitro* for 14 and 28 days in basal (control) (i) and (ii) and chondrogenic medium (iii) and (iv) on FDM-fabricated PEU scaffolds, BMSCs were immunostained for F-actin (Phalloidin, red), nucleus (Hoechst, yellow), collagen I (green) and collagen II (blue), scale bar is 100 µm; µCT images of PEU scaffolds after 28 days of culture in differentiation (v) and basal medium (vi),

scale bar is 1 mm and insets are 700x700 μm (reproduced with permission [692]). (b) Representative pictures showing the high flexibility and excellent shape recovery after compression of waterborne PU/HA scaffolds fabricated by SE-AM (i); histological images based on safranin O/fast green stained sections from the regenerated cartilage in New Zealand white rabbit MSCs-seeded scaffolds 1 month after their implantation into an osteochondral defect created in the rabbit knee joints: PU/HA scaffold loaded with the chondrogenic induction factor Y27632 in comparison with PU/HA and PLGA scaffolds, the box indicates the repair region, S: scaffold debris (reproduced with permission [823]).

An **Inkjet printing** approach to pattern pH-sensitive PUs based on PCL diols was developed by employing an ionizable chain extender. It involves the controlled deposition of an acid aqueous medium onto a film of an alkaline solution of the neutralized polymer that precipitates due to a local pH change. 2D patterns were fabricated with this method by employing HMDI as a hard segment and bicine as an ionizable chain extender [704], or methylene di-*p*-phenyl-diisocyanate and N,N-bis (2-hydorxyethyl)-2-aminoethane-sulfonic acid as a hard segment and an ionizable chain extender, respectively [705].

4.2.5 Other synthetic polymers

Poly(trimethylene carbonate) (**PTMC**) (**Figure 20a**) has been recently employed as a macromer functionalized with methacrylate end groups to enable SLA photocrosslinking. In addition, as previously mentioned, PTMC has been also investigated as a copolymer either with PCL [141, 142] or trimethylolpropane [142] to develop acrylate-endcapped macromers for SLA, as well as with PLA to achieve optimized melt rheological properties for FDM [708, 709]. Biocompatible PTMC is typically synthesized by ring-opening polymerization of trimethylene carbonate [824]. PTMC undergoes slow enzyme-mediated surface erosion enabling the maintenance of mechanical properties for long time, without sudden implant failure related to bulk degradation [825]. In addition, unlike poly(α-hydroxy acids), acidic moieties responsible of autocatalytic degradation and tissue necrosis are not produced upon PTMC degradation. PTMC is an amorphous polymer with a T_g ~ −17 °C, low Young's modulus (~3 MPa) and relatively high strain at break (~160%) [826]. As a consequence of its low stiffness, PTMC has been mainly employed in the biomedical area for soft tissue engineering, and in the development of copolymers, generally with glycolides, for applications as flexible sutures (Biosyn™) tissue fixation devices (Suretac™) and orthopedic screws (Acufex®) [827].

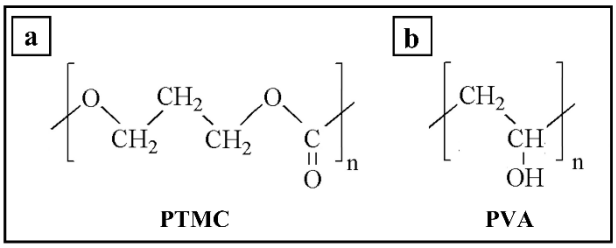

Figure 20. Chemical structure of potential biodegradable polymers under biomedical AM implementation. (a) Poly(trimethylene carbonate) (PTMC). (b) Poly(vinyl alcohol) (PVA).

Genev *et al*. [143] synthesized three-armed PTMC macromers by ring-opening polymerization and then reacted them with methacrylic anhydride to prepare a photocrosslinkable resin. They processed by **SLA** reactive formulations, composed of PTMC macromers with methacrylate end-groups (PTMC-MA), Hap particles, and propylene carbonate as a non-reactive diluent, to fabricate customized orbital floor implants. The variation of PTMC-MA/Hap ratio in this kind of formulations allowed the fabrication of porous scaffolds with tunable surface roughness, wettability, stiffness, *in vitro* cell adhesion, and *in vivo* bone healing in rabbits calvarial defects [144, 706]. By following the same approach, PTMC-based composite scaffolds loaded with up 51 wt.% β-TCP were endowed with a patient-specific shape for the regeneration of large mandibular defects (**Figure 21a**) [707]. PTMC porous constructs by SLA were also investigated *in vitro* as scaffolds for hASCs differentiation towards annulus fibrosus cells when exposed to growth factors under optimized cell seeding [828].

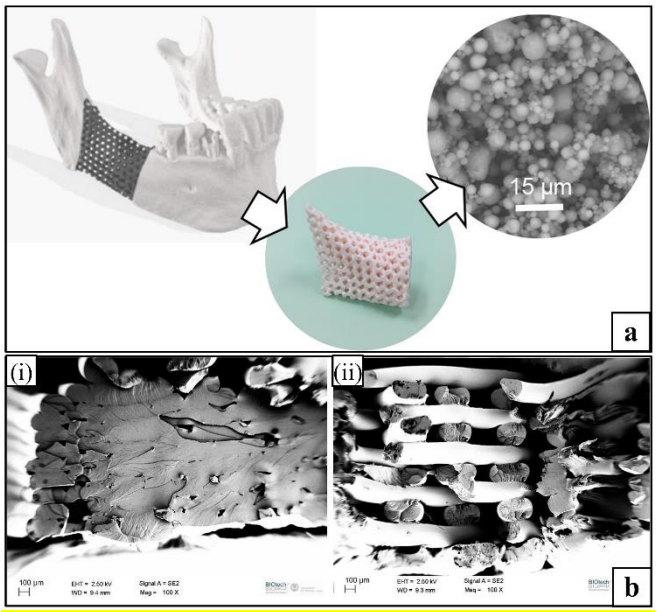

Figure 21. AM of PTMC: (a) engineering route from imaging data of a large mandibular defect to SLA manufacturing of a porous individualized implant made of PTMC/β-TCP [707]. AM of PVA: (b) representative SEM micrographs of fracture surface after tensile test of FDM-printed samples made of neat PVA (i) or PVA loaded with 5 wt.% nanocellulose (ii) [712].

Poly(vinyl alcohol) (**PVA**) (**Figure 21b**) is a hydrophilic vinyl polymer, typically manufactured on an industrial scale by free-radical polymerization of vinyl acetate, followed by alkaline hydrolysis (alcoholysis) of poly(vinyl acetate) [829]. PVA commercial batches can have a different deacetylation degree, in the range 70 to 99%, which significantly affects polymer water solubility, chemical properties, and crystallinity. Besides being employed in different industrial sectors, such as food packaging, cleaning and detergent products, and water treatment, PVA has FDA approval for clinical uses in humans [830]. It can be enzymatically degraded in aerobic and anaerobic conditions under the action of specific microorganisms [829, 831]. Although its biodegradability and/or elimination in animals is still under debate [832], PVA has been extensively investigated as a potential biodegradable polymer to develop biomedical hydrogels, often in combination with a wide range of natural or synthetic polymers [833].

As previously discussed, PVA has been used in aqueous binders for **BJ** of polysaccharides [8], as a hydrophilic matrix in multilayer drug-loaded systems by **SE-AM** [106], or as a water-leachable blend component in PEU filaments for **FDM** [693]. In addition, few recent studies focused on PVA as the main polymer matrix component for AM. Two recent articles by the same research group described the development of PVA filaments loaded with either carbon nanotubes [711] or cellulose nanocrystals [712], through blending in aqueous solution followed by drying and single screw extrusion. In both cases, a variation of the organic nanofiller content resulted in significant changes of T_g and mechanical properties of nanocomposites samples fabricated by **FDM** (**Figure 21b**). Another study dealt with the optimization of PVA-based aqueous inks formulated with the addition of additives (e.g., humectant and pigments), for **inkjet printing** of multilayer structures [710].

5 Conclusions

AM is revolutionizing the approach to a wide range of biomedical applications, including, among others, exoprostheses, surgical implants, tissue engineering, *in vitro* tissue modelling, and controlled drug release. The interest of the scientific and industrial communities is justified by the great versatility and tremendous technological potential of advanced AM strategies to customization of biodegradable systems composition, micro/nanostructure, macroshape, mechanical behavior, and functional properties.

Recent progress in the design and development of biodegradable polymers and relevant processing approaches is providing unique means for AM development of biomedical devices. Preclinical and clinical trials are giving promising results for the next generation of implantable

medical devices that will likely improve and save the life of thousands of adults and pediatric patients all around the world. In parallel, AM is supplying always new *in vitro* technological tools needed in the modern healthcare ecosystem for advanced diagnostics, pharmaceutical development, and tissue physiology studies. AM impact is also consolidating in the pharmaceutical industry, as witnessed by the presence in the market of relevant drug formulations and the growing scientific literature on this topic.

To date, many studies have reported the successful application of experimental protocols for processing natural polymers and their functional derivatives by means of different AM techniques. Industrial processing methods, as well as consolidated AM approaches, have been adapted and extended for fabricating 3D constructs based on proteins and/or polysaccharides, possibly encapsulating cells and other biologics. Various SLA and SE-AM technologies, together with relevant ad-hoc processing protocols are currently under industrial implementation to this purpose, and some of them are likely to be integrated in the next future in approved diagnostic and therapeutic procedures.

AM application to PHA is solving the great challenge of coupling the sustainable development concept, peculiar of natural polymers, with the advanced control over the fabrication accuracy and reproducibility achievable with aliphatic polyesters. In addition, the wide experience gained on synthetic polymers processing by conventional techniques is fastening the translation to clinic of additive manufactured devices made of thermoplastic polyesters. In particular, decades-long history of clinical exploitation of polymer thermal processing is likely to be further implemented in AM. FDM, MEW, and SLS would consequently find increasing industrial application to consolidate their ongoing biomedical translation for the fabrication, among others, of surgical devices and exoprostheses. Biostable polymers, such as those engineered for advanced applications (e.g., PEEK), are also fully involved in this technological revolution. In this context, SE-AM will offer advanced technological tools for polymer structuring at multi-scale levels, and for device biofunctionalization through drug loading strategies.

Cutting-edge advancements on 4D printing, nano/microfabrication, and smart drug release are leading to the next frontiers of biomedical AM. These, together with the development of advanced materials engineering tools, the always increasing automation and digital control of the design and fabrication processes, in relationship to the resulting properties of the fabricated items, are expected in the near future to tremendously impact the biomedical industry.

Acknowledgments

The financial support of the University of Pisa PRA-2016-50 and PRA-2018-23 projects entitled “Functional Materials”, the Tuscany Region (Italy) funded Project “Nuovi Supporti Bioattivi a Matrice Polimerica per la Rigenerazione Ossea in Applicazioni Odontoiatriche (R.E.O.S.S.)” as part of the program POR CReO FESR 2007–2013—Le ali alle tue idee, and the European Eranet+ project, BI-TRE—BIophotonic technologies for Tissue Repair (2014–2016), is gratefully acknowledged.

References

[1] International A. ASTM, Standard Terminology for Additive Manufacturing Technologies: Designation F2792-12a. West Conshohocken, PA20122012.
[2] Chhaya MP, Poh PSP, Balmayor ER, van Griensven M, Schantz J-T, Hutmacher DW Additive manufacturing in biomedical sciences and the need for definitions and norms, Expert Rev Med Devices, 12 (2015), pp. 537-43.
[3] Chartrain NA, Williams CB, Whittington AR A review on fabricating tissue scaffolds using vat photopolymerization, Acta Biomater, 74 (2018), pp. 90-111.
[4] Williams JM, Adewunmi A, Schek RM, Flanagan CL, Krebsbach PH, Feinberg SE, et al. Bone tissue engineering using polycaprolactone scaffolds fabricated via selective laser sintering, Biomaterials, 26 (2005), pp. 4817-27.
[5] Butscher A, Bohner M, Hofmann S, Gauckler L, Müller R Structural and material approaches to bone tissue engineering in powder-based three-dimensional printing, Acta Biomater, 7 (2011), pp. 907-20.
[6] A. Gold S, Strong R, N. Turner B A review of melt extrusion additive manufacturing processes: I. Process design and modeling, Rapid Prototyp J, 20 (2014), pp. 192-204.
[7] Puppi D, Chiellini F Wet-spinning of biomedical polymers: from single-fibre production to additive manufacturing of three-dimensional scaffolds, Polym Int, 66 (2017), pp. 1690–6.
[8] Ligon SC, Liska R, Stampfl J, Gurr M, Mülhaupt R Polymers for 3D Printing and Customized Additive Manufacturing, Chem Rev, 117 (2017), pp. 10212-90.
[9] Wunner Felix M, Wille ML, Noonan Thomas G, Bas O, Dalton Paul D, De‐Juan‐Pardo Elena M, et al. Melt Electrospinning Writing of Highly Ordered Large Volume Scaffold Architectures, Adv Mater, 30 (2018), pp. 1706570.
[10] Giannitelli SM, Mozetic P, Trombetta M, Rainer A Combined additive manufacturing approaches in tissue engineering, Acta Biomater, 24 (2015), pp. 1-11.
[11] Puppi D, Chiellini F. Biofabrication via integrated additive manufacturing and electrofluidodynamics. In: Guarino V, Ambrosio L, editors. Electrofluidodynamic Technologies (EFDTs) for Biomaterials and Medical Devices. Woodhead Publishing; 2018. p. 71-85.
[12] Ning F, Cong W, Qiu J, Wei J, Wang S Additive manufacturing of carbon fiber reinforced thermoplastic composites using fused deposition modeling, Compos Part B Eng, 80 (2015), pp. 369-78.
[13] Kruth JP, Levy G, Klocke F, Childs THC Consolidation phenomena in laser and powder-bed based layered manufacturing, CIRP Annals, 56 (2007), pp. 730-59.
[14] Kotlinski J Mechanical properties of commercial rapid prototyping materials, Rapid Prototyp J, 20 (2014), pp. 499-510.
[15] Chacón JM, Caminero MA, García-Plaza E, Núñez PJ Additive manufacturing of PLA structures using fused deposition modelling: Effect of process parameters on mechanical properties and their optimal selection, Mater Des, 124 (2017), pp. 143-57.

[16] Wang YW, Yang F, Wu Q, Cheng YC, Yu PH, Chen J, et al. Effect of composition of poly(3-hydroxybutyrate-co-3-hydroxyhexanoate) on growth of fibroblast and osteoblast, Biomaterials, 26 (2005), pp. 755-61.
[17] Louvrier A, Marty P, Barrabé A, Euvrard E, Chatelain B, Weber E, et al. How useful is 3D printing in maxillofacial surgery?, J Stomatol Oral Maxi, 118 (2017), pp. 206-12.
[18] Melchels FPW, Feijen J, Grijpma DW A review on stereolithography and its applications in biomedical engineering, Biomaterials, 31 (2010), pp. 6121-30.
[19] Gonçalves FAMM, Fonseca AC, Domingos M, Gloria A, Serra AC, Coelho JFJ The potential of unsaturated polyesters in biomedicine and tissue engineering: Synthesis, structure-properties relationships and additive manufacturing, Prog Polym Sci, 68 (2017), pp. 1-34.
[20] Ratner BD, Hoffman AS, Schoen FJ, Lemons JE. Introduction - Biomaterials Science: An Evolving, Multidisciplinary Endeavor. In: Ratner BD, Hoffman AS, Schoen FJ, Lemons JE, editors. Biomater Sci. Academic Press; 2013. p. 25-39.
[21] Youssef A, Hollister SJ, Dalton PD Additive manufacturing of polymer melts for implantable medical devices and scaffolds, Biofabrication, 9 (2017), pp. 012002.
[22] Zopf DA, Hollister SJ, Nelson ME, Ohye RG, Green GE Bioresorbable Airway Splint Created with a Three-Dimensional Printer, N Engl J Med, 368 (2013), pp. 2043-5.
[23] Han Y, Yin Q, Wang Y, Zhao H, He J, Gu C Three-dimensional printed degradable splint in the treatment of pulmonary artery sling associated with severe bilateral bronchus stenosis, Cardiol Young, 28 (2018), pp. 1477-80.
[24] Xu W, Wang X, Yan Y, Zheng W, Xiong Z, Lin F, et al. Rapid Prototyping Three-Dimensional Cell/Gelatin/Fibrinogen Constructs for Medical Regeneration, J Bioact Compatible Polym, 22 (2007), pp. 363-77.
[25] Blatchley MR, Gerecht S Acellular implantable and injectable hydrogels for vascular regeneration, Biomed Mater, 10 (2015), pp. 034001.
[26] Puppi D, Mota C, Gazzarri M, Dinucci D, Gloria A, Myrzabekova M, et al. Additive manufacturing of wet-spun polymeric scaffolds for bone tissue engineering, Biomed Microdevices, 14 (2012), pp. 1115-27.
[27] Wubneh A, Tsekoura EK, Ayranci C, Uludağ H Current state of fabrication technologies and materials for bone tissue engineering, Acta Biomater, 80 (2018), pp. 1-30.
[28] Puppi D, Russo A, Parrini G, Chiellini F. Development of customized polymeric scaffolds with multiscale porosity by a hybrid additive manufacturing technique. IXth ECNP International Conference on Nanostructured Polymers and Nanocomposites. Rome, ItalySeptember 19 to 21, 2016.
[29] George M, Aroom KR, Hawes HG, Gill BS, Love J 3D Printed Surgical Instruments: The Design and Fabrication Process, World J Surg, 41 (2017), pp. 314-9.
[30] Andrianesis K, Tzes A Development and Control of a Multifunctional Prosthetic Hand with Shape Memory Alloy Actuators, J Intell Robotic Syst, 78 (2015), pp. 257-89.
[31] Puppi D, Morelli A, Bello F, Valentini S, Chiellini F Additive Manufacturing of Poly(methyl methacrylate) Biomedical Implants with Dual-scale Porosity, Macromol Mater Eng, 303 (2018), pp. 1800247.
[32] 3D-Printed Tracheal Splints Used in Groundbreaking Pediatric Surgery, https://www.news.gatech.edu; 2018 [September 18, 2018].
[33] Ding C, Qiao Z, Jiang W, Li H, Wei J, Zhou G, et al. Regeneration of a goat femoral head using a tissue-specific, biphasic scaffold fabricated with CAD/CAM technology, Biomaterials, 34 (2013), pp. 6706-16.
[34] Chiellini F, Puppi D, Piras AM, Morelli A, Bartoli C, Migone C Modelling of pancreatic ductal adenocarcinoma in vitro with three-dimensional microstructured hydrogels, RSC Adv, 6 (2016), pp. 54226-35.

[35] Ma X, Qu X, Zhu W, Li Y-S, Yuan S, Zhang H, et al. Deterministically patterned biomimetic human iPSC-derived hepatic model via rapid 3D bioprinting, Proc Natl Acad Sci, 113 (2016), pp. 2206.
[36] Haring AP, Tong Y, Halper J, Johnson BN Programming of Multicomponent Temporal Release Profiles in 3D Printed Polypills via Core–Shell, Multilayer, and Gradient Concentration Profiles, Adv Healthcare Mater, 7 (2018), pp. 1800213.
[37] D'Urso PS, Effeney DJ, Earwaker WJ, Barker TM, Redmond MJ, Thompson RG, et al. Custom cranioplasty using stereolithography and acrylic, Br J Plast Surg, 53 (2000), pp. 200-4.
[38] Müller A, Krishnan KG, Uhl E, Mast G The Application of Rapid Prototyping Techniques in Cranial Reconstruction and Preoperative Planning in Neurosurgery, J Craniofac Surg, 14 (2003), pp.
[39] Mavili ME, Canter HI, Saglam-Aydinatay B, Kamaci S, Kocadereli I Use of Three-Dimensional Medical Modeling Methods for Precise Planning of Orthognathic Surgery, J Craniofac Surg, 18 (2007), pp.
[40] Wanibuchi M, Ohtaki M, Fukushima T, Friedman AH, Houkin K Skull base training and education using an artificial skull model created by selective laser sintering, Acta Neurochir (Wien), 152 (2010), pp. 1055-60.
[41] Gabriele W, Berndt T, Peter P, Kurt H, Johannes T Cerebrovascular stereolithographic biomodeling for aneurysm surgery, J Neurosurg, 100 (2004), pp. 139-45.
[42] Giesel FL, Hart AR, Hahn HK, Wignall E, Rengier F, Talanow R, et al. 3D Reconstructions of the Cerebral Ventricles and Volume Quantification in Children with Brain Malformations, Acad Radiol, 16 (2009), pp. 610-7.
[43] Lan Q, Chen A, Zhang T, Li G, Zhu Q, Fan X, et al. Development of Three-Dimensional Printed Craniocerebral Models for Simulated Neurosurgery, World Neurosurg, 91 (2016), pp. 434-42.
[44] Paiva WS, Amorim R, Bezerra DAF, Masini M Aplication of the stereolithography technique in complex spine surgery, Arq Neuropsiquiatr, 65 (2007), pp. 443-5.
[45] Wilcox B, Mobbs RJ, Wu A-M, Phan K Systematic review of 3D printing in spinal surgery: the current state of play, J Spine Surg, 3 (2017), pp. 433-43.
[46] Ling Q, He E, Ouyang H, Guo J, Yin Z, Huang W Design of mulitlevel OLF approach ("V"-shaped decompressive laminoplasty) based on 3D printing technology, Eur Spine J, 27 (2018), pp. 323-9.
[47] Armillotta A, Bonhoeffer P, Dubini G, Ferragina S, Migliavacca F, Sala G, et al. Use of rapid prototyping models in the planning of percutaneous pulmonary valved stent implantation, Proc Inst Mech Eng, Part H, 221 (2007), pp. 407-16.
[48] Olivieri L, Krieger A, Chen MY, Kim P, Kanter JP 3D heart model guides complex stent angioplasty of pulmonary venous baffle obstruction in a Mustard repair of D-TGA, Int J Cardiol, 172 (2014), pp. e297-e8.
[49] Ripley B, Kelil T, Cheezum MK, Goncalves A, Di Carli MF, Rybicki FJ, et al. 3D printing based on cardiac CT assists anatomic visualization prior to transcatheter aortic valve replacement, J Cardiovasc Comput Tomogr, 10 (2016), pp. 28-36.
[50] Guarino J, Tennyson S, McCain G, Bond L, Shea K, King H Rapid Prototyping Technology for Surgeries of the Pediatric Spine and Pelvis: Benefits Analysis, Journal of Pediatric Orthopaedics, 27 (2007), pp.
[51] Hurson C, Tansey A, O'Donnchadha B, Nicholson P, Rice J, McElwain J Rapid prototyping in the assessment, classification and preoperative planning of acetabular fractures, Injury, 38 (2007), pp. 1158-62.
[52] Wu X-B, Wang J-Q, Zhao C-P, Sun X, Shi Y, Zhang Z-A, et al. Printed Three-dimensional Anatomic Templates for Virtual Preoperative Planning Before Reconstruction of Old Pelvic Injuries: Initial Results, Chin Med J (Engl), 128 (2015), pp. 477-82.

[53] Martelli N, Serrano C, van den Brink H, Pineau J, Prognon P, Borget I, et al. Advantages and disadvantages of 3-dimensional printing in surgery: A systematic review, Surgery, 159 (2016), pp. 1485-500.
[54] Kondor S, Grant CG, Liacouras P, Schmid MAJJR, Michael Parsons LTC, Rastogi VK, et al. On Demand Additive Manufacturing of a Basic Surgical Kit, J Med Devices, 7 (2013), pp. 030916--2.
[55] Kondor S, Grant CG, Liacouras P, Schmid MAJJR, Michael Parsons LTC, Macy B, et al. Personalized Surgical Instruments, J Med Devices, 7 (2013), pp. 030934--2.
[56] Resnik L, Meucci MR, Lieberman-Klinger S, Fantini C, Kelty DL, Disla R, et al. Advanced Upper Limb Prosthetic Devices: Implications for Upper Limb Prosthetic Rehabilitation, Arch Phys Med Rehabil, 93 (2012), pp. 710-7.
[57] Ten Kate J, Smit G, Breedveld P 3D-printed upper limb prostheses: a review, Disabil Rehabil Assist Technol, 12 (2017), pp. 300-14.
[58] van Baar GJC, Forouzanfar T, Liberton NPTJ, Winters HAH, Leusink FKJ Accuracy of computer-assisted surgery in mandibular reconstruction: A systematic review, Oral Oncol, 84 (2018), pp. 52-60.
[59] Tarsitano A, Ciocca L, Scotti R, Marchetti C Morphological results of customized microvascular mandibular reconstruction: A comparative study, J Craniomaxillofac Surg, 44 (2016), pp. 697-702.
[60] Honigmann P, Sharma N, Okolo B, Popp U, Msallem B, Thieringer FM Patient-Specific Surgical Implants Made of 3D Printed PEEK: Material, Technology, and Scope of Surgical Application, Biomed Res Int, 2018 (2018), pp. 4520636-.
[61] Espalin D, Arcaute K, Rodriguez D, Medina F, Posner M, Wicker R Fused deposition modeling of patient-specific polymethylmethacrylate implants, Rapid Prototyp J, 16 (2010), pp. 164-73.
[62] Velu R, Singamneni S Evaluation of the influences of process parameters while selective laser sintering PMMA powders, Proc Inst Mech Eng, Part C, 229 (2015), pp. 603-13.
[63] Vaezi M, Yang S Extrusion-based additive manufacturing of PEEK for biomedical applications, Virtual Phys Prototyp, 10 (2015), pp. 123-35.
[64] Melchels FPW, Domingos MAN, Klein TJ, Malda J, Bartolo PJ, Hutmacher DW Additive manufacturing of tissues and organs, Prog Polym Sci, 37 (2012), pp. 1079-104.
[65] Mota C, Puppi D, Chiellini F, Chiellini E Additive manufacturing techniques for the production of tissue engineering constructs, J Tissue Eng Regener Med, 9 (2015), pp. 174-90.
[66] Puppi D, Chiellini F, Piras AM, Chiellini E Polymeric materials for bone and cartilage repair, Prog Polym Sci, 35 (2010), pp. 403-40.
[67] Stevens MM, George JH Exploring and engineering the cell surface interface, Science, 310 (2005), pp. 1135-8.
[68] Engler AJ, Sen S, Sweeney HL, Discher DE Matrix Elasticity Directs Stem Cell Lineage Specification, Cell, 126 (2006), pp. 677-89.
[69] Nikkhah M, Edalat F, Manoucheri S, Khademhosseini A Engineering microscale topographies to control the cell–substrate interface, Biomaterials, 33 (2012), pp. 5230-46.
[70] Kim HN, Jiao A, Hwang NS, Kim MS, Kang DH, Kim D-H, et al. Nanotopography-guided tissue engineering and regenerative medicine, Adv Drug Del Rev, 65 (2013), pp. 536-58.
[71] Dalton PD, Vaquette C, Farrugia BL, Dargaville TR, Brown TD, Hutmacher DW Electrospinning and additive manufacturing: converging technologies, Biomater Sci, 1 (2013), pp. 171-85.
[72] Weiß T, Hildebrand G, Schade R, Liefeith K Two-Photon polymerization for microfabrication of three-dimensional scaffolds for tissue engineering application, Eng Life Sci, 9 (2009), pp. 384-90.

[73] Temple JP, Hutton DL, Hung BP, Huri PY, Cook CA, Kondragunta R, et al. Engineering anatomically shaped vascularized bone grafts with hASCs and 3D-printed PCL scaffolds, J Biomed Mater Res A, 102 (2014), pp. 4317-25.
[74] Dini F, Barsotti G, Puppi D, Coli A, Briganti A, Giannessi E, et al. Tailored star poly (ε-caprolactone) wet-spun scaffolds for in vivo regeneration of long bone critical size defects, J Bioact Compatible Polym, 31 (2016), pp. 15-30.
[75] Lu T, Li Y, Chen T Techniques for fabrication and construction of three-dimensional scaffolds for tissue engineering, Int J Nanomedicine, 8 (2013), pp. 337-50.
[76] Atala A, Kasper FK, Mikos AG Engineering Complex Tissues, Sci Transl Med, 4 (2012), pp. 160rv12.
[77] Woodruff MA, Lange C, Reichert J, Berner A, Chen F, Fratzl P, et al. Bone tissue engineering: from bench to bedside, Mater Today, 15 (2012), pp. 430-5.
[78] Ingber DE Can cancer be reversed by engineering the tumor microenvironment?, Semin Cancer Biol, 18 (2008), pp. 356-64.
[79] Hutmacher DW, Loessner D, Rizzi S, Kaplan DL, Mooney DJ, Clements JA Can tissue engineering concepts advance tumor biology research?, Trends Biotechnol, 28 (2010), pp. 125-33.
[80] Arya N, Sardana V, Saxena M, Rangarajan A, Katti DS Recapitulating tumour microenvironment in chitosan–gelatin three-dimensional scaffolds: an improved in vitro tumour model, J Royal Soc Interface, 9 (2012), pp. 3288-302.
[81] Talukdar S, Kundu SC A Non-Mulberry Silk Fibroin Protein Based 3D In Vitro Tumor Model for Evaluation of Anticancer Drug Activity, Adv Funct Mater, 22 (2012), pp. 4778-88.
[82] Grzesiak JJ, Bouvet M Determination of the Ligand-Binding Specificities of the α2β1 and α1β1 Integrins in a Novel 3-Dimensional In Vitro Model of Pancreatic Cancer, Pancreas, 34 (2007), pp.
[83] Deramaudt TB, Takaoka M, Upadhyay R, Bowser MJ, Porter J, Lee A, et al. N-Cadherin and Keratinocyte Growth Factor Receptor Mediate the Functional Interplay between Ki-RAS(G12V) and p53(V143A) in Promoting Pancreatic Cell Migration, Invasion, and Tissue Architecture Disruption, Mol Cell Biol, 26 (2006), pp. 4185-200.
[84] Gutierrez-Barrera AM, Menter DG, Abbruzzese JL, Reddy SAG Establishment of three-dimensional cultures of human pancreatic duct epithelial cells, Biochem Biophys Res Commun, 358 (2007), pp. 698-703.
[85] He Q, Wang X, Zhang X, Han H, Han B, Xu J, et al. A tissue-engineered subcutaneous pancreatic cancer model for antitumor drug evaluation, Int J Nanomedicine, 8 (2013), pp. 1167-76.
[86] Wang X, Zhang X, Fu Z, Yin H A bioengineered metastatic pancreatic tumor model for mechanistic investigation of chemotherapeutic drugs, J Biotechnol, 166 (2013), pp. 166-73.
[87] Vanderburgh J, Sterling JA, Guelcher SA 3D Printing of Tissue Engineered Constructs for in vitro Modeling of Disease Progression and Drug Screening, Ann Biomed Eng, 45 (2017), pp. 164-79.
[88] Xu X, Farach-Carson MC, Jia X Three-dimensional in vitro tumor models for cancer research and drug evaluation, Biotechnol Adv, 32 (2014), pp. 1256-68.
[89] Martine LC, Holzapfel BM, McGovern JA, Wagner F, Quent VM, Hesami P, et al. Engineering a humanized bone organ model in mice to study bone metastases, Nat Protoc, 12 (2017), pp. 639.
[90] Gurkan UA, El Assal R, Yildiz SE, Sung Y, Trachtenberg AJ, Kuo WP, et al. Engineering Anisotropic Biomimetic Fibrocartilage Microenvironment by Bioprinting Mesenchymal Stem Cells in Nanoliter Gel Droplets, Mol Pharm, 11 (2014), pp. 2151-9.
[91] Kolesky DB, Truby RL, Gladman AS, Busbee TA, Homan KA, Lewis JA 3D Bioprinting of Vascularized, Heterogeneous Cell-Laden Tissue Constructs, Adv Mater, 26 (2014), pp. 3124-30.

[92] Holzapfel BM, Wagner F, Thibaudeau L, Levesque J-P, Hutmacher DW Concise Review: Humanized Models of Tumor Immunology in the 21st Century: Convergence of Cancer Research and Tissue Engineering, Stem Cells, 33 (2015), pp. 1696-704.
[93] Quent Verena MC, Theodoropoulos C, Hutmacher Dietmar W, Reichert Johannes C Differential osteogenicity of multiple donor-derived human mesenchymal stem cells and osteoblasts in monolayer, scaffold-based 3D culture and in vivo, Biomed Eng (NY), 61 (2016), pp. 253-66.
[94] Holzapfel BM, Wagner F, Loessner D, Holzapfel NP, Thibaudeau L, Crawford R, et al. Species-specific homing mechanisms of human prostate cancer metastasis in tissue engineered bone, Biomaterials, 35 (2014), pp. 4108-15.
[95] Thibaudeau L, Taubenberger AV, Holzapfel BM, Quent VM, Fuehrmann T, Hesami P, et al. A tissue-engineered humanized xenograft model of human breast cancer metastasis to bone, Dis Model Mech, 7 (2014), pp. 299.
[96] Yang Q, Lian Q, Xu F Perspective: Fabrication of integrated organ-on-a-chip via bioprinting, Biomicrofluidics, 11 (2017), pp. 031301-.
[97] Schaffner M, Rühs PA, Coulter F, Kilcher S, Studart AR 3D printing of bacteria into functional complex materials, Sci Adv, 3 (2017), pp. eaao6804.
[98] Mandrycky C, Wang Z, Kim K, Kim D-H 3D bioprinting for engineering complex tissues, Biotechnol Adv, 34 (2016), pp. 422-34.
[99] Junaid A, Mashaghi A, Hankemeier T, Vulto P An end-user perspective on Organ-on-a-Chip: Assays and usability aspects, Curr Opin Biomed Eng, 1 (2017), pp. 15-22.
[100] Li Y, Poon CT, Li M, Lu TJ, Pingguan-Murphy B, Xu F Chinese-Noodle-Inspired Muscle Myofiber Fabrication, Adv Funct Mater, 25 (2015), pp. 5999-6008.
[101] Gao B, Yang Q, Zhao X, Jin G, Ma Y, Xu F 4D Bioprinting for Biomedical Applications, Trends Biotechnol, 34 (2016), pp. 746-56.
[102] Bose S, Ke D, Sahasrabudhe H, Bandyopadhyay A Additive Manufacturing of Biomaterials, Prog Mater Sci, 93 (2017), pp. 45-111.
[103] Buwalda SJ, Vermonden T, Hennink WE Hydrogels for Therapeutic Delivery: Current Developments and Future Directions, Biomacromolecules, 18 (2017), pp. 316-30.
[104] van Tienderen GS, Berthel M, Yue Z, Cook M, Liu X, Beirne S, et al. Advanced fabrication approaches to controlled delivery systems for epilepsy treatment, Expert Opin Drug Deliv, 15 (2018), pp. 915-25.
[105] Puppi D, Piras AM, Pirosa A, Sandreschi S, Chiellini F Levofloxacin-loaded Star Poly(ε-caprolactone) Scaffolds by Additive Manufacturing, J Mater Sci - Mater Med, 27 (2016), pp. 44.
[106] Rattanakit P, Moulton SE, Santiago KS, Liawruangrath S, Wallace GG Extrusion printed polymer structures: A facile and versatile approach to tailored drug delivery platforms, Int J Pharm, 422 (2012), pp. 254-63.
[107] Zhang J, Vo AQ, Feng X, Bandari S, Repka MA Pharmaceutical Additive Manufacturing: a Novel Tool for Complex and Personalized Drug Delivery Systems, AAPS PharmSciTech, 19 (2018), pp. 3388-402.
[108] Goyanes A, Robles Martinez P, Buanz A, Basit AW, Gaisford S Effect of geometry on drug release from 3D printed tablets, Int J Pharm, 494 (2015), pp. 657-63.
[109] Zhang J, Yang W, Vo AQ, Feng X, Ye X, Kim DW, et al. Hydroxypropyl methylcellulose-based controlled release dosage by melt extrusion and 3D printing: Structure and drug release correlation, Carbohydr Polym, 177 (2017), pp. 49-57.
[110] Sadia M, Arafat B, Ahmed W, Forbes RT, Alhnan MA Channelled tablets: An innovative approach to accelerating drug release from 3D printed tablets, J Controlled Release, 269 (2018), pp. 355-63.
[111] Ma H, Feng C, Chang J, Wu C 3D-printed bioceramic scaffolds: From bone tissue engineering to tumor therapy, Acta Biomater, 79 (2018), pp. 37-59.

[112] Park SH, Kim TG, Kim HC, Yang D-Y, Park TG Development of dual scale scaffolds via direct polymer melt deposition and electrospinning for applications in tissue regeneration, Acta Biomater, 4 (2008), pp. 1198-207.
[113] Visscher LE, Dang HP, Knackstedt MA, Hutmacher DW, Tran PA 3D printed Polycaprolactone scaffolds with dual macro-microporosity for applications in local delivery of antibiotics, Mater Sci Eng, C, 87 (2018), pp. 78-89.
[114] Zhou C, Yang K, Wang K, Pei X, Dong Z, Hong Y, et al. Combination of fused deposition modeling and gas foaming technique to fabricated hierarchical macro/microporous polymer scaffolds, Mater Des, 109 (2016), pp. 415-24.
[115] Pham CB, Leong KF, Lim TC, Chian KS Rapid freeze prototyping technique in bio-plotters for tissue scaffold fabrication, Rapid Prototyp J, 14 (2008), pp. 246-53.
[116] Mueller B Additive Manufacturing Technologies – Rapid Prototyping to Direct Digital Manufacturing, Assembly Autom, 32 (2012), pp.
[117] Suri S, Han L-H, Zhang W, Singh A, Chen S, Schmidt CE Solid freeform fabrication of designer scaffolds of hyaluronic acid for nerve tissue engineering, Biomed Microdevices, 13 (2011), pp. 983-93.
[118] Hinze U, Chichkov B. Light Sources and Systems for Multiphoton Lithography. In: Stampfl J, Liska R, Ovsianikov A, editors. Multiphoton Lithography: Techniques, Materials and Applications. 2017 Wiley&VCH Verlag GmbH & Co. KGaA; 2016.
[119] Sun H-B, Kawata S. Two-photon Photopolymerization and 3D Lithographic Microfabrication. NMR; 3D Analysis; Photopolymerization. Berlin Heidelberg, New York: Springer-Verlag; 2004. p. 169-273.
[120] Wong BH Invisalign A to Z, Am J Orthod Dentofacial Orthop, 121 (2002), pp. 540-1.
[121] Jacquel N, Lo CW, Wu HS, Wei YH, Wang Shaw S Solubility of polyhydroxyalkanoates by experiment and thermodynamic correlations, AlChE J, 53 (2007), pp. 2704-14.
[122] Christensen AM, Weimer K, Beaudreau C, Rensberger M, Johnson B. The Digital Thread for Personalized Craniomaxillofacial Surgery. In: Greenberg AM, editor. Digital Technologies in Craniomaxillofacial Surgery. New York, NY: Springer New York; 2018. p. 23-45.
[123] Lin H, Zhang D, Alexander PG, Yang G, Tan J, Cheng AW-M, et al. Application of visible light-based projection stereolithography for live cell-scaffold fabrication with designed architecture, Biomaterials, 34 (2013), pp. 331-9.
[124] Wang Z, Abdulla R, Parker B, Samanipour R, Ghosh S, Kim K A simple and high-resolution stereolithography-based 3D bioprinting system using visible light crosslinkable bioinks, Biofabrication, 7 (2015), pp. 045009.
[125] Crivello JV, Reichmanis E Photopolymer Materials and Processes for Advanced Technologies, Chem Mater, 26 (2014), pp. 533-48.
[126] Hinczewski C, Corbel S, Chartier T Ceramic suspensions suitable for stereolithography, J Eur Ceram Soc, 18 (1998), pp. 583-90.
[127] Lee K-W, Wang S, Fox BC, Ritman EL, Yaszemski MJ, Lu L Poly(propylene fumarate) Bone Tissue Engineering Scaffold Fabrication Using Stereolithography: Effects of Resin Formulations and Laser Parameters, Biomacromolecules, 8 (2007), pp. 1077-84.
[128] Kwon IK, Matsuda T Photo-polymerized microarchitectural constructs prepared by microstereolithography (μSL) using liquid acrylate-end-capped trimethylene carbonate-based prepolymers, Biomaterials, 26 (2005), pp. 1675-84.
[129] Melchels FPW, Feijen J, Grijpma DW A poly(d,l-lactide) resin for the preparation of tissue engineering scaffolds by stereolithography, Biomaterials, 30 (2009), pp. 3801-9.
[130] Mondschein RJ, Kanitkar A, Williams CB, Verbridge SS, Long TE Polymer structure-property requirements for stereolithographic 3D printing of soft tissue engineering scaffolds, Biomaterials, 140 (2017), pp. 170-88.

[131] Pansky A, Tille C, Seitz H, Emons M, Bens A, Roitzheim B, et al. Non‐toxic flexible photopolymers for medical stereolithography technology, Rapid Prototyp J, 13 (2007), pp. 38-47.
[132] Dhariwala B, Hunt E, Boland T Rapid Prototyping of Tissue-Engineering Constructs, Using Photopolymerizable Hydrogels and Stereolithography, Tissue Eng, 10 (2004), pp. 1316-22.
[133] Mapili G, Lu Y, Chen S, Roy K Laser-layered microfabrication of spatially patterned functionalized tissue-engineering scaffolds, J Biomed Mater Res B Appl Biomater, 75B (2005), pp. 414-24.
[134] Ge Q, Sakhaei AH, Lee H, Dunn CK, Fang NX, Dunn ML Multimaterial 4D Printing with Tailorable Shape Memory Polymers, Sci Rep, 6 (2016), pp. 31110.
[135] Schultz AR, Lambert PM, Chartrain NA, Ruohoniemi DM, Zhang Z, Jangu C, et al. 3D Printing Phosphonium Ionic Liquid Networks with Mask Projection Microstereolithography, ACS Macro Lett, 3 (2014), pp. 1205-9.
[136] Hegde M, Meenakshisundaram V, Chartrain N, Sekhar S, Tafti D, Williams CB, et al. 3D Printing All-Aromatic Polyimides using Mask-Projection Stereolithography: Processing the Nonprocessable, Adv Mater, 29 (2017), pp. 1701240.
[137] Lin W-S, Harris BT, Pellerito J, Morton D Fabrication of an interim complete removable dental prosthesis with an in-office digital light processing three-dimensional printer: A proof-of-concept technique, J Prosthet Dent, 120 (2018), pp. 331-4.
[138] Lan PX, Lee JW, Seol Y-J, Cho D-W Development of 3D PPF/DEF scaffolds using micro-stereolithography and surface modification, J Mater Sci Mater Med, 20 (2009), pp. 271-9.
[139] Shin JH, Lee JW, Jung JH, Cho D-W, Lim G Evaluation of cell proliferation and differentiation on a poly(propylene fumarate) 3D scaffold treated with functional peptides, J Mater Sci, 46 (2011), pp. 5282-7.
[140] Cooke MN, Fisher JP, Dean D, Rimnac C, Mikos AG Use of stereolithography to manufacture critical-sized 3D biodegradable scaffolds for bone ingrowth, J Biomed Mater Res B Appl Biomater, 64B (2002), pp. 65-9.
[141] Matsuda T, Mizutani M Liquid acrylate-endcapped biodegradable poly(ϵ-caprolactone-co-trimethylene carbonate). II. Computer-aided stereolithographic microarchitectural surface photoconstructs, J Biomed Mater Res, 62 (2002), pp. 395-403.
[142] Lee S-J, Kang H-W, Park JK, Rhie J-W, Hahn SK, Cho D-W Application of microstereolithography in the development of three-dimensional cartilage regeneration scaffolds, Biomed Microdevices, 10 (2008), pp. 233-41.
[143] Geven MA, Varjas V, Kamer L, Wang X, Peng J, Eglin D, et al. Fabrication of patient specific composite orbital floor implants by stereolithography, Polym Adv Technol, 26 (2015), pp. 1433-8.
[144] Guillaume O, Geven MA, Sprecher CM, Stadelmann VA, Grijpma DW, Tang TT, et al. Surface-enrichment with hydroxyapatite nanoparticles in stereolithography-fabricated composite polymer scaffolds promotes bone repair, Acta Biomater, 54 (2017), pp. 386-98.
[145] Jansen J, Melchels FPW, Grijpma DW, Feijen J Fumaric Acid Monoethyl Ester-Functionalized Poly(d,l-lactide)/N-vinyl-2-pyrrolidone Resins for the Preparation of Tissue Engineering Scaffolds by Stereolithography, Biomacromolecules, 10 (2009), pp. 214-20.
[146] Ronca A, Ronca S, Forte G, Zeppetelli S, Gloria A, De Santis R, et al. Synthesis and characterization of divinyl-fumarate poly-ε-caprolactone for scaffolds with controlled architectures, J Tissue Eng Regener Med, 12 (2016), pp. e523-e31.
[147] Xia C, Fang NX 3D microfabricated bioreactor with capillaries, Biomed Microdevices, 11 (2009), pp. 1309-15.
[148] Arcaute K, Mann B, Wicker R Stereolithography of spatially controlled multi-material bioactive poly(ethylene glycol) scaffolds, Acta Biomater, 6 (2010), pp. 1047-54.

[149] Leigh SJ, Gilbert HTJ, Barker IA, Becker JM, Richardson SM, Hoyland JA, et al. Fabrication of 3-Dimensional Cellular Constructs via Microstereolithography Using a Simple, Three-Component, Poly(Ethylene Glycol) Acrylate-Based System, Biomacromolecules, 14 (2013), pp. 186-92.
[150] Nichol JW, Koshy ST, Bae H, Hwang CM, Yamanlar S, Khademhosseini A Cell-laden microengineered gelatin methacrylate hydrogels, Biomaterials, 31 (2010), pp. 5536-44.
[151] Placone JK, Navarro J, Laslo GW, Lerman MJ, Gabard AR, Herendeen GJ, et al. Development and Characterization of a 3D Printed, Keratin-Based Hydrogel, Ann Biomed Eng, 45 (2017), pp. 237-48.
[152] Zhang W, Li D, Wang K, Bian W, Li X, Lian Q, et al. Fabrication of a bio‐inspired beta‐Tricalcium phosphate/collagen scaffold based on ceramic stereolithography and gel casting for osteochondral tissue engineering, Rapid Prototyp J, 18 (2012), pp. 68-80.
[153] Morris VB, Nimbalkar S, Younesi M, McClellan P, Akkus O Mechanical Properties, Cytocompatibility and Manufacturability of Chitosan:PEGDA Hybrid-Gel Scaffolds by Stereolithography, Ann Biomed Eng, 45 (2017), pp. 286-96.
[154] Zhang AP, Qu X, Soman P, Hribar KC, Lee JW, Chen S, et al. Rapid Fabrication of Complex 3D Extracellular Microenvironments by Dynamic Optical Projection Stereolithography, Adv Mater, 24 (2012), pp. 4266-70.
[155] Gauvin R, Chen Y-C, Lee JW, Soman P, Zorlutuna P, Nichol JW, et al. Microfabrication of complex porous tissue engineering scaffolds using 3D projection stereolithography, Biomaterials, 33 (2012), pp. 3824-34.
[156] Miao S, Zhu W, Castro NJ, Nowicki M, Zhou X, Cui H, et al. 4D printing smart biomedical scaffolds with novel soybean oil epoxidized acrylate, Sci Rep, 6 (2016), pp. 27226.
[157] Froyen L, Kruth JP, Laoui T, Wang X Lasers and materials in selective laser sintering, Assembly Autom, 23 (2003), pp. 357-71.
[158] Fina F, Goyanes A, Gaisford S, Basit AW Selective laser sintering (SLS) 3D printing of medicines, Int J Pharm, 529 (2017), pp. 285-93.
[159] Mazzoli A Selective laser sintering in biomedical engineering, Med Biol Eng Comput, 51 (2013), pp. 245-56.
[160] http://oxfordpm.com, May, 2019
[161] Adamzyk C, Kachel P, Hoss M, Gremse F, Modabber A, Hölzle F, et al. Bone tissue engineering using polyetherketoneketone scaffolds combined with autologous mesenchymal stem cells in a sheep calvarial defect model, J Craniomaxillofac Surg, 44 (2016), pp. 985-94.
[162] Morrison RJ, Hollister SJ, Niedner MF, Mahani MG, Park AH, Mehta DK, et al. Mitigation of tracheobronchomalacia with 3D-printed personalized medical devices in pediatric patients, Sci Transl Med, 7 (2015), pp. 285ra64-ra64.
[163] Schmid M, Amado A, Wegener K Materials perspective of polymers for additive manufacturing with selective laser sintering, J Mater Res, 29 (2014), pp. 1824-32.
[164] Schmid M, Wegener K Additive Manufacturing: Polymers Applicable for Laser Sintering (LS), Procedia Eng, 149 (2016), pp. 457-64.
[165] Schmid M, Wegener K Thermal and molecular properties of polymer powders for Selective Laser Sintering (SLS), AIP Conf Proc, 1779 (2016), pp. 100003.
[166] Gayer C, Abert J, Bullemer M, Grom S, Jauer L, Meiners W, et al. Influence of the material properties of a poly(D,L-lactide)/β-tricalcium phosphate composite on the processability by selective laser sintering, J Mech Behav Biomed Mater, 87 (2018), pp. 267-78.
[167] Drummer D, Rietzel D, Kühnlein F Development of a characterization approach for the sintering behavior of new thermoplastics for selective laser sintering, Phys Procedia, 5 (2010), pp. 533-42.
[168] Du Y, Liu H, Shuang J, Wang J, Ma J, Zhang S Microsphere-based selective laser sintering for building macroporous bone scaffolds with controlled microstructure and excellent biocompatibility, Colloids Surf B Biointerfaces, 135 (2015), pp. 81-9.

[169] Schmid M, Amado A, Wegener K Polymer powders for selective laser sintering (SLS), AIP Conf Proc, 1664 (2015), pp. 160009.
[170] Velu R, Singamneni S Selective laser sintering of polymer biocomposites based on polymethyl methacrylate, J Mater Res, 29 (2014), pp. 1883-92.
[171] Shi Y, Chen J, Wang Y, Li Z, Huang S Study of the selective laser sintering of polycarbonate and postprocess for parts reinforcement, Proc Inst Mech Eng, Part L, 221 (2007), pp. 37-42.
[172] Antonov EN, Bagratashvili VN, Whitaker MJ, Barry JJA, Shakesheff KM, Konovalov AN, et al. Three-Dimensional Bioactive and Biodegradable Scaffolds Fabricated by Surface-Selective Laser Sintering, Adv Mater, 17 (2004), pp. 327-30.
[173] Lindner M, Hoeges S, Meiners W, Wissenbach K, Smeets R, Telle R, et al. Manufacturing of individual biodegradable bone substitute implants using selective laser melting technique, J Biomed Mater Res A, 97A (2011), pp. 466-71.
[174] Lee P-H, Chang E, Yu S, Lee SW, Kim IW, Park S, et al. Modification and characteristics of biodegradable polymer suitable for selective laser sintering, Int J, Precis, Eng, Manuf,, 14 (2013), pp. 1079-86.
[175] Wiria FE, Leong KF, Chua CK, Liu Y Poly-ε-caprolactone/hydroxyapatite for tissue engineering scaffold fabrication via selective laser sintering, Acta Biomater, 3 (2007), pp. 1-12.
[176] Eosoly S, Lohfeld S, Brabazon D Effect of Hydroxyapatite on Biodegradable Scaffolds Fabricated by SLS, Key Eng Mater, 396-398 (2009), pp. 659-62.
[177] Eshraghi S, Das S Mechanical and microstructural properties of polycaprolactone scaffolds with one-dimensional, two-dimensional, and three-dimensional orthogonally oriented porous architectures produced by selective laser sintering, Acta Biomater, 6 (2010), pp. 2467-76.
[178] Antonov EN, Bagratashvili VN, Howdle SM, Konovalov AN, Popov VK, Panchenko VY Fabrication of polymer scaffolds for tissue engineering using surface selective laser sintering, Laser Phys, 16 (2006), pp. 774-87.
[179] Duan B, Wang M, Zhou WY, Cheung WL, Li ZY, Lu WW Three-dimensional nanocomposite scaffolds fabricated via selective laser sintering for bone tissue engineering, Acta Biomater, 6 (2010), pp. 4495-505.
[180] Duan B, Wang M Customized Ca–P/PHBV nanocomposite scaffolds for bone tissue engineering: design, fabrication, surface modification and sustained release of growth factor, J Royal Soc Interface, 7 (2010), pp. S615-S29.
[181] Duan B, Cheung WL, Wang M Optimized fabrication of Ca–P/PHBV nanocomposite scaffolds via selective laser sintering for bone tissue engineering, Biofabrication, 3 (2011), pp. 015001.
[182] Sachs E, Cima M, Williams P, Brancazio D, Cornie J Three Dimensional Printing: Rapid Tooling and Prototypes Directly from a CAD Model, J Eng Ind, 114 (1992), pp. 481-8.
[183] Utela B, Storti D, Anderson R, Ganter M A review of process development steps for new material systems in three dimensional printing (3DP), J Manuf Process, 10 (2008), pp. 96-104.
[184] Gbureck U, Hölzel T, Biermann I, Barralet JE, Grover LM Preparation of tricalcium phosphate/calcium pyrophosphate structures via rapid prototyping, J Mater Sci Mater Med, 19 (2008), pp. 1559-63.
[185] Shanjani Y, De Croos JNA, Pilliar RM, Kandel RA, Toyserkani E Solid freeform fabrication and characterization of porous calcium polyphosphate structures for tissue engineering purposes, J Biomed Mater Res B Appl Biomater, 93B (2010), pp. 510-9.
[186] Pravin S, Sudhir A Integration of 3D printing with dosage forms: A new perspective for modern healthcare, Biomed Pharmacother, 107 (2018), pp. 146-54.
[187] Garzón EO, Alves JL, Neto RJ. Post-process Influence of Infiltration on Binder Jetting Technology. In: Silva LFMd, editor. Materials Design and Applications. Cham: Springer International Publishing; 2017. p. 233-55.

[188] Cima L, Cima M. Preparation of medical devices by solid free-form fabrication methods. US Patent and Trademark Office. United States: Massachusetts Institute of Technology; 1996.
[189] Wei Q, Wang Y, Chai W, Zhang Y, Chen X Molecular dynamics simulation and experimental study of the bonding properties of polymer binders in 3D powder printed hydroxyapatite bioceramic bone scaffolds, Ceram Int, 43 (2017), pp. 13702-9.
[190] Wei Q, Wang Y, Li X, Yang M, Chai W, Wang K, et al. Study the bonding mechanism of binders on hydroxyapatite surface and mechanical properties for 3DP fabrication bone scaffolds, J Mech Behav Biomed Mater, 57 (2016), pp. 190-200.
[191] Shao H, Sun M, Zhang F, Liu A, He Y, Fu J, et al. Custom Repair of Mandibular Bone Defects with 3D Printed Bioceramic Scaffolds, J Dent Res, 97 (2017), pp. 68-76.
[192] Seidenstuecker M, Kerr L, Bernstein A, Mayr OH, Suedkamp PN, Gadow R, et al. 3D Powder Printed Bioglass and β-Tricalcium Phosphate Bone Scaffolds, Materials, 11 (2018), pp.
[193] Deng Y, Jiang C, Li C, Li T, Peng M, Wang J, et al. 3D printed scaffolds of calcium silicate-doped β-TCP synergize with co-cultured endothelial and stromal cells to promote vascularization and bone formation, Sci Rep, 7 (2017), pp. 5588.
[194] Miguel C, Marta D, Uwe G, Jürgen G, Paulo F, Inês P, et al. Fabrication of computationally designed scaffolds by low temperature 3D printing, Biofabrication, 5 (2013), pp. 035012.
[195] Trombetta R, Inzana JA, Schwarz EM, Kates SL, Awad HA 3D Printing of Calcium Phosphate Ceramics for Bone Tissue Engineering and Drug Delivery, Ann Biomed Eng, 45 (2017), pp. 23-44.
[196] Barba A, Diez-Escudero A, Maazouz Y, Rappe K, Espanol M, Montufar EB, et al. Osteoinduction by Foamed and 3D-Printed Calcium Phosphate Scaffolds: Effect of Nanostructure and Pore Architecture, ACS Appl Mater Interfaces, 9 (2017), pp. 41722-36.
[197] Khalyfa A, Vogt S, Weisser J, Grimm G, Rechtenbach A, Meyer W, et al. Development of a new calcium phosphate powder-binder system for the 3D printing of patient specific implants, J Mater Sci Mater Med, 18 (2007), pp. 909-16.
[198] Lin S, Chao PY, Chien YW, Sayani S, Kuma S, Mason M, et al. In vitro and in vivo evaluations of biodegradable implants for hormone replacement therapy: effect of system design and PK-PD relationship, AAPS PharmSciTech, 2 (2001), pp. E16.
[199] Lam CXF, Mo XM, Teoh SH, Hutmacher DW Scaffold development using 3D printing with a starch-based polymer, Mater Sci Eng, C, 20 (2002), pp. 49-56.
[200] Huang W, Zheng Q, Sun W, Xu H, Yang X Levofloxacin implants with predefined microstructure fabricated by three-dimensional printing technique, Int J Pharm, 339 (2007), pp. 33-8.
[201] Wu W, Zheng Q, Guo X, Sun J, Liu Y A programmed release multi-drug implant fabricated by three-dimensional printing technology for bone tuberculosis therapy, Biomed Mater, 4 (2009), pp. 065005.
[202] Wu W, Ye C, Zheng Q, Wu G, Cheng Z A therapeutic delivery system for chronic osteomyelitis via a multi-drug implant based on three-dimensional printing technology, J Biomater Appl, 31 (2016), pp. 250-60.
[203] Hutmacher DW Scaffolds in tissue engineering bone and cartilage, Biomaterials, 21 (2000), pp. 2529-43.
[204] Wang F, Shor L, Darling A, Khalil S, Sun W, Güçeri S, et al. Precision extruding deposition and characterization of cellular poly‐ε‐caprolactone tissue scaffolds, Rapid Prototyp J, 10 (2004), pp. 42-9.
[205] Gloria A, Russo T, De Santis R, Ambrosio L 3d Fiber Deposition Technique to Make Multifunctional and Tailor-Made Scaffolds for Tissue Engineering Applications, J Appl Biomater Biomech, 7 (2009), pp. 141-52.
[206] Landers R, Mülhaupt R Desktop manufacturing of complex objects, prototypes and biomedical scaffolds by means of computer‐assisted design combined with computer‐

guided 3D plotting of polymers and reactive oligomers, Macromol Mater Eng, 282 (2000), pp. 17-21.
[207] Mota C, Puppi D, Dinucci D, Errico C, Bártolo P, Chiellini F Dual-Scale Polymeric Constructs as Scaffolds for Tissue Engineering, Materials, 4 (2011), pp.
[208] Kim G, Son J, Park S, Kim W Hybrid process for fabricating 3D hierarchical scaffolds combining rapid prototyping and electrospinning, Macromol Rapid Commun, 29 (2008), pp. 1577-81.
[209] Moroni L, Schotel R, Hamann D, de Wijn JR, van Blitterswijk CA 3D Fiber-Deposited Electrospun Integrated Scaffolds Enhance Cartilage Tissue Formation, Adv Funct Mater, 18 (2008), pp. 53-60.
[210] Brown TD, Dalton PD, Hutmacher DW Melt electrospinning today: An opportune time for an emerging polymer process, Prog Polym Sci, 56 (2016), pp. 116-66.
[211] Brown TD, Dalton PD, Hutmacher DW Direct Writing By Way of Melt Electrospinning, Adv Mater, 23 (2011), pp. 5651-7.
[212] Gernot H, Tomasz J, Toby DB, Kathrin H, Claus M, Franz J, et al. Additive manufacturing of scaffolds with sub-micron filaments via melt electrospinning writing, Biofabrication, 7 (2015), pp. 035002.
[213] Marascio MGM, Antons J, Pioletti DP, Bourban P-E 3D Printing of Polymers with Hierarchical Continuous Porosity, Adv Mater Technol, 2 (2017), pp. 1700145.
[214] Rohner D, Hutmacher Dietmar W, Cheng Tan K, Oberholzer M, Hammer B In vivo efficacy of bone-marrow-coated polycaprolactone scaffolds for the reconstruction of orbital defects in the pig, J Biomed Mater Res B Appl Biomater, 66B (2003), pp. 574-80.
[215] Park SH, Park DS, Shin JW, Kang YG, Kim HK, Yoon TR, et al. Scaffolds for bone tissue engineering fabricated from two different materials by the rapid prototyping technique: PCL versus PLGA, J Mater Sci Mater Med, 23 (2012), pp. 2671-8.
[216] Jinku K, Sean M, Brandi T, Pedro A-U, Young-Hye S, David DD, et al. Rapid-prototyped PLGA/β-TCP/hydroxyapatite nanocomposite scaffolds in a rabbit femoral defect model, Biofabrication, 4 (2012), pp. 025003.
[217] Adeola DO, Zohreh I, Jennifer LS, David MLC, Eames BF, Daniel XBC Modulating mechanical behaviour of 3D-printed cartilage-mimetic PCL scaffolds: influence of molecular weight and pore geometry, Biofabrication, 8 (2016), pp. 025020.
[218] Chhaya MP, Melchels FPW, Holzapfel BM, Baldwin JG, Hutmacher DW Sustained regeneration of high-volume adipose tissue for breast reconstruction using computer aided design and biomanufacturing, Biomaterials, 52 (2015), pp. 551-60.
[219] Fuenmayor E, Forde M, Healy AV, Devine DM, Lyons JG, McConville C, et al. Material Considerations for Fused-Filament Fabrication of Solid Dosage Forms, Pharmaceutics, 10 (2018), pp. 44.
[220] Fitzharris ER, Watanabe N, Rosen DW, Shofner ML Effects of material properties on warpage in fused deposition modeling parts, Int J Adv Manuf Technol, 95 (2018), pp. 2059-70.
[221] Love LJ, Kunc V, Rios O, Duty CE, Elliott AM, Post BK, et al. The importance of carbon fiber to polymer additive manufacturing, J Mater Res, 29 (2014), pp. 1893-8.
[222] McIlroy C, Olmsted PD Disentanglement effects on welding behaviour of polymer melts during the fused-filament-fabrication method for additive manufacturing, Polymer, 123 (2017), pp. 376-91.
[223] Seppala JE, Migler KD Infrared thermography of welding zones produced by polymer extrusion additive manufacturing, Addit Manuf, 12 (2016), pp. 71-6.
[224] Costa SF, Duarte FM, Covas JA Estimation of filament temperature and adhesion development in fused deposition techniques, J Mater Process Technol, 245 (2017), pp. 167-79.
[225] Taubner V, Shishoo R Influence of processing parameters on the degradation of poly(L-lactide) during extrusion, J Appl Polym Sci, 79 (2001), pp. 2128-35.

[226] Cuiffo MA, Snyder J, Elliott AM, Romero N, Kannan S, Halada GP Impact of the Fused Deposition (FDM) Printing Process on Polylactic Acid (PLA) Chemistry and Structure, Applied Sciences, 7 (2017), pp.
[227] Carrasco F, Pagès P, Gámez-Pérez J, Santana OO, Maspoch ML Processing of poly(lactic acid): Characterization of chemical structure, thermal stability and mechanical properties, Polym Degrad Stab, 95 (2010), pp. 116-25.
[228] Woodruff MA, Hutmacher DW The return of a forgotten polymer—Polycaprolactone in the 21st century, Prog Polym Sci, 35 (2010), pp. 1217-56.
[229] Kempin W, Franz C, Koster L-C, Schneider F, Bogdahn M, Weitschies W, et al. Assessment of different polymers and drug loads for fused deposition modeling of drug loaded implants, Eur J Pharm Biopharm, 115 (2017), pp. 84-93.
[230] Aho J, Bøtker JP, Genina N, Edinger M, Arnfast L, Rantanen J Roadmap to 3D-Printed Oral Pharmaceutical Dosage Forms: Feedstock Filament Properties and Characterization for Fused Deposition Modeling, J Pharm Sci, 108 (2019), pp. 26-35.
[231] Li H, Tan C, Li L Review of 3D printable hydrogels and constructs, Mater Des, 159 (2018), pp. 20-38.
[232] Guo S-Z, Gosselin F, Guerin N, Lanouette A-M, Heuzey M-C, Therriault D Solvent-Cast Three-Dimensional Printing of Multifunctional Microsystems, Small, 9 (2013), pp. 4118-22.
[233] Khalil S, Sun W Bioprinting Endothelial Cells With Alginate for 3D Tissue Constructs, J Biomech Eng, 131 (2009), pp. 111002--8.
[234] Wang X, Yan Y, Pan Y, Xiong Z, Liu H, Cheng J, et al. Generation of Three-Dimensional Hepatocyte/Gelatin Structures with Rapid Prototyping System, Tissue Eng, 12 (2006), pp. 83-90.
[235] Billiet T, Gevaert E, De Schryver T, Cornelissen M, Dubruel P The 3D printing of gelatin methacrylamide cell-laden tissue-engineered constructs with high cell viability, Biomaterials, 35 (2014), pp. 49-62.
[236] Puppi D, Migone C, Morelli A, Bartoli C, Gazzarri M, Pasini D, et al. Microstructured chitosan/poly(γ-glutamic acid) polyelectrolyte complex hydrogels by computer-aided wet-spinning for biomedical three-dimensional scaffolds, J Bioact Compatible Polym, 31 (2016), pp. 531-49.
[237] Hansen CJ, Saksena R, Kolesky DB, Vericella JJ, Kranz SJ, Muldowney GP, et al. High-Throughput Printing via Microvascular Multinozzle Arrays, Adv Mater, 25 (2013), pp. 96-102.
[238] Mota C, Wang SY, Puppi D, Gazzarri M, Migone C, Chiellini F, et al. Additive manufacturing of poly[(R)-3-hydroxybutyrate-co-(R)-3-hydroxyhexanoate] scaffolds for engineered bone development, J Tissue Eng Regener Med, 11 (2017), pp. 175-86.
[239] Puppi D, Morelli A, Chiellini F Additive Manufacturing of Poly(3-hydroxybutyrate-co-3-hydroxyhexanoate)/poly(ε-caprolactone) Blend Scaffolds for Tissue Engineering, Bioengineering, 4 (2017), pp. 49.
[240] Zhang B, He J, Li X, Xu F, Li D Micro/nanoscale electrohydrodynamic printing: from 2D to 3D, Nanoscale, 8 (2016), pp. 15376-88.
[241] Bu N, Huang Y, Wang X, Yin Z Continuously Tunable and Oriented Nanofiber Direct-Written by Mechano-Electrospinning, Mater Manuf Processes, 27 (2012), pp. 1318-23.
[242] Huang Y, Duan Y, Ding Y, Bu N, Pan Y, Lu N, et al. Versatile, kinetically controlled, high precision electrohydrodynamic writing of micro/nanofibers, Sci Rep, 4 (2014), pp. 5949.
[243] Huihua Y, Qihui Z, Biyun L, Min B, Xiangxin L, Yanzhong Z Direct printing of patterned three-dimensional ultrafine fibrous scaffolds by stable jet electrospinning for cellular ingrowth, Biofabrication, 7 (2015), pp. 045004.
[244] Luo G, Teh KS, Liu Y, Zang X, Wen Z, Lin L Direct-Write, Self-Aligned Electrospinning on Paper for Controllable Fabrication of Three-Dimensional Structures, ACS Appl Mater Interfaces, 7 (2015), pp. 27765-70.

[245] Lee M, Kim H-Y Toward Nanoscale Three-Dimensional Printing: Nanowalls Built of Electrospun Nanofibers, Langmuir, 30 (2014), pp. 1210-4.
[246] Lee J, Lee SY, Jang J, Jeong YH, Cho D-W Fabrication of Patterned Nanofibrous Mats Using Direct-Write Electrospinning, Langmuir, 28 (2012), pp. 7267-75.
[247] Wang J-C, Chang M-W, Ahmad Z, Li J-S Fabrication of patterned polymer-antibiotic composite fibers via electrohydrodynamic (EHD) printing, J Drug Deliv Sci Technol, 35 (2016), pp. 114-23.
[248] Puppi D, Chiellini F. 12 - Drug release kinetics of electrospun fibrous systems. In: Focarete ML, Tampieri A, editors. Core-Shell Nanostructures for Drug Delivery and Theranostics. Woodhead Publishing; 2018. p. 349-74.
[249] Altobelli R, Guarino V, Ambrosio L Micro- and nanocarriers by electrofludodynamic technologies for cell and molecular therapies, Process Biochem, 51 (2016), pp. 2143-54.
[250] Dorj B, Park J-H, Kim H-W Robocasting chitosan/nanobioactive glass dual-pore structured scaffolds for bone engineering, Mater Lett, 73 (2012), pp. 119-22.
[251] Mota C, Puppi D, Dinucci D, Gazzarri M, Chiellini F Additive manufacturing of star poly(ε-caprolactone) wet-spun scaffolds for bone tissue engineering applications, J Bioact Compatible Polym, 28 (2013), pp. 320-40.
[252] Puppi D, Migone C, Grassi L, Pirosa A, Maisetta G, Batoni G, et al. Integrated three-dimensional fiber/hydrogel biphasic scaffolds for periodontal bone tissue engineering, Polym Int, 65 (2016), pp. 631-40.
[253] Puppi D, Pirosa A, Lupi G, Erba PA, Giachi G, Chiellini F Design and fabrication of novel polymeric biodegradable stents for small caliber blood vessels by computer-aided wet-spinning, Biomed Mater, 12 (2017), pp. 035011.
[254] Puppi D, Braccini S, Ranaudo A, Federica C Poly(3-hydroxybutyrate-co-3-hydroxyexanoate) scaffolds with tunable macro- and microstructural features by additive manufacturing, J Biotechnol, 308 (2020), pp. 96-107.
[255] Xiong Z, Yan Y, Wang S, Zhang R, Zhang C Fabrication of porous scaffolds for bone tissue engineering via low-temperature deposition, Scripta Mater, 46 (2002), pp. 771-6.
[256] Zhu N, Li MG, Cooper D, Chen XB Development of novel hybrid poly(l-lactide)/chitosan scaffolds using the rapid freeze prototyping technique, Biofabrication, 3 (2011), pp. 034105.
[257] Kim G, Ahn S, Yoon H, Kim Y, Chun W A cryogenic direct-plotting system for fabrication of 3D collagen scaffolds for tissue engineering, J Mater Chem, 19 (2009), pp. 8817-23.
[258] Puppi D, Pirosa A, Morelli A, Chiellini F Design, fabrication and characterization of tailored poly[(R)-3-hydroxybutyrate-*co*-(R)-3-hydroxyexanoate] scaffolds by Computer-aided Wet-spinning, Rapid Prototyp J, 24 (2018), pp. 1-8.
[259] Vozzi G, Previti A, De Rossi D, Ahluwalia A Microsyringe-Based Deposition of Two-Dimensional and Three-Dimensional Polymer Scaffolds with a Well-Defined Geometry for Application to Tissue Engineering, Tissue Eng, 8 (2002), pp. 1089-98.
[260] Vozzi G, Flaim C, Ahluwalia A, Bhatia S Fabrication of PLGA scaffolds using soft lithography and microsyringe deposition, Biomaterials, 24 (2003), pp. 2533-40.
[261] Serra T, Planell JA, Navarro M High-resolution PLA-based composite scaffolds via 3-D printing technology, Acta Biomater, 9 (2013), pp. 5521-30.
[262] Serra T, Ortiz-Hernandez M, Engel E, Planell JA, Navarro M Relevance of PEG in PLA-based blends for tissue engineering 3D-printed scaffolds, Mater Sci Eng, C, 38 (2014), pp. 55-62.
[263] Deitzel JM, Kleinmeyer J, Harris D, Beck Tan NC The effect of processing variables on the morphology of electrospun nanofibers and textiles, Polymer, 42 (2001), pp. 261-72.
[264] Tan SH, Inai R, Kotaki M, Ramakrishna S Systematic parameter study for ultra-fine fiber fabrication via electrospinning process, Polymer, 46 (2005), pp. 6128-34.

[265] Chung JHY, Naficy S, Yue Z, Kapsa R, Quigley A, Moulton SE, et al. Bio-ink properties and printability for extrusion printing living cells, Biomater Sci, 1 (2013), pp. 763-73.
[266] Draget KI, Skjåk-Bræk G, Smidsrød O Alginate based new materials, Int J Biol Macromol, 21 (1997), pp. 47-55.
[267] Sakai S, Kamei H, Mori T, Hotta T, Ohi H, Nakahata M, et al. Visible Light-Induced Hydrogelation of an Alginate Derivative and Application to Stereolithographic Bioprinting Using a Visible Light Projector and Acid Red, Biomacromolecules, 19 (2018), pp. 672-9.
[268] Ouyang L, Highley CB, Sun W, Burdick JA A Generalizable Strategy for the 3D Bioprinting of Hydrogels from Nonviscous Photo-crosslinkable Inks, Adv Mater, 29 (2016), pp. 1604983.
[269] Wang Z, Jin X, Dai R, Holzman JF, Kim K An ultrafast hydrogel photocrosslinking method for direct laser bioprinting, RSC Adv, 6 (2016), pp. 21099-104.
[270] Liu S, Li L Recoverable and Self-Healing Double Network Hydrogel Based on κ-Carrageenan, ACS Appl Mater Interfaces, 8 (2016), pp. 29749-58.
[271] Liu S, Li L Ultrastretchable and Self-Healing Double-Network Hydrogel for 3D Printing and Strain Sensor, ACS Appl Mater Interfaces, 9 (2017), pp. 26429-37.
[272] Kim JE, Kim SH, Jung Y Current status of three-dimensional printing inks for soft tissue regeneration, Tissue Eng Regen Med, 13 (2016), pp. 636-46.
[273] Bertlein S, Brown G, Lim KS, Jungst T, Boeck T, Blunk T, et al. Thiol–Ene Clickable Gelatin: A Platform Bioink for Multiple 3D Biofabrication Technologies, Adv Mater, 29 (2017), pp. 1703404.
[274] Ooi HW, Mota C, ten Cate AT, Calore A, Moroni L, Baker MB Thiol–Ene Alginate Hydrogels as Versatile Bioinks for Bioprinting, Biomacromolecules, 19 (2018), pp. 3390-400.
[275] Hoyle CE, Bowman CN Thiol–Ene Click Chemistry, Angew Chem, 49 (2010), pp. 1540-73.
[276] Stichler S, Jungst T, Schamel M, Zilkowski I, Kuhlmann M, Böck T, et al. Thiol-ene Clickable Poly(glycidol) Hydrogels for Biofabrication, Ann Biomed Eng, 45 (2017), pp. 273-85.
[277] Hoch E, Schuh C, Hirth T, Tovar GEM, Borchers K Stiff gelatin hydrogels can be photochemically synthesized from low viscous gelatin solutions using molecularly functionalized gelatin with a high degree of methacrylation, J Mater Sci Mater Med, 23 (2012), pp. 2607-17.
[278] Lee BH, Lum N, Seow LY, Lim PQ, Tan LP Synthesis and Characterization of Types A and B Gelatin Methacryloyl for Bioink Applications, Materials, 9 (2016), pp. 797.
[279] Hinton TJ, Jallerat Q, Palchesko RN, Park JH, Grodzicki MS, Shue H-J, et al. Three-dimensional printing of complex biological structures by freeform reversible embedding of suspended hydrogels, Sci Adv, 1 (2015), pp. e1500758-e.
[280] Ozbolat IT, Peng W, Ozbolat V Application areas of 3D bioprinting, Drug Discov Today, 21 (2016), pp. 1257-71.
[281] Groll J, Burdick JA, Cho DW, Derby B, Gelinsky M, Heilshorn SC, et al. A definition of bioinks and their distinction from biomaterial inks, Biofabrication, 11 (2018), pp. 013001.
[282] Chan V, Zorlutuna P, Jeong JH, Kong H, Bashir R Three-dimensional photopatterning of hydrogels using stereolithography for long-term cell encapsulation, Lab Chip, 10 (2010), pp. 2062-70.
[283] Li S, Yan Y, Xiong Z, Zhang CWR, Wang X Gradient Hydrogel Construct Based on an Improved Cell Assembling System, J Bioact Compatible Polym, 24 (2009), pp. 84-99.
[284] Shengjie L, Zhuo X, Xiaohong W, Yongnian Y, Haixia L, Renji Z Direct Fabrication of a Hybrid Cell/Hydrogel Construct by a Double-nozzle Assembling Technology, J Bioact Compatible Polym, 24 (2009), pp. 249-65.
[285] Xu M, Van Y, Liu H, Yag R, Wang X Controlled Adipose-derived Stromal Cells Differentiation into Adipose and Endothelial Cells in a 3D Structure Established by Cell-assembly Technique, J Bioact Compatible Polym, 24 (2009), pp. 31-47.

[286] Xu M, Wang X, Yan Y, Yao R, Ge Y An cell-assembly derived physiological 3D model of the metabolic syndrome, based on adipose-derived stromal cells and a gelatin/alginate/fibrinogen matrix, Biomaterials, 31 (2010), pp. 3868-77.
[287] Xu W, Wang X, Yan Y, Zhang R A Polyurethane-Gelatin Hybrid Construct for Manufacturing Implantable Bioartificial Livers, J Bioact Compatible Polym, 23 (2008), pp. 409-22.
[288] Wang X, He K, Zhang W Optimizing the fabrication processes for manufacturing a hybrid hierarchical polyurethane–cell/hydrogel construct, J Bioact Compatible Polym, 28 (2013), pp. 303-19.
[289] Huang Y, He K, Wang X Rapid prototyping of a hybrid hierarchical polyurethane-cell/hydrogel construct for regenerative medicine, Mater Sci Eng, C, 33 (2013), pp. 3220-9.
[290] Costantini M, Colosi C, Święszkowski W, Barbetta A Co-axial wet-spinning in 3D bioprinting: state of the art and future perspective of microfluidic integration, Biofabrication, 11 (2018), pp. 012001.
[291] Ji S, Guvendiren M Recent Advances in Bioink Design for 3D Bioprinting of Tissues and Organs, Front Bioeng Biotechnol, 5 (2017), pp. 23-.
[292] Xu T, Zhao W, Zhu J-M, Albanna MZ, Yoo JJ, Atala A Complex heterogeneous tissue constructs containing multiple cell types prepared by inkjet printing technology, Biomaterials, 34 (2013), pp. 130-9.
[293] Xu T, Gregory CA, Molnar P, Cui X, Jalota S, Bhaduri SB, et al. Viability and electrophysiology of neural cell structures generated by the inkjet printing method, Biomaterials, 27 (2006), pp. 3580-8.
[294] Barron JA, Spargo BJ, Ringeisen BR Biological laser printing of three dimensional cellular structures, Appl Phys A, 79 (2004), pp. 1027-30.
[295] Koch L, Kuhn S, Sorg H, Gruene M, Schlie S, Gaebel R, et al. Laser Printing of Skin Cells and Human Stem Cells2009.
[296] Doraiswamy A, Narayan RJ, Lippert T, Urech L, Wokaun A, Nagel M, et al. Excimer laser forward transfer of mammalian cells using a novel triazene absorbing layer, Appl Surf Sci, 252 (2006), pp. 4743-7.
[297] Rhee S, Puetzer JL, Mason BN, Reinhart-King CA, Bonassar LJ 3D Bioprinting of Spatially Heterogeneous Collagen Constructs for Cartilage Tissue Engineering, ACS Biomater Sci Eng, 2 (2016), pp. 1800-5.
[298] Gao G, Yonezawa T, Hubbell K, Dai G, Cui X Inkjet-bioprinted acrylated peptides and PEG hydrogel with human mesenchymal stem cells promote robust bone and cartilage formation with minimal printhead clogging, Biotechnol J, 10 (2015), pp. 1568-77.
[299] Michael M, Jana B, Matthias S, Marcy Z-W Nanostructured Pluronic hydrogels as bioinks for 3D bioprinting, Biofabrication, 7 (2015), pp. 035006.
[300] Ng WL, Yeong WY, Naing MW Polyvinylpyrrolidone-Based Bio-Ink Improves Cell Viability and Homogeneity during Drop-On-Demand Printing, Materials, 10 (2017), pp. 190.
[301] Gilbert F, O'Connell CD, Mladenovska T, Dodds S Print Me an Organ? Ethical and Regulatory Issues Emerging from 3D Bioprinting in Medicine, Sci Eng Ethics, 24 (2018), pp. 73-91.
[302] Ozbolat IT, Moncal KK, Gudapati H Evaluation of bioprinter technologies, Addit Manuf, 13 (2017), pp. 179-200.
[303] Ouyang L, Highley CB, Rodell CB, Sun W, Burdick JA 3D Printing of Shear-Thinning Hyaluronic Acid Hydrogels with Secondary Cross-Linking, ACS Biomater Sci Eng, 2 (2016), pp. 1743-51.
[304] Liu W, Heinrich MA, Zhou Y, Akpek A, Hu N, Liu X, et al. Extrusion Bioprinting of Shear-Thinning Gelatin Methacryloyl Bioinks, Adv Healthcare Mater, 6 (2017), pp. 10.1002/adhm.201601451.

[305] Pereira RF, Sousa A, Barrias CC, Bayat A, Granja PL, Bártolo PJ Advances in bioprinted cell-laden hydrogels for skin tissue engineering, Biomanufact Rev, 2 (2017), pp. 1.
[306] Pereira RF, Bártolo PJ 3D bioprinting of photocrosslinkable hydrogel constructs, J Appl Polym Sci, 132 (2015), pp.
[307] Lim KS, Schon BS, Mekhileri NV, Brown GCJ, Chia CM, Prabakar S, et al. New Visible-Light Photoinitiating System for Improved Print Fidelity in Gelatin-Based Bioinks, ACS Biomater Sci Eng, 2 (2016), pp. 1752-62.
[308] Ashammakhi N, Ahadian S, Xu C, Montazerian H, Ko H, Nasiri R, et al. Bioinks and bioprinting technologies to make heterogeneous and biomimetic tissue constructs, Materials Today Bio, 1 (2019), pp. 100008.
[309] Morelli A, Puppi D, Chiellini F Polymers from Renewable Resources, J Renewable Mater, 1 (2013), pp. 83-112.
[310] Van Hoorick J, Declercq H, De Muynck A, Houben A, Van Hoorebeke L, Cornelissen R, et al. Indirect additive manufacturing as an elegant tool for the production of self-supporting low density gelatin scaffolds, J Mater Sci Mater Med, 26 (2015), pp. 247.
[311] Puppi D, Pecorini G, Chiellini F Biomedical Processing of Polyhydroxyalkanoates, Bioengineering, 6 (2019), pp. 108.
[312] Miranda-Nieves D, Chaikof EL Collagen and Elastin Biomaterials for the Fabrication of Engineered Living Tissues, ACS Biomater Sci Eng, 3 (2017), pp. 694-711.
[313] Gopinathan J, Noh I Recent trends in bioinks for 3D printing, Biomater Res, 22 (2018), pp. 11.
[314] SeungHyun A, Young Ho K, GeunHyung K A three-dimensional hierarchical collagen scaffold fabricated by a combined solid freeform fabrication (SFF) and electrospinning process to enhance mesenchymal stem cell (MSC) proliferation, J Micromech Microeng, 20 (2010), pp. 065015.
[315] Lee V, Singh G, Trasatti JP, Bjornsson C, Xu X, Tran TN, et al. Design and Fabrication of Human Skin by Three-Dimensional Bioprinting, Tissue Eng Part C, 20 (2013), pp. 473-84.
[316] Tao X, Kyle WB, Mohammad ZA, Dennis D, Weixin Z, James JY, et al. Hybrid printing of mechanically and biologically improved constructs for cartilage tissue engineering applications, Biofabrication, 5 (2013), pp. 015001.
[317] Yang X, Lu Z, Wu H, Li W, Zheng L, Zhao J Collagen-alginate as bioink for three-dimensional (3D) cell printing based cartilage tissue engineering, Mater Sci Eng, C, 83 (2018), pp. 195-201.
[318] Anja L, Michael M, Sophie B, Birgit P, Hagen B, Michaela S, et al. Additive manufacturing of collagen scaffolds by three-dimensional plotting of highly viscous dispersions, Biofabrication, 8 (2016), pp. 015015.
[319] Nocera AD, Comín R, Salvatierra NA, Cid MP Development of 3D printed fibrillar collagen scaffold for tissue engineering, Biomed Microdevices, 20 (2018), pp. 26.
[320] Inzana JA, Olvera D, Fuller SM, Kelly JP, Graeve OA, Schwarz EM, et al. 3D printing of composite calcium phosphate and collagen scaffolds for bone regeneration, Biomaterials, 35 (2014), pp. 4026-34.
[321] Irvine SA, Agrawal A, Lee BH, Chua HY, Low KY, Lau BC, et al. Printing cell-laden gelatin constructs by free-form fabrication and enzymatic protein crosslinking, Biomed Microdevices, 17 (2015), pp. 16.
[322] Yan Y, Wang X, Xiong Z, Liu H, Liu F, Lin F, et al. Direct Construction of a Three-dimensional Structure with Cells and Hydrogel, J Bioact Compatible Polym, 20 (2005), pp. 259-69.
[323] Rui Y, Renji Z, Yongnian Y, Xiaohong W In Vitro Angiogenesis of 3D Tissue Engineered Adipose Tissue, J Bioact Compatible Polym, 24 (2009), pp. 5-24.
[324] Yan Y, Wang X, Pan Y, Liu H, Cheng J, Xiong Z, et al. Fabrication of viable tissue-engineered constructs with 3D cell-assembly technique, Biomaterials, 26 (2005), pp. 5864-71.

[325] Zhang T, Yan Y, Wang X, Xiong Z, Lin F, Wu R, et al. Three-dimensional Gelatin and Gelatin/Hyaluronan Hydrogel Structures for Traumatic Brain Injury, J Bioact Compatible Polym, 22 (2007), pp. 19-29.
[326] Mũnoz Z, Shih H, Lin C-C Gelatin hydrogels formed by orthogonal thiol–norbornene photochemistry for cell encapsulation, Biomater Sci, 2 (2014), pp. 1063-72.
[327] Greene T, Lin C-C Modular Cross-Linking of Gelatin-Based Thiol–Norbornene Hydrogels for in Vitro 3D Culture of Hepatocellular Carcinoma Cells, ACS Biomater Sci Eng, 1 (2015), pp. 1314-23.
[328] Cui X, Boland T Human microvasculature fabrication using thermal inkjet printing technology, Biomaterials, 30 (2009), pp. 6221-7.
[329] Lee Y-B, Polio S, Lee W, Dai G, Menon L, Carroll RS, et al. Bio-printing of collagen and VEGF-releasing fibrin gel scaffolds for neural stem cell culture, Exp Neurol, 223 (2010), pp. 645-52.
[330] Ozbolat IT, Hospodiuk M Current advances and future perspectives in extrusion-based bioprinting, Biomaterials, 76 (2016), pp. 321-43.
[331] Gruene M, Pflaum M, Hess C, Diamantouros S, Schlie S, Deiwick A, et al. Laser Printing of Three-Dimensional Multicellular Arrays for Studies of Cell–Cell and Cell–Environment Interactions, Tissue Eng Part C, 17 (2011), pp. 973-82.
[332] Kolesky DB, Homan KA, Skylar-Scott MA, Lewis JA Three-dimensional bioprinting of thick vascularized tissues, Proc Natl Acad Sci, 113 (2016), pp. 3179.
[333] Hospodiuk M, Dey M, Sosnoski D, Ozbolat IT The bioink: A comprehensive review on bioprintable materials, Biotechnol Adv, 35 (2017), pp. 217-39.
[334] Jose RR, Brown JE, Polido KE, Omenetto FG, Kaplan DL Polyol-Silk Bioink Formulations as Two-Part Room-Temperature Curable Materials for 3D Printing, ACS Biomater Sci Eng, 1 (2015), pp. 780-8.
[335] Rodriguez MJ, Brown J, Giordano J, Lin SJ, Omenetto FG, Kaplan DL Silk based bioinks for soft tissue reconstruction using 3-dimensional (3D) printing with in vitro and in vivo assessments, Biomaterials, 117 (2017), pp. 105-15.
[336] Rodriguez MJ, Dixon TA, Cohen E, Huang W, Omenetto FG, Kaplan DL 3D freeform printing of silk fibroin, Acta Biomater, 71 (2018), pp. 379-87.
[337] Compaan AM, Christensen K, Huang Y Inkjet Bioprinting of 3D Silk Fibroin Cellular Constructs Using Sacrificial Alginate, ACS Biomater Sci Eng, 3 (2017), pp. 1519-26.
[338] Das S, Pati F, Choi Y-J, Rijal G, Shim J-H, Kim SW, et al. Bioprintable, cell-laden silk fibroin–gelatin hydrogel supporting multilineage differentiation of stem cells for fabrication of three-dimensional tissue constructs, Acta Biomater, 11 (2015), pp. 233-46.
[339] Kim SH, Yeon YK, Lee JM, Chao JR, Lee YJ, Seo YB, et al. Precisely printable and biocompatible silk fibroin bioink for digital light processing 3D printing, Nat Commun, 9 (2018), pp. 1620.
[340] Fuh JYH, Feng W, Geng L, Tong Loh H, San Wong Y, Hutmacher DW Direct writing of chitosan scaffolds using a robotic system, Rapid Prototyp J, 11 (2005), pp. 90-7.
[341] Ang TH, Sultana FSA, Hutmacher DW, Wong YS, Fuh JYH, Mo XM, et al. Fabrication of 3D chitosan–hydroxyapatite scaffolds using a robotic dispensing system, Mater Sci Eng, C, 20 (2002), pp. 35-42.
[342] Ye K, Felimban R, Traianedes K, Moulton SE, Wallace GG, Chung J, et al. Chondrogenesis of Infrapatellar Fat Pad Derived Adipose Stem Cells in 3D Printed Chitosan Scaffold, PLOS ONE, 9 (2014), pp. e99410.
[343] Wu Q, Maire M, Lerouge S, Therriault D, Heuzey M-C 3D Printing of Microstructured and Stretchable Chitosan Hydrogel for Guided Cell Growth, Adv Biosyst, 1 (2017), pp. 1700058.
[344] Wu Q, Therriault D, Heuzey M-C Processing and Properties of Chitosan Inks for 3D Printing of Hydrogel Microstructures, ACS Biomater Sci Eng, 4 (2018), pp. 2643-52.

[345] Shan-hui H, Chen-Huan L, Ching-Shiow T Air plasma treated chitosan fibers-stacked scaffolds, Biofabrication, 4 (2012), pp. 015002.
[346] Lisa E, Ruben F, Carlo B, Francesca Z, Cinzia M, Annalisa B, et al. Highly defined 3D printed chitosan scaffolds featuring improved cell growth, Biomed Mater, 12 (2017), pp. 045009.
[347] Intini C, Elviri L, Cabral J, Mros S, Bergonzi C, Bianchera A, et al. 3D-printed chitosan-based scaffolds: An in vitro study of human skin cell growth and an in-vivo wound healing evaluation in experimental diabetes in rats, Carbohydr Polym, 199 (2018), pp. 593-602.
[348] Liu Q, Li Q, Xu S, Zheng Q, Cao X Preparation and Properties of 3D Printed Alginate–Chitosan Polyion Complex Hydrogels for Tissue Engineering, Polymers, 10 (2018), pp.
[349] Shi P, Laude A, Yeong WY Investigation of cell viability and morphology in 3D bio-printed alginate constructs with tunable stiffness, J Biomed Mater Res A, 105 (2016), pp. 1009-18.
[350] Marchioli G, Gurp Lv, Krieken PPv, Stamatialis D, Engelse M, Blitterswijk CAv, et al. Fabrication of three-dimensional bioplotted hydrogel scaffolds for islets of Langerhans transplantation, Biofabrication, 7 (2015), pp. 025009.
[351] Ning L, Guillemot A, Zhao J, Kipouros G, Chen X Influence of Flow Behavior of Alginate–Cell Suspensions on Cell Viability and Proliferation, Tissue Eng Part C, 22 (2016), pp. 652-62.
[352] Leppiniemi J, Lahtinen P, Paajanen A, Mahlberg R, Metsä-Kortelainen S, Pinomaa T, et al. 3D-Printable Bioactivated Nanocellulose–Alginate Hydrogels, ACS Appl Mater Interfaces, 9 (2017), pp. 21959-70.
[353] Markstedt K, Mantas A, Tournier I, Martínez Ávila H, Hägg D, Gatenholm P 3D Bioprinting Human Chondrocytes with Nanocellulose–Alginate Bioink for Cartilage Tissue Engineering Applications, Biomacromolecules, 16 (2015), pp. 1489-96.
[354] Ahn S, Lee H, Kim G Functional cell-laden alginate scaffolds consisting of core/shell struts for tissue regeneration, Carbohydr Polym, 98 (2013), pp. 936-42.
[355] Martínez Ávila H, Schwarz S, Rotter N, Gatenholm P 3D bioprinting of human chondrocyte-laden nanocellulose hydrogels for patient-specific auricular cartilage regeneration, Bioprinting, 1-2 (2016), pp. 22-35.
[356] Håkansson KMO, Henriksson IC, de la Peña Vázquez C, Kuzmenko V, Markstedt K, Enoksson P, et al. Solidification of 3D Printed Nanofibril Hydrogels into Functional 3D Cellulose Structures, Adv Mater Technol, 1 (2016), pp. 1600096.
[357] Müller M, Öztürk E, Arlov Ø, Gatenholm P, Zenobi-Wong M Alginate Sulfate–Nanocellulose Bioinks for Cartilage Bioprinting Applications, Ann Biomed Eng, 45 (2017), pp. 210-23.
[358] Nguyen D, Hägg DA, Forsman A, Ekholm J, Nimkingratana P, Brantsing C, et al. Cartilage Tissue Engineering by the 3D Bioprinting of iPS Cells in a Nanocellulose/Alginate Bioink, Sci Rep, 7 (2017), pp. 658.
[359] Markstedt K, Sundberg J, Gatenholm P 3D Bioprinting of Cellulose Structures from an Ionic Liquid, 3D Print Addit Manuf, 1 (2014), pp. 115-21.
[360] Li VCF, Mulyadi A, Dunn CK, Deng Y, Qi HJ Direct Ink Write 3D Printed Cellulose Nanofiber Aerogel Structures with Highly Deformable, Shape Recoverable, and Functionalizable Properties, ACS Sustain Chem Eng, 6 (2018), pp. 2011-22.
[361] Markstedt K, Escalante A, Toriz G, Gatenholm P Biomimetic Inks Based on Cellulose Nanofibrils and Cross-Linkable Xylans for 3D Printing, ACS Appl Mater Interfaces, 9 (2017), pp. 40878-86.
[362] Pattinson SW, Hart AJ Additive Manufacturing of Cellulosic Materials with Robust Mechanics and Antimicrobial Functionality, Adv Mater Technol, 2 (2017), pp. 1600084.
[363] Wang Q, Sun J, Yao Q, Ji C, Liu J, Zhu Q 3D printing with cellulose materials, Cellulose, 25 (2018), pp. 4275-301.

[364] Kumar S, Hofmann M, Steinmann B, Foster EJ, Weder C Reinforcement of Stereolithographic Resins for Rapid Prototyping with Cellulose Nanocrystals, ACS Appl Mater Interfaces, 4 (2012), pp. 5399-407.
[365] Palaganas NB, Mangadlao JD, de Leon ACC, Palaganas JO, Pangilinan KD, Lee YJ, et al. 3D Printing of Photocurable Cellulose Nanocrystal Composite for Fabrication of Complex Architectures via Stereolithography, ACS Appl Mater Interfaces, 9 (2017), pp. 34314-24.
[366] Schuurman W, Levett PA, Pot MW, van Weeren PR, Dhert WJA, Hutmacher DW, et al. Gelatin-Methacrylamide Hydrogels as Potential Biomaterials for Fabrication of Tissue-Engineered Cartilage Constructs, Macromol Biosci, 13 (2013), pp. 551-61.
[367] Pescosolido L, Schuurman W, Malda J, Matricardi P, Alhaique F, Coviello T, et al. Hyaluronic Acid and Dextran-Based Semi-IPN Hydrogels as Biomaterials for Bioprinting, Biomacromolecules, 12 (2011), pp. 1831-8.
[368] Skardal A, Zhang J, McCoard L, Xu X, Oottamasathien S, Prestwich GD Photocrosslinkable hyaluronan-gelatin hydrogels for two-step bioprinting, Tissue Eng Part A, 16 (2010), pp. 2675-85.
[369] Kesti M, Müller M, Becher J, Schnabelrauch M, D'Este M, Eglin D, et al. A versatile bioink for three-dimensional printing of cellular scaffolds based on thermally and photo-triggered tandem gelation, Acta Biomater, 11 (2015), pp. 162-72.
[370] Highley CB, Rodell CB, Burdick JA Direct 3D Printing of Shear-Thinning Hydrogels into Self-Healing Hydrogels, Adv Mater, 27 (2015), pp. 5075-9.
[371] Skardal A, Zhang J, Prestwich GD Bioprinting vessel-like constructs using hyaluronan hydrogels crosslinked with tetrahedral polyethylene glycol tetracrylates, Biomaterials, 31 (2010), pp. 6173-81.
[372] Skardal A, Zhang J, McCoard L, Oottamasathien S, Prestwich GD Dynamically Crosslinked Gold Nanoparticle – Hyaluronan Hydrogels, Adv Mater, 22 (2010), pp. 4736-40.
[373] Stichler S, Böck T, Paxton N, Bertlein S, Levato R, Schill V, et al. Double printing of hyaluronic acid/poly(glycidol) hybrid hydrogels with poly(ε-caprolactone) for MSC chondrogenesis, Biofabrication, 9 (2017), pp. 044108.
[374] Poldervaart MT, Goversen B, de Ruijter M, Abbadessa A, Melchels FPW, Öner FC, et al. 3D bioprinting of methacrylated hyaluronic acid (MeHA) hydrogel with intrinsic osteogenicity, PLOS ONE, 12 (2017), pp. e0177628.
[375] Oliveira MF, Maia IA, Noritomi PY, Nargi GC, Silva JVL, Ferreira BMP, et al. Construção de Scaffolds para engenharia tecidual utilizando prototipagem rápida, Matéria, 12 (2007), pp. 373-82.
[376] Pereira TF, Silva MAC, Oliveira MF, Maia IA, Silva JVL, Costa MF, et al. Effect of process parameters on the properties of selective laser sintered Poly(3-hydroxybutyrate) scaffolds for bone tissue engineering AU - Pereira, T.F, Virtual Phys Prototyp, 7 (2012), pp. 275-85.
[377] Pereira TF, Oliveira MF, Maia IA, Silva JVL, Costa MF, Thiré RMSM 3D Printing of Poly(3-hydroxybutyrate) Porous Structures Using Selective Laser Sintering, Macromol Symp, 319 (2012), pp. 64-73.
[378] Kosorn W, Sakulsumbat M, Uppanan P, Kaewkong P, Chantaweroad S, Jitsaard J, et al. PCL/PHBV blended three dimensional scaffolds fabricated by fused deposition modeling and responses of chondrocytes to the scaffolds, J Biomed Mater Res B Appl Biomater, (2016), pp.
[379] Menčík P, Přikryl R, Stehnová I, Melčová V, Kontárová S, Figalla S, et al. Effect of Selected Commercial Plasticizers on Mechanical, Thermal, and Morphological Properties of Poly(3-hydroxybutyrate)/Poly(lactic acid)/Plasticizer Biodegradable Blends for Three-Dimensional (3D) Print, Materials, 11 (2018), pp.
[380] Hu X, Cebe P, Weiss AS, Omenetto F, Kaplan DL Protein-based composite materials, Mater Today, 15 (2012), pp. 208-15.

[381] Yue K, Trujillo-de Santiago G, Alvarez MM, Tamayol A, Annabi N, Khademhosseini A Synthesis, properties, and biomedical applications of gelatin methacryloyl (GelMA) hydrogels, Biomaterials, 73 (2015), pp. 254-71.
[382] Brown AC, Barker TH Fibrin-based biomaterials: Modulation of macroscopic properties through rational design at the molecular level, Acta Biomater, 10 (2014), pp. 1502-14.
[383] Volkov V, Ferreira AV, Cavaco-Paulo A On the Routines of Wild-Type Silk Fibroin Processing Toward Silk-Inspired Materials: A Review, Macromol Mater Eng, 300 (2015), pp. 1199-216.
[384] Lee CH, Singla A, Lee Y Biomedical applications of collagen, Int J Pharm, 221 (2001), pp. 1-22.
[385] Luis MD, Naledi S, Kieran F, Dimitrios IZ Acetic acid and pepsin result in high yield, high purity and low macrophage response collagen for biomedical applications, Biomed Mater, 12 (2017), pp. 065009.
[386] An B, Kaplan DL, Brodsky B Engineered recombinant bacterial collagen as an alternative collagen-based biomaterial for tissue engineering, Front Chem, 2 (2014), pp. 40-.
[387] Brodsky B, Werkmeister J, Ramshaw JA. Collagens and Gelatins. In: Fahnestock SR, Steinbüchel A, editors. Biopolymers. Weinheim: Wiley-VCH; 2003. p. 119-53.
[388] Gelse K, Pöschl E, Aigner T Collagens--structure, function, and biosynthesis, Adv Drug Del Rev, 55 (2003), pp. 1531-46.
[389] Angele P, Abke J, Kujat R, Faltermeier H, Schumann D, Nerlich M, et al. Influence of different collagen species on physico-chemical properties of crosslinked collagen matrices, Biomaterials, 25 (2004), pp. 2831-41.
[390] Yaylaoglu MB, Yıldız C, Korkusuz F, Hasırcı V Novel osteochondral implant, Biomaterials, 20 (1999), pp. 1513-20.
[391] Daamen WF, van Moerkerk HTB, Hafmans T, Buttafoco L, Poot AA, Veerkamp JH, et al. Preparation and evaluation of molecularly-defined collagen-elastin-glycosaminoglycan scaffolds for tissue engineering, Biomaterials, 24 (2003), pp. 4001-9.
[392] Liu L-S, Thompson AY, Heidaran MA, Poser JW, Spiro RC An osteoconductive collagen/hyaluronate matrix for bone regeneration, Biomaterials, 20 (1999), pp. 1097-108.
[393] Woerly S, Marchand R, Lavallée G Interactions of copolymeric poly(glyceryl methacrylate)-collagen hydrogels with neural tissue: effects of structure and polar groups, Biomaterials, 12 (1991), pp. 197-203.
[394] Rao JK, Ramesh DV, Rao KP Implantable controlled delivery systems for proteins based on collagenpHEMA hydrogels, Biomaterials, 15 (1994), pp. 383-9.
[395] Harriger MD, Supp AP, Warden GD, Boyce ST Glutaraldehyde crosslinking of collagen substrates inhibits degradation in skin substitutes grafted to athymic mice, J Biomed Mater Res, 35 (1997), pp. 137-45.
[396] Brinkman WT, Nagapudi K, Thomas BS, Chaikoff EL Photo-cross-linking of type I collagen gels in the presence of smooth muscle cells: Mechanical properties, cell viability, and function, Biomacromolecules, 4 (2003), pp. 890-5.
[397] Elbjeirami WM, Yonter EO, Starcher BC, West JL Enhancing mechanical properties of tissue-engineered constructs via lysyl oxidase crosslinking activity, J Biomed Mater Res A, 66A (2003), pp. 513-21.
[398] Fujioka-Kobayashi M, Schaller B, Saulacic N, Pippenger BE, Zhang Y, Miron RJ Absorbable collagen sponges loaded with recombinant bone morphogenetic protein 9 induces greater osteoblast differentiation when compared to bone morphogenetic protein 2, Clin, Exp, Dent Res, 3 (2017), pp. 32-40.
[399] Pulkkinen HJ, Tiitu V, Valonen P, Jurvelin JS, Lammi MJ, Kiviranta I Engineering of cartilage in recombinant human type II collagen gel in nude mouse model *in vivo*, Osteoarthritis Cartilage, 18 (2010), pp. 1077-87.

[400] Chamieh F, Collignon A-M, Coyac BR, Lesieur J, Ribes S, Sadoine J, et al. Accelerated craniofacial bone regeneration through dense collagen gel scaffolds seeded with dental pulp stem cells, Sci Rep, 6 (2016), pp. 38814.
[401] Dhand C, Ong ST, Dwivedi N, Diaz SM, Venugopal JR, Navaneethan B, et al. Bio-inspired in situ crosslinking and mineralization of electrospun collagen scaffolds for bone tissue engineering, Biomaterials, 104 (2016), pp. 323-38.
[402] Boland ED, Matthews JA, Pawlowski KJ, Simpson DG, Wnek GE, Bowlin GL Electrospinning collagen and elastin: preliminary vascular tissue engineering, Front Biosci, 9 (2004), pp. 1422-32.
[403] Venugopal J, Ma LL, Yong T, Ramakrishna S In vitro study of smooth muscle cells on polycaprolactone and collagen nanofibrous matrices, Cell Biol Int, 29 (2005), pp. 861-7.
[404] Stitzel J, Liu J, Lee SJ, Komura M, Berry J, Soker S, et al. Controlled fabrication of a biological vascular substitute, Biomaterials, 27 (2006), pp. 1088-94.
[405] Blanco NM, Edwards J, Zamboni WA Dermal Substitute (Integra) for Open Nasal Wounds, Plast Reconstr Surg, 113 (2004), pp. 2224-5.
[406] Priya SG, Jungvid H, Kumar A Skin Tissue Engineering for Tissue Repair and Regeneration, Tissue Eng Part B, 14 (2008), pp. 105-18.
[407] Bello YM, Falabella AF The role of Graftskin (Apligraf) in difficult-to-heal venous leg ulcers, J Wound Care, 11 (2002), pp. 182 - 3
[408] Nair LS, Laurencin CT Biodegradable polymers as biomaterials, Prog Polym Sci, 32 (2007), pp. 762-98.
[409] Atala A, Bauer SB, Soker S, Yoo JJ, Retik AB Tissue-engineered autologous bladders for patients needing cystoplasty, The Lancet, 367 (2006), pp. 1241-6.
[410] Raya-Rivera AM, Esquiliano D, Fierro-Pastrana R, López-Bayghen E, Valencia P, Ordorica-Flores R, et al. Tissue-engineered autologous vaginal organs in patients: a pilot cohort study, The Lancet, 384 (2014), pp. 329-36.
[411] Murphy SV, Skardal A, Atala A Evaluation of hydrogels for bio-printing applications, J Biomed Mater Res A, 101A (2012), pp. 272-84.
[412] Vaidya M Startups tout commercially 3D-printed tissue for drug screening, Nat Med, 21 (2015), pp. 2.
[413] Rimann M, Laternser S, Keller H, Leupin O, Graf-Hausner U 3D Bioprinted Muscle and Tendon Tissues for Drug Development, CHIMIA, 69 (2015), pp. 65-7.
[414] Hockaday L 3D Bioprinting: A Deliberate Business, Genetic Engineering & Biotechnology News, 35 (2014), pp. 14-7.
[415] https://www.bioprintabm.com/, 2018 [11/2018].
[416] Reiffel AJ, Kafka C, Hernandez KA, Popa S, Perez JL, Zhou S, et al. High-Fidelity Tissue Engineering of Patient-Specific Auricles for Reconstruction of Pediatric Microtia and Other Auricular Deformities, PLOS ONE, 8 (2013), pp. e56506.
[417] Li Y, Rodrigues J, Tomás H Injectable and biodegradable hydrogels: gelation, biodegradation and biomedical applications, Chem Soc Rev, 41 (2012), pp. 2193-221.
[418] Tabata Y, Ikada Y Protein release from gelatin matrices, Adv Drug Del Rev, 31 (1998), pp. 287-301.
[419] Young S, Wong M, Tabata Y, Mikos AG Gelatin as a delivery vehicle for the controlled release of bioactive molecules, J Controlled Release, 109 (2005), pp. 256-74.
[420] Maurer PH II. Antigenicity of Gelatin in Rabbits and other Species, J Exp Med, 100 (1954), pp. 515.
[421] Hellio D, Djabourov M Physically and Chemically Crosslinked Gelatin Gels, Macromol Symp, 241 (2006), pp. 23-7.
[422] Malafaya PB, Silva GA, Reis RL Natural-origin polymers as carriers and scaffolds for biomolecules and cell delivery in tissue engineering applications, Adv Drug Del Rev, 59 (2007), pp. 207-33.

[423] Yamada K, Tabata Y, Yamamoto K, Miyamoto S, Nagata I, Kikuchi H, et al. Potential efficacy of basic fibroblast growth factor incorporated in biodegradable hydrogels for skull bone regeneration, J Neurosurg, 86 (1997), pp. 871-5.
[424] Tabata Y, Nagano A, Muniruzzaman M, Ikada Y In vitro sorption and desorption of basic fibroblast growth factor from biodegradable hydrogels, Biomaterials, 19 (1998), pp. 1781-9.
[425] Yamamoto M, Takahashi Y, Tabata Y Controlled release by biodegradable hydrogels enhances the ectopic bone formation of bone morphogenetic protein, Biomaterials, 24 (2003), pp. 4375-83.
[426] Patel ZS, Yamamoto M, Ueda H, Tabata Y, Mikos AG Biodegradable gelatin microparticles as delivery systems for the controlled release of bone morphogenetic protein-2, Acta Biomater, 4 (2008), pp. 1126-38.
[427] Park H, Temenoff JS, Holland TA, Tabata Y, Mikos AG Delivery of TGF-[beta]1 and chondrocytes via injectable, biodegradable hydrogels for cartilage tissue engineering applications, Biomaterials, 26 (2005), pp. 7095-103.
[428] Malda J, Kreijveld E, Temenoff JS, Blitterswijk CAv, Riesle J Expansion of human nasal chondrocytes on macroporous microcarriers enhances redifferentiation, Biomaterials, 24 (2003), pp. 5153-61.
[429] Payne RG, Yaszemski MJ, Yasko AW, Mikos AG Development of an injectable, in situ crosslinkable, degradable polymeric carrier for osteogenic cell populations. Part 1. Encapsulation of marrow stromal osteoblasts in surface crosslinked gelatin microparticles, Biomaterials, 23 (2002), pp. 4359-71.
[430] Ponticiello MS, Schinagl RM, Kadiyala S, Barry FP Gelatin-based resorbable sponge as a carrier matrix for human mesenchymal stem cells in cartilage regeneration therapy, J Biomed Mater Res, 52 (2000), pp. 246-55.
[431] Liu Y, Shu XZ, Prestwich GD Osteochondral Defect Repair with Autologous Bone Marrowâ€“Derived Mesenchymal Stem Cells in an Injectable, In Situ, Cross-Linked Synthetic Extracellular Matrix, Tissue Eng, 12 (2006), pp. 3405-16.
[432] Kimura Y, Ozeki M, Inamoto T, Tabata Y Adipose tissue engineering based on human preadipocytes combined with gelatin microspheres containing basic fibroblast growth factor, Biomaterials, 24 (2003), pp. 2513-21.
[433] Detta N, Errico C, Dinucci D, Puppi D, Clarke D, Reilly G, et al. Novel electrospun polyurethane/gelatin composite meshes for vascular grafts, J Mater Sci Mater Med, 21 (2010), pp. 1761-9.
[434] Luo Y, Li Y, Qin X, Wa Q 3D printing of concentrated alginate/gelatin scaffolds with homogeneous nano apatite coating for bone tissue engineering, Mater Des, 146 (2018), pp. 12-9.
[435] Wu Z, Su X, Xu Y, Kong B, Sun W, Mi S Bioprinting three-dimensional cell-laden tissue constructs with controllable degradation, Sci Rep, 6 (2016), pp. 24474.
[436] Tse C, Zhang Y, Smith PJ. The use of reactive inkjet printing in tissue engineering. In: Smith PJ, Morrin A, editors. Reactive Inkjet Printing: A Chemical Synthesis Tool. Croydon, UK: CPI Group; 2018.
[437] Van Den Bulcke AI, Bogdanov B, De Rooze N, Schacht EH, Cornelissen M, Berghmans H Structural and Rheological Properties of Methacrylamide Modified Gelatin Hydrogels, Biomacromolecules, 1 (2000), pp. 31-8.
[438] Grogan SP, Chung PH, Soman P, Chen P, Lotz MK, Chen S, et al. Digital micromirror device projection printing system for meniscus tissue engineering, Acta Biomater, 9 (2013), pp. 7218-26.
[439] Melchels FPW, Dhert WJA, Hutmacher DW, Malda J Development and characterisation of a new bioink for additive tissue manufacturing, J Mater Chem B, 2 (2014), pp. 2282-9.

[440] Mouser VHM, Melchels FPW, Visser J, Dhert WJA, Gawlitta D, Malda J Yield stress determines bioprintability of hydrogels based on gelatin-methacryloyl and gellan gum for cartilage bioprinting, Biofabrication, 8 (2016), pp. 035003.
[441] Melchels FPW, Blokzijl MM, Levato R, Peiffer QC, Ruijter Md, Hennink WE, et al. Hydrogel-based reinforcement of 3D bioprinted constructs, Biofabrication, 8 (2016), pp. 035004.
[442] Ahmed TAE, Dare EV, Hincke M Fibrin: A Versatile Scaffold for Tissue Engineering Applications, Tissue Eng Part B, (2008), pp.
[443] Litvinov RI, Weisel JW What Is the Biological and Clinical Relevance of Fibrin?, Semin Thromb Hemost, 42 (2016), pp. 333-43.
[444] Ryan E, Mockros L, Weisel J, Lorand L Structural origins of fibrin clot rheology, Biophys J, 77 (1999), pp. 2813–26.
[445] Spotnitz WD Fibrin Sealant: Past, Present, and Future: A Brief Review, World J Surg, 34 (2010), pp. 632-4.
[446] Chapin JC, Hajjar KA Fibrinolysis and the control of blood coagulation, Blood Rev, 29 (2015), pp. 17-24.
[447] Ho W, Tawil B, Dunn JCY, Wu BM The Behavior of Human Mesenchymal Stem Cells in 3D Fibrin Clots: Dependence on Fibrinogen Concentration and Clot Structure, Tissue Eng, 12 (2006), pp. 1587-95.
[448] Jing P, Rudra JS, Herr AB, Collier JH Self-Assembling Peptide-Polymer Hydrogels Designed From the Coiled Coil Region of Fibrin, Biomacromolecules, 9 (2008), pp. 2438-46.
[449] Zhang G, Wang X, Wang Z, Zhang J, Suggs L A PEGylated Fibrin Patch for Mesenchymal Stem Cell Delivery, Tissue Eng, 12 (2006), pp. 9-19.
[450] Gamboa-Martínez TC, Luque-Guillén V, González-García C, Gómez Ribelles JL, Gallego-Ferrer G Crosslinked fibrin gels for tissue engineering: Two approaches to improve their properties, J Biomed Mater Res A, 103 (2014), pp. 614-21.
[451] Lieshout MV, Peters G, Rutten M, Baaijens F A Knitted, Fibrin-Covered Polycaprolactone Scaffold for Tissue Engineering of the Aortic Valve, Tissue Eng, 12 (2006), pp. 481-7.
[452] Rao RR, Peterson AW, Ceccarelli J, Putnam AJ, Stegemann JP Matrix composition regulates three-dimensional network formation by endothelial cells and mesenchymal stem cells in collagen/fibrin materials, Angiogenesis, 15 (2012), pp. 253-64.
[453] Vepari C, Kaplan DL Silk as a biomaterial, Prog Polym Sci, 32 (2007), pp. 991-1007.
[454] Rockwood DN, Preda RC, Yücel T, Wang X, Lovett ML, Kaplan DL Materials fabrication from Bombyx mori silk fibroin, Nat Protoc, 6 (2011), pp. 1612.
[455] Vepari C, Kaplan DL Silk as a biomaterial, Prog Polym Sci, 32 (2007), pp. 991-1007.
[456] Vollrath F, Knight DP Liquid crystalline spinning of spider silk, Nature, 410 (2001), pp. 541-8.
[457] Panilaitis B, Altman GH, Chen J, Jin H-J, Karageorgiou V, Kaplan DL Macrophage responses to silk, Biomaterials, 24 (2003), pp. 3079-85.
[458] Glisovic A, Vehoff T, Davies R, Salditt T Correlation between structure and mechanical properties of spider silk, Comp Biochem Physiol, A: Mol Integr Physiol, 146 (2007), pp. S138-S.
[459] Jin H-J, Kaplan DL Mechanism of silk processing in insects and spiders, Nature, 424 (2003), pp. 1057-61.
[460] Altman GH, Diaz F, Jakuba C, Calabro T, Horan RL, Chen J, et al. Silk-based biomaterials, Biomaterials, 24 (2003), pp. 401-16.
[461] Kundu B, Rajkhowa R, Kundu SC, Wang X Silk fibroin biomaterials for tissue regenerations, Adv Drug Del Rev, 65 (2013), pp. 457-70.

[462] Unger RE, Wolf M, Peters K, Motta A, Migliaresi C, James Kirkpatrick C Growth of human cells on a non-woven silk fibroin net: a potential for use in tissue engineering, Biomaterials, 25 (2004), pp. 1069-75.
[463] Zhang F, Zhang Z, Zhu X, Kang E-T, Neoh K-G Silk-functionalized titanium surfaces for enhancing osteoblast functions and reducing bacterial adhesion, Biomaterials, 29 (2008), pp. 4751-9.
[464] Unger RE, Peters K, Wolf M, Motta A, Migliaresi C, Kirkpatrick CJ Endothelialization of a non-woven silk fibroin net for use in tissue engineering: growth and gene regulation of human endothelial cells, Biomaterials, 25 (2004), pp. 5137-46.
[465] Fuchs S, Motta A, Migliaresi C, Kirkpatrick CJ Outgrowth endothelial cells isolated and expanded from human peripheral blood progenitor cells as a potential source of autologous cells for endothelialization of silk fibroin biomaterials, Biomaterials, 27 (2006), pp. 5399-408.
[466] Jin H-J, Chen J, Karageorgiou V, Altman GH, Kaplan DL Human bone marrow stromal cell responses on electrospun silk fibroin mats, Biomaterials, 25 (2004), pp. 1039-47.
[467] Pignatelli C, Perotto G, Nardini M, Cancedda R, Mastrogiacomo M, Athanassiou A Electrospun silk fibroin fibers for storage and controlled release of human platelet lysate, Acta Biomater, 73 (2018), pp. 365-76.
[468] Meinel L, Hofmann S, Karageorgiou V, Zichner L, Langer R, Kaplan D, et al. Engineering cartilage-like tissue using human mesenchymal stem cells and silk protein scaffolds, Biotechnol Bioeng, 88 (2004), pp. 379-91.
[469] Meinel L, Hofmann S, Betz O, Fajardo R, Merkle HP, Langer R, et al. Osteogenesis by human mesenchymal stem cells cultured on silk biomaterials: Comparison of adenovirus mediated gene transfer and protein delivery of BMP-2, Biomaterials, 27 (2006), pp. 4993-5002.
[470] Zhang X, Cao C, Ma X, Li Y Optimization of macroporous 3-D silk fibroin scaffolds by salt-leaching procedure in organic solvent-free conditions, J Mater Sci Mater Med, 23 (2012), pp. 315-24.
[471] Karageorgiou V, Meinel L, Hofmann S, Malhotra A, Volloch V, Kaplan D Bone morphogenetic protein-2 decorated silk fibroin films induce osteogenic differentiation of human bone marrow stromal cells, J Biomed Mater Res A, 71A (2004), pp. 528-37.
[472] Uebersax L, Merkle HP, Meinel L Insulin-like growth factor I releasing silk fibroin scaffolds induce chondrogenic differentiation of human mesenchymal stem cells, J Controlled Release, 127 (2008), pp. 12-21.
[473] Farokhi M, Mottaghitalab F, Samani S, Shokrgozar MA, Kundu SC, Reis RL, et al. Silk fibroin/hydroxyapatite composites for bone tissue engineering, Biotechnol Adv, 36 (2018), pp. 68-91.
[474] Kim HJ, Kim U-J, Kim HS, Li C, Wada M, Leisk GG, et al. Bone tissue engineering with premineralized silk scaffolds, Bone, 42 (2008), pp. 1226-34.
[475] Li C, Vepari C, Jin H-J, Kim HJ, Kaplan DL Electrospun silk-BMP-2 scaffolds for bone tissue engineering, Biomaterials, 27 (2006), pp. 3115-24.
[476] Holland C, Numata K, Rnjak-Kovacina J, Seib FP The Biomedical Use of Silk: Past, Present, Future, Adv Healthcare Mater, 8 (2019), pp. 1800465.
[477] Di Donato P, Poli A, Taurisano V, Nicolaus B. Polysaccharides from Bioagro-Waste for New Biomolecules. In: Ramawat KG, Mérillon J-M, editors. Polysaccharides: Bioactivity and Biotechnology. Cham: Springer International Publishing; 2015. p. 603-37.
[478] Morelli A, Puppi D, Chiellini F. Chapter 16 - Perspectives on Biomedical Applications of Ulvan. In: Venkatesan J, Anil S, Kim S-K, editors. Seaweed Polysaccharides. Radarweg 29, PO Box 211, 1000 AE Amsterdam, Netherlands: Elsevier; 2017. p. 305-30.
[479] Lee KY, Mooney DJ Alginate: Properties and biomedical applications, Prog Polym Sci, 37 (2012), pp. 106-26.
[480] George M, Abraham TE Polyionic hydrocolloids for the intestinal delivery of protein drugs: Alginate and chitosan -- a review, J Controlled Release, 114 (2006), pp. 1-14.

[481] Vauchel P, Leroux K, Kaas R, Arhaliass A, Baron R, Legrand J Kinetics modeling of alginate alkaline extraction from Laminaria digitata, Bioresour Technol, 100 (2009), pp. 1291-6.
[482] M. Otterlei, K. Ostgaard, G. Skjakbraek, O. Smidsrod, P. Soonshiong, Espevik T Induction of cytokine production from human monocytes stimulated with alginate, J Immunother, 10 (1991), pp. 286.
[483] U. Zimmermann, G. Klock, K. Federlin, K. Haning, M. Kowaslski, R.G. Bretzel, et al. Production of mitogen contamination free alginates with variable ratios of mannuronic to guluronic acid by free flow electrophoresis, Electrophoresis, 13 (1992), pp. 269.
[484] Holme HK, Davidsen L, Kristiansen A, Smidsrød O Kinetics and mechanisms of depolymerization of alginate and chitosan in aqueous solution, Carbohydr Polym, 73 (2008), pp. 656-64.
[485] Machluff M. Protein therapeutic delivery using encapsulated cell platform. In: V. Nedovic, R. Villaert, editors. Application of cell immobilization Biotechnology. Dordrecht: Springer; 2005. p. 200.
[486] Rowley JA, Madlambayan G, Mooney DJ Alginate hydrogels as synthetic extracellular matrix materials, Biomaterials, 20 (1999), pp. 45-53.
[487] O. Jeon, C. Powell, S.M. Ahmed, E. Alsberg Biodegradable, photocrosslinked alginate hydrogels with independently tailorable physical properties and cell adhesivity, Tissue Eng Part A, 16 (2010), pp. 2915.
[488] Degala S, Zipfel WR, Bonassar LJ Chondrocyte calcium signaling in response to fluid flow is regulated by matrix adhesion in 3-D alginate scaffolds, Arch Biochem Biophys, 505 (2011), pp. 112-7.
[489] Evangelista MB, Hsiong SX, Fernandes R, Sampaio P, Kong H-J, Barrias CC, et al. Upregulation of bone cell differentiation through immobilization within a synthetic extracellular matrix, Biomaterials, 28 (2007), pp. 3644-55.
[490] Kreeger PK, Deck JW, Woodruff TK, Shea LD The in vitro regulation of ovarian follicle development using alginate-extracellular matrix gels, Biomaterials, 27 (2006), pp. 714-23.
[491] Lee KY, Alsberg E, Hsiong S, Comisar W, Linderman J, Ziff R, et al. Nanoscale Adhesion Ligand Organization Regulates Osteoblast Proliferation and Differentiation, Nano Lett, 4 (2004), pp. 1501-6.
[492] Comisar WA, Hsiong SX, Kong H-J, Mooney DJ, Linderman JJ Multi-scale modeling to predict ligand presentation within RGD nanopatterned hydrogels, Biomaterials, 27 (2006), pp. 2322-9.
[493] Al-Shamkhani A, Duncan R Radioiodination of Alginate via Covalently-Bound Tyrosinamide Allows Monitoring of its Fate In Vivo, J Bioact Compatible Polym, 10 (1995), pp. 4-13.
[494] Bouhadir KH, Lee KY, Alsberg E, Damm KL, Anderson KW, Mooney DJ Degradation of Partially Oxidized Alginate and Its Potential Application for Tissue Engineering, Biotechnol Prog, 17 (2001), pp. 945-50.
[495] Lueckgen A, Garske DS, Ellinghaus A, Desai RM, Stafford AG, Mooney DJ, et al. Hydrolytically-degradable click-crosslinked alginate hydrogels, Biomaterials, 181 (2018), pp. 189-98.
[496] Grant GT, Morris ER, Rees DA, Smith PJC, Thom D Biological interactions between polysaccharides and divalent cations: the egg box model, FEBS Lett, 32 (1973), pp. 195-8.
[497] Hunt NC, Smith AM, Gbureck U, Shelton RM, Grover LM Encapsulation of fibroblasts causes accelerated alginate hydrogel degradation, Acta Biomater, 6 (2010), pp. 3649-56.
[498] Eiselt P, Lee KY, Mooney DJ Rigidity of Two-Component Hydrogels Prepared from Alginate and Poly(ethylene glycol)−Diamines, Macromolecules, 32 (1999), pp. 5561-6.
[499] Bouhadir KH, Hausman DS, Mooney DJ Synthesis of cross-linked poly(aldehyde guluronate) hydrogels, Polymer, 40 (1999), pp. 3575-84.

[500] Lee KY, Rowley JA, Eiselt P, Moy EM, Bouhadir KH, Mooney DJ Controlling Mechanical and Swelling Properties of Alginate Hydrogels Independently by Cross-Linker Type and Cross-Linking Density, Macromolecules, 33 (2000), pp. 4291-4.
[501] Jeon O, Bouhadir KH, Mansour JM, Alsberg E Photocrosslinked alginate hydrogels with tunable biodegradation rates and mechanical properties, Biomaterials, 30 (2009), pp. 2724-34.
[502] Seliktar D Designing Cell-Compatible Hydrogels for Biomedical Applications, Science, 336 (2012), pp. 1124.
[503] Desai RM, Koshy ST, Hilderbrand SA, Mooney DJ, Joshi NS Versatile click alginate hydrogels crosslinked via tetrazine–norbornene chemistry, Biomaterials, 50 (2015), pp. 30-7.
[504] Hafeez S, Ooi WH, Morgan LF, Mota C, Dettin M, Van Blitterswijk C, et al. Viscoelastic Oxidized Alginates with Reversible Imine Type Crosslinks: Self-Healing, Injectable, and Bioprintable Hydrogels, Gels, 4 (2018), pp.
[505] Di Martino A, Sittinger M, Risbud MV Chitosan: A versatile biopolymer for orthopaedic tissue-engineering, Biomaterials, 26 (2005), pp. 5983-90.
[506] Peter MG. Chitin and Chitosan from Animal Sources. In: Steinbüchel A, editor. Biopolymers. Weinheim: WILEY-VCH; 2002. p. 481-574.
[507] Jang M-K, Kong B-G, Jeong Y-I, Lee CH, Nah J-W Physicochemical characterization of α-chitin, β-chitin, and γ-chitin separated from natural resources, J Polym Sci, Part A: Polym Chem, 42 (2004), pp. 3423-32.
[508] Dash M, Chiellini F, Ottenbrite RM, Chiellini E Chitosan—A versatile semi-synthetic polymer in biomedical applications, Prog Polym Sci, 36 (2011), pp. 981-1014.
[509] Aranaz I, Mengibar M, Harris R, Panos I, Miralles B, Acosta N, et al. Functional Characterization of Chitin and Chitosan, Curr Chem Biol, 3 (2009), pp. 203-30.
[510] Kong M, Chen XG, Xing K, Park HJ Antimicrobial properties of chitosan and mode of action: A state of the art review, Int J Food Microbiol, 144 (2010), pp. 51-63.
[511] Kurita K Chitin and Chitosan: Functional Biopolymers from Marine Crustaceans, Mar Biotechnol, 8 (2006), pp. 203-26.
[512] Hirano S Chitin and chitosan as novel biotechnological materials, Polym Int, 48 (1999), pp. 732-4.
[513] Kean T, Thanou M Biodegradation, biodistribution and toxicity of chitosan, Adv Drug Del Rev, 62 (2010), pp. 3-11.
[514] Chatelet C, Damour O, Domard A Influence of the degree of acetylation on some biological properties of chitosan films, Biomaterials, 22 (2001), pp. 261-8.
[515] Ren D, Yi H, Wang W, Ma X The enzymatic degradation and swelling properties of chitosan matrices with different degrees of N-acetylation, Carbohydr Res, 340 (2005), pp. 2403-10.
[516] Divya K, Jisha MS Chitosan nanoparticles preparation and applications, Environmental Chemistry Letters, 16 (2018), pp. 101-12.
[517] Croisier F, Jérôme C Chitosan-based biomaterials for tissue engineering, Eur Polym J, 49 (2013), pp. 780-92.
[518] Duan B, Yuan X, Zhu Y, Zhang Y, Li X, Zhang Y, et al. A nanofibrous composite membrane of PLGA-chitosan/PVA prepared by electrospinning, Eur Polym J, 42 (2006), pp. 2013-22.
[519] Cai X, Tong H, Shen X, Chen W, Yan J, Hu J. Preparation and characterization of homogeneous chitosan-polylactic acid/hydroxyapatite nanocomposite for bone tissue engineering and evaluation of its mechanical properties. Acta Biomater2009.
[520] Li Z, Ramay HR, Hauch KD, Xiao D, Zhang M Chitosan-alginate hybrid scaffolds for bone tissue engineering, Biomaterials, 26 (2005), pp. 3919-28.
[521] Cuy JL, Beckstead BL, Brown CD, Hoffman AS, Giachelli CM Adhesive protein interactions with chitosan: Consequences for valve endothelial cell growth on tissue-engineering materials, J Biomed Mater Res A, 67A (2003), pp. 538-47.

[522] Zhang Y, Zhang M Microstructural and mechanical characterization of chitosan scaffolds reinforced by calcium phosphates, J Non-Cryst Solids, 282 (2001), pp. 159-64.
[523] Gravel M, Vago R, Tabrizian M Use of Natural Coralline Biomaterials As Reinforcing and Gas-Forming Agent for Developing Novel Hybrid Biomatrices: Microarchitectural and Mechanical Studies, Tissue Eng, 12 (2006), pp. 589-600.
[524] Park KM, Joung YK, Na JS, Lee MC, Park KD Thermosensitive chitosan-Pluronic hydrogel as an injectable cell delivery carrier for cartilage regeneration, Acta Biomater, 5 (2009), pp. 1956-65
[525] Almeida CR, Serra T, Oliveira MI, Planell JA, Barbosa MA, Navarro M Impact of 3-D printed PLA- and chitosan-based scaffolds on human monocyte/macrophage responses: Unraveling the effect of 3-D structures on inflammation, Acta Biomater, 10 (2014), pp. 613-22.
[526] Zhang J, Allardyce BJ, Rajkhowa R, Zhao Y, Dilley RJ, Redmond SL, et al. 3D Printing of Silk Particle-Reinforced Chitosan Hydrogel Structures and Their Properties, ACS Biomater Sci Eng, 4 (2018), pp. 3036-46.
[527] Stephanie R, Grace L, Benjamin D, David Don L, Antoni PT, Benjamin MW Macro- and micro-designed chitosan-alginate scaffold architecture by three-dimensional printing and directional freezing, Biofabrication, 8 (2016), pp. 015003.
[528] Picheth GF, Pirich CL, Sierakowski MR, Woehl MA, Sakakibara CN, de Souza CF, et al. Bacterial cellulose in biomedical applications: A review, Int J Biol Macromol, 104 (2017), pp. 97-106.
[529] Klemm D, Schmauder H-P, Heinze T. Cellulose. In: Steinbüchel A, editor. Biopolymers. Weinheim: WILEY-VCH; 2002. p. 275-319.
[530] Park S, Baker JO, Himmel ME, Parilla PA, Johnson DK Cellulose crystallinity index: measurement techniques and their impact on interpreting cellulase performance, Biotechnol Biofuels, 3 (2010), pp. 10.
[531] Jedvert K, Heinze T Cellulose modification and shaping – a review, J Polym Eng, 37 (2017), pp. 845.
[532] Courtenay JC, Sharma RI, Scott JL Recent Advances in Modified Cellulose for Tissue Culture Applications, Molecules, 23 (2018), pp. 654.
[533] Shoda M, Sugano Y Recent advances in bacterial cellulose production, Biotechnol Bioprocess Eng, 10 (2005), pp. 1.
[534] Gatenholm P, Klemm D Bacterial Nanocellulose as a Renewable Material for Biomedical Applications, MRS Bull, 35 (2010), pp. 208.
[535] Sulaeva I, Henniges U, Rosenau T, Potthast A Bacterial cellulose as a material for wound treatment: Properties and modifications. A review, Biotechnol Adv, 33 (2015), pp. 1547-71.
[536] Kucińska-Lipka J, Gubanska I, Janik H Bacterial cellulose in the field of wound healing and regenerative medicine of skin: recent trends and future prospectives, Polym Bull, 72 (2015), pp. 2399-419.
[537] Stumpf TR, Yang X, Zhang J, Cao X In situ and ex situ modifications of bacterial cellulose for applications in tissue engineering, Mater Sci Eng, C, 82 (2018), pp. 372-83.
[538] Torgbo S, Sukyai P Bacterial cellulose-based scaffold materials for bone tissue engineering, Appl Mater Today, 11 (2018), pp. 34-49.
[539] Schütz K, Placht A-M, Paul B, Brüggemeier S, Gelinsky M, Lode A Three-dimensional plotting of a cell-laden alginate/methylcellulose blend: towards biofabrication of tissue engineering constructs with clinically relevant dimensions, J Tissue Eng Regener Med, 11 (2017), pp. 1574-87.
[540] Gunasekera DHAT, Kuek S, Hasanaj D, He Y, Tuck C, Croft AK, et al. Three dimensional ink-jet printing of biomaterials using ionic liquids and co-solvents, Faraday Discuss, 190 (2016), pp. 509-23.
[541] Allison DD, Grande-Allen KJ Review. Hyaluronan: A Powerful Tissue Engineering Tool, Tissue Eng, 12 (2006), pp. 2131-40.

[542] Campoccia D, Doherty P, Radice M, Brun P, Abatangelo G, Williams DF Semisynthetic resorbable materials from hyaluronan esterification, Biomaterials, 19 (1998), pp. 2101-27.
[543] Laurent TC, Laurent UG, Fraser JE Functions of hyaluronan, Ann Rheum Dis, 54 (1995), pp. 429-32.
[544] Liu L, Liu Y, Li J, Du G, Chen J Microbial production of hyaluronic acid: current state, challenges, and perspectives, Microb Cell Fact, 10 (2011), pp. 99.
[545] Kogan G, Šoltés L, Stern R, Gemeiner P Hyaluronic acid: a natural biopolymer with a broad range of biomedical and industrial applications, Biotechnol Lett, 29 (2007), pp. 17-25.
[546] Highley CB, Prestwich GD, Burdick JA Recent advances in hyaluronic acid hydrogels for biomedical applications, Curr Opin Biotechnol, 40 (2016), pp. 35-40.
[547] Collins MN, Birkinshaw C Hyaluronic acid based scaffolds for tissue engineering—A review, Carbohydr Polym, 92 (2013), pp. 1262-79.
[548] Scott JE, Heatley F Biological Properties of Hyaluronan in Aqueous Solution Are Controlled and Sequestered by Reversible Tertiary Structures, Defined by NMR Spectroscopy, Biomacromolecules, 3 (2002), pp. 547-53.
[549] Park JK, Shim J-H, Kang KS, Yeom J, Jung HS, Kim JY, et al. Solid Free-Form Fabrication of Tissue-Engineering Scaffolds with a Poly(lactic-co-glycolic acid) Grafted Hyaluronic Acid Conjugate Encapsulating an Intact Bone Morphogenetic Protein–2/Poly(ethylene glycol) Complex, Adv Funct Mater, 21 (2011), pp. 2906-12.
[550] Schellauf F, Grillo Fernandes E, Braunegg G, Chiellini E. Properties of PHAs and Their Correlation to Fermentation Conditions in Biorelated Polymers. In: Chiellini E, Gil H, Braunegg G, Buchert J, Gatenholm P, van der Zee M, editors. Sustainable Polymer Science and Technology. New York Kluwer Academic/Plenum Publishers; 2001. p. 115.
[551] Zinn M, Witholt B, Egli T Occurrence, synthesis and medical application of bacterial polyhydroxyalkanoate, Adv Drug Del Rev, 53 (2001), pp. 5-21.
[552] Fernández-Dacosta C, Posada JA, Kleerebezem R, Cuellar MC, Ramirez A Microbial community-based polyhydroxyalkanoates (PHAs) production from wastewater: Techno-economic analysis and ex-ante environmental assessment, Bioresour Technol, 185 (2015), pp. 368-77.
[553] Koller M, Maršálek L, de Sousa Dias MM, Braunegg G Producing microbial polyhydroxyalkanoate (PHA) biopolyesters in a sustainable manner, New Biotechnology, 37 (2017), pp. 24-38.
[554] Koller M Advances in Polyhydroxyalkanoate (PHA) Production, Bioengineering, 4 (2017), pp. 88.
[555] Coats ER, Watson BS, Brinkman CK Polyhydroxyalkanoate Synthesis by Mixed Microbial Consortia Cultured on Fermented Dairy Manure: Effect of Aeration on Process Rates/Yields and the Associated Microbial Ecology, Water Res, 106 (2016), pp. 26-40.
[556] Lemoigne M Produits de deshydration et de polymerisation de l'acide b-oxobutyrique, Bull Soc Chem Biol, 8 (1926), pp. 770-82.
[557] Martin DP, Williams SF Medical applications of poly-4-hydroxybutyrate: a strong flexible absorbable biomaterial, Biochem Eng J, 16 (2003), pp. 97-105.
[558] Miranda De Sousa Dias M, Koller M, Puppi D, Morelli A, Chiellini F, Braunegg G Fed-Batch Synthesis of Poly(3-Hydroxybutyrate) and Poly(3-Hydroxybutyrate-co-4-Hydroxybutyrate) from Sucrose and 4-Hydroxybutyrate Precursors by Burkholderia sacchari Strain DSM 17165, Bioengineering, 4 (2017), pp.
[559] Radecka IK, Jiang G, Hill DJ, Kowalczuk MM. Poly(hydroxyalkanoates) composites and their applications. In: Inamuddin, editor. Green Polymer Composites Technology: Properties and Applications. Boca Raton: CRC Press; 2016. p. 163-75.
[560] Padermshoke A, Katsumoto Y, Sato H, Ekgasit S, Noda I, Ozaki Y Surface melting and crystallization behavior of polyhydroxyalkanoates studied by attenuated total reflection infrared spectroscopy, Polymer, 45 (2004), pp. 6547-54.

[561] Feng L, Watanabe T, Wang Y, Kichise T, Fukuchi T, Chen G-Q, et al. Studies on Comonomer Compositional Distribution of Bacterial Poly(3-hydroxybutyrate-co-3-hydroxyhexanoate)s and Thermal Characteristics of Their Factions, Biomacromolecules, 3 (2002), pp. 1071-7.
[562] Yang Q, Wang J, Zhang S, Tang X, Shang G, Peng Q, et al. The Properties of Poly(3-hydroxybutyrate-co-3-hydroxyhexanoate) and its Applications in Tissue Engineering, Curr Stem Cell Res Ther, 9 (2014), pp. 215-22.
[563] Abe H, Doi Y Side-Chain Effect of Second Monomer Units on Crystalline Morphology, Thermal Properties, and Enzymatic Degradability for Random Copolyesters of (R)-3-Hydroxybutyric Acid with (R)-3-Hydroxyalkanoic Acids, Biomacromolecules, 3 (2002), pp. 133-8.
[564] Shrivastav A, Kim H-Y, Kim Y-R Advances in the Applications of Polyhydroxyalkanoate Nanoparticles for Novel Drug Delivery System, Biomed Res Int, 2013 (2013), pp. 12.
[565] Koller M Biodegradable and Biocompatible Polyhydroxy-alkanoates (PHA): Auspicious Microbial Macromolecules for Pharmaceutical and Therapeutic Applications, Molecules, 23 (2018), pp.
[566] Södergård A, Stolt M Properties of lactic acid based polymers and their correlation with composition, Prog Polym Sci, 27 (2002), pp. 1123-63.
[567] Cooke MN, Fisher JP, Dean D, Rimnac C, Mikos AG Use of stereolithography to manufacture critical-sized 3D biodegradable scaffolds for bone ingrowth, J Biomed Mater Res B Appl Biomater, 64B (2003), pp. 65-9.
[568] Sarasua JR, Arraiza AL, Balerdi P, Maiza I Crystallinity and mechanical properties of optically pure polylactides and their blends, Polym Eng Sci, 45 (2005), pp. 745-53.
[569] Madhavan Nampoothiri K, Nair NR, John RP An overview of the recent developments in polylactide (PLA) research, Bioresour Technol, 101 (2010), pp. 8493-501.
[570] Lasprilla AJR, Martinez GAR, Lunelli BH, Jardini AL, Filho RM Poly-lactic acid synthesis for application in biomedical devices — A review, Biotechnol Adv, 30 (2012), pp. 321-8.
[571] Rudnik E. 13 - Compostable Polymer Properties and Packaging Applications. In: Ebnesajjad S, editor. Plastic Films in Food Packaging. Oxford: William Andrew Publishing; 2013. p. 217-48.
[572] Bergström JS, Hayman D An Overview of Mechanical Properties and Material Modeling of Polylactide (PLA) for Medical Applications, Ann Biomed Eng, 44 (2016), pp. 330-40.
[573] Farah S, Anderson DG, Langer R Physical and mechanical properties of PLA, and their functions in widespread applications — A comprehensive review, Adv Drug Del Rev, 107 (2016), pp. 367-92.
[574] Biron M. 4 - Renewable Plastics Derived From Natural Polymers. In: Biron M, editor. Industrial Applications of Renewable Plastics. William Andrew Publishing; 2017. p. 115-54.
[575] Manoukian OS, Sardashti N, Stedman T, Gailiunas K, Ojha A, Penalosa A, et al. Biomaterials for Tissue Engineering and Regenerative Medicine. In: Narayan R, editor. Encyclopedia of Biomedical Engineering. Oxford: Elsevier; 2019. p. 462-82.
[576] Narayanan G, Vernekar VN, Kuyinu EL, Laurencin CT Poly (lactic acid)-based biomaterials for orthopaedic regenerative engineering, Adv Drug Del Rev, 107 (2016), pp. 247-76.
[577] Niaounakis M. 2 - Properties. In: Niaounakis M, editor. Biopolymers: Applications and Trends. Oxford: William Andrew Publishing; 2015. p. 91-138.
[578] Gunatillake PA, Adhikari R Biodegradable synthetic polymers for tissue engineering, eCM Journal, 5 (2003), pp. 1-16.

[579] Hutmacher DW, Schantz T, Zein I, Ng KW, Teoh SH, Tan KC Mechanical properties and cell cultural response of polycaprolactone scaffolds designed and fabricated via fused deposition modeling, J Biomed Mater Res, 55 (2001), pp. 203-16.
[580] Shao XX, Hutmacher DW, Ho ST, Goh JCH, Lee EH Evaluation of a hybrid scaffold/cell construct in repair of high-load-bearing osteochondral defects in rabbits, Biomaterials, 27 (2006), pp. 1071-80.
[581] Zhou Y, Chen F, Ho ST, Woodruff MA, Lim TM, Hutmacher DW Combined marrow stromal cell-sheet techniques and high-strength biodegradable composite scaffolds for engineered functional bone grafts, Biomaterials, 28 (2007), pp. 814-24.
[582] Shim J-H, Moon T-S, Yun M-J, Jeon Y-C, Jeong C-M, Cho D-W, et al. Stimulation of healing within a rabbit calvarial defect by a PCL/PLGA scaffold blended with TCP using solid freeform fabrication technology, J Mater Sci Mater Med, 23 (2012), pp. 2993-3002.
[583] Jiang W, Shi J, Li W, Sun K Three dimensional melt-deposition of polycaprolactone/bio-derived hydroxyapatite composite into scaffold for bone repair, J Biomater Sci Polym Ed, 24 (2013), pp. 539-50.
[584] Lohfeld S, Cahill S, Barron V, McHugh P, Dürselen L, Kreja L, et al. Fabrication, mechanical and in vivo performance of polycaprolactone/tricalcium phosphate composite scaffolds, Acta Biomater, 8 (2012), pp. 3446-56.
[585] Liao H-T, Lee M-Y, Tsai W-W, Wang H-C, Lu W-C Osteogenesis of adipose-derived stem cells on polycaprolactone–β-tricalcium phosphate scaffold fabricated via selective laser sintering and surface coating with collagen type I, J Tissue Eng Regener Med, 10 (2016), pp. E337-E53.
[586] Xiong Z, Yan Y, Zhang R, Sun L Fabrication of porous poly(l-lactic acid) scaffolds for bone tissue engineering via precise extrusion, Scripta Mater, 45 (2001), pp. 773-9.
[587] Fairag R, Rosenzweig DH, Ramirez-Garcialuna JL, Weber MH, Haglund L Three-Dimensional Printed Polylactic Acid Scaffolds Promote Bone-like Matrix Deposition in Vitro, ACS Appl Mater Interfaces, 11 (2019), pp. 15306-15.
[588] Gregor A, Filová E, Novák M, Kronek J, Chlup H, Buzgo M, et al. Designing of PLA scaffolds for bone tissue replacement fabricated by ordinary commercial 3D printer, J Biol Eng, 11 (2017), pp. 31-.
[589] Cui H, Zhu W, Holmes B, Zhang LG Biologically Inspired Smart Release System Based on 3D Bioprinted Perfused Scaffold for Vascularized Tissue Regeneration, Adv Sci, 3 (2016), pp. 1600058.
[590] Barbeck M, Serra T, Booms P, Stojanovic S, Najman S, Engel E, et al. Analysis of the in vitro degradation and the in vivo tissue response to bi-layered 3D-printed scaffolds combining PLA and biphasic PLA/bioglass components – Guidance of the inflammatory response as basis for osteochondral regeneration, Bioact Mater, 2 (2017), pp. 208-23.
[591] Antonov EN, Barinov SM, Vakhrushev IV, Komlev VS, Popov VK, Fedotov AY, et al. Selective laser sintering of bioactive composite matrices for bone tissue engineering, Inorg Mater Appl Res, 6 (2015), pp. 171-8.
[592] Melchels FPW, Velders AH, Feijen J, Grijpma DW Photo-Cross-Linked Poly(dl-lactide)-Based Networks. Structural Characterization by HR-MAS NMR Spectroscopy and Hydrolytic Degradation Behavior, Macromolecules, 43 (2010), pp. 8570-9.
[593] Melchels FPW, Bertoldi K, Gabbrielli R, Velders AH, Feijen J, Grijpma DW Mathematically defined tissue engineering scaffold architectures prepared by stereolithography, Biomaterials, 31 (2010), pp. 6909-16.
[594] Ronca A, Ambrosio L, Grijpma DW Design of Porous Three-Dimensional PDLLA/nano-hap Composite Scaffolds Using Stereolithography, J Appl Biomater Func, 10 (2012), pp. 249-58.

[595] Hong JM, Kim BJ, Shim J-H, Kang KS, Kim K-J, Rhie JW, et al. Enhancement of bone regeneration through facile surface functionalization of solid freeform fabrication-based three-dimensional scaffolds using mussel adhesive proteins, Acta Biomater, 8 (2012), pp. 2578-86.
[596] Yu D, Li Q, Mu X, Chang T, Xiong Z Bone regeneration of critical calvarial defect in goat model by PLGA/TCP/rhBMP-2 scaffolds prepared by low-temperature rapid-prototyping technology, Int J Oral Maxillofac Surg, 37 (2008), pp. 929-34.
[597] Xu M, Li Y, Suo H, Yan Y, Liu L, Wang Q, et al. Fabricating a pearl/PLGA composite scaffold by the low-temperature deposition manufacturing technique for bone tissue engineering, Biofabrication, 2 (2010), pp. 025002.
[598] Simpson RL, Wiria FE, Amis AA, Chua CK, Leong KF, Hansen UN, et al. Development of a 95/5 poly(L-lactide-co-glycolide)/hydroxylapatite and β-tricalcium phosphate scaffold as bone replacement material via selective laser sintering, J Biomed Mater Res B Appl Biomater, 84B (2008), pp. 17-25.
[599] Lee JW, Lan PX, Kim B, Lim G, Cho D-W Fabrication and characteristic analysis of a poly(propylene fumarate) scaffold using micro-stereolithography technology, J Biomed Mater Res B Appl Biomater, 87B (2008), pp. 1-9.
[600] Lee JW, Ahn G, Kim JY, Cho D-W Evaluating cell proliferation based on internal pore size and 3D scaffold architecture fabricated using solid freeform fabrication technology, J Mater Sci Mater Med, 21 (2010), pp. 3195-205.
[601] Kim K, Dean D, Wallace J, Breithaupt R, Mikos AG, Fisher JP The influence of stereolithographic scaffold architecture and composition on osteogenic signal expression with rat bone marrow stromal cells, Biomaterials, 32 (2011), pp. 3750-63.
[602] Wallace J, Wang MO, Thompson P, Busso M, Belle V, Mammoser N, et al. Validating continuous digital light processing (cDLP) additive manufacturing accuracy and tissue engineering utility of a dye-initiator package, Biofabrication, 6 (2014), pp. 015003.
[603] Trachtenberg JE, Placone JK, Smith BT, Fisher JP, Mikos AG Extrusion-based 3D printing of poly(propylene fumarate) scaffolds with hydroxyapatite gradients, J Biomater Sci Polym Ed, 28 (2017), pp. 532-54.
[604] Lim LT, Auras R, Rubino M Processing technologies for poly(lactic acid), Prog Polym Sci, 33 (2008), pp. 820-52.
[605] Nigmatullin R, Thomas P, Lukasiewicz B, Puthussery H, Roy I Polyhydroxyalkanoates, a family of natural polymers, and their applications in drug delivery, J Chem Technol Biotechnol, 90 (2015), pp. 1209-21.
[606] Manavitehrani I, Fathi A, Badr H, Daly S, Negahi Shirazi A, Dehghani F Biomedical Applications of Biodegradable Polyesters, Polymers, 8 (2016), pp.
[607] Chen G-Q, Zhang J Microbial polyhydroxyalkanoates as medical implant biomaterials AU - Chen, Guo-Qiang, Artif Cells Nanomed Biotechnol, 46 (2018), pp. 1-18.
[608] Aluthge DC, Xu C, Othman N, Noroozi N, Hatzikiriakos SG, Mehrkhodavandi P PLA–PHB–PLA Triblock Copolymers: Synthesis by Sequential Addition and Investigation of Mechanical and Rheological Properties, Macromolecules, 46 (2013), pp. 3965-74.
[609] Winnacker M, Rieger B Copolymers of polyhydroxyalkanoates and polyethylene glycols: recent advancements with biological and medical significance, Polym Int, 66 (2017), pp. 497-503.
[610] Kwon H-S, Jung S-G, Kim H-Y, Parker SA, Batt CA, Kim Y-R A multi-functional polyhydroxybutyrate nanoparticle for theranostic applications, J Mater Chem B, 2 (2014), pp. 3965-71.
[611] Utsunomia C, Saito T, Matsumoto Ki, Hori C, Isono T, Satoh T, et al. Synthesis of lactate (LA)-based poly(ester-urethane) using hydroxyl-terminated LA-based oligomers from a microbial secretion system, J Polym Res, 24 (2017), pp. 167.
[612] Ramachandran H, Kannusamy S, Huong K-H, Mathava R, Amirul AA. Blends of Polyhydroxyalkanoates (PHAs). In: Roy I, Visakh PM, editors. Polyhydroxyalkanoate (PHA)

based Blends, Composites and Nanocomposites. Thomas Graham House, Science Park, Milton Road, Cambridge CB4 0WF, UK: The Royal Society of Chemistry; 2015. p. 66-97.
[613] Madkour MH, Heinrich D, Alghamdi MA, Shabbaj II, Steinbüchel A PHA Recovery from Biomass, Biomacromolecules, 14 (2013), pp. 2963-72.
[614] Leroy E, Petit I, Audic JL, Colomines G, Deterre R Rheological characterization of a thermally unstable bioplastic in injection molding conditions, Polym Degrad Stab, 97 (2012), pp. 1915-21.
[615] Wu C-S, Liao H-T, Cai Y-X Characterisation, biodegradability and application of palm fibre-reinforced polyhydroxyalkanoate composites, Polym Degrad Stab, 140 (2017), pp. 55-63.
[616] Wu C-S, Liao H-T Fabrication, characterization, and application of polyester/wood flour composites, J Polym Eng, 37 (2017), pp. 689.
[617] Wu CS, Liao HT Interface design of environmentally friendly carbon nanotube-filled polyester composites: Fabrication, characterisation, functionality and application, Express Polym Lett, 11 (2017), pp. 187-98.
[618] Tian H, Tang Z, Zhuang X, Chen X, Jing X Biodegradable synthetic polymers: Preparation, functionalization and biomedical application, Prog Polym Sci, 37 (2012), pp. 237-80.
[619] Coulembier O, Degée P, Hedrick JL, Dubois P From controlled ring-opening polymerization to biodegradable aliphatic polyester: Especially poly(β-malic acid) derivatives, Prog Polym Sci, 31 (2006), pp. 723-47.
[620] Puppi D, Chiellini F, Dash M, Chiellini E. Biodegradable Polymers for Biomedical Applications. In: Felton GP, editor. Biodegradable Polymers: Processing, Degradation & Applications. New York: Nova Science Publishers; 2011. p. 545-60.
[621] Teo EY, Ong S-Y, Khoon Chong MS, Zhang Z, Lu J, Moochhala S, et al. Polycaprolactone-based fused deposition modeled mesh for delivery of antibacterial agents to infected wounds, Biomaterials, 32 (2011), pp. 279-87.
[622] Yilgor P, Yilmaz G, Onal MB, Solmaz I, Gundogdu S, Keskil S, et al. An in vivo study on the effect of scaffold geometry and growth factor release on the healing of bone defects, J Tissue Eng Regener Med, 7 (2013), pp. 687-96.
[623] Kundu J, Shim J-H, Jang J, Kim S-W, Cho D-W An additive manufacturing-based PCL–alginate–chondrocyte bioprinted scaffold for cartilage tissue engineering, J Tissue Eng Regener Med, 9 (2015), pp. 1286-97.
[624] Pati F, Song T-H, Rijal G, Jang J, Kim SW, Cho D-W Ornamenting 3D printed scaffolds with cell-laid extracellular matrix for bone tissue regeneration, Biomaterials, 37 (2015), pp. 230-41.
[625] Jiang W, Shi J, Li W, Sun K Morphology, wettability, and mechanical properties of polycaprolactone/hydroxyapatite composite scaffolds with interconnected pore structures fabricated by a mini-deposition system, Polym Eng Sci, 52 (2012), pp. 2396-402.
[626] Shor L, Güçeri S, Chang R, Gordon J, Kang Q, Hartsock L, et al. Precision extruding deposition (PED) fabrication of polycaprolactone (PCL) scaffolds for bone tissue engineering, Biofabrication, 1 (2009), pp. 015003.
[627] Lee K, Jin G, Jang CH, Jung W-K, Kim G Preparation and characterization of multi-layered poly(ε-caprolactone)/chitosan scaffolds fabricated with a combination of melt-plotting/in situ plasma treatment and a coating method for hard tissue regeneration, J Mater Chem B, 1 (2013), pp. 5831-41.
[628] Domingos M, Chiellini F, Gloria A, Ambrosio L, Bartolo P, Chiellini E Effect of process parameters on the morphological and mechanical properties of 3D Bioextruded poly(ε -caprolactone) scaffolds, Rapid Prototyp J, 18 (2012), pp. 56-67.
[629] Fiedler T, Videira AC, Bártolo P, Strauch M, Murch GE, Ferreira JMF On the mechanical properties of PLC–bioactive glass scaffolds fabricated via BioExtrusion, Mater Sci Eng, C, 57 (2015), pp. 288-93.

[630] Liu F, Wang W, Mirihanage W, Hinduja S, Bartolo PJ A plasma-assisted bioextrusion system for tissue engineering, CIRP Annals, 67 (2018), pp. 229-32.
[631] Martins A, Chung S, Pedro AJ, Sousa RA, Marques AP, Reis RL, et al. Hierarchical starch-based fibrous scaffold for bone tissue engineering applications, J Tissue Eng Regener Med, 3 (2009), pp. 37-42.
[632] Yoon H, Ahn S, Kim G Three-Dimensional Polycaprolactone Hierarchical Scaffolds Supplemented with Natural Biomaterials to Enhance Mesenchymal Stem Cell Proliferation, Macromol Rapid Commun, 30 (2009), pp. 1632-7.
[633] Lee H, Yeo M, Ahn S, Kang D-O, Jang CH, Lee H, et al. Designed hybrid scaffolds consisting of polycaprolactone microstrands and electrospun collagen-nanofibers for bone tissue regeneration, J Biomed Mater Res B Appl Biomater, 97B (2011), pp. 263-70.
[634] Yeo M, Kim G Cell-printed hierarchical scaffolds consisting of micro-sized polycaprolactone (PCL) and electrospun PCL nanofibers/cell-laden alginate struts for tissue regeneration, J Mater Chem B, 2 (2014), pp. 314-24.
[635] Yoon H, Kim G A three-dimensional polycaprolactone scaffold combined with a drug delivery system consisting of electrospun nanofibers, J Pharm Sci, 100 (2011), pp. 424-30.
[636] Hochleitner G, Jüngst T, Brown TD, Hahn K, Moseke C, Jakob F, et al. Additive manufacturing of scaffolds with sub-micron filaments via melt electrospinning writing, Biofabrication, 7 (2015), pp. 035002.
[637] Brown TD, Slotosch A, Thibaudeau L, Taubenberger A, Loessner D, Vaquette C, et al. Design and Fabrication of Tubular Scaffolds via Direct Writing in a Melt Electrospinning Mode, Biointerphases, 7 (2012), pp. 13.
[638] Jungst T, Muerza-Cascante ML, Brown TD, Standfest M, Hutmacher DW, Groll J, et al. Melt electrospinning onto cylinders: effects of rotational velocity and collector diameter on morphology of tubular structures, Polym Int, 64 (2015), pp. 1086-95.
[639] Haigh JN, Chuang Y-m, Farrugia B, Hoogenboom R, Dalton PD, Dargaville TR Hierarchically Structured Porous Poly(2-oxazoline) Hydrogels, Macromol Rapid Commun, 37 (2016), pp. 93-9.
[640] Visser J, Melchels FPW, Jeon JE, van Bussel EM, Kimpton LS, Byrne HM, et al. Reinforcement of hydrogels using three-dimensionally printed microfibres, Nat Commun, 6 (2015), pp. 6933.
[641] Jensen J, Rölfing JHD, Svend Le DQ, Kristiansen AA, Nygaard JV, Hokland LB, et al. Surface-modified functionalized polycaprolactone scaffolds for bone repair: In vitro and in vivo experiments, J Biomed Mater Res A, 102 (2014), pp. 2993-3003.
[642] Dang HP, Shabab T, Shafiee A, Peiffer QC, Fox K, Tran N, et al. 3D printed dual macro-, microscale porous network as a tissue engineering scaffold with drug delivering function, Biofabrication, 11 (2019), pp. 035014.
[643] Chen F, Hochleitner G, Woodfield T, Groll J, Dalton PD, Amsden BG Additive Manufacturing of a Photo-Cross-Linkable Polymer via Direct Melt Electrospinning Writing for Producing High Strength Structures, Biomacromolecules, 17 (2016), pp. 208-14.
[644] Romagnoli C, Zonefrati R, Puppi D, Rosati C, Aldinucci A, Palmini G, et al. Human Adipose Tissue-Derived Stem Cells and a Poly(ε-Caprolactone) Scaffold Produced by Computer-Aided Wet Spinning for Bone Tissue Engineering, Journal of Biomaterials and Tissue Engineering, 7 (2017), pp. 622-33.
[645] He Y, Tuck CJ, Prina E, Kilsby S, Christie SDR, Edmondson S, et al. A new photocrosslinkable polycaprolactone-based ink for three-dimensional inkjet printing, J Biomed Mater Res B Appl Biomater, 105 (2017), pp. 1645-57.
[646] Smith MH, Flanagan CL, Kemppainen JM, Sack JA, Chung H, Das S, et al. Computed tomography-based tissue-engineered scaffolds in craniomaxillofacial surgery, Int J Med Robot Comp, 3 (2007), pp. 207-16.

[647] Hollister SJ, Flanagan CL, Zopf DA, Morrison RJ, Nasser H, Patel JJ, et al. Design Control for Clinical Translation of 3D Printed Modular Scaffolds, Ann Biomed Eng, 43 (2015), pp. 774-86.
[648] Morrison RJ, Nasser HB, Kashlan KN, Zopf DA, Milner DJ, Flanangan CL, et al. Co-culture of adipose-derived stem cells and chondrocytes on three-dimensionally printed bioscaffolds for craniofacial cartilage engineering, The Laryngoscope, 128 (2018), pp. E251-E7.
[649] Zopf DA, Mitsak AG, Flanagan CL, Wheeler M, Green GE, Hollister SJ Computer aided-designed, 3-dimensionally printed porous tissue bioscaffolds for craniofacial soft tissue reconstruction, Otolaryngol Head Neck Surg, 152 (2015), pp. 57-62.
[650] Zopf DA, Flanagan CL, Mitsak AG, Brennan JR, Hollister SJ Pore architecture effects on chondrogenic potential of patient-specific 3-dimensionally printed porous tissue bioscaffolds for auricular tissue engineering, Int J Pediatr Otorhinolaryngol, 114 (2018), pp. 170-4.
[651] Ciardelli G, Chiono V, Vozzi G, Pracella M, Ahluwalia A, Barbani N, et al. Blends of Poly-(ε-caprolactone) and Polysaccharides in Tissue Engineering Applications, Biomacromolecules, 6 (2005), pp. 1961-76.
[652] Xia Y, Zhou P, Cheng X, Xie Y, Liang C, Li C, et al. Selective laser sintering fabrication of nano-hydroxyapatite/poly-ε-caprolactone scaffolds for bone tissue engineering applications, Int J Nanomedicine, 8 (2013), pp. 4197-213.
[653] Chen C-H, Lee M-Y, Shyu VB-H, Chen Y-C, Chen C-T, Chen J-P Surface modification of polycaprolactone scaffolds fabricated via selective laser sintering for cartilage tissue engineering, Mater Sci Eng, C, 40 (2014), pp. 389-97.
[654] Elomaa L, Teixeira S, Hakala R, Korhonen H, Grijpma DW, Seppälä JV Preparation of poly(ε-caprolactone)-based tissue engineering scaffolds by stereolithography, Acta Biomater, 7 (2011), pp. 3850-6.
[655] Ronca A, Ronca S, Forte G, Zeppetelli S, Gloria A, De Santis R, et al. Synthesis and characterization of divinyl-fumarate poly-ε-caprolactone for scaffolds with controlled architectures, J Tissue Eng Regener Med, 12 (2018), pp. e523-e31.
[656] Elomaa L, Kang Y, Seppälä JV, Yang Y Biodegradable photocrosslinkable poly(depsipeptide-co-ε-caprolactone) for tissue engineering: Synthesis, characterization, and In vitro evaluation, J Polym Sci, Part A: Polym Chem, 52 (2014), pp. 3307-15.
[657] Drummer D, Rietzel D, Cifuentes‐Cuéllar S Suitability of PLA/TCP for fused deposition modeling, Rapid Prototyp J, 18 (2012), pp. 500-7.
[658] Lanzotti A, Grasso M, Martorelli M, Staiano G The impact of process parameters on mechanical properties of parts fabricated in PLA with an open-source 3-D printer, Rapid Prototyp J, 21 (2015), pp. 604-17.
[659] Liu A, Xue G-h, Sun M, Shao H-f, Ma C-y, Gao Q, et al. 3D Printing Surgical Implants at the clinic: A Experimental Study on Anterior Cruciate Ligament Reconstruction, Sci Rep, 6 (2016), pp. 21704.
[660] Grémare A, Guduric V, Bareille R, Heroguez V, Latour S, L'Heureux N, et al. Characterization of printed PLA scaffolds for bone tissue engineering, J Biomed Mater Res A, 106 (2017), pp. 887-94.
[661] Sandler N, Salmela I, Fallarero A, Rosling A, Khajeheian M, Kolakovic R, et al. Towards fabrication of 3D printed medical devices to prevent biofilm formation, Int J Pharm, 459 (2014), pp. 62-4.
[662] Water JJ, Bohr A, Boetker J, Aho J, Sandler N, Nielsen HM, et al. Three-Dimensional Printing of Drug-Eluting Implants: Preparation of an Antimicrobial Polylactide Feedstock Material, J Pharm Sci, 104 (2015), pp. 1099-107.
[663] Boetker J, Water JJ, Aho J, Arnfast L, Bohr A, Rantanen J Modifying release characteristics from 3D printed drug-eluting products, Eur J Pharm Sci, 90 (2016), pp. 47-52.

[664] Kim J, McBride S, Tellis B, Alvarez-Urena P, Song Y-H, Dean DD, et al. Rapid-prototyped PLGA/β-TCP/hydroxyapatite nanocomposite scaffolds in a rabbit femoral defect model, Biofabrication, 4 (2012), pp. 025003.
[665] Zhang H, Mao X, Zhao D, Jiang W, Du Z, Li Q, et al. Three dimensional printed polylactic acid-hydroxyapatite composite scaffolds for prefabricating vascularized tissue engineered bone: An in vivo bioreactor model, Sci Rep, 7 (2017), pp. 15255.
[666] Shim J-H, Won J-Y, Sung S-J, Lim D-H, Yun W-S, Jeon Y-C, et al. Comparative Efficacies of a 3D-Printed PCL/PLGA/β-TCP Membrane and a Titanium Membrane for Guided Bone Regeneration in Beagle Dogs, Polymers, 7 (2015), pp.
[667] Won JY, Park CY, Bae JH, Ahn G, Kim C, Lim DH, et al. Evaluation of 3D printed PCL/PLGA/β-TCP versus collagen membranes for guided bone regeneration in a beagle implant model, Biomed Mater, 11 (2016), pp. 055013.
[668] Song T-H, Jang J, Choi Y-J, Shim J-H, Cho D-W 3D-Printed Drug/Cell Carrier Enabling Effective Release of Cyclosporin a for Xenogeneic Cell-Based Therapy, Cell Transplant, 24 (2015), pp. 2513-25.
[669] Kim JD, Choi JS, Kim BS, Chan Choi Y, Cho YW Piezoelectric inkjet printing of polymers: Stem cell patterning on polymer substrates, Polymer, 51 (2010), pp. 2147-54.
[670] Yan Y, Xiong Z, Hu Y, Wang S, Zhang R, Zhang C Layered manufacturing of tissue engineering scaffolds via multi-nozzle deposition, Mater Lett, 57 (2003), pp. 2623-8.
[671] Liu C, Li Y, Zhang L, Mi S, Xu Y, Sun W Development of a novel low-temperature deposition machine using screw extrusion to fabricate poly(l-lactide-co-glycolide) acid scaffolds, Proc Inst Mech Eng, Part H, 228 (2014), pp. 593-606.
[672] Mironov AV, Grigoryev AM, Krotova LI, Skaletsky NN, Popov VK, Sevastianov VI 3D printing of PLGA scaffolds for tissue engineering, J Biomed Mater Res A, 105 (2017), pp. 104-9.
[673] Zhou WY, Lee SH, Wang M, Cheung WL Selective Laser Sintering of Tissue Engineering Scaffolds Using Poly(L-Lactide) Microspheres, Key Eng Mater, 334-335 (2007), pp. 1225-8.
[674] Zhou WY, Lee SH, Wang M, Cheung WL, Ip WY Selective laser sintering of porous tissue engineering scaffolds from poly(l-lactide)/carbonated hydroxyapatite nanocomposite microspheres, J Mater Sci Mater Med, 19 (2008), pp. 2535-40.
[675] Zhou WY, Wang M, Cheung WL, Ip WY Selective laser sintering of poly(l-lactide)/carbonated hydroxyapatite nanocomposite porous scaffolds for bone tissue engineering, Tissue Eng, (2010), pp. 179-204.
[676] Hoeges S, Lindner M, Fischer H, Meiners W, Wissenbach K. Manufacturing of bone substitute implants using Selective Laser Melting. In: Vander Sloten J, Verdonck P, Nyssen M, Haueisen J, editors. 4th European Conference of the International Federation for Medical and Biological Engineering. Berlin, Heidelberg: Springer Berlin Heidelberg; 2009. p. 2230-4.
[677] Kanczler JM, Mirmalek-Sani S-H, Hanley NA, Ivanov AL, Barry JJA, Upton C, et al. Biocompatibility and osteogenic potential of human fetal femur-derived cells on surface selective laser sintered scaffolds, Acta Biomater, 5 (2009), pp. 2063-71.
[678] Bukharova TB, Antonov EN, Popov VK, Fatkhudinov TK, Popova AV, Volkov AV, et al. Biocompatibility of Tissue Engineering Constructions from Porous Polylactide Carriers Obtained by the Method of Selective Laser Sintering and Bone Marrow-Derived Multipotent Stromal Cells, Bull Exp Biol Med, 149 (2010), pp. 148-53.
[679] Koegler WS, Griffith LG Osteoblast response to PLGA tissue engineering scaffolds with PEO modified surface chemistries and demonstration of patterned cell response, Biomaterials, 25 (2004), pp. 2819-30.
[680] Wu W, Zheng Q, Guo X, Huang W The controlled-releasing drug implant based on the three dimensional printing technology: Fabrication and properties of drug releasing in vivo, J Wuhan Univ Technol, 24 (2009), pp. 977.

[681] Melchels FPW, Tonnarelli B, Olivares AL, Martin I, Lacroix D, Feijen J, et al. The influence of the scaffold design on the distribution of adhering cells after perfusion cell seeding, Biomaterials, 32 (2011), pp. 2878-84.
[682] Tanodekaew S, Channasanon S, Kaewkong P, Uppanan P PLA-HA Scaffolds: Preparation and Bioactivity, Procedia Eng, 59 (2013), pp. 144-9.
[683] Ronca A, Ambrosio L, Grijpma DW Preparation of designed poly(d,l-lactide)/nanosized hydroxyapatite composite structures by stereolithography, Acta Biomater, 9 (2013), pp. 5989-96.
[684] Choi J-W, Wicker R, Lee S-H, Choi K-H, Ha C-S, Chung I Fabrication of 3D biocompatible/biodegradable micro-scaffolds using dynamic mask projection microstereolithography, J Mater Process Technol, 209 (2009), pp. 5494-503.
[685] Dadsetan M, Guda T, Runge MB, Mijares D, LeGeros RZ, LeGeros JP, et al. Effect of calcium phosphate coating and rhBMP-2 on bone regeneration in rabbit calvaria using poly(propylene fumarate) scaffolds, Acta Biomater, 18 (2015), pp. 9-20.
[686] Luangphakdy V, Walker E, Shinohara K, Pan H, Hefferan T, Bauer TW, et al. Evaluation of osteoconductive scaffolds in the canine femoral multi-defect model, Tissue Eng Part A, 19 (2013), pp. 634-48.
[687] Lee JW, Kang KS, Lee SH, Kim J-Y, Lee B-K, Cho D-W Bone regeneration using a microstereolithography-produced customized poly(propylene fumarate)/diethyl fumarate photopolymer 3D scaffold incorporating BMP-2 loaded PLGA microspheres, Biomaterials, 32 (2011), pp. 744-52.
[688] Lee JW, Kim K-J, Kang KS, Chen S, Rhie J-W, Cho D-W Development of a bone reconstruction technique using a solid free-form fabrication (SFF)-based drug releasing scaffold and adipose-derived stem cells, J Biomed Mater Res A, 101A (2013), pp. 1865-75.
[689] Moore T, Adhikari R, Barton P, Gunatillake PA. Biodegradable polyurethane for fused deposition modelling. 7th World Biomaterials Congress. Sidney, Australia: Curran Associates, Inc.; 2004. p. 885.
[690] Haryńska A, Kucinska-Lipka J, Sulowska A, Gubanska I, Kostrzewa M, Janik H Medical-Grade PCL Based Polyurethane System for FDM 3D Printing—Characterization and Fabrication, Materials, 12 (2019), pp. 887.
[691] Güney A, Gardiner C, McCormack A, Malda J, Grijpma DW Thermoplastic PCL-b-PEG-b-PCL and HDI Polyurethanes for Extrusion-Based 3D-Printing of Tough Hydrogels, Bioengineering, 5 (2018), pp. 99.
[692] Camarero-Espinosa S, Tomasina C, Calore A, Moroni L Additive Manufactured, Highly Resilient, Elastic and Biodegradable Poly(ester)urethane Scaffolds with Chondroinductive Properties for Cartilage Tissue Engineering, Materials Today Bio, (2020), pp. 100051.
[693] Castro NJ, Tan WN, Shen C, Zhang LG Simulated Body Fluid Nucleation of Three-Dimensional Printed Elastomeric Scaffolds for Enhanced Osteogenesis, Tissue Eng Part A, 22 (2016), pp. 940-8.
[694] Agrawal A, Rahbar N, Calvert PD Strong fiber-reinforced hydrogel, Acta Biomater, 9 (2013), pp. 5313-8.
[695] Perkins J, Hong Y, Ye S-H, Wagner WR, Desai S Direct writing of bio-functional coatings for cardiovascular applications, J Biomed Mater Res A, 102 (2014), pp. 4290-300.
[696] Xu W, Wang X, Yan Y, Zhang R Rapid Prototyping of Polyurethane for the Creation of Vascular Systems, J Bioact Compatible Polym, 23 (2008), pp. 103-14.
[697] Cui T, Yan Y, Zhang R, Liu L, Xu W, Wang X Rapid Prototyping of a Double-Layer Polyurethane–Collagen Conduit for Peripheral Nerve Regeneration, Tissue Eng Part C, 15 (2008), pp. 1-9.
[698] Xiahong W, Tongkui C, Yongnian Y, Renji Z Peroneal Nerve Regeneration Using a Unique Bilayer Polyurethane-collagen Guide Conduit, J Bioact Compatible Polym, 24 (2009), pp. 109-27.

[699] Kai H, Xiaohong W Rapid prototyping of tubular polyurethane and cell/hydrogel constructs, J Bioact Compatible Polym, 26 (2011), pp. 363-74.
[700] Hsu S-h, Hung K-C, Lin Y-Y, Su C-H, Yeh H-Y, Jeng US, et al. Water-based synthesis and processing of novel biodegradable elastomers for medical applications, J Mater Chem B, 2 (2014), pp. 5083-92.
[701] Hsieh F-Y, Lin H-H, Hsu S-h 3D bioprinting of neural stem cell-laden thermoresponsive biodegradable polyurethane hydrogel and potential in central nervous system repair, Biomaterials, 71 (2015), pp. 48-57.
[702] Tsai Y-C, Li S, Hu S-G, Chang W-C, Jeng US, Hsu S-h Synthesis of thermoresponsive amphiphilic polyurethane gel as a new cell printing material near body temperature, ACS Appl Mater Interfaces, 7 (2015), pp. 27613-23.
[703] Lin H-H, Hsieh F-Y, Tseng C-S, Hsu S-h Preparation and characterization of a biodegradable polyurethane hydrogel and the hybrid gel with soy protein for 3D cell-laden bioprinting, J Mater Chem B, 4 (2016), pp. 6694-705.
[704] Zhang C, Zhao K, Hu T, Cui X, Brown N, Boland T Loading dependent swelling and release properties of novel biodegradable, elastic and environmental stimuli-sensitive polyurethanes, J Controlled Release, 131 (2008), pp. 128-36.
[705] Zhang C, Wen X, Vyavahare NR, Boland T Synthesis and characterization of biodegradable elastomeric polyurethane scaffolds fabricated by the inkjet technique, Biomaterials, 29 (2008), pp. 3781-91.
[706] Guillaume O, Geven MA, Grijpma DW, Tang TT, Qin L, Lai YX, et al. Poly(trimethylene carbonate) and nano-hydroxyapatite porous scaffolds manufactured by stereolithography, Polym Adv Technol, 28 (2017), pp. 1219-25.
[707] Dienel KEG, van Bochove B, Seppälä JV Additive Manufacturing of Bioactive Poly(trimethylene carbonate)/β-Tricalcium Phosphate Composites for Bone Regeneration, Biomacromolecules, 21 (2020), pp. 366-75.
[708] Fukushima K Poly(trimethylene carbonate)-based polymers engineered for biodegradable functional biomaterials, Biomater Sci, 4 (2016), pp. 9-24.
[709] Ahlinder A, Fuoco T, Finne-Wistrand A Medical grade polylactide, copolyesters and polydioxanone: Rheological properties and melt stability, Polym Test, 72 (2018), pp. 214-22.
[710] Salaoru I, Zhou Z, Morris P, Gibbons GJ Inkjet printing of polyvinyl alcohol multilayers for additive manufacturing applications, J Appl Polym Sci, 133 (2016), pp. 43572.
[711] Rigotti D, Fambri L, Pegoretti A Polyvinyl alcohol reinforced with carbon nanotubes for fused deposition modeling, J Reinf Plast Compos, 37 (2018), pp. 716-27.
[712] Cataldi A, Rigotti D, Nguyen VDH, Pegoretti A Polyvinyl alcohol reinforced with crystalline nanocellulose for 3D printing application, Materials Today Communications, 15 (2018), pp. 236-44.
[713] Sun H, Mei L, Song C, Cui X, Wang P The in vivo degradation, absorption and excretion of PCL-based implant, Biomaterials, 27 (2006), pp. 1735-40.
[714] Bartnikowski M, Dargaville TR, Ivanovski S, Hutmacher DW Degradation mechanisms of polycaprolactone in the context of chemistry, geometry and environment, Prog Polym Sci, 96 (2019), pp. 1-20.
[715] Ye WP, Du FS, Jin WH, Yang JY, Xu Y In vitro degradation of poly(caprolactone), poly(lactide) and their block copolymers: influence of composition, temperature and morphology, React Funct Polym, 32 (1997), pp. 161-8.
[716] Gupta D, Venugopal J, Mitra S, Giri Dev VR, Ramakrishna S Nanostructured biocomposite substrates by electrospinning and electrospraying for the mineralization of osteoblasts, Biomaterials, 30 (2009), pp. 2085-94.
[717] Chew SY, Mi R, Hoke A, Leong KW Aligned Protein-Polymer Composite Fibers Enhance Nerve Regeneration: A Potential Tissue-Engineering Platform, Adv Funct Mater, 17 (2007), pp. 1288-96.

[718] Albertsson A-C, Varma IK. Aliphatic Polyesters: Synthesis, Properties and Applications. Degradable Aliphatic Polyesters. Berlin, Heidelberg: Springer Berlin Heidelberg; 2002. p. 1-40.
[719] Malikmammadov E, Tanir TE, Kiziltay A, Hasirci V, Hasirci N PCL and PCL-based materials in biomedical applications, J Biomater Sci Polym Ed, 29 (2018), pp. 863-93.
[720] Cipitria A, Skelton A, Dargaville TR, Dalton PD, Hutmacher DW Design, fabrication and characterization of PCL electrospun scaffolds—a review, J Mater Chem, 21 (2011), pp. 9419-53.
[721] Puppi D, Piras AM, Chiellini F, Chiellini E, Martins A, Leonor IB, et al. Optimized electro- and wet-spinning techniques for the production of polymeric fibrous scaffolds loaded with bisphosphonate and hydroxyapatite, J Tissue Eng Regener Med, 5 (2011), pp. 253-63.
[722] Bezwada RS, Jamiolkowski DD, Lee I-Y, Agarwal V, Persivale J, Trenka-Benthin S, et al. Monocryl® suture, a new ultra-pliable absorbable monofilament suture, Biomaterials, 16 (1995), pp. 1141-8.
[723] Darney PD, Monroe SE, Klaisle CM, Alvarado A Clinical evaluation of the Capronor contraceptive implant: Preliminary report, Am J Obstet Gynecol, 160 (1989), pp. 1292-5.
[724] Rohner D, Hutmacher DW, Cheng TK, Oberholzer M, Hammer B In vivo efficacy of bone-marrow-coated polycaprolactone scaffolds for the reconstruction of orbital defects in the pig, J Biomed Mater Res B Appl Biomater, 66B (2003), pp. 574-80.
[725] Schantz JT, Lim TC, Ning C, Teoh SH, Tan KC, Wang SC, et al. Cranioplasty after trephination using a novel biodegradable burr hole cover: technical case report, Neurosurgery, 58 (2006), pp. ONS-E176; discussion ONS-E.
[726] http://www.osteopore.com; 2019
[727] Low SW, Ng YJ, Yeo TT, Chou N Use of Osteoplug polycaprolactone implants as novel burr-hole covers, Singapore Med J, 50 (2009), pp. 777-80.
[728] Teo L, Teoh SH, Liu Y, Lim L, Tan B, Schantz J-T, et al. A Novel Bioresorbable Implant for Repair of Orbital Floor Fractures, Orbit, 34 (2015), pp. 192-200.
[729] Goh Bee T, Teh Luan Y, Tan Danny Ben P, Zhang Z, Teoh Swee H Novel 3D polycaprolactone scaffold for ridge preservation – a pilot randomised controlled clinical trial, Clin Oral Implants Res, 26 (2015), pp. 271-7.
[730] Wiggenhauser PS, Müller DF, Melchels FPW, Egaña JT, Storck K, Mayer H, et al. Engineering of vascularized adipose constructs, Cell Tissue Res, (2011), pp. 1-11.
[731] Zein I, Hutmacher DW, Tan KC, Teoh SH Fused deposition modeling of novel scaffold architectures for tissue engineering applications, Biomaterials, 23 (2002), pp. 1169-85.
[732] Abbah SA, Lam CXL, Hutmacher DW, Goh JCH, Wong H-K Biological performance of a polycaprolactone-based scaffold used as fusion cage device in a large animal model of spinal reconstructive surgery, Biomaterials, 30 (2009), pp. 5086-93.
[733] Kim S-J, Kim M-R, Oh J-S, Han I, Shin S-W Effects of Polycaprolactone-Tricalcium Phosphate, Recombinant Human Bone Morphogenetic Protein-2 and Dog Mesenchymal Stem Cells on Bone Formation: Pilot Study in Dogs, Yonsei Med J, 50 (2009), pp. 825-31.
[734] Lam CXF, Hutmacher DW, Schantz J-T, Woodruff MA, Teoh SH Evaluation of polycaprolactone scaffold degradation for 6 months in vitro and in vivo, J Biomed Mater Res A, 90A (2009), pp. 906-19.
[735] Sawyer AA, Song SJ, Susanto E, Chuan P, Lam CXF, Woodruff MA, et al. The stimulation of healing within a rat calvarial defect by mPCL–TCP/collagen scaffolds loaded with rhBMP-2, Biomaterials, 30 (2009), pp. 2479-88.
[736] Rai B, Lin JL, Lim ZXH, Guldberg RE, Hutmacher DW, Cool SM Differences between in vitro viability and differentiation and in vivo bone-forming efficacy of human mesenchymal stem cells cultured on PCL-TCP scaffolds, Biomaterials, 31 (2010), pp. 7960-70.

[737] Ho ST, Hutmacher DW, Ekaputra AK, Hitendra D, Hui JH The evaluation of a biphasic osteochondral implant coupled with an electrospun membrane in a large animal model, Tissue Eng Part A, 16 (2010), pp. 1123-41.
[738] Yeo A, Wong WJ, Teoh S-H Surface modification of PCL-TCP scaffolds in rabbit calvaria defects: Evaluation of scaffold degradation profile, biomechanical properties and bone healing patterns, J Biomed Mater Res A, 93A (2010), pp. 1358-67.
[739] Probst FA, Hutmacher DW, Muller DF, Machens HG, Schantz JT [Calvarial reconstruction by customized bioactive implant], Handchir Mikrochir Plast Chir, 42 (2010), pp. 369-73.
[740] Rai B, Oest ME, Dupont KM, Ho KH, Teoh SH, Guldberg RE Combination of platelet-rich plasma with polycaprolactone-tricalcium phosphate scaffolds for segmental bone defect repair, J Biomed Mater Res A, 81A (2007), pp. 888-99.
[741] Reichert JC, Cipitria A, Epari DR, Saifzadeh S, Krishnakanth P, Berner A, et al. A Tissue Engineering Solution for Segmental Defect Regeneration in Load-Bearing Long Bones, Sci Transl Med, 4 (2012), pp. 141ra93.
[742] Cipitria A, Wagermaier W, Zaslansky P, Schell H, Reichert JC, Fratzl P, et al. BMP delivery complements the guiding effect of scaffold architecture without altering bone microstructure in critical-sized long bone defects: A multiscale analysis, Acta Biomater, 23 (2015), pp. 282-94.
[743] Holländer J, Genina N, Jukarainen H, Khajeheian M, Rosling A, Mäkilä E, et al. Three-Dimensional Printed PCL-Based Implantable Prototypes of Medical Devices for Controlled Drug Delivery, J Pharm Sci, 105 (2016), pp. 2665-76.
[744] Costa PF, Vaquette C, Zhang Q, Reis RL, Ivanovski S, Hutmacher DW Advanced tissue engineering scaffold design for regeneration of the complex hierarchical periodontal structure, J Clin Periodontol, 41 (2014), pp. 283-94.
[745] Jeon June E, Vaquette C, Theodoropoulos C, Klein Travis J, Hutmacher Dietmar W Multiphasic construct studied in an ectopic osteochondral defect model, J Royal Soc Interface, 11 (2014), pp. 20140184.
[746] Muerza-Cascante ML, Haylock D, Hutmacher DW, Dalton PD Melt Electrospinning and Its Technologization in Tissue Engineering, Tissue Eng Part B, 21 (2014), pp. 187-202.
[747] Les AS, Ohye RG, Filbrun AG, Ghadimi Mahani M, Flanagan CL, Daniels RC, et al. 3D-printed, externally-implanted, bioresorbable airway splints for severe tracheobronchomalacia, The Laryngoscope, 0 (2019), pp.
[748] Datta R, Henry M Lactic acid: recent advances in products, processes and technologies — a review, J Chem Technol Biotechnol, 81 (2006), pp. 1119-29.
[749] Bigg DM Polylactide copolymers: Effect of copolymer ratio and end capping on their properties, Adv Polym Tech, 24 (2005), pp. 69-82.
[750] Rabnawaz M, Wyman I, Auras R, Cheng S A roadmap towards green packaging: the current status and future outlook for polyesters in the packaging industry, Green Chemistry, 19 (2017), pp. 4737-53.
[751] Nair LS, Laurencin CT Polymers as Biomaterials for Tissue Engineering and Controlled Drug Delivery, Adv Biochem Eng/Biotechnol, 102 (2006), pp. 47-90.
[752] Doppalapudi S, Jain A, Khan W, Domb AJ Biodegradable polymers—an overview, Polym Adv Technol, 25 (2014), pp. 427-35.
[753] Alexy RD, Levi DS Materials and Manufacturing Technologies Available for Production of a Pediatric Bioabsorbable Stent, Biomed Res Int, 2013 (2013), pp. 11.
[754] An YH, Woolf SK, Friedman RJ Pre-clinical in vivo evaluation of orthopaedic bioabsorbable devices, Biomaterials, 21 (2000), pp. 2635-52.
[755] Barber FA, Dockery WD Long-Term Absorption of Poly-L-Lactic Acid Interference Screws, Arthroscopy, 22 (2006), pp. 820-6.

[756] Warden WH, Chooljian D, Jackson DW Ten-Year Magnetic Resonance Imaging Follow-Up of Bioabsorbable Poly-L-Lactic Acid Interference Screws After Anterior Cruciate Ligament Reconstruction, Arthroscopy, 24 (2008), pp. 370.e1-.e3.
[757] Rezwan K, Chen QZ, Blaker JJ, Boccaccini AR Biodegradable and bioactive porous polymer/inorganic composite scaffolds for bone tissue engineering, Biomaterials, 27 (2006), pp. 3413-31.
[758] Bergsma EJ, Rozema FR, Bos RR, Debruijn WC Foreign body reaction to resorbable poly(L-lactic) bone plates and screws used for the fixation of unstable zygomatic fractures, J Oral Maxillofac Surg, 51 (1993), pp. 666-70.
[759] Martin C, Winet H, Bao JY Acidity near eroding polylactide-polyglycolide in vitro and in vivo in rabbit tibial bone chambers, Biomaterials, 17 (1996), pp. 2373-80.
[760] Deng X-L, Sui G, Zhao M-L, Chen G-Q, Yang X-P Poly(L-lactic acid)/hydroxyapatite hybrid nanofibrous scaffolds prepared by electrospinning, J Biomater Sci Polym Ed, 18 (2007), pp. 117-30.
[761] Chou Y-F, Dunn JCY, Wu BM *In vitro* response of MC3T3-E1 preosteoblasts within three-dimensional apatite-coated PLGA scaffolds, J Biomed Mater Res B Appl Biomater, 75B (2005), pp. 81-90.
[762] Dunn AS, Campbell PG, Marra KG The influence of polymer blend composition on the degradation of polymer/hydroxyapatite biomaterials, J Mater Sci Mater Med, 12 (2001), pp. 673-7.
[763] Heidemann W, Jeschkeit S, Ruffieux K, Fischer JH, Wagner M, Kruger G, et al. Degradation of poly(d,l)lactide implants with or without addition of calciumphosphates in vivo, Biomaterials, 22 (2001), pp. 2371-81.
[764] Rahman MS, Way S Polyglycolic acid surgical sutures ingynaecological surgery, BJOG, 79 (1972), pp. 849-51.
[765] Burns AE Biofix fixation techniques and results in foot surgery, J Foot Ankle Surg, 34 (1995), pp. 276-82.
[766] Otto J, Binnebösel M, Pietsch S, Anurov M, Titkova S, Öttinger AP, et al. Large-Pore PDS Mesh Compared to Small-Pore PG Mesh, J Invest Surg, 23 (2010), pp. 190-6.
[767] Knecht S, Erggelet C, Endres M, Sittinger M, Kaps C, Stüssi E Mechanical testing of fixation techniques for scaffold-based tissue-engineered grafts, J Biomed Mater Res B Appl Biomater, 83B (2007), pp. 50-7.
[768] Wang L, Dormer NH, Bonewald LF, Detamore MS Osteogenic Differentiation of Human Umbilical Cord Mesenchymal Stromal Cells in Polyglycolic Acid Scaffolds, Tissue Eng Part A, 16 (2010), pp. 1937-48.
[769] Erggelet C, Neumann K, Endres M, Haberstroh K, Sittinger M, Kaps C Regeneration of ovine articular cartilage defects by cell-free polymer-based implants, Biomaterials, 28 (2007), pp. 5570-80.
[770] Mahmoudifar N, Doran PM Chondrogenic differentiation of human adipose-derived stem cells in polyglycolic acid mesh scaffolds under dynamic culture conditions, Biomaterials, 31 (2010), pp. 3858-67.
[771] Xu L, Cao D, Liu W, Zhou G, Zhang WJ, Cao Y In vivo engineering of a functional tendon sheath in a hen model, Biomaterials, 31 (2010), pp. 3894-902.
[772] Martins C, Sousa F, Araújo F, Sarmento B Functionalizing PLGA and PLGA Derivatives for Drug Delivery and Tissue Regeneration Applications, Adv Healthcare Mater, 7 (2018), pp. 1701035.
[773] Puppi D, Piras AM, Detta N, Dinucci D, Chiellini F Poly(lactic-co-glycolic acid) electrospun fibrous meshes for the controlled release of retinoic acid, Acta Biomater, 6 (2010), pp. 1258-68.

[774] Danhier F, Ansorena E, Silva JM, Coco R, Le Breton A, Préat V PLGA-based nanoparticles: An overview of biomedical applications, J Controlled Release, 161 (2012), pp. 505-22.
[775] Gentile P, Chiono V, Carmagnola I, Hatton VP An Overview of Poly(lactic-co-glycolic) Acid (PLGA)-Based Biomaterials for Bone Tissue Engineering, Int J Mol Sci, 15 (2014), pp.
[776] Ulery BD, Nair LS, Laurencin CT Biomedical Applications of Biodegradable Polymers, J Polym Sci, Part B: Polym Phys, 49 (2011), pp. 832-64.
[777] Tymrak BM, Kreiger M, Pearce JM Mechanical properties of components fabricated with open-source 3-D printers under realistic environmental conditions, Mater Des, 58 (2014), pp. 242-6.
[778] Joziasse CAP, Veenstra H, Grijpma DW, Pennings AJ On the chain stiffness of poly(lactide)s, Macromol Chem Phys, 197 (1996), pp. 2219-29.
[779] Dorgan JR, Williams JS, Lewis DN Melt rheology of poly(lactic acid): Entanglement and chain architecture effects, J Rheol, 43 (1999), pp. 1141-55.
[780] Heo DN, Castro NJ, Lee S-J, Noh H, Zhu W, Zhang LG Enhanced bone tissue regeneration using a 3D printed microstructure incorporated with a hybrid nano hydrogel, Nanoscale, 9 (2017), pp. 5055-62.
[781] Yuan S, Shen F, Chua CK, Zhou K Polymeric composites for powder-based additive manufacturing: Materials and applications, Prog Polym Sci, 91 (2019), pp. 141-68.
[782] Leong KF, Chua CK, Gui WS, Verani Building Porous Biopolymeric Microstructures for Controlled Drug Delivery Devices Using Selective Laser Sintering, Int J Adv Manuf Technol, 31 (2006), pp. 483-9.
[783] Lim SH, Kathuria H, Tan JJY, Kang L 3D printed drug delivery and testing systems — a passing fad or the future?, Adv Drug Del Rev, 132 (2018), pp. 139-68.
[784] Wu G, Wu W, Zheng Q, Li J, Zhou J, Hu Z Experimental study of PLLA/INH slow release implant fabricated by three dimensional printing technique and drug release characteristics in vitro, BioMedical Engineering OnLine, 13 (2014), pp. 97.
[785] Kasper FK, Tanahashi K, Fisher JP, Mikos AG Synthesis of poly(propylene fumarate), Nat Protoc, 4 (2009), pp. 518-25.
[786] Yaszemski MJ, Payne RG, Mikos AG. Poly(propylene fumarate). US: No. 5,733,951.; 31 Mar 1998.
[787] Domb AJ. Poly(propylene glycol fumarate) compositions for biomedical applications. US patent 4888413; 1989.
[788] Luo Y, Dolder CK, Walker JM, Mishra R, Dean D, Becker ML Synthesis and Biological Evaluation of Well-Defined Poly(propylene fumarate) Oligomers and Their Use in 3D Printed Scaffolds, Biomacromolecules, 17 (2016), pp. 690-7.
[789] Peter SJ, Kim P, Yasko AW, Yaszemski MJ, Mikos AG Crosslinking characteristics of an injectable poly(propylene fumarate)/β-tricalcium phosphate paste and mechanical properties of the crosslinked composite for use as a biodegradable bone cement, J Biomed Mater Res, 44 (1999), pp. 314-21.
[790] Hedberg EL, Kroese-Deutman HC, Shih CK, Crowther RS, Carney DH, Mikos AG, et al. In vivo degradation of porous poly(propylene fumarate)/poly(DL-lactic-co-glycolic acid) composite scaffolds, Biomaterials, 26 (2005), pp. 4616-23.
[791] Timmer MD, Shin H, Horch RA, Ambrose CG, Mikos AG In Vitro Cytotoxicity of Injectable and Biodegradable Poly(propylene fumarate)-Based Networks: Unreacted Macromers, Cross-Linked Networks, and Degradation Products, Biomacromolecules, 4 (2003), pp. 1026-33.
[792] Frazier DD, Lathi VK, Gerhart TN, Hayes WC Ex vivo degradation of a poly(propylene glycol-fumarate) biodegradable particulate composite bone cement, J Biomed Mater Res, 35 (1997), pp. 383-9.

[793] Fisher JP, Dean D, Mikos AG Photocrosslinking characteristics and mechanical properties of diethyl fumarate/poly(propylene fumarate) biomaterials, Biomaterials, 23 (2002), pp. 4333-43.
[794] Pal S. Mechanical Properties of Biological Materials. In: Pal S, editor. Design of Artificial Human Joints & Organs. Boston, MA: Springer US; 2014. p. 23-40.
[795] Liu X, Miller Ii AL, Waletzki BE, Yaszemski MJ, Lu L Novel biodegradable poly(propylene fumarate)-co-poly(l-lactic acid) porous scaffolds fabricated by phase separation for tissue engineering applications, RSC Adv, 5 (2015), pp. 21301-9.
[796] Yaszemski MJ, Payne RG, Hayes WC, Langer RS, Aufdemorte TB, Mikos AG The Ingrowth of New Bone Tissue and Initial Mechanical Properties of a Degrading Polymeric Composite Scaffold, Tissue Eng, 1 (1995), pp. 41-52.
[797] Vehof JWM, Fisher JP, Dean D, van der Waerden J-PCM, Spauwen PHM, Mikos AG, et al. Bone formation in transforming growth factor β-1-coated porous poly(propylene fumarate) scaffolds, J Biomed Mater Res, 60 (2002), pp. 241-51.
[798] Timmer MD, Ambrose CG, Mikos AG In vitro degradation of polymeric networks of poly(propylene fumarate) and the crosslinking macromer poly(propylene fumarate)-diacrylate, Biomaterials, 24 (2003), pp. 571-7.
[799] Peter SJ, Nolley JA, Widmer MS, Merwin JE, Yaszemski MJ, Yasko AW, et al. In Vitro Degradation of a Poly(Propylene Fumarate)/ β-Tricalcium Phosphate Composite Orthopaedic Scaffold, Tissue Eng, 3 (1997), pp. 207-15.
[800] Kharas GB, Kamenetsky M, Simantirakis J, Beinlich KC, Rizzo A-MT, Caywood GA, et al. Synthesis and characterization of fumarate-based polyesters for use in bioresorbable bone cement composites, J Appl Polym Sci, 66 (1997), pp. 1123-37.
[801] Cai Z-Y, Yang D-A, Zhang N, Ji C-G, Zhu L, Zhang T Poly(propylene fumarate)/(calcium sulphate/[beta]-tricalcium phosphate) composites: Preparation, characterization and in vitro degradation, Acta Biomater, 5 (2009), pp. 628-35.
[802] Lee K-W, Wang S, Yaszemski MJ, Lu L Physical properties and cellular responses to crosslinkable poly(propylene fumarate)/hydroxyapatite nanocomposites, Biomaterials, 29 (2008), pp. 2839-48.
[803] Hedberg EL, Tang A, Crowther RS, Carney DH, Mikos AG Controlled release of an osteogenic peptide from injectable biodegradable polymeric composites, J Controlled Release, 84 (2002), pp. 137-50.
[804] Hedberg EL, Kroese-Deutman HC, Shih CK, Crowther RS, Carney DH, Mikos AG, et al. Effect of varied release kinetics of the osteogenic thrombin peptide TP508 from biodegradable, polymeric scaffolds on bone formation *in vivo*, J Biomed Mater Res A, 72A (2005), pp. 343-53.
[805] Hedberg EL, Shih CK, Lemoine JJ, Timmer MD, K. Liebschner MA, Jansen JA, et al. In vitro degradation of porous poly(propylene fumarate)/poly(dl-lactic-co-glycolic acid) composite scaffolds, Biomaterials, 26 (2005), pp. 3215-25.
[806] Dilla RA, Motta CMM, Snyder SR, Wilson JA, Wesdemiotis C, Becker ML Synthesis and 3D Printing of PEG–Poly(propylene fumarate) Diblock and Triblock Copolymer Hydrogels, ACS Macro Lett, 7 (2018), pp. 1254-60.
[807] Rychlý J, Lattuati-Derieux A, Lavédrine B, Matisová-Rychlá L, Malíková M, Csomorová K, et al. Assessing the progress of degradation in polyurethanes by chemiluminescence and thermal analysis. II. Flexible polyether- and polyester-type polyurethane foams, Polym Degrad Stab, 96 (2011), pp. 462-9.
[808] Thompson DG, Osborn JC, Kober EM, Schoonover JR Effects of hydrolysis-induced molecular weight changes on the phase separation of a polyester polyurethane, Polym Degrad Stab, 91 (2006), pp. 3360-70.
[809] Anderson JM, Rodriguez A, Chang DT Foreign body reaction to biomaterials, Semin Immunol, 20 (2008), pp. 86-100.

[810] Penczek P, Frisch KC, Szczepaniak B, Rudnik E Synthesis and properties of liquid crystalline polyurethanes, J Polym Sci, Part A: Polym Chem, 31 (1993), pp. 1211-20.
[811] Honarkar H Waterborne polyurethanes: A review, J Dispersion Sci Technol, 39 (2018), pp. 507-16.
[812] Li Z, Li J Control of Hyperbranched Structure of Polycaprolactone/Poly(ethylene glycol) Polyurethane Block Copolymers by Glycerol and Their Hydrogels for Potential Cell Delivery, The Journal of Physical Chemistry B, 117 (2013), pp. 14763-74.
[813] Cooper SL, Tobolsky AV Properties of linear elastomeric polyurethanes, J Appl Polym Sci, 10 (1966), pp. 1837-44.
[814] Lan PN, Corneillie S, Schacht E, Davies M, Shard A Synthesis and characterization of segmented polyurethanes based on amphiphilic polyether diols, Biomaterials, 17 (1996), pp. 2273-80.
[815] Alves P, Ferreira P, Gil H. Biomedical Polyurethane-Based Materials. Polyurethane: Properties, Structure and Applications. New York: Nova Publishers; 2012.
[816] Joseph J, Patel RM, Wenham A, Smith JR Biomedical applications of polyurethane materials and coatings, Transactions of the IMF, 96 (2018), pp. 121-9.
[817] Guelcher SA Biodegradable Polyurethanes: Synthesis and Applications in Regenerative Medicine, Tissue Eng Part B, 14 (2008), pp. 3-17.
[818] Tatai L, Moore TG, Adhikari R, Malherbe F, Jayasekara R, Griffiths I, et al. Thermoplastic biodegradable polyurethanes: The effect of chain extender structure on properties and in-vitro degradation, Biomaterials, 28 (2007), pp. 5407-17.
[819] Caracciolo PC, Lores NJ, Abraham GA. Chapter 8 - Polyurethane-based structures obtained by additive manufacturing technologies. In: Holban A-M, Grumezescu AM, editors. Materials for Biomedical Engineering. Elsevier; 2019. p. 235-58.
[820] Hung KC, Tseng CS, Hsu SH. 5 - 3D printing of polyurethane biomaterials. In: Cooper SL, Guan J, editors. Advances in Polyurethane Biomaterials. Woodhead Publishing; 2016. p. 149-70.
[821] Merceron TK, Burt M, Seol Y-J, Kang H-W, Lee SJ, Yoo JJ, et al. A 3D bioprinted complex structure for engineering the muscle–tendon unit, Biofabrication, 7 (2015), pp. 035003.
[822] Hung K-C, Tseng C-S, Hsu S-h Synthesis and 3D Printing of Biodegradable Polyurethane Elastomer by a Water-Based Process for Cartilage Tissue Engineering Applications, Adv Healthcare Mater, 3 (2014), pp. 1578-87.
[823] Hung K-C, Tseng C-S, Dai L-G, Hsu S-h Water-based polyurethane 3D printed scaffolds with controlled release function for customized cartilage tissue engineering, Biomaterials, 83 (2016), pp. 156-68.
[824] Tamura M, Matsuda K, Nakagawa Y, Tomishige K Ring-opening polymerization of trimethylene carbonate to poly(trimethylene carbonate) diol over a heterogeneous high-temperature calcined CeO2 catalyst, Chem Commun, 54 (2018), pp. 14017-20.
[825] Zhang Z, Kuijer R, Bulstra SK, Grijpma DW, Feijen J The in vivo and in vitro degradation behavior of poly(trimethylene carbonate), Biomaterials, 27 (2006), pp. 1741-8.
[826] Engelberg I, Kohn J Physico-mechanical properties of degradable polymers used in medical applications: A comparative study, Biomaterials, 12 (1991), pp. 292-304.
[827] Brannigan RP, Dove AP Synthesis, properties and biomedical applications of hydrolytically degradable materials based on aliphatic polyesters and polycarbonates, Biomater Sci, 5 (2017), pp. 9-21.
[828] Blanquer SBG, Gebraad AWH, Miettinen S, Poot AA, Grijpma DW, Haimi SP Differentiation of adipose stem cells seeded towards annulus fibrosus cells on a designed poly(trimethylene carbonate) scaffold prepared by stereolithography, J Tissue Eng Regener Med, 11 (2017), pp. 2752-62.
[829] Chiellini E, Corti A, D'Antone S, Solaro R Biodegradation of poly (vinyl alcohol) based materials, Prog Polym Sci, 28 (2003), pp. 963-1014.

[830] Chong S-F, Smith AAA, Zelikin AN Microstructured, Functional PVA Hydrogels through Bioconjugation with Oligopeptides under Physiological Conditions, Small, 9 (2013), pp. 942-50.
[831] Ben Halima N Poly(vinyl alcohol): review of its promising applications and insights into biodegradation, RSC Adv, 6 (2016), pp. 39823-32.
[832] Cerroni B, Cicconi R, Oddo L, Scimeca M, Bonfiglio R, Bernardini R, et al. In vivo biological fate of poly(vinylalcohol) microbubbles in mice, Heliyon, 4 (2018), pp. e00770-e.
[833] Kumar A, Han SS PVA-based hydrogels for tissue engineering: A review, International Journal of Polymeric Materials and Polymeric Biomaterials, 66 (2017), pp. 159-82.